IN-1336
NASA CR-72550
October 1969

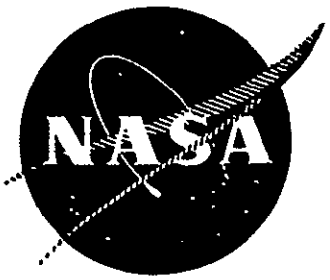

CAVITY REACTOR CRITICAL EXPERIMENT
VOLUME IV
(Waves and Control Methods)

G.D. Pincock and J. F. Kunze

Prepared for

NATIONAL AERONAUTICS AND SPACE ADMINISTRATION

Contract C-67747-A

IDAHO NUCLEAR CORPORATION
National Reactor Testing Station
Idaho Falls, Idaho

LEGAL NOTICE

This report was prepared as an account of Government sponsored work. Neither the United States, nor the Commission, nor any person acting on behalf of the Commission:

A. Makes any warranty or representation, express or implied, with respect to the accuracy, completeness, or usefulness of the information contained in this report, or that the use of any information, apparatus, method, or process disclosed in this report may not infringe privately owned rights; or

B. Assumes any liabilities with respect to the use of, or for damages resulting from the use of any information, apparatus, method, or process disclosed in this report.

As used in the above, "person acting on behalf of the Commission" includes any employee or contractor of the Commission, or employee of such contractor, to the extent that such employee or contractor of the Commission, or employee of such contractor prepares, disseminates, or provides access to, any information pursuant to his employment or contract with the Commission, or his employment with such contractor.

PRINTED IN USA

IN-1336
NASA CR-72550
Issued: October 1969
Limited Distribution

CAVITY REACTOR CRITICAL EXPERIMENT

VOLUME IV

(Waves and Control Methods)

BY

G. D. Pincock and J. F. Kunze

Prepared for
NATIONAL AERONAUTICS AND SPACE ADMINISTRATION
Contract C-67747-A

Technical Management
NASA-Lewis Research Center
Cleveland, Ohio

Nuclear Systems Division
Robert E. Hyland, Project Manager

Space Nuclear Propulsion Office
Capt. C. E. Franklin, USAF

IDAHO NUCLEAR CORPORATION

A JOINTLY OWNED SUBSIDIARY OF
AEROJET GENERAL CORPORATION
ALLIED CHEMICAL CORPORATION
PHILLIPS PETROLEUM COMPANY

U. S. Atomic Energy Commission Research and Development Report
Issued Under Contract AT(10-1)-1230
Idaho Operations Office

ABSTRACT

This report is volume four of a set covering critical experiments performed on a large cavity reactor system at the National Reactor Testing Station. This volume contains experiments which evaluate the effects of fuel wave formations on the outer boundary of the active core as a function of wave size and axial position. Also included are effects of rounding off the core at the ends and evaluation of reactor control methods such as a poison sleeve and rotating runs.

ACKNOWLEDGEMENTS

The authors wish to acknowledge the contributions of Mrs. P. L. Chase in data reduction, graph preparation, and proof reading-editing of the report; and to the reactor operations crew of C. G. Cooper, R. R. Jones, and D. H. Suckling.

TABLE OF CONTENTS

TABLE OF CONTENTS

(Cont'd)

TABLE OF CONTENTS

(Cont 'd)

FIGURES

TABLE OF CONTENTS

(Cont'd)

Page

FIGURES

(Cont'd)

TABLE OF CONTENTS

(Cont'd)

Page

FIGURES

(Cont'd)

TABLE OF CONTENTS

(Cont'd)

Page

FIGURES

(Cont'd)

TABLE OF CONTENTS

(Cont'd)

Page

FIGURES

(Cont'd)

TABLE OF CONTENTS

(Cont'd)

Page

FIGURES

(Cont'd)

TABLE OF CONTENTS

(Cont'd)

Page

FIGURES

(Cont'd)

TABLE OF CONTENTS

(Cont'd)

Page

FIGURES

(Cont'd)

TABLE OF CONTENTS

(Cont'd)

Page

TABLES

TABLE OF CONTENTS

(Cont'd)

Page

TABLES

(Cont'd)

TABLE OF CONTENTS

(Cont'd)

Page

TABLES

(Cont'd)

1.0 SUMMARY

In the actual coaxial flowing gas system of the cavity reactor concept, mixing of the fuel and propellant and distortions of the flow patterns will occur inside the cavity. Scale model flow tests conducted at other installations have provided information on the extent that these disturbances perturb ideal smooth boundry between core and propellant. The major type of disturbances are herein called "waves," in which an undulation develops in the outer fuel boundary and moves through the cavity and out the exhaust nozzle. These "waves" have been simulated in the critical experiment within a 183 cm diameter by 122 cm long cavity. Of principal interest was the reactivity worth of the waves with respect to a smooth core boundary that was 122 cm in diameter. Two major wave configurations and two basic wave amplitudes were considered. The nominal maximum reactivity worths are listed below.

a. Wave crest develops, giving a net fuel addition to the reactor

i)	7.3 cm crest height	+ 0.7%Δk
ii)	22 cm crest height	+ 6%Δk

b. Wave crest and trough develops, with no net fuel addition to the reactor

i)	7.3 cm amplitude	+ 0.3%Δk
ii)	22 cm amplitude	+ 2.8%Δk

The data show that as the wave progresses down the length of the core the worth of the fuel in the wave does not substantially vary.

In addition to the occurrence of waves, the flowing fuel shape in practice will not be the uniform cylinder that has generally been simulated in the critical experiments (so as to simplify the nuclear model used in reactor physics calculations). The sharp "corners" will be gone, resulting in a "tear drop" shaped fuel boundary. The measured reactivity penalty for the loss of the "corners" was 5.5%Δk, with 70% of this loss occurring at the heavily fueled inlet end.* Also, displacement of the fuel away from the end wall of the cavity will be required in practice so that the wall will not contact the extremely high temperature fuel. A 7.5 cm space between the end wall and the core created an additional 2.8%Δk reactivity penalty.*

The "waves" represent potentially rapid reactivity fluctuations that could occur during flowing gas operation. The control system used to date in the critical experiment has consisted of twenty to thirty 1.7 cm diameter boron carbide control rods in one of the end reflectors. These have generally provided control worths of 4 to 6%Δk. Two other control schemes were evaluated. One of these was a cadmium sleeve to be moved longitudinally so as to encircle the core radially; the other scheme consisted of rotating control drums in the reflector. A complete control system of either type would incorporate at least 10%Δk in reactivity, thus providing more than adequate shutdown margin for any unexpected perturbations occurring in the cavity.

* The fuel density in the remainder of the core was unchanged, resulting in a net reduction in total fuel loading.

2.0 INTRODUCTION

This report contains the experimental results from a series of critical experiments which have been conducted on the Cavity Reactor by the General Electric Company at the Idaho Test Station for the Space Nuclear Propulsion Office of NASA and the AEC. This report covers an operating period from May 1968, through December 1968.

Previous critical experiments on a large cavity reactor configuration (183 cm diameter by 122 cm long cavity) have studied the critical mass requirements, power and flux distributions, and structural material effects on reactivity (1), (2), (3). These configurations have generally been of a shape that can be conveniently described by simple two dimensional cylindrical nuclear models (and even by one dimensional spherical models) for the purpose of performing reactor physics calculations. However, the smooth boundaries that have been depicted for the core in the previous experiments will not occur in actual operation of the coaxial flowing gas system. Scale model tests using flow gases (5), (6) have shown what distortions are to be expected in the core-coolant flow boundary. These distortions, nominally labeled as waves, were simulated in the critical experiment.

Sheet fuel approximately 7.3 cm x 7.3 cm by 0.0025 cm thick was used in all the experiments. The fuel element boxes had a square cross section to accommodate the fuel, and all core shapes were created with these square boxes. Various sizes and wave shapes were measured on different core configurations including both uniform core and core with variable fuel density and variable non-cylindrical shapes. The fuel wave experiments were designed to obtain the data needed to predict reactivity fluctuations during operation and hence reactor control requirements as waves are formed along the boundary between the active core and the coolant. In all cases the formation of waves along the active core boundary result in a positive change in reactivity. The larger the wave the larger the reactivity increase; however, the magnitude of reactivity increase in the extreme cases appears to be well within the ability to design an adequate control system.

Under power operation, the coaxial flow cavity reactor will not have the sharp boundary at the ends of the reactor that have existed on the critical experiment configurations. Therefore, measurements were made to determine the reactivity penalty of rounding off the ends of the active core. In addition, the core was shortened, at what would correspond to the entrance end, 7.3 cm (one stage of fuel) and the reactivity loss was measured.

The control system used for the critical experiments has consisted of numerous small diameter boron carbide rods positioned in the end reflector. Other means of reactor control were evaluated such as rotating drums in the radial reflector and a poison sleeve inserted around the cavity from within the end reflector. These measurements were performed using a sheet of cadmium. The cadmium sheet used represented only a very small fraction of the complete control system design. Measurements were made to determine the linearity of the effects with cadmium

sheet size so that a somewhat reliable extrapolation could be made to the complete control system worth.

Though the results in this report are given in terms of reactivity (change in multiplication factor), one should be cautioned about the interpretation and usefulness of large reactivity values. All of the reported measured results are essentially extrapolations of small reactivity values determined by period measurements. The inevitable uncertainty of interaction effects, non-linearities of extrapolations, and major flux distribution changes will be involved. However, despite these "experimental uncertainties," the relationship to the design and operation of the cavity reactor system is of principal concern. Here, it is the fuel loading, which is a major operational variable, that should be related to the reactivity values reported from these experiments. The final section on conclusions and recommendations attempts to show these relationships by drawing on the information in Reference 1, 2, and 3.

3.0 DESCRIPTION OF TEST ASSEMBLY AND TEST PROCEDURES

3.1 Reactor Description

The overall reactor assembly used for the experiments reported herein was the same as used on earlier cavity reactor critical experiments performed by the General Electric Company. References 1, 2, and 3 contain descriptions of the reactor as well as details of the previous experiments and test results. The cavity region of the reactor was 121.9 cm long by 182.9 cm in diameter and was surrounded by 88.9 cm of D_2O. The D_2O contained 0.22 mole percent H_2O and served as both a moderator and reflector. The total overall reactor assembly was a right cylinder 365.8 cm (12 ft) in diameter by 304.8 cm (10 ft) long. The D_2O was contained in two tanks, a fixed tank and a movable tank. The movable tank was mounted on a four-wheel dolly and could be separated from the fixed tank by 132 cm to provide access to the cavity region. The movable tank served as one of the end reflectors while the fixed tank contained the cavity region. Both tanks were made of type 6061 aluminum.

The control system was contained in the end reflector region of the fixed tank as shown in Figure 3.1. Stainless steel clad boron carbide rods were used for control and these rods were attached to actuators which had both shim and scram functions. When fully inserted, the rods penetrated the end reflector to the cavity wall. Additional shutdown was provided by separating the two reactor tanks. The position of the movable table was remotely controlled and the drive system was connected to the reactor control circuits.

All of the experiments described herein contained an annulus of MTR-type fuel elements in the radial reflector as shown in Figure 3.2. This annulus contained 823.2 grams of U-235 and was 19 cm from the wet surface of the cavity wall. The composition and size of the MTR-type fuel plates used in this experiment are given in Table 3.1. These fuel plates were used in earlier experiments as noted in Reference 1.

The core support structure which was used for the initial reactor assembly is shown in Figure 3.3. This was modified later and the extent of the modification will be described in a subsequent section of this report. The base structure shown in Figure 3.3 contained 15.15 kg of type 6061 aluminum and 38.6 kg of type 1100 aluminum. The core structure consisted of several cells into which fuel elements could be inserted. A typical fuel element is shown in Figure 3.4. In order to identify the several fuel element positions within the reactor a numbering system was used as shown in Figure 3.5. By specifying a cell and fuel element number, any position within the core structure could be identified. Each fuel element can consisted of 511 gm of type 1100 aluminum. In addition, when the elements were loaded with fuel, spacers were used to hold the fuel in the configuration shown in Figure 3.4. Each spacer weighed 3.46 gm and there were two of these in each stage of fuel. Each fuel element also contained a lid of type 1100 aluminum which weighed 29.6 gm. The base core configuration contained 208 fuel elements when fully loaded. Thus the total aluminum mass in the core was:

Type 1100 in fuel element cans, rings, and lids	133.2 kg
Type 1100 in fuel element support structure	38.6 kg
Type 6061 in rear yoke support	15.2 kg

3.2 Experimental Procedures

All power distribution measurements were made with catcher foils. The foils consisted of thin discs of aluminum, normally 1.429 cm (9/16 in.) in diameter placed against a bare disc of uranium. After exposure in the reactor, the catcher foils were counted in beta scintillation counters. The activity in the foils was due to fission products embedded in the outer surface of the aluminum and was proportional to power in the specific location in the reactor. Variations in fuel surface and pressure of contact account for uncertainties of less than 1% in count rate. Both bare and cadmium covered foils were exposed. The cadmium was 0.0508 cm (0.020 in.) thick. All foil exposure runs were for 20 minutes from P/e to shutdown where P was the level reactor power for the exposure and e is the natural logarithm base.

All foil locations within the reactor were referenced to an axial and radial zero position. The axial zero reference point was the wet surface of the outer D_2O tank all of the fixed table end reflector (Reference 1, p. 29). The radial zero reference point was the radial center of the reactor.

Neutron flux measurements were obtained from bare and cadmium covered gold foils. The foils were all nominally 0.00127 cm thick and were 1.429 cm in diameter. After exposure in the reactor, these foils were counted in a 256-channel gamma ray analyzer to determine the activity under the 0.41 Mev gamma energy peak, and hence the absolute disintegration rate.

The control rods were remotely operated from the control room and rod positions were monitored on a digital voltmeter or ratiometer. Rod worth curves were not normally measured on the various configurations since the curves are generally insensitive to conditions within the cavity. The curves from previous measurements were generally checked for accuracy by a rod pull or rod insertion measurement using inverse kinetics. These curves were used to evaluate k-excess and rod worth and are found in Reference 1, pp. 26 and 27.

All reactor periods were reduced to reactivity by using the normal inhour equation. The effective delayed neutron parameters used in this equation are given in Reference 1, p. 28. The value of the delayed neutron fraction (the dollar), including gamma-neutron production in the D_2O was 0.765%Δk with an uncertainty of $\pm$0.02%Δk. The neutron lifetime was assumed to be 4.0 milliseconds.

There were two general types of waves tested. The first type consisted of a single wave addition to the outer surface of the reactor

which was either 7.3 or 21.9 cm square. The wave resulted in a net increase in fuel mass. Both single and multiple waves were tested. The second type consisted of a wave with both trough and crest and was created by shifting the fuel from the active core to the outer surface of the core, thus conserving fuel. The waves were the same size as noted above and were both single and multiple waves.

TABLE 3.1

Composition and Dimensions for MTR Type Fuel Plates

Fuel Plate		
Length	50.8	cm
Width	6.2	cm
Thickness	0.094	cm
Al weight	70.25	g
U-235	8.4	g
Aluminum Backup Plate (one per fuel plate)		
Length	56.44	cm
Width	6.985	cm
Thickness	0.099	cm
Al weight	101.3	g

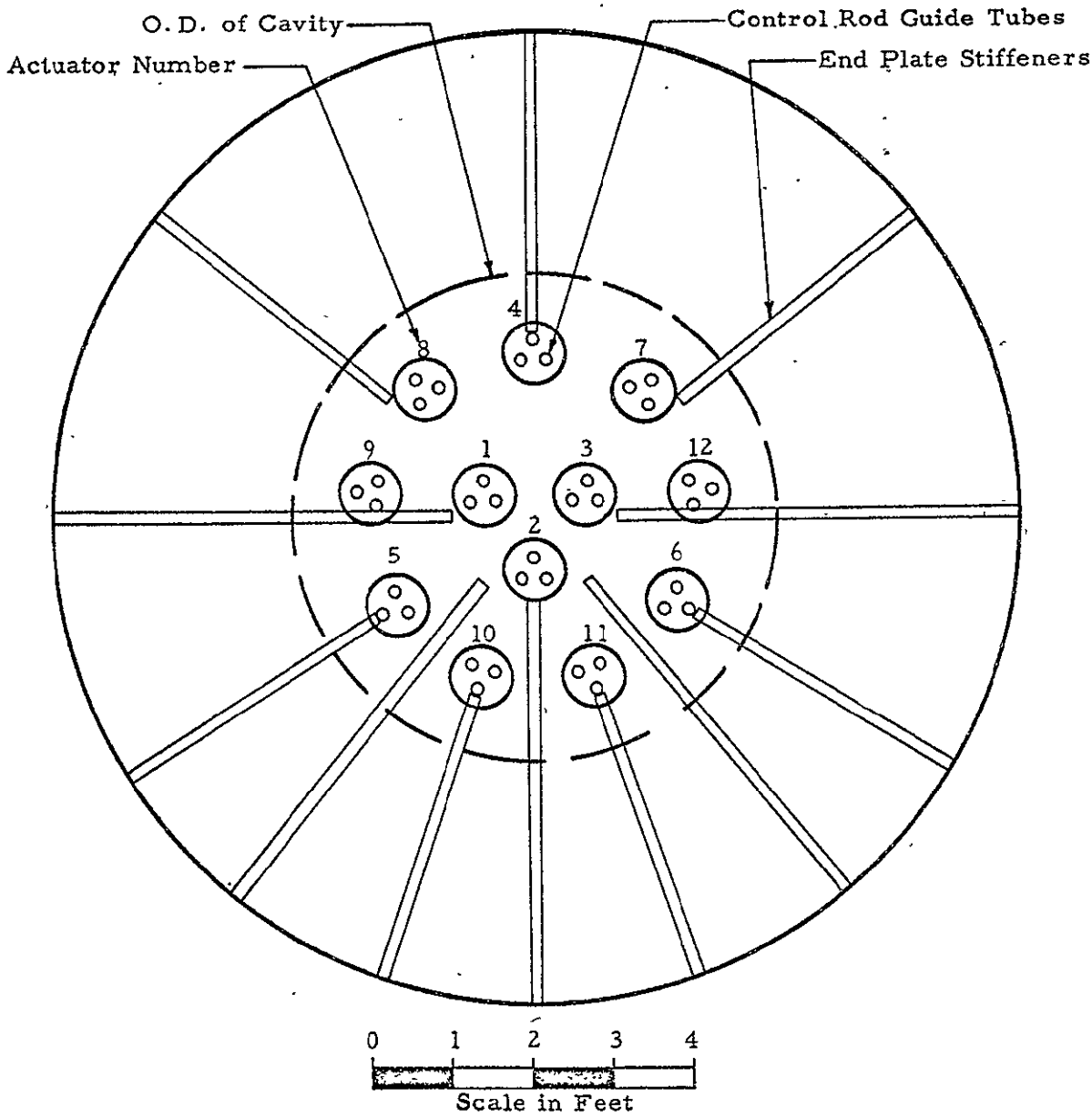

Fig. 3.1 Control rod configuration

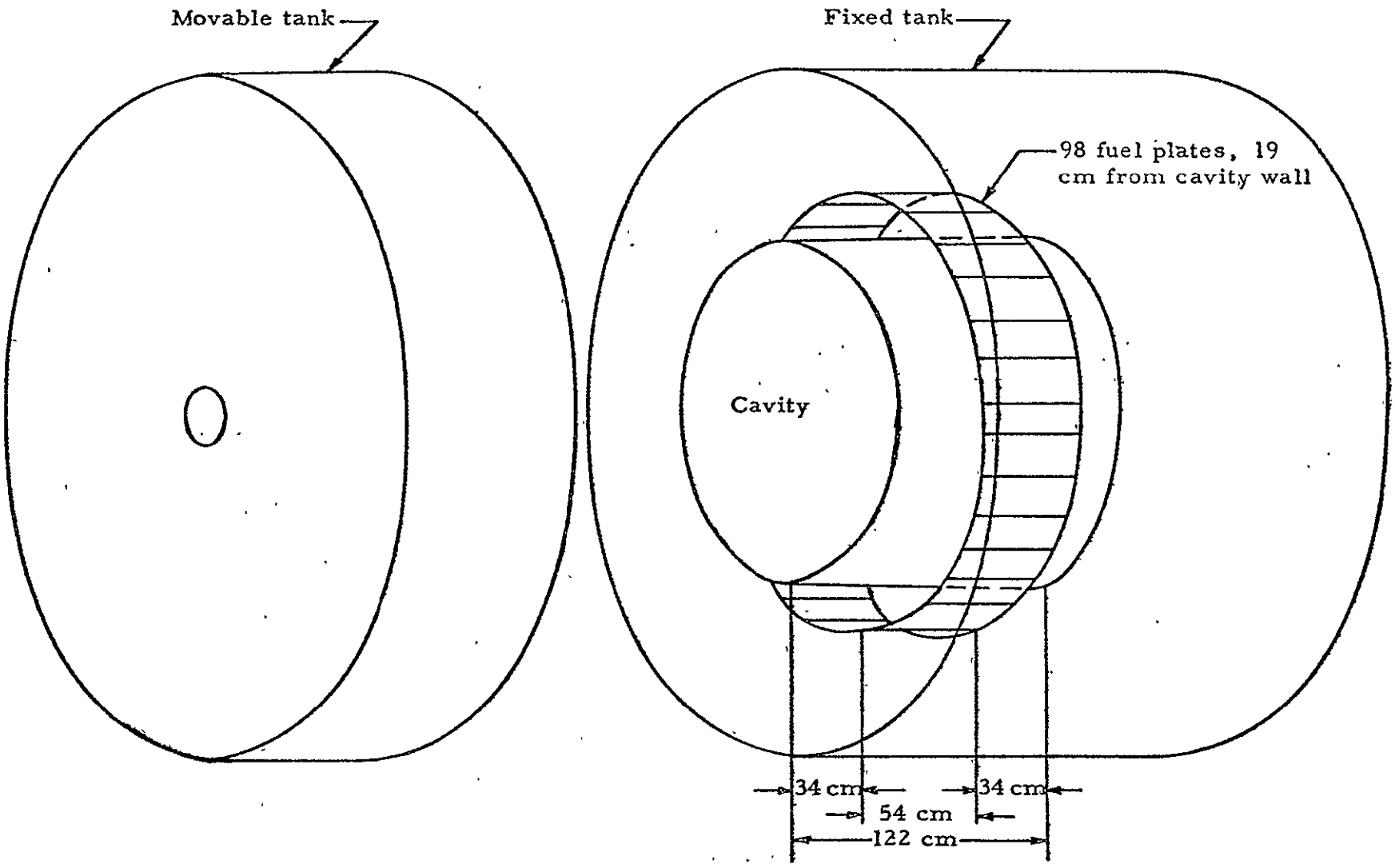

Fig. 3.2 Reflector tank configuration showing booster fuel in the reflector

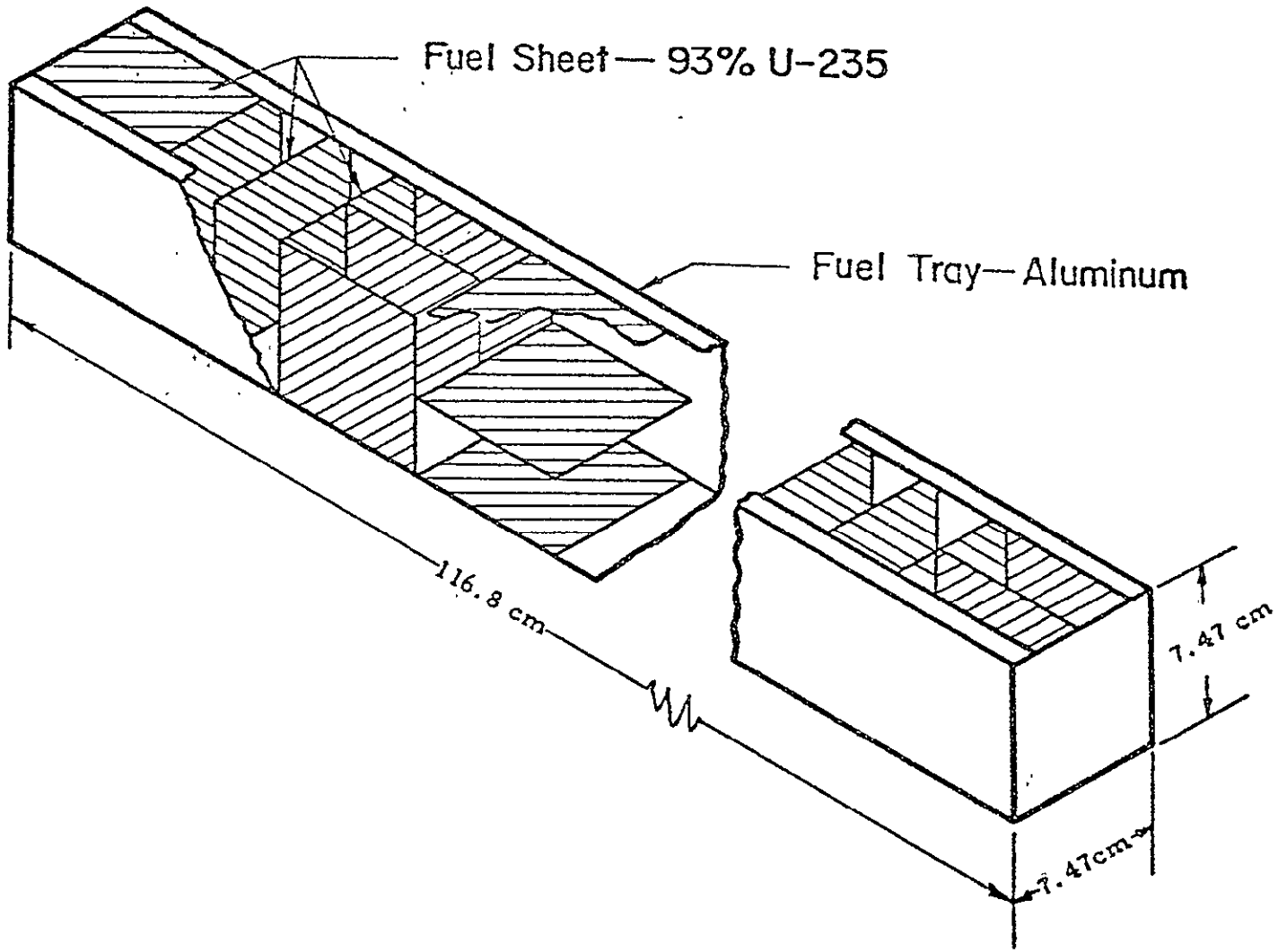

Fig. 3.4 Typical fuel element configuration

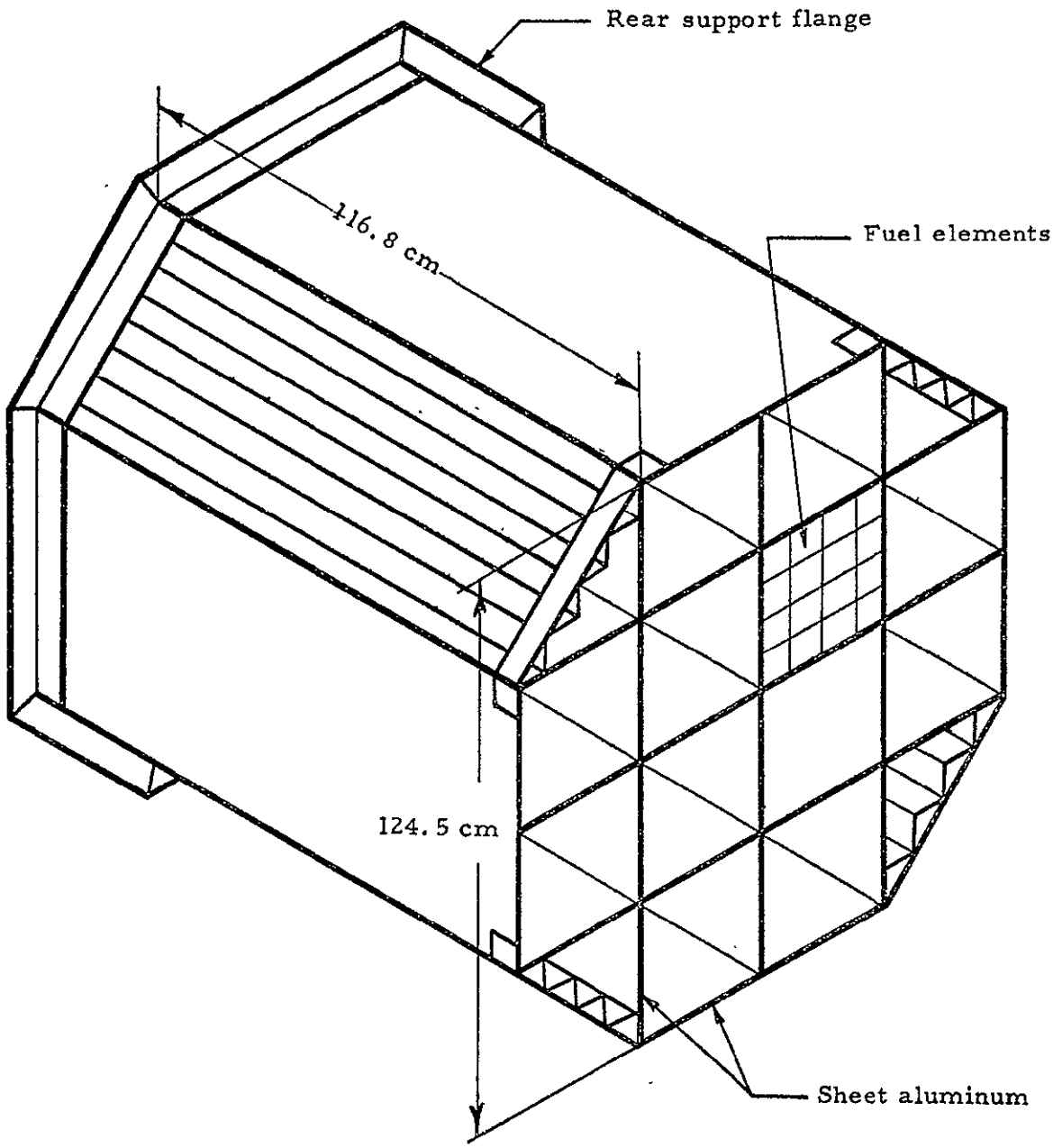

Fig. 3.3 Core support-fuel element structure

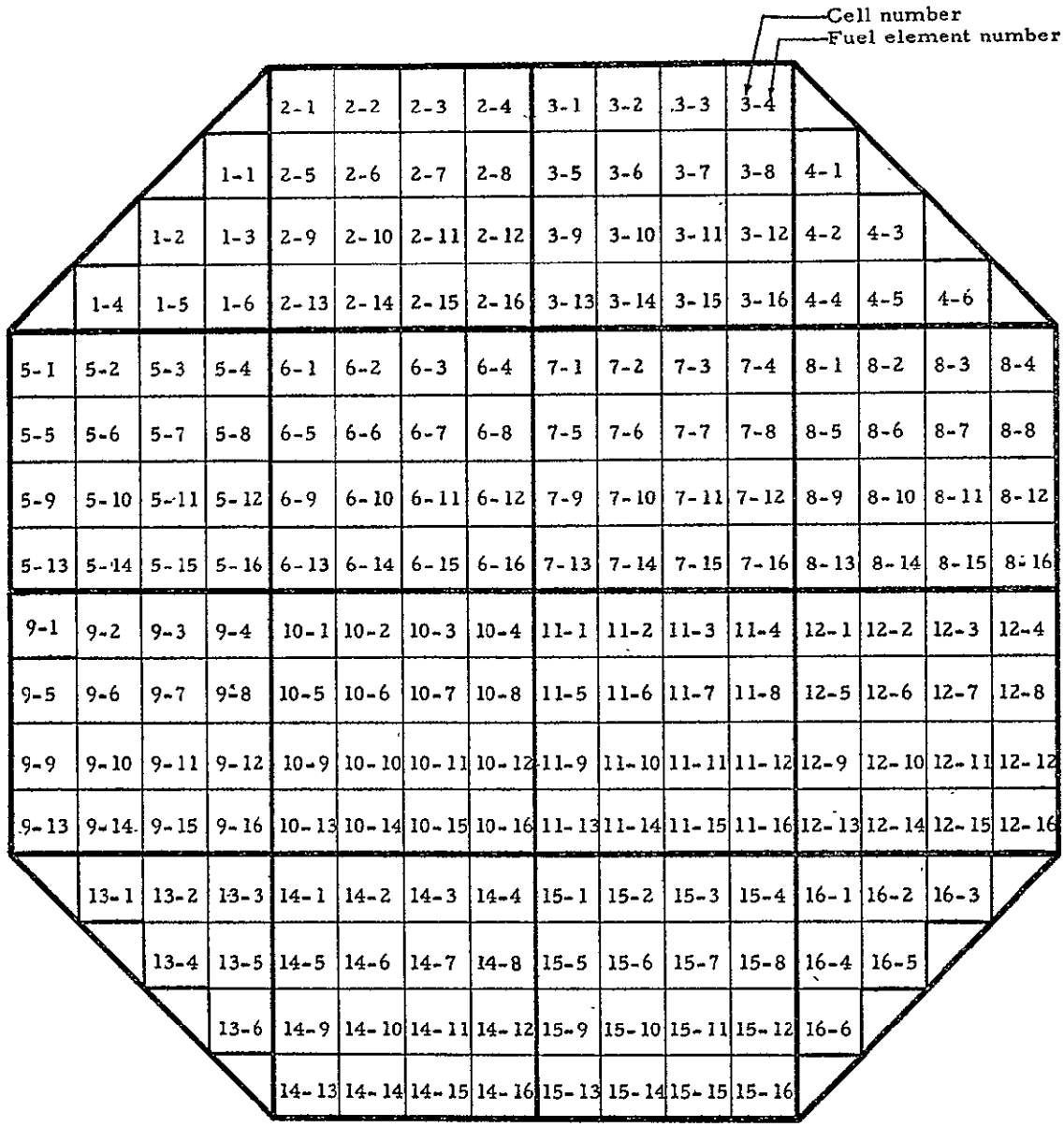

End view facing the fixed table

Fig. 3.5 Numbering scheme for fuel elements

4.0 PRE-WAVE CONFIGURATION

Prior to making the required modifications to the core for the wave experiments, a reactor configuration was assembled to determine the critical mass with the fuel annulus in the radial reflector, the stainless steel liner(83.1 kg, 0.096 cm thick) on the cavity wall, and polyethylene distributed through the region between the active core and cavity wall. It was required that the fuel loading in the active core be around 30 kg of uranium, and in order to keep the critical loading within this limit, the polyethylene concentration was varied. The fuel annulus was placed 19 cm from the wet surface of the cavity wall in the radial reflector and contained 823.2 gm of U-235. The polyethylene was the same structure as used for a previous experiment and is described in Reference 1, p. 82. The base structure contained about 18 kg of polyethylene; however, this weight could be increased by adding tubes of polyethylene to the main structure. In order to properly support the polyethylene structure, 14.7 kg of aluminum structure was used for this purpose.

4.1 Initial Loading

Initial loading began May 1, 1968. The fuel elements were each loaded with 56 size 1.0 fuel sheets. Since there were 16 stages of fuel per fuel element, the average number of sheets per stage was 3.5. Half fuel sheets were not used so the stages contained either 3 or 4 sheets. The elements were loaded so that the odd numbered stages contained 3 sheets of fuel and the even numbered stages contained 4 sheets of fuel or visa versa. The total loading in 208 fuel elements was 11648 sheets of fuel or 30.5 kg of uranium.

The reactor assembly, prior to any modification for the above configuration, contained 23.25 kg of uranium, no polyethylene, the stainless steel liner on the cavity wall. K-excess was 3.543%Δk. Therefore, the major changes to create the new configuration were in the addition of polyethylene and the increase in fuel loading. Polyethylene was added, 20.6 kg was selected, and then the fuel elements were modified in several increments and multiplication data obtained after each step as noted in Table 4.1 and Figure 4.1. The reactor was critical after the core was fully loaded with 30.5 kg of uranium, 20.6 kg of polyethylene, and k-excess was 0.177%Δk.

4.2 Rod Worth Measurements

The reactivity worth of Actuator 5 and Actuator 6 was measured during the course of this experiment. Two separate measurements of Actuator 5 gave a worth of -0.5504±0.0380%Δk and four measurements of Actuator 6 produced an average worth of -0.5541±0.0176%Δk.

4.3 Material Worth Measurements

Prior to the fuel worth measurement, 2.55 kg of polyethylene were removed from the region between the active core and cavity wall

in order to increase k-excess. Measurements were then taken of fuel worth at several radial positions (longitudinal averages) as shown in Table 4.2 and Figure 4.2. The volume weighted average fuel worth was then calculated from this curve, and found to be 0.451%Δk/kg.

Removing the above polyethylene increased k-excess 0.60%Δk which gives a worth of -0.235%Δk of CH_2.

Additional fuel worth measurements were obtained as a function of distance from the end reflector region (Table 4.3) to further verify the values reported in Reference 1, p. 210 (Table 11.3). There were some variations from the earlier data but nothing unusual which would change the distribution of fuel worth vs axial position.

4.4 Power Distribution Measurements

Bare catcher foils were exposed within the cavity and on the fuel annulus to define the power distribution and determine the power fraction in the annulus. The individual foil data are given in Table 4.4. Figure 4.3 shows the relative axial distribution through the cavity. The axial profiles were averaged and these were plotted to give the radial profile as shown in Figure 4.4. The volume weighted average was 2.051 over the active core. The active core power calculates to be 12.8 watts and the annulus power 1.96 watts. A linear extrapolation of the annulus power from 823.2 to 1000 gm of U-235 gives an annulus power of 2.38 watts. The power fraction in a fuel annulus containing 1 kg of U-235 is, therefore, 0.157, where as the ratio of fuel in the annulus to the total fuel loading is 0.034. (The reference value of 1 kg of U-235 in the reflector annulus was adopted in Reference 1.) This power fraction agrees well with the previous results for a light core loading, reported in Reference 1.

A sector of the fuel annulus was then moved to 12 cm from the cavity wall to measure the annulus power fraction at this point. Only bare catcher foils were exposed along the radial centerline of the core and on the sector of fuel annulus which was moved in closer to the cavity. The data are given in Table 4.5. A plot was made of the axial profile at the core center, as shown in Figure 4.5, and the curve average was 1.230 with respect to the core center value.

The core power was calculated to be 14.7 watts, assuming the radial power profile was the same as shown in Figure 4.4, for the fuel annulus of 19 cm. The fuel annulus power was 2.19 watts if containing 1 kg of U-235 which gives a power fraction in the annulus of 0.130. This value is about 10% lower than expected from previous results. These data substantiate the fact that there is a peak in power fraction with the fuel annulus around 19 cm from the wet surface of the cavity wall. A result that had been concluded from earlier measurements (Reference 1, p. 269).

The above power mapping was done with the D_2O temperature at 21°C and Actuator 6 withdrawn from 23.4 cm to 28.1 cm. All other control rods were completely withdrawn.

TABLE 4.1

Inverse Multiplication After Addition of 20.6 kg of Polyethylene to the Cavity Reactor

Increment	No. Fuel Elements Modified	Channel No. 1		Channel No. 2		Channel No. 3		Average	Rod
		CR	CRo/CR	CR	CRo/CR	CR	CRo/CR	CRo/CR	Positions
Base	0	10575	.0757	7047	.0732	8088	.0775	.0755	In
		24250	.0366	16265	.0360	18577	.0387	.0371	Out
1	19	10948	.0731	7413	.0696	8517	.0736	.0721	In
	19	27147	.0327	18488	.0316	20751	.0330	.0330	Out
2	38	11546	.0690	7696	.0667	8980	.0695	.0684	In
2	38	30522	.0289	20724	.0281	23492	.0304	.0291	Out
3	74	13168	.0605	8731	.0588	10054	.0621	.0605	In
3	74	41918	.0211	28693	.0203	32141	.0222	.0212	Out
4	110	14769	.0540	9930	.0517	11481	.0544	.0534	In
4	110	61770	.0143	42054	.0138	46167	.0155	.0145	Out
5	146	16742	.0474	11269	.0453	12822	.0484	.0470	In
5	146	110862	.0079	74525	.0078	80015	.0089	.0082	Out
6	182	19177	.0414	12976	.0394	14738	.0421	.0410	In
6	182	393716	.0022	259010	.0022	262186	.0027	.0024	Out
7	208	21190	.0368	14606	.0344	16467	.0372	.0361	In
7		Reactor critical with k-excess = 0.177%Δk							

TABLE 4.2

Uranium Worth Measurement

Stainless Steel Liner and 18.1 kg Polyethylene in Cavity

Fuel Annulus in Radial Reflector at 19 cm from Cavity Wall

30.5 kg Loading in Core

Run No.	Radial Distance (cm from core center)	Uranium Weight Difference (gm)	Reactivity Change (%Δk)	Uranium Worth (%Δk/kg)
562	5.4	77.37	0.0231	0.299
563	43.5	77.37	0.0323	0.417
565	26.9	77.37	0.0249	0.322
566	50.8	77.37	0.0369	0.477
569	60.2	77.37	0.0563	0.728
570	59.2	77.37	0.0535	0.691
547	63.2	180.30	0.1732	0.930

TABLE 4.3

Fuel Worth in Reflector Region

Fuel Annulus at 19 cm in Radial Reflector

18.1 kg Polyethylene in Cavity

Position		Fuel Weight	Worth of fuel and wand	Worth of wand	Worth/kg U^{235}
Radial (cm)	Axial * (cm)	(gm U^{235})	(%Δk)	(%Δk)	(%Δk)
21.8	81.2	8.54	0.0372	-0.0246	7.24
21.8	73.6	8.54	0.0609	-0.0240	9.94
21.8	58.3	8.54	0.0415	-0.0175	8.07
21.8	27.8	8.54	0.0060	-0.0069	1.51

* From one end of the reactor, that opposite the separation plane. Zero cm is at the outside edge of the end reflector.

TABLE 4.4

Bare Catcher Foil Data

Fuel Annulus 19 cm and 18.1 kg Polyethylene in Core

Foil No.	Location Radial (cm)	Location Axial (cm)	Normalized Counts	Ratio of Local to Core Center (Foil No. X)
Run 1133				
1	0	90.8	51726	2.361
2	0	102.8	30601	1.397
3	0	118.0	28120	1.283
4	0	133.3	24629	1.124
5	0	148.5	21909	1.000 (X)
6	0	163.8	24279	1.108
7	0	179.0	27080	1.236
8	0	194.2	33846	1.545
9	0	206.2	57922	2.644
10	30.5	90.8	53231	2.430
11	30.5	102.8	37722	1.722
12	30.5	118.0	35064	1.600
13	30.5	133.3	33218	1.516
14	30.5	148.5	30816	1.407
15	30.5	163.8	30622	1.398
16	30.5	179.0	33506	1.529
17	30.5	194.2	39581	1.807
18	30.5	206.2	54735	2.498
19	45.7	90.8	59681	2.724
20	45.7	102.8	48659	2.221
21	45.7	118.0	40757	1.860
22	45.7	133.3	42638	1.946
23	45.7	148.5	39043	1.782
24	45.7	163.8	40673	1.856
25	45.7	179.0	41911	1.913
26	45.7	194.2	48964	2.235
27	45.7	206.2	61557	2.810
28	61.0	90.5	80992	3.697
29	61.0	102.8	78254	3.572
30	61.0	118.0	64008	2.922
31	61.0	133.3	65377	2.984
32	61.0	148.5	62746	2.864
33	61.0	163.8	62287	2.843
34	61.0	179.0	63500	2.898
35	61.0	194.2	72999	3.332
36	61.0	206.2	79453	3.626
37	76.2	90.8	127002	5.797
38	76.2	102.8	126436	5.771

TABLE 4.4

(Continued)

Foil No.	Location Radial (cm)	Location Axial (cm)	Normalized Counts	Ratio of Local to Core Center (Foil No. X)
Run 1133 (Cont'd)				
39	76.2	118.0	134866	6.156
40	76.2	133.3	120987	5.522
41	76.2	148.5	126769	5.786
42	76.2	163.8	115409	5.268
43	76.2	179.0	115094	5.253
44	76.2	194.2	111689	5.098
45	76.2	206.2	114874	5.243
46	91.4	90.8	130075	5.937
47	91.4	102.8	127491	5.819
48	91.4	118.0	119282	5.444
49	91.4	133.3	116812	5.332
50	91.4	148.5	117837	5.378
51	91.4	163.8	122029	5.570
52	91.4	179.0	120376	5.494
53	91.4	194.2	121217	5.533
54	91.4	206.2	117047	5.342
55	111.1	128.2	260598	11.894
56	111.7	128.2	242866	11.085
57	111.1	151.1	239959	10.952
58	111.7	151.1	237253	10.829
59	111.1	174.0	216040	9.861
60	111.7	174.0	228128	10.412

TABLE 4.5

Bare Catcher Foil Data

Fuel Annulus 19 cm Except Sector at 12 cm from the Cavity

Wall and 18.1 kg Polyethylene in Core

Foil No.	Location Radial (cm)	Location Axial (cm)	Normalized Counts	Ratio of Local to Core Center (Foil No. X)
Run 1134				
1	0	90.8	50099	1.993
2	0	102.8	33308	1.325
3	0	118.0	27024	1.075
4	0	133.3	26541	1.056
5	0	148.5	25131	1.000 (X)
6	0	163.8	22695	0.903
7	0	179.0	27124	1.079
8	0	194.2	34825	1.386
9	0	206.2	59759	2.378
10		128.2	222130	8.839
11		128.2	245686	9.776
12		151.1	225344	8.967
13		151.1	210028	8.357
14		174.0	212688	8.463
15		174.0	202857	8.072

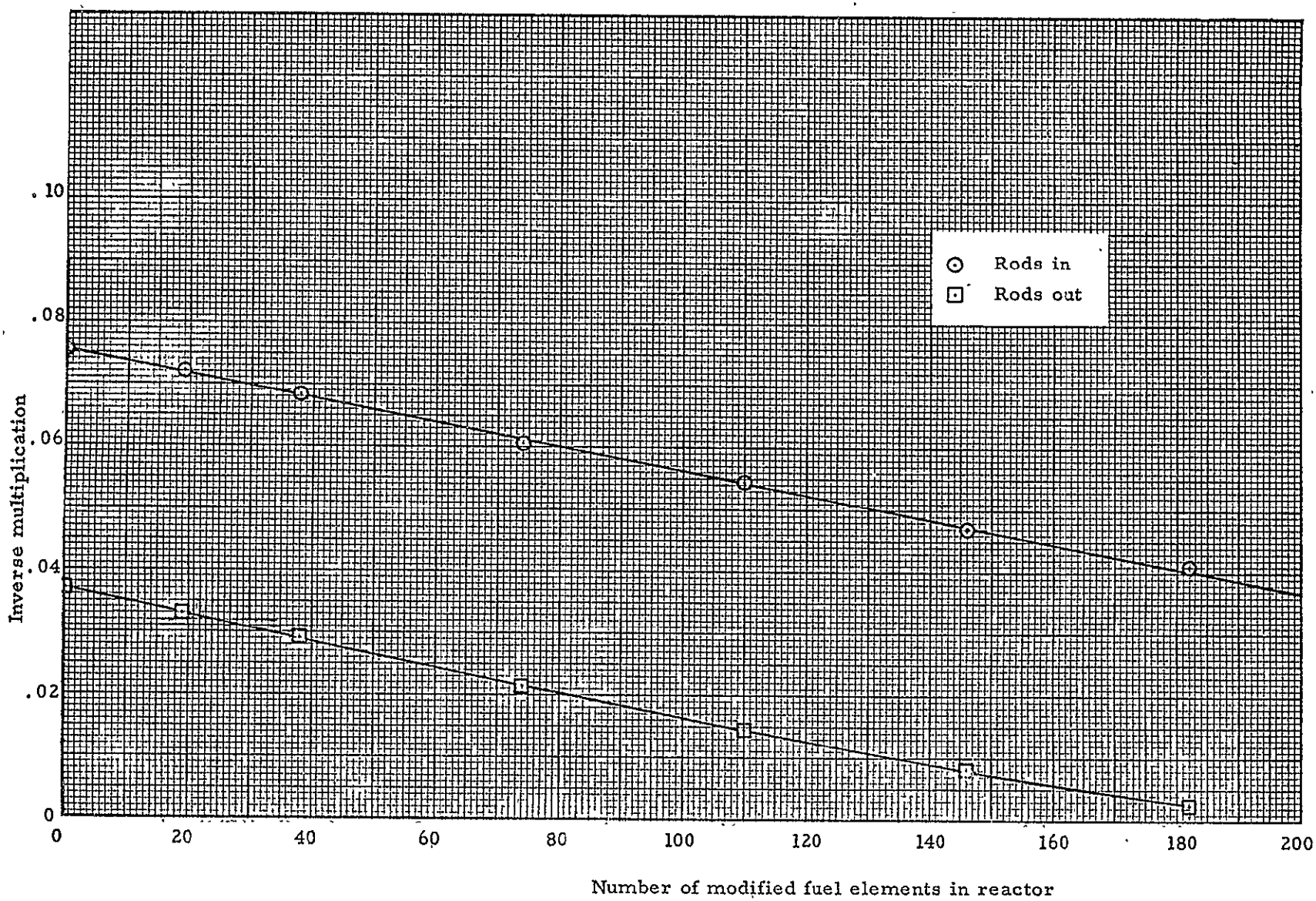

Fig. 4.1 Inverse multiplication curve for base configuration

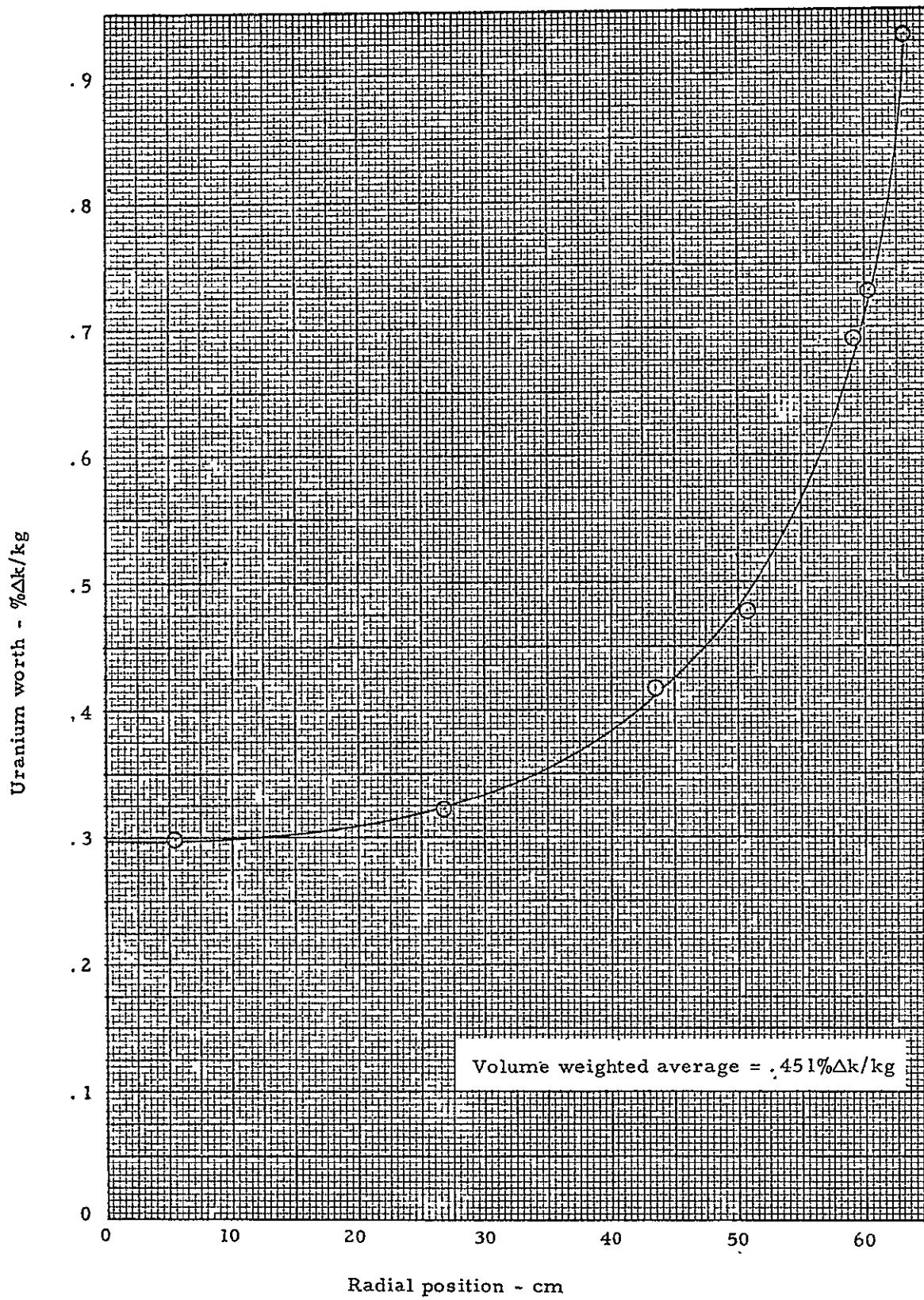

Fig. 4.2 Average uranium worth vs radial position-base configuration

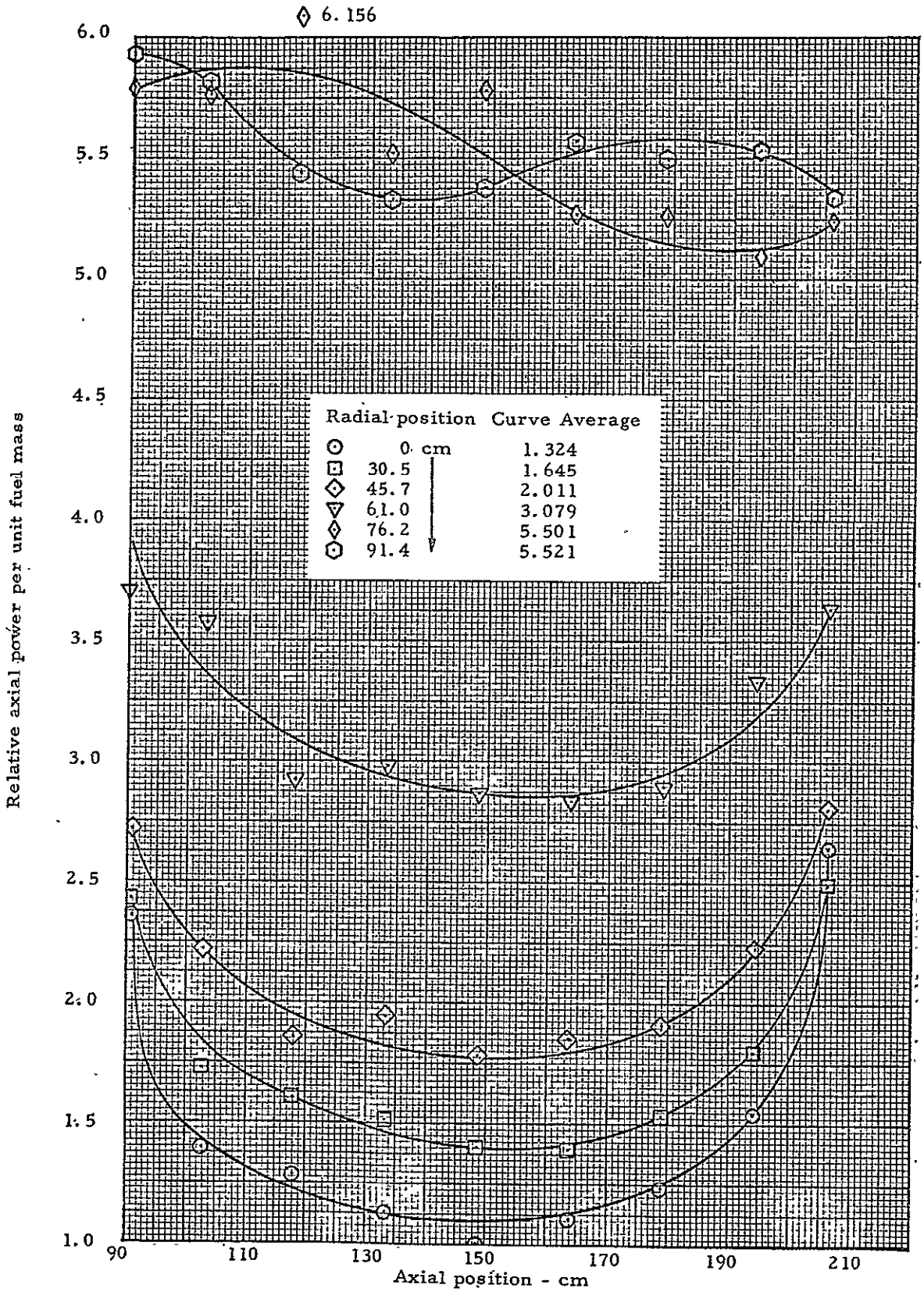

Fig. 4.3 Longitudinal power distribution - base configuration

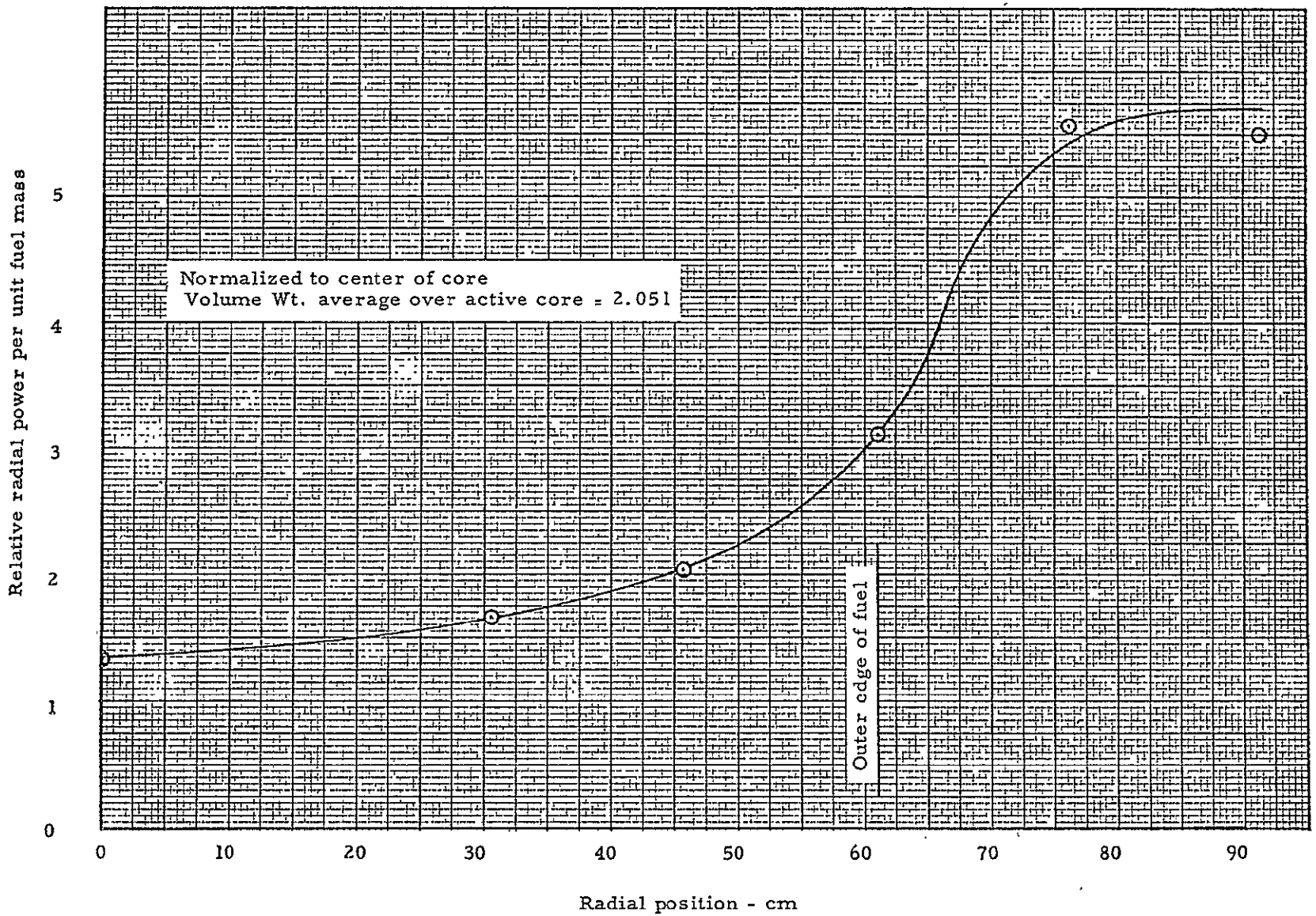

Fig. 4.4 Power distribution (longitudinal average vs radius)

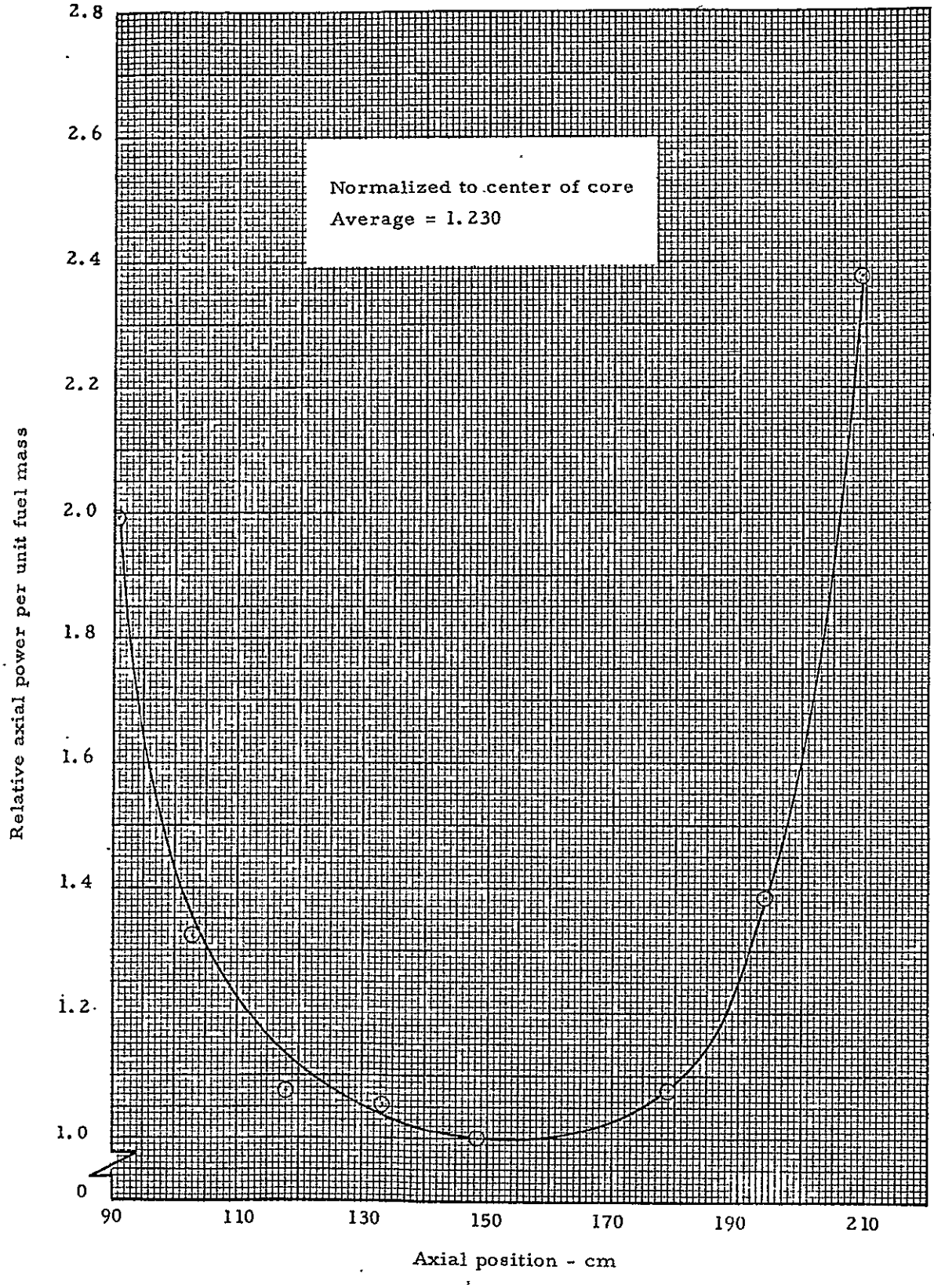

Fig. 4.5 Longitudinal power distribution along axial centerline

5.0 CONFIGURATION 1 (Bare Core For Wave Measurements)

In order to perform the fuel wave experiments, it was necessary to extend the main core structure radially outward. The largest waves to be tested were 21.9 cm square and were to extend beyond the normal active core by this distance. The layout of the new core support structure is shown in Figure 5.1. As will be noted, the cells varied considerably in size outside of the normal active core. It was convenient to re-number the fuel element positions within the cells and the new numbering system is given in Figure 5.2. To specify a particular location in the reactor, two numbers were used, such as 14-12, where the first number was the cell location and the second number was the fuel element position within the cell. The new, expanded core support structure weighed 91.5 kg which is an increase of 37.75 kg of type 1100 aluminum over the original structure (Reference 2, p. 138).

Polyethylene to simulate hydrogen was again required between the core structure and cavity wall. However, now the space in the region between the core structure and the cavity wall was only 8 cm thick. It was decided not to complicate unduly the experimental arrangement. Therefore, the hydrogen simulation (CH_2) was placed only in this annulus by using tubes and sheets of polyethylene to fill the annulus. Initial loading began with 20.6 kg of polyethylene in this annulus.

The 0.096 cm thick stainless steel liner was still on the cavity wall. The total weight in the liner was 83.1 kg distributed over both ends and radial wall of the cavity.

Previous to this reactor assembly, the fuel elements were inserted into the cavity until they butted against the cavity end plate. This placed the center of the fuel elements 2.55 cm off the axial center of the cavity since the cavity was 121.9 cm long and the fuel elements were 116.8 cm long. At this time, however, aluminum spacers were made and inserted at the back of the cavity against the end plate so as to center the fuel elements in the cavity. The spacers weighed 2572 grams.

5.1 Initial Loading

The anticipated fuel loading for this configuration was the same as for the reactor described in Section 4.0 of this report. Two major changes were made in establishing this assembly; (1) the core structure size was increased which increased the aluminum mass in the core 40.3 kg, (2) the polyethylene was moved to the outer 8 cm of the radial wall of the cavity. It was known from earlier measurements that polyethylene has about twice the negative reactivity effect when against the active core as when near the cavity wall. Therefore, the effects of adding the extra aluminum in the support structure and moving the polyethylene nearer to the cavity wall were expected to cancel each other, approximately. Prior to loading the core, the 20.6 kg of polyethylene were placed in the outer 8 cm of the cavity and all the additional aluminum core support structure and rear spacers were installed.

The fuel element loading was unchanged from the 56 sheets per element described in Section 4.1. The first increment placed in the core was 104 elements or one-half of the anticipated critical mass of 30.5 kg of uranium. The loading proceeded, as shown in Table 5.1 and Figure 5.3, until 182 elements (26.7 kg of uranium) were in the reactor at which point the reactor was critical with 0.0835%Δk excess reactivity. It was obvious that k-excess would be greater than the allowable operation limit if all 208 fuel elements were added to the reactor without reducing the fuel density or otherwise compensating for the reactivity. It was decided to increase the polyethylene mass so an additional 7.26 kg were placed in the annulus between the core structure and cavity wall, bringing the total to 27.86 kg. The fuel loading was increased to 198 fuel elements or 29.1 kg and again the reactor was critical and k-excess was 0.526%Δk. An additional 7.04 kg of polyethylene were then placed in the cavity, making a total of 34.9 kg (all distributed in the outer 8 cm thick annulus) and the remaining fuel elements were added.. With 30.5 kg of uranium in the core, k-excess was 0.179%Δk.

5.2 Rod Worth Measurements

A single measurement of the worth of Actuator 6 gave -0.515%Δk and the worth of Actuators 3 and 6 together was -1.254%Δk, also a single measurement. These data were obtained while completing the fuel loading after the reactor was a critical assembly. There were no other reactivity measurements with this reactor assembly until the wave tests were started.

5.3 Power Distribution

5.3.1 Bare Catcher Foil Data

The catcher foil data, both bare and cadmium covered, are contained in Table 5.2. Axial power distribution profiles were measured at several radial positions within the cavity as shown in Figure 5.4. The axial averages were then plotted to show the radial profile as seen in Figure 5.5. The volume weight average power density (obtained from the composite radial distribution) over the active core was 1.786 with respect to the foil at the center of the core. It will be noted from the radial distribution curve that the polyethylene (CH_2) has an appreciable effect on the curve, as there was a significant attenuation through this material.

The power for both the active core and the fuel annulus was calculated from the bare foil data and it was determined that the active core generated 13.2 watts and the annulus 2.06 watts. The annulus contained 823.2 gm of U^{235}. When referenced to 1 kg of U^{235}, the annulus power to total reactor power fraction was 0.161. This compares to 0.157 reported in Section 4.4 of this report with the fuel annulus at the same position, and the same fuel mass ratio between the annulus and the core.

Except for Run 1135 all foil exposures were made with Actuators 4, 5, and 6 equally withdrawn about 26 cm with the remaining rods in the fully withdrawn position. Run 1135 had Actuators 3 and 6 equally withdrawn 22.4 cm and the other rods fully withdrawn. The D_2O temperature averaged near 21°C during all the measurements.

5.3.2 Catcher Foil Cadmium Ratios

Sufficient cadmium covered foils were exposed to generate an axial distribution through the radial center and a radial profile through axial center of the core. The cadmium ratios are given at the bottom of Table 5.2, and the plotted distributions are presented in Figures 5.6 and 5.7. The high value at the separation plane in Figure 5.6 is due to the "exhaust" hole in the center of the end reflector (movable table). Figure 5.7 shows a considerable hardening of the fission spectrum across the polyethylene since the cadmium ratio decreases from 33.5 to 19.4 in crossing this annulus toward the center of the reactor.

5.4 Resonance Detector Data

5.4.1 Bare Gold Foils

Extensive mapping was performed with 0.0005 cm thick gold foils both in the cavity and reflector regions and the results are given in Table 5.3. All of the gold foil data are contained in this table including both bare and cadmium covered foils. All of the gold foil activities were power normalized to Run 1135 by using the counts from the power normalizer foils as shown in Table 5.4. There were scrams near the middle of Runs 1140 and 1142, and therefore, the normalization factors for these runs are more uncertain than for the other runs. On Run 1142, some of the foil positions were repeated and these were used to determine the normalization factor. No such repeat data were available on Run 1140, and catcher foil activity had to be interpolated for the effective length of the shortened run.

Within the cavity region, several axial profiles were measured with the bare gold foils across the core radius as shown in Figure 5.8. The data were normalized to the core center as was done with the bare catcher foils. The curves were averaged and the averages were plotted as a radial profile in Figure 5.9. The volume weighted average over the active core was then detetermined to be 1.314 of the value at the core center.

The profiles within the radial and end reflectors are shown in Figures 5.10 and 5.11, respectively. Run 1135 was performed with Actuators 3 and 6 equally withdrawn about 22 cm. Actuator 3 is next to the center hole in the end reflector where the measurements are taken and this caused some attenuation of the flux in the end reflector as noted in Figure 5.11. The rod pattern was changed on subsequent runs so that Actuators 1, 2, and 3 were fully withdrawn and Actuators 4, 5, and 6 were about 26 cm withdrawn. The radial reflector shows a slightly higher bare gold foil activity which is normal with the fuel annulus in the radial reflector.

5.4.2 Gold Foil Cadmium Ratios

Where both bare and cadmium covered gold foil activities were available, cadmium ratios were calculated. The foil data were first reduced to infinitely dilute activities as described in Reference 2, p. 49,50. The values thus calculated are given in Table 5.5. The axial and radial

distributions in the cavity are shown in Figure 5.12 and 5.13, respectively. There were some cadmium ratio data which were obviously bad so repeat measurements were obtained. These points can be observed in the two figures where double points appear. In general, however, the data appeared to be consistent within the typical experimental error of about ±5%. At the core center, the infinitely dilute cadmium ratio was about 1.2 and this increased to 1.7 at the outer edge of the fuel along the axial centerline of the core. The big change occurred over the polyethylene annulus, where the cadmium ratio increased from around 1.7 on the inner surface to 2.3 on the outer surface of the polyethylene. This material acts as a flux trap which not only absorbs neutrons but reflects the neutrons back into the reflector thus causing a significant attenuation in the number of low energy neutrons reaching the active core.

The cadmium ratios in the radial and end reflectors are shown in Figure 5.14. The crossover in the two curves around 20 cm from the cavity wall is caused by the high concentration of polyethylene near the cavity wall and the fuel annulus in the reflector. The polyethylene enhances the thermal neutrons in the radial reflector near the cavity wall and the production of fission neutrons in the fuel annulus increases the epi-thermal neutrons level between the annulus and outer regions of the reflector.

5.5 Thermal Neutron Flux

The thermal neutron flux is readily calculated from those locations where both bare and cadmium covered gold foil data are available. The standard equations given in Reference 3, p. 69 were used. The thermal cross section used for gold was 98.8 barns. The resulting flux values per watt of active core power are given in Table 5.6. The active core power for Run 1135, the foil exposure run to which subsequent runs were normalized, was 13.2 watts. The thermal flux distribution within the active core is shown in Figure 5.15. The thermal flux at the core center is about 0.4×10^6 n/cm^2/sec/watt. This increases to approximately 1.4×10^6 n/cm^2/sec/watt at the outer edge of the fuel along the axial centerline of the core. Although there is some data scatter noted in Figure 5.15, the points generally fall on a smooth curve within 10% or less.

Figures 5.16 and 5.17 show the thermal flux distributions radially and axially through the core and reflector regions. Only the data through the axial or radial centerline are plotted. The composite two dimensional effects are shown in Figure 5.15. It will be noted from this figure that the point at an axial position of 151.1 cm (midplane) and a radial position of 30.5 cm was about 50% low. Another point in Figure 5.16 which appears to be in error is at a 84.5 cm. This is apparently 50% too high when compared to the center foil on the axial profile at a radial position of 84.5 cm given in Figure 5.15. It appears from the smooth curve that this point should have been around 2.3 rather than near 2.9.

TABLE 5.1

Inverse Multiplication for Initial Loading of Configuration 1

Increment	Number Elements in Core	Channel No. 1 CR	Channel No. 1 CRo/CR	Channel No. 2 CR	Channel No. 2 CRo/CR	Channel No. 3 CR	Channel No. 3 CRo/CR	Average	Rod Positions
0	0	658	1.000	466	1.000	545	1.000	1.000	In
0	0	722	1.000	529	1.000	606	1.000	1.000	Out
1	104	5055	0.130	3792	0.123	4287	0.127	0.127	In
1	104	7422	0.097	5451	0.097	6174	0.098	0.097	Out
2	134	8102	0.081	5960	0.078	6808	0.080	0.080	In
2	134	14470	0.050	10633	0.050	12063	0.050	0.050	Out
3	161	14353	0.046	10499	0.044	11800	0.046	0.045	In
3	161	44557	0.016	33165	0.016	36522	0.017	0.016	Out
4	182	23313	0.028	17014	0.027	19128	0.028	0.028	In
4	182	Critical with 0.0835%Δk k-excess							
		Added 7.26 kg polyethylene to core							
5	182	17529	0.0375	12007	0.0388	13734	0.0397	0.0387	In
5	182	81097	0.0089	55380	0.0096	60281	0.0101	0.0095	Out
6	192	22901	0.0287	15869	0.0294	17782	0.0306	0.0296	In
6	192	817485	0.0009	531680	0.0010	539272	0.0011	0.0010	Out
7	198	28581	0.0230	19755	0.0236	21772	0.0250	0.0239	In
7	198	Critical with 0.5257%Δk k-excess							

TABLE 5.2

Catcher Foil Data

Configuration 1 (Base Configuration for Wave Experiments)

Foil No.	Type	Location Radial (cm)	Location Axial (cm)	Normalized Count	Local to Foil (X)
Run 1135					
1	Bare	0	93.3	49264	1.890
2	Bare	0	105.3	32461	1.245
3	Bare	0	120.6	37808	1.067
4	Bare	0	135.8	25658	0.984
5	Bare	0	151.1	26066	1.000 (X)
6	Bare	0	166.3	23942	0.918
7	Bare	0	181.5	30182	1.158
8	Bare	0	196.8	38942	1.494
9	Bare	0	208.8	62541	2.399
10	Bare	30.5	93.3	56558	2.170
11	Bare	30.5	105.3	36658	1.406
12	Bare	30.5	120.6	35854	1.375
13	Bare	30.5	135.8	31390	1.204
14	Bare	30.5	151.1	32042	1.229
15	Bare	30.5	166.3	30618	1.175
16	Bare	30.5	181.5	35877	1.376
17	Bare	30.5	196.8	40914	1.569
18	Bare	30.5	208.8	52632	2.019
19	Bare	45.7	93.3	62376	2.393
20	Bare	45.7	105.3	54006	2.072
21	Bare	45.7	120.6	40386	1.549
22	Bare	45.7	135.8	40088	1.538
23	Bare	45.7	151.1	40843	1.567
24	Bare	45.7	166.3	44579	1.710
25	Bare	45.7	181.5	37123	1.424
26	Bare	45.7	196.8	47319	1.815
27	Bare	45.7	208.8	59746	2.292
28	Bare	61.0	93.3	80016	3.069
29	Bare	61.0	105.3	74015	2.839
30	Bare	61.0	120.6	76254	2.925
31	Bare	61.0	135.8	71852	2.756
32	Bare	61.0	151.1	71394	2.739
33	Bare	61.0	166.3	72312	2.774
34	Bare	61.0	181.5	70386	2.700
35	Bare	61.0	196.8	80047	3.071
36	Bare	61.0	208.8	85264	3.271
37	Bare	84.5	93.3	113968	4.372
38	Bare	84.5	105.3	109507	4.201
39	Bare	84.5	120.6	101905	3.909

TABLE 5.2

(Continued)

Foil No.	Type	Location Radial (cm)	Axial (cm)	Normalized Count	Local to Foil (X)
Run 1135 (Cont'd)					
40	Bare	84.5	135.8	104426	4.006
41	Bare	84.5	151.1	99059	3.800
42	Bare	84.5	166.3	96801	3.713
43	Bare	84.5	181.5	97252	3.731
44	Bare	84.5	196.8	93222	3.576
45	Bare	84.5	208.8	108629	4.167
46	Bare	90.8	93.3	139341	5.345
47	Bare	90.8	105.3	148704	5.704
48	Bare	90.8	120.6	166332	6.380
49	Bare	90.8	135.8	165873	6.363
50	Bare	90.8	151.1	169934	6.519
51	Bare	90.8	166.3	152638	5.855
52	Bare	90.8	181.5	149464	5.733
53	Bare	90.8	196.8	129870	4.982
54	Bare	90.8	208.8	112070	4.299
55	Bare	111.1	128.2	270901	10.39
56	Bare	111.7	128.2	259087	9.939
57	Bare	111.1	151.1	254534	9.764
58	Bare	111.7	151.1	238363	9.144
59	Bare	111.1	174.0	238258	9.140
60	Bare	111.7	174.0	239890	9.202
Run 1140					Cd Ratio
1	Cd	0	93.3	4798	10.268
2	Cd	0	120.6	4013	6.929
3	Cd	0	151.1	3345	7.793
4	Cd	0	181.5	3679	8.204
5	Cd	0	208.8	3789	16.506
Run 1141					
1	Cd	30.5	151.1	4247	7.545
2	Cd	61.0	151.1	4805	14.858
3	Cd	84.5	151.1	5104	19.408
4	Cd	90.8	151.1	5069	33.524

TABLE 5.3

Gold Foil Data - (0.0005 cm thick)

Configuration 1 (Base Configuration for Wave Experiments)

Foil No.	Foil Type	Location Radial (cm)	Location Axial (cm)	Foil Weight (gm)	Specific Activity d/cm/gm x 10^{-6}	Local to Foil (X)
Run 1135						
1	Bare	0	89.4	0.0184	2.681	
2	Bare	0	74.9	0.0163	5.694	
3	Bare	0	59.6	0.0184	4.480	
4	Bare	0	44.4	0.0192	2.964	
5	Bare	0	29.1	0.0174	1.723	
6	Bare	0	13.9	0.0166	0.805	
7	Bare	0	0	0.0179	0.136	
8	Bare	93.2	151.1	0.0184	5.049	
9	Bare	107.7	151.1	0.0178	6.234	
10	Bare	123.0	151.1	0.0168	5.205	
11	Bare	138.2	151.1	0.0166	3.531	
12	Bare	153.5	151.1	0.0155	2.038	
13	Bare	168.7	151.1	0.0153	0.877	
14	Bare	183.9	151.1	0.0203	0.121	
Run 1136						
1	Bare	0	93.3	0.0162	2.434	1.559
2	Bare	0	105.3	0.0147	2.029	1.300
3	Bare	0	120.6	0.0147	1.590	1.019
4	Bare	0	135.8	0.0164	1.561	1.000
5	Bare	0	151.1	0.0161	1.561	1.000 (X)
6	Bare	0	166.3	0.0147	1.620	1.038
7	Bare	0	181.5	0.0156	1.691	1.083
8	Bare	0	196.8	0.0146	1.807	1.158
9	Bare	0	208.8	0.0137	2.313	1.482
10	Bare	30.5	93.3	0.0164	2.305	1.477
11	Bare	30.5	105.3	0.0178	1.880	1.204
12	Bare	30.5	120.6	0.0172	1.824	1.168
13	Bare	30.5	135.8	0.0162	1.749	1.120
14	Bare	30.5	151.1	0.01555	1.739	1.114
15	Bare	30.5	166.3	0.0145	1.825	1.169
16	Bare	30.5	181.5	0.0202	1.705	1.092
17	Bare	30.5	196.8	0.01935	1.854	1.188
18	Bare	30.5	208.8	0.0187	2.247	1.439
19	Bare	45.7	93.3	0.0175	2.267	1.452
20	Bare	45.7	105.3	0.0166	2.155	1.381

TABLE 5.3

(Continued)

Foil No.	Foil Type	Location Radial (cm)	Location Axial (cm)	Foil Weight (gm)	Specific Activity d/cm/gm x 10^{-6}	Local to Foil (X)
Run 1136 (Cont'd)						
21	Bare	45.7	120.6	0.0169	1.975	1.265
22	Bare	45.7	135.8	0.0170	1.988	1.274
23	Bare	45.7	151.1	0.0178	1.954	1.252
24	Bare	45.7	166.3	0.0178	1.719	1.101
25	Bare	45.7	181.5	0.0200	1.897	1.215
26	Bare	45.7	196.8	0.0216	2.017	1.292
27	Bare	45.7	208.8	0.0197	2.327	1.491
28	Bare	61.0	93.3	0.0160	2.890	1.851
29	Bare	61.0	105.3	0.0166	2.778	1.780
30	Bare	61.0	120.6	0.0206	2.632	1.686
31	Bare	61.0	135.8	0.0162	2.717	1.741
32	Bare	61.0	151.1	0.0143	2.573	1.648
33	Bare	61.0	166.3	0.0200	2.536	1.625
34	Bare	61.0	181.5	0.0183	2.559	1.639
35	Bare	61.0	196.8	0.0171	2.593	1.661
36	Bare	61.0	208.8	0.0159	2.757	1.766
37	Bare	84.5	93.3	0.0151	3.322	2.128
38	Bare	84.5	105.3	0.0186	3.198	2.049
39	Bare	84.5	120.6	0.0145	3.272	2.096
40	Bare	84.5	135.8	0.0171	3.202	2.051
41	Bare	84.5	151.1	0.0176	3.245	2.079
42	Bare	84.5	166.3	0.0160	3.257	2.086
43	Bare	84.5	181.5	0.0182	3.200	2.050
44	Bare	84.5	196.8	0.0161	3.132	2.006
45	Bare	84.5	208.8	0.0170	2.962	1.897
46	Bare	87.6	93.3	0.0163	3.500	2.242
47	Bare	87.6	105.3	0.0182	3.475	2.226
48	Bare	87.6	120.6	0.0154	3.703	2.372
49	Bare	87.6	135.8	0.0153	3.679	2.357
50	Bare	87.6	151.1	0.0158	3.690	2.364
51	Bare	87.6	166.3	0.0142	3.630	2.325
52	Bare	87.6	181.5	0.0200	3.566	2.284
53	Bare	87.6	196.8	0.0193	3.293	2.110
54	Bare	87.6	208.8	0.0171	3.150	2.018
55	Bare	90.8	93.3	0.0163	3.758	2.407
56	Bare	90.8	105.3	0.0177	4.103	2.628
57	Bare	90.8	120.6	0.0143	4.493	2.878
58	Bare	90.8	135.8	0.0155	4.437	2.842
59	Bare	90.8	151.1	0.0134	4.664	2.988

TABLE 5.3

(Continued)

Foil No.	Foil Type	Location Radial (cm)	Location Axial (cm)	Foil Weight (gm)	Specific Activity d/m/gm x 10^{-6}	Local to Foil (X)
Run 1136 (Cont'd)						
60	Bare	90.8	166.3	0.0171	4.390	2.812
61	Bare	90.8	181.5	0.0177	4.306	2.758
62	Bare	90.8	196.8	0.0152	4.061	2.602
63	Bare	90.8	208.8	0.0202	3.066	1.964
64	Cd	0	59.6	0.0198	0.301	--
65	Cd	0	29.1	0.0147	0.0048	--
66	Cd	123.0	151.1	0.0163	0.429	--
67	Cd	153.5	151.1	0.0204	0.0095	--
Run 1137						
1	Cd	0	93.3	0.0177	1.291	
2	Cd	0	120.6	0.0194	1.164	
3	Cd	0	151.1	0.0156	1.154	
4	Cd	0	181.5	0.0194	1.152	
5	Cd	0	208.8	0.0165	1.192	
6	Cd	61.0	93.3	0.0161	1.362	
7	Cd	61.0	151.1	0.0154	1.411	
8	Cd	61.0	208.8	0.0156	1.363	
9	Cd	87.6	120.6	0.0206	1.404	
10	Cd	87.6	181.5	0.0163	1.538	
11	Bare	100.1	151.1	0.01965	6.235	
12	Bare	115.4	151.1	0.0175	5.523	
13	Bare	130.6	151.1	0.01965	4.177	
14	Bare	0	52.0	0.0141	4.301	
15	Bare	0	67.2	0.0159	5.755	
16	Bare	0	82.5	0.0199	3.634	
Run 1138						
1	Cd	0	44.4	0.0188	0.0447	
2	Cd	0	89.4	0.0171	1.427	
3	Cd	107.7	151.1	0.0193	1.148	
4	Cd	138.2	151.1	0.0161	0.0761	
5	Cd	30.5	93.3	0.01835	1.285	
6	Cd	30.5	120.6	0.0158	1.249	
7	Cd	30.5	151.1	0.0135	1.617	
8	Cd	30.5	181.5	0.0178	1.221	
9	Cd	30.5	208.8	0.0160	1.356	
10	Cd	61.0	120.6	0.0193	1.288	

TABLE 5.3

(Continued)

Foil No.	Foil Type	Location Radial (cm)	Location Axial (cm)	Foil Weight (gm)	Specific Activity d/m/gm x 10^{-6}	Local to Foil (X)
Run 1138 (Cont'd)						
11	Cd	61.0	181.5	0.0211	1.233	
12	Cd	87.6	93.3	0.0187	1.186	
13	Cd	87.6	151.1	0.0164	1.606	
14	Cd	87.6	208.8	0.0180	1.172	
Run 1139						
1	Cd	0	74.9	0.0179	1.398	
2	Cd	93.2	151.1	0.0221	1.378	
3	Cd	45.7	93.3	0.0221	1.203	
4	Cd	45.7	120.6	0.0212	1.183	
5	Cd	45.7	151.1	0.0169	1.245	
6	Cd	45.7	181.5	0.0205	1.189	
7	Cd	45.7	208.8	0.0164	1.366	
8	Cd	84.5	93.3	0.0153	1.266	
9	Cd	84.5	151.1	0.0184	1.416	
10	Cd	84.5	208.8	0.0183	1.230	
11	Cd	90.8	120.6	0.0167	1.545	
12	Cd	90.8	181.5	0.0189	1.436	
Run 1140						
1	Cd	84.5	120.6	0.0182	1.232	
2	Cd	84.5	181.5	0.0173	1.235	
3	Cd	90.8	93.3	0.0190	1.005	
4	Cd	90.8	151.1	0.0178	1.337	
5	Cd	90.8	208.8	0.0173	1.020	
Run 1141						
1	Bare	0	0	0.0161	0.162	
2	Bare	0	13.9	0.0160	1.104	
3	Bare	0	29.1	0.0164	2.203	
4	Bare	0	44.4	0.0193	3.463	
5	Bare	0	59.6	0.0152	5.110	
6	Bare	0	74.9	0.0157	5.907	
7	Bare	0	89.4	0.0159	2.727	

TABLE 5.3

(Continued)

Foil No.	Foil Type	Location Radial (cm)	Location Axial (cm)	Foil Weight (gm)	Specific Activity d/m/gm x 10^{-6}	Local to Foil (X)
Run 1142						
1	Cd	0	120.6	0.0210	1.123	
2	Cd	0	151.1	0.0186	1.141	
3	Cd	0	181.5	0.0172	1.182	
4	Cd	0	208.8	0.0187	1.202	
5	Cd	30.5	151.1	0.0142	1.257	
6	Cd	84.5	151.1	0.0199	1.417	
7	Cd	90.8	120.6	0.0194	1.426	
8	Cd	90.8	151.1	0.0207	1.477	
9	Bare	90.8	208.8	0.0198	3.198	
10	Bare	0	89.4	0.0169	2.636	
11	Bare	0	82.5	0.0161	4.927	
12	Bare	0	74.9	0.0125	5.756	
13	Bare	0	67.2	0.0149	5.438	
14	Bare	0	59.6	0.0167	4.887	
15	Bare	0	52.0	0.0150	4.164	
16	Bare	93.2	151.1	0.01695	5.029	
17	Bare	100.1	151.1	0.0194	6.167	
18	Bare	107.7	151.1	0.0216	6.075	
19	Bare	115.4	151.1	0.0163	5.809	
20	Bare	123.0	151.1	0.0213	5.099	
21	Bare	130.6	151.1	0.0161	4.322	

TABLE 5.4

Power Normalization Factors

Run No.	Count Time	Decay Time (min)	Decay Factor	Activity (cpm)	Corrected Activity (cpm)	Normalization Factor
1135	1450.88	43.50	0.852	295633	251879	
	1452.88	45.50	0.897	281195	252232	
	1454.88	47.50	0.942	267076	251586	
					251899	1.000
1136	1409.10	49.31	0.984	256946	252835	
	1411.30	51.51	1.035	244169	252715	
	1413.60	53.81	1.091	231962	253071	
					252874	0.996
1137	1605.60	23.47	0.460	560838	257985	
	1607.53	25.40	0.494	522755	258241	
	1609.35	27.22	0.527	489541	257988	
					258071	0.976
1138	1044.44	44.48	0.874	290413	253821	
	1046.32	46.36	0.916	277987	254636	
	1048.30	48.34	0.960	264952	254354	
					254270	0.991
1139	1241.73	39.96	0.777	329133	255736	
	1243.59	41.82	0.815	312248	254482	
	1245.56	43.79	0.858	294150	252381	
					254200	0.991
1140	1506.00	67.901	1.565	193099	302200	
	1507.81	69.711	1.612	186441	300543	
	1509.80	71.701	1.663	179360	298276	
					300340	0.839
1141	1631.89	22.68	0.447	569223	254443	
	1623.80	24.59	0.480	531229	254990	
	1635.55	26.34	0.511	499183	255083	
					254839	0.988
1142	1235.13	92.93	2.108	125004	263508	
	1237.13	94.93	2.106	121587	262689	
	1239.13	96.93	2.213	117974	261135	
					262444	0.960

Normalization factor based on comparison of repeated foil positions is 0.987 and this value was used to power normalize the data for Run 1142.

TABLE 5.5

Gold Cadmium Ratios

Base Core for Wave Experiments

Location		Infinitely Dilute Foil Activity		Cadmium Ratio (Infinitely Dilute)
Radial (cm)	Axial (cm)	Cd Foil Activity d/m/gm x 10^{-6}	Bare Foil Activity d/m/gm x 10^{-6}	
0	93.3	2.320	3.423	1.476
0	120.6	2.160	2.471	1.144
0	120.6	2.144	2.464	1.149
0	151.1	1.987	2.406	1.211
0	151.1	2.086	2.448	1.174
0	181.5	2.138	2.587	1.210
0	181.5	2.103	2.573	1.223
0	208.8	2.091	3.137	1.500
0	208.8	2.202	3.181	1.445
30.5	93.3	2.338	3.308	1.415
30.5	120.6	2.160	2.770	1.283
30.5	151.1	2.657	2.851	1.073
30.5	151.1	2.099	2.618	1.247
30.5	181.5	2.198	2.735	1.244
30.5	208.8	2.354	3.316	1.408
45.7	93.3	2.340	3.300	1.410
45.7	120.6	2.266	2.960	1.306
45.7	151.1	2.202	2.933	1.332
45.7	181.5	2.250	2.948	1.310
45.7	208.8	2.392	3.437	1.437
61.0	93.3	2.370	3.895	1.644
61.0	120.6	2.385	3.759	1.576
61.0	151.1	2.419	3.547	1.466
61.0	181.5	2.358	3.620	1.535
61.0	208.8	2.347	3.749	1.598
84.5	93.3	2.166	4.216	1.947
84.5	120.6	2.235	4.178	1.869
84.5	151.1	2.579	4.386	1.701
84.5	151.1	2.653	4.419	1.665
84.5	181.5	2.202	4.188	1.902
84.5	208.8	2.236	4.106	1.837
87.6	93.3	2.172	4.429	2.039
87.6	120.6	2.662	4.812	1.808
87.6	151.1	2.812	4.876	1.734
87.6	181.5	2.687	4.821	1.794
87.6	208.8	2.118	4.075	1.924
90.8	93.3	1.851	4.550	2.458
90.8	120.6	2.722	5.588	2.053
90.8	120.6	2.646	5.558	2.101
90.8	151.1	2.407	5.603	2.328

TABLE 5.5

(Continued)

Location		Infinitely Dilute Foil Activity		Cadmium Ratio (Infinitely Dilute)
Radial (cm)	Axial (cm)	Cd Foil Activity d/m/gm x 10^{-6}	Bare Foil Activity d/m/gm x 10^{-6}	
90.8	151.1	2.805	5.758	2.053
90.8	181.5	2.640	5.477	2.075
90.8	208.8	1.818	3.918	2.155
0	89.4	2.534	3.798	1.499
0	74.9	2.522	6.967	2.763
0	59.6	0.562	3.501	42.68
0	29.1	0.008	2.206	272.2
93.2	151.1	2.681	6.258	2.335
107.7	151.1	2.126	7.179	3.377
123.0	151.1	0.750	5.529	7.377
138.2	151.1	0.132	3.588	27.10
153.5	151.1	0.018	2.046	114.0

TABLE 5.6

Thermal Neutron Flux

Configuration 1 (Base Core for Wave Experiments)

Location		Thermal Neutron Flux
Radial (cm)	Axial (cm)	$n/cm^2/sec/watt \times 10^{-6}$
0	93.3	1.297
0	120.6	0.366
0	151.1	0.493
0	181.5	0.529
0	208.8	1.231
30.5	93.3	1.141
30.5	120.6	0.718
30.5	151.1	0.239
30.5	181.5	0.632
30.5	208.8	1.131
45.7	93.3	1.130
45.7	120.6	0.816
45.7	151.1	0.861
45.7	181.5	0.820
45.7	208.8	1.230
61.0	93.3	1.794
61.0	120.6	1.616
61.0	151.1	1.326
61.0	181.5	1.485
61.0	208.8	1.650
84.5	93.3	2.411
84.5	120.6	2.283
84.5	151.1	2.881
84.5	181.5	2.388
84.5	208.8	2.200
87.6	93.3	2.655
87.6	120.6	2.531
87.6	151.1	2.429
87.6	181.5	2.510
87.6	208.8	2.301
90.8	93.3	3.177
90.8	120.6	3.373
90.8	151.1	3.760
90.8	181.5	3.338
90.8	208.8	1.714
0	89.4	1.487
0	74.9	5.230
0	59.6	5.625
0	44.4	4.021
0	29.1	2.587
0	13.9	1.299
0	0	0.191

TABLE 5.6

(Continued)

Location		
Radial (cm)	Axial (cm)	Thermal Neutron Flux $m/cm^2/sec/watt \times 10^{-6}$
93.2	151.1	4.221
107.7	151.1	5.945
123.0	151.1	5.625
138.2	151.1	4.068
153.5	151.1	2.387
168.7	151.1	1.030
183.9	151.1	0.024

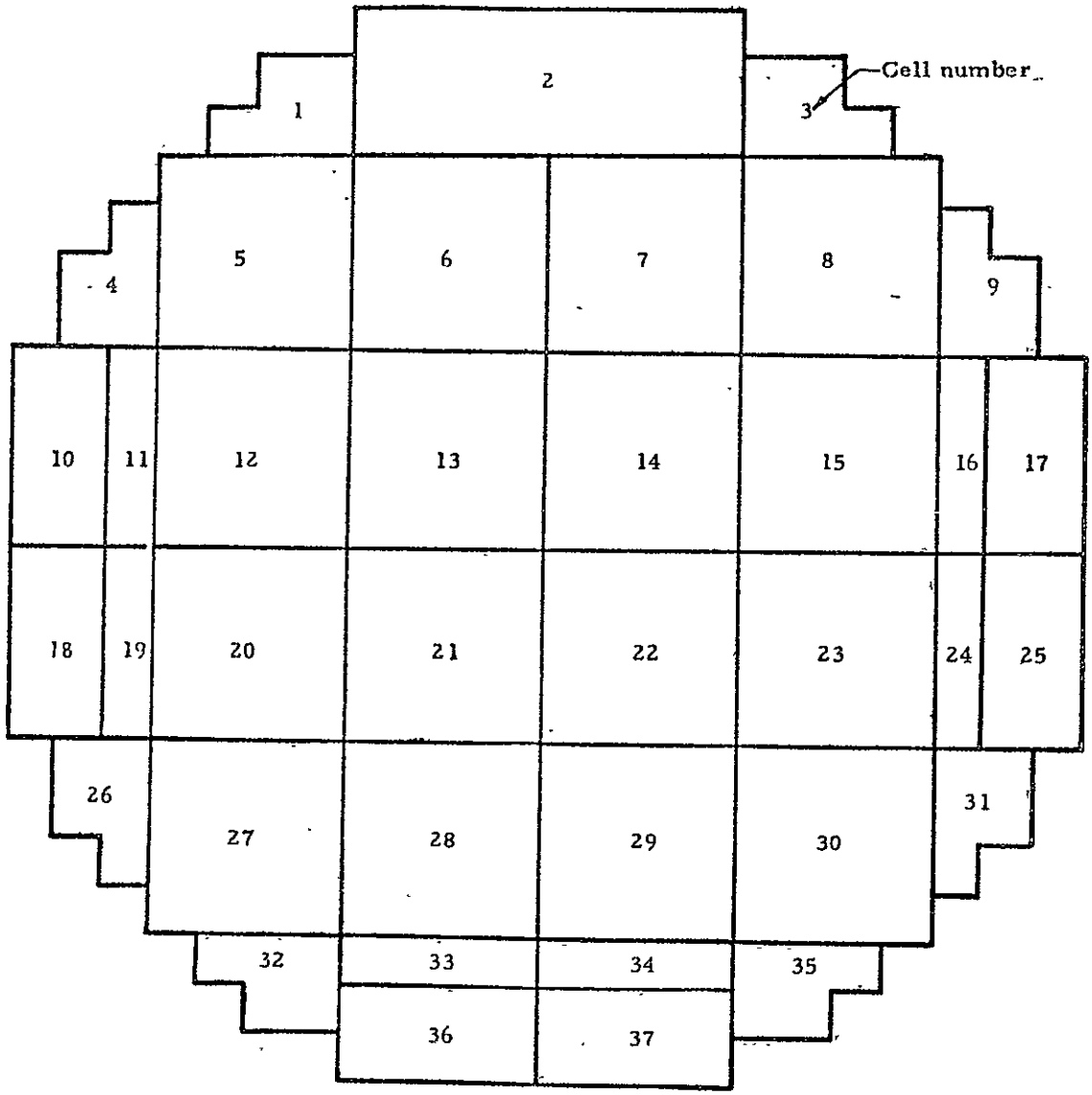

Fig. 5.1 Cross section view at separation plane of cell arrangement of modified core structure

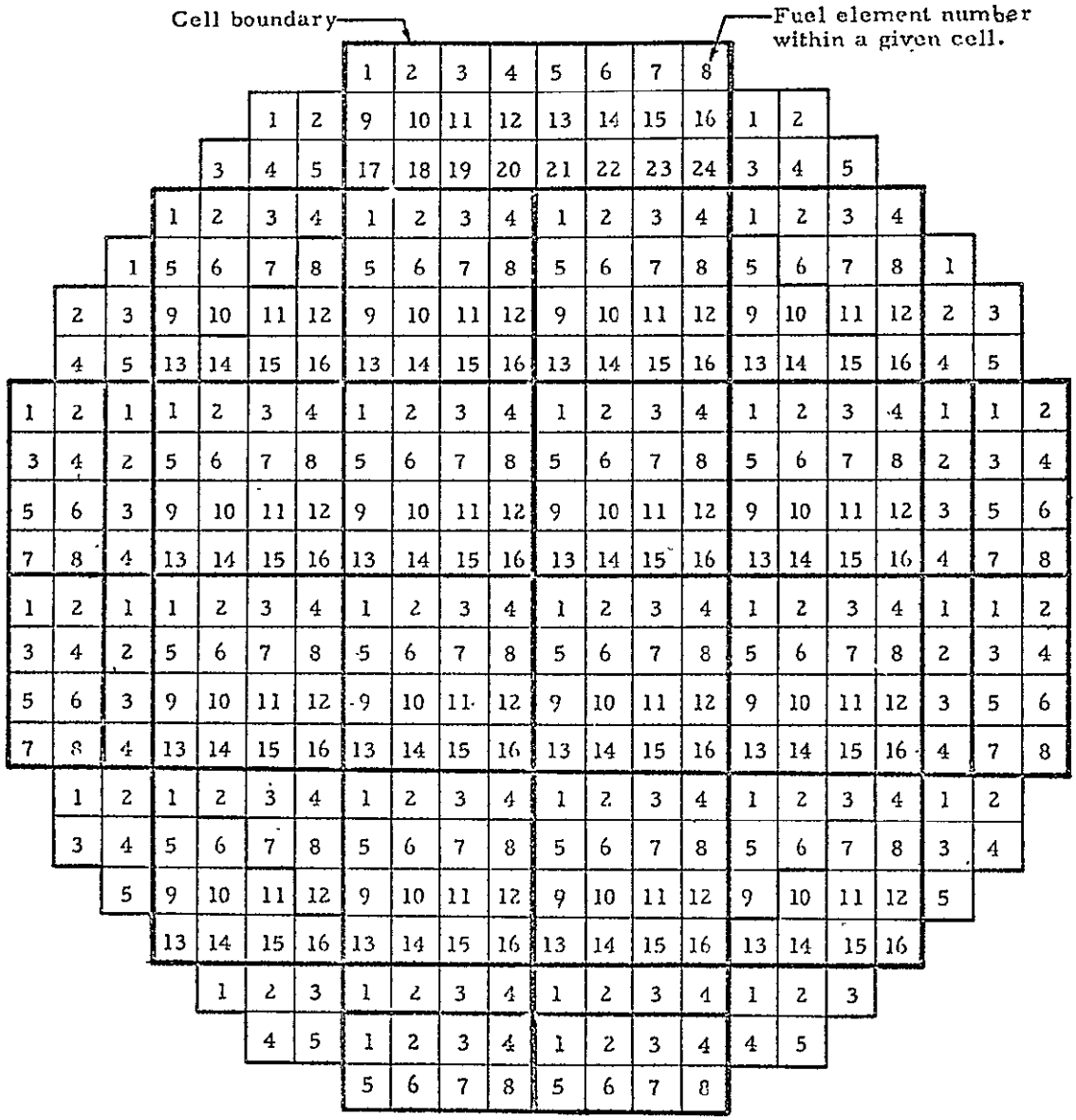

Fig. 5.2 Cross section view at separation plane of fuel element numbers in the several cells of the modified core structure

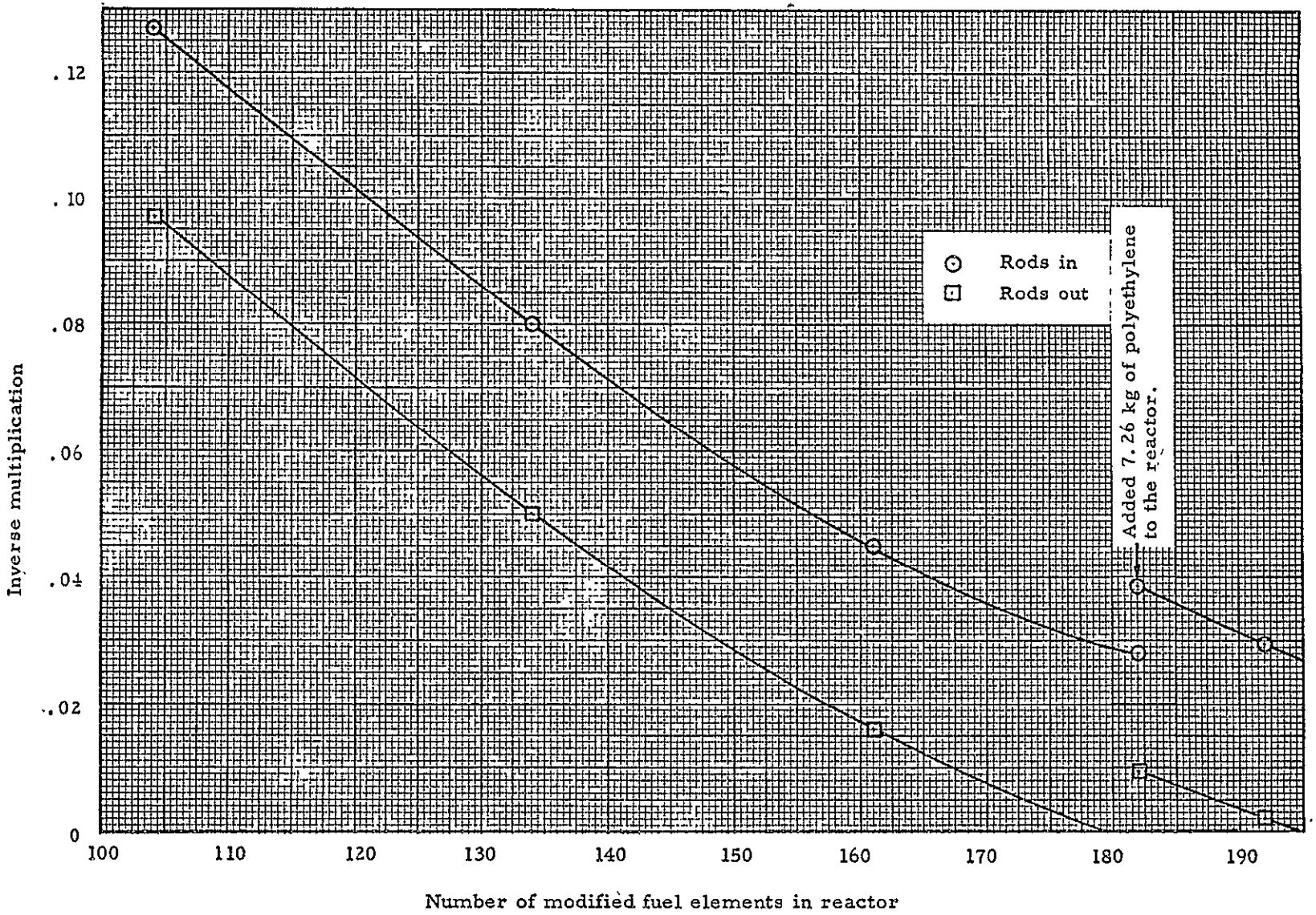

Fig. 5.3 Inverse multiplication curves and modified base wave configuration

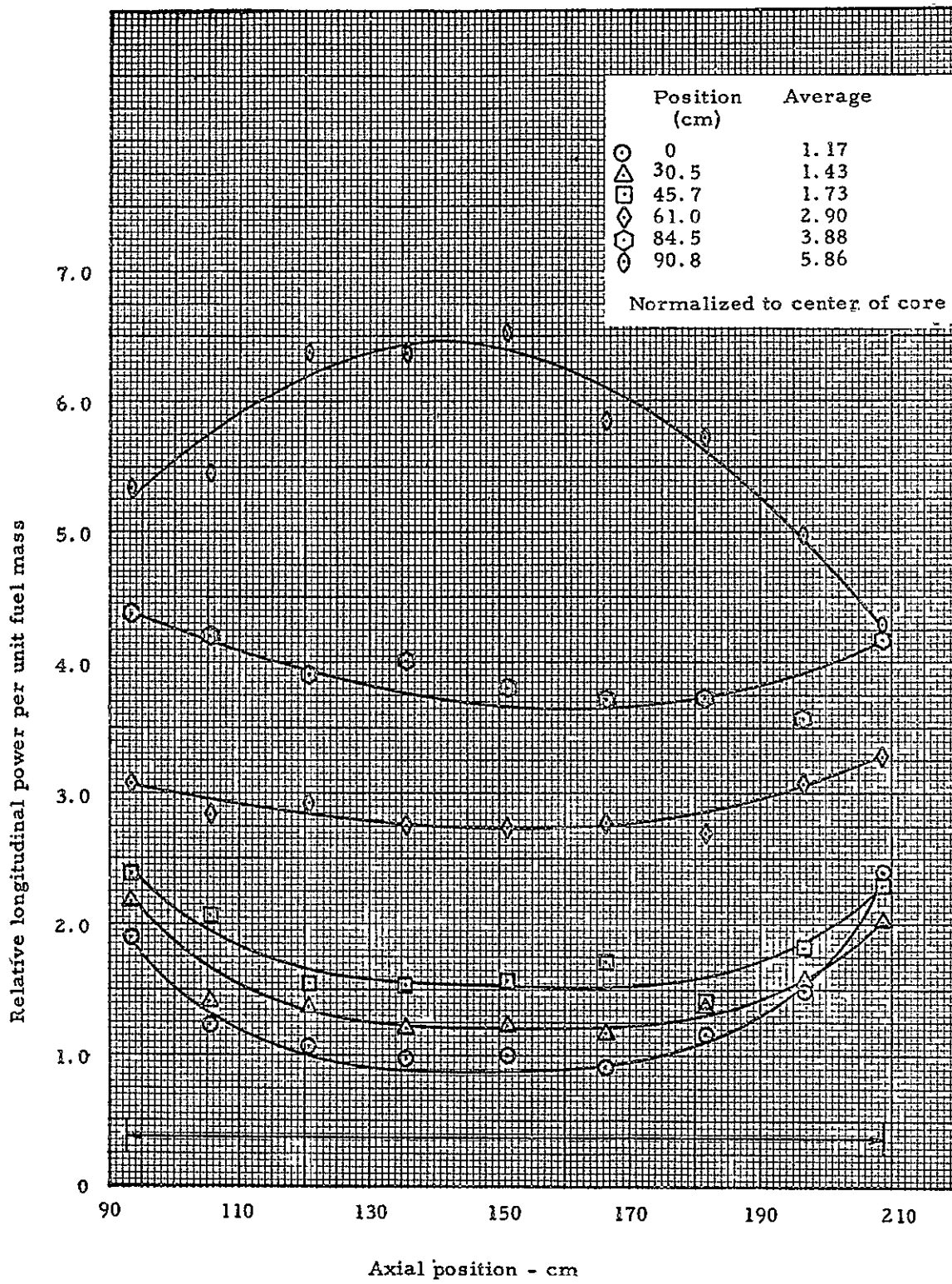

Fig. 5.4 Relative axial distribution of bare catcher foil activity in the cavity of the bare configuration for the fuel wave experiments 30.5 kg fuel in core

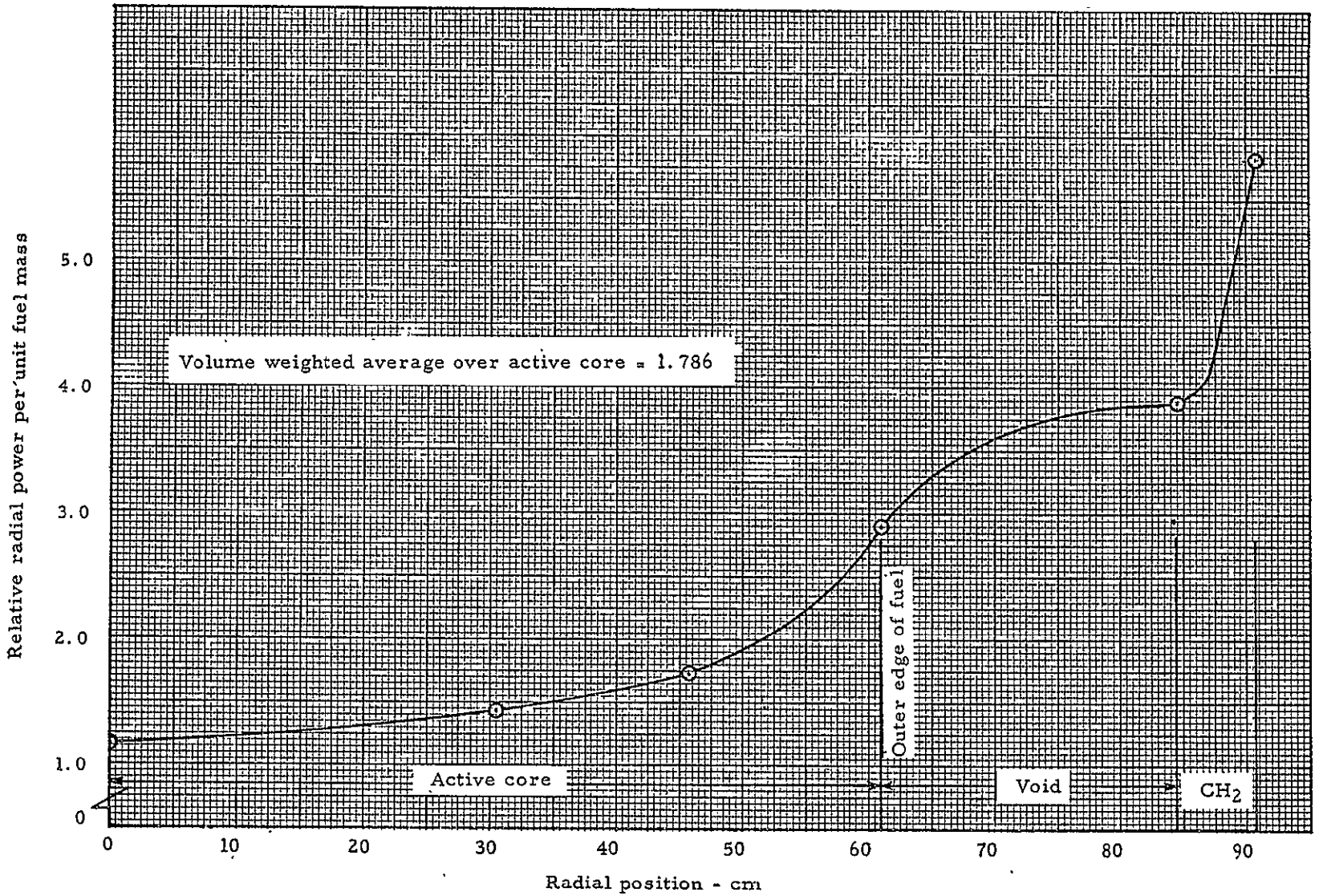

Fig. 5.5 Relative radial distribution of axial averages of bare foil activity in the cavity of the base configuration for the fuel wave experiments. 30.5 kg fuel in core

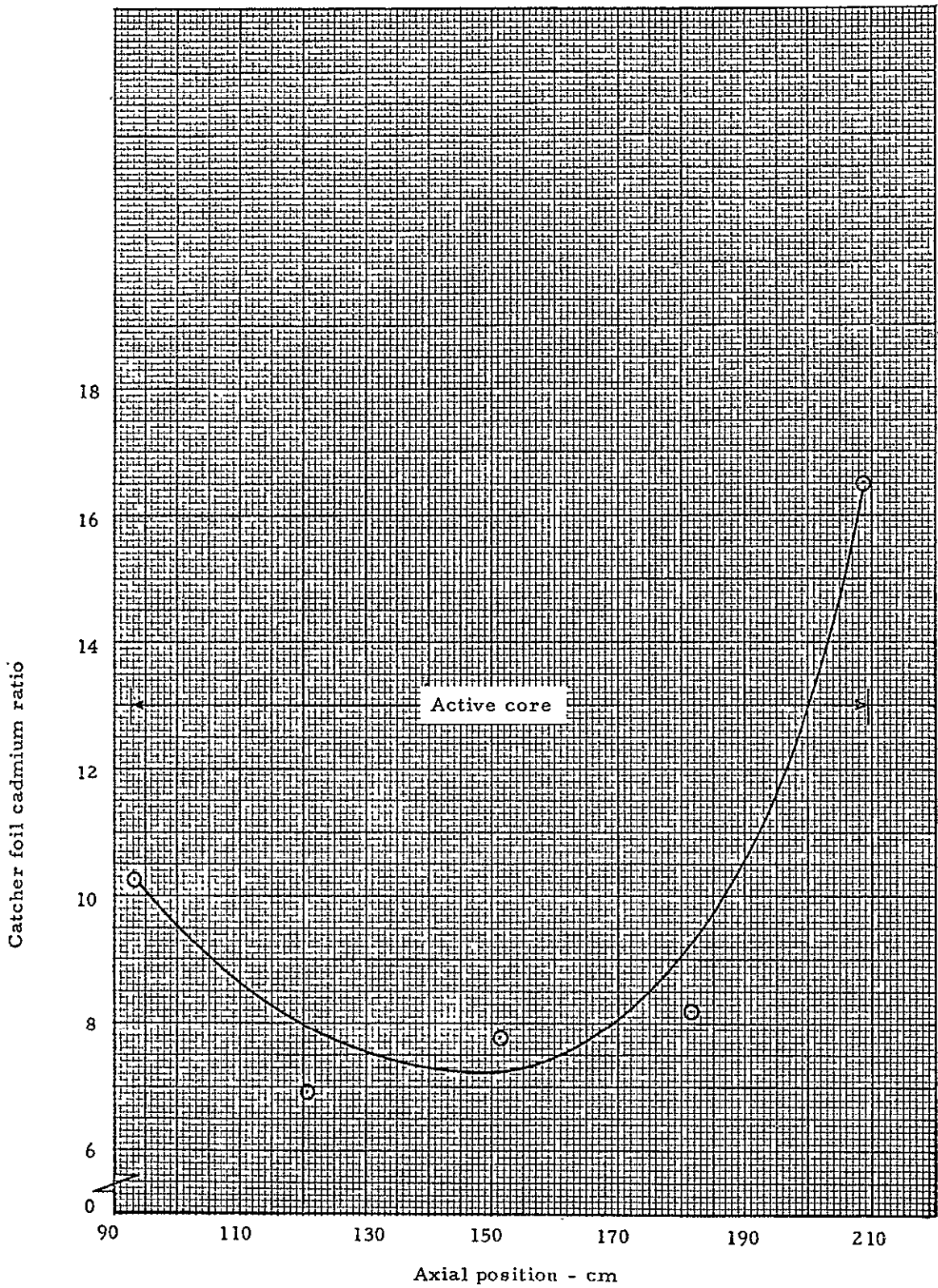

Fig. 5.6 U^{235} cadmium ratio on axial centerline

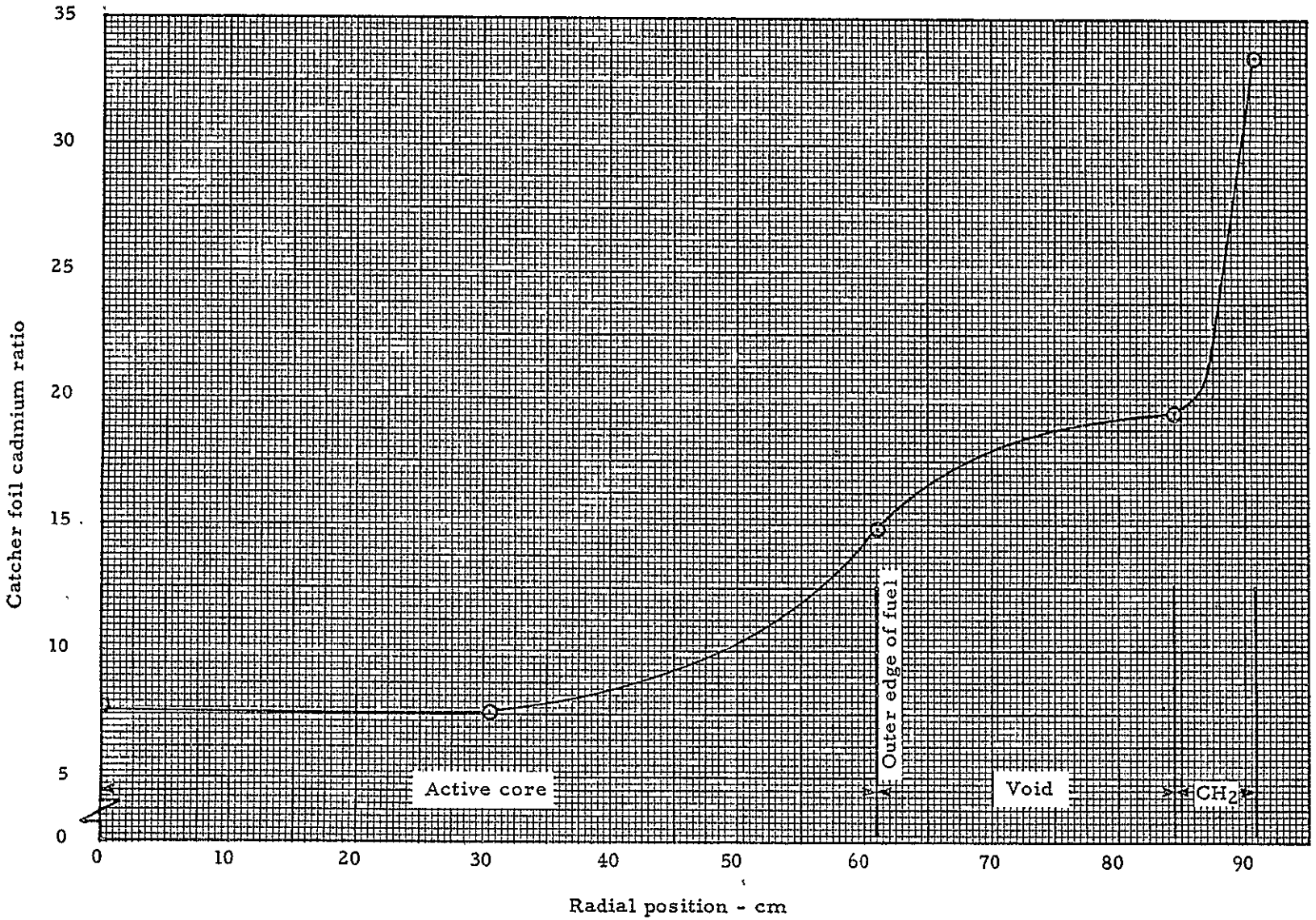

Fig. 5.7 U^{235} cadmium ratio vs radius at axial centerline

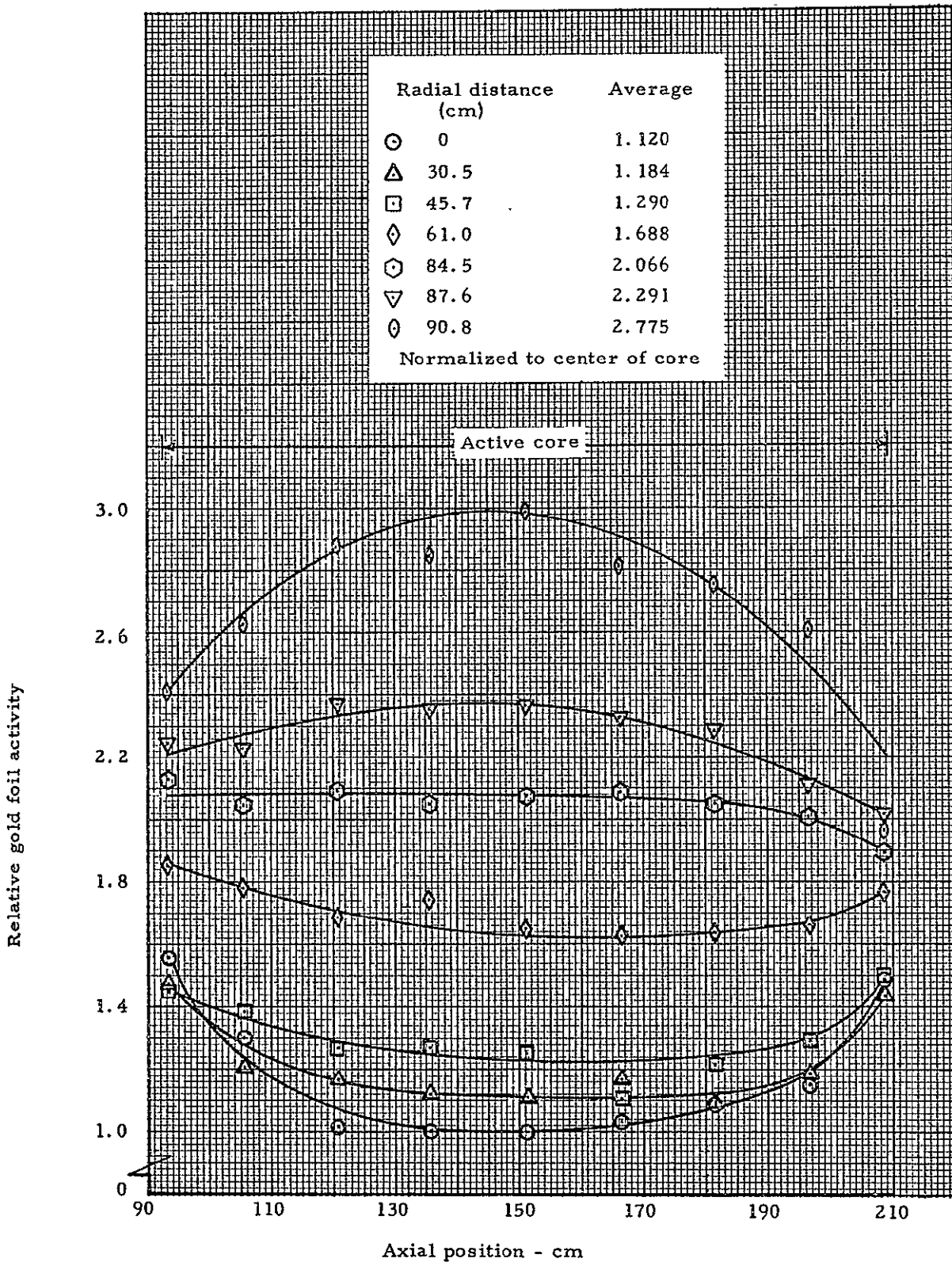

Fig. 5.8 Gold foil (0.0005 cm thick) activity in the core

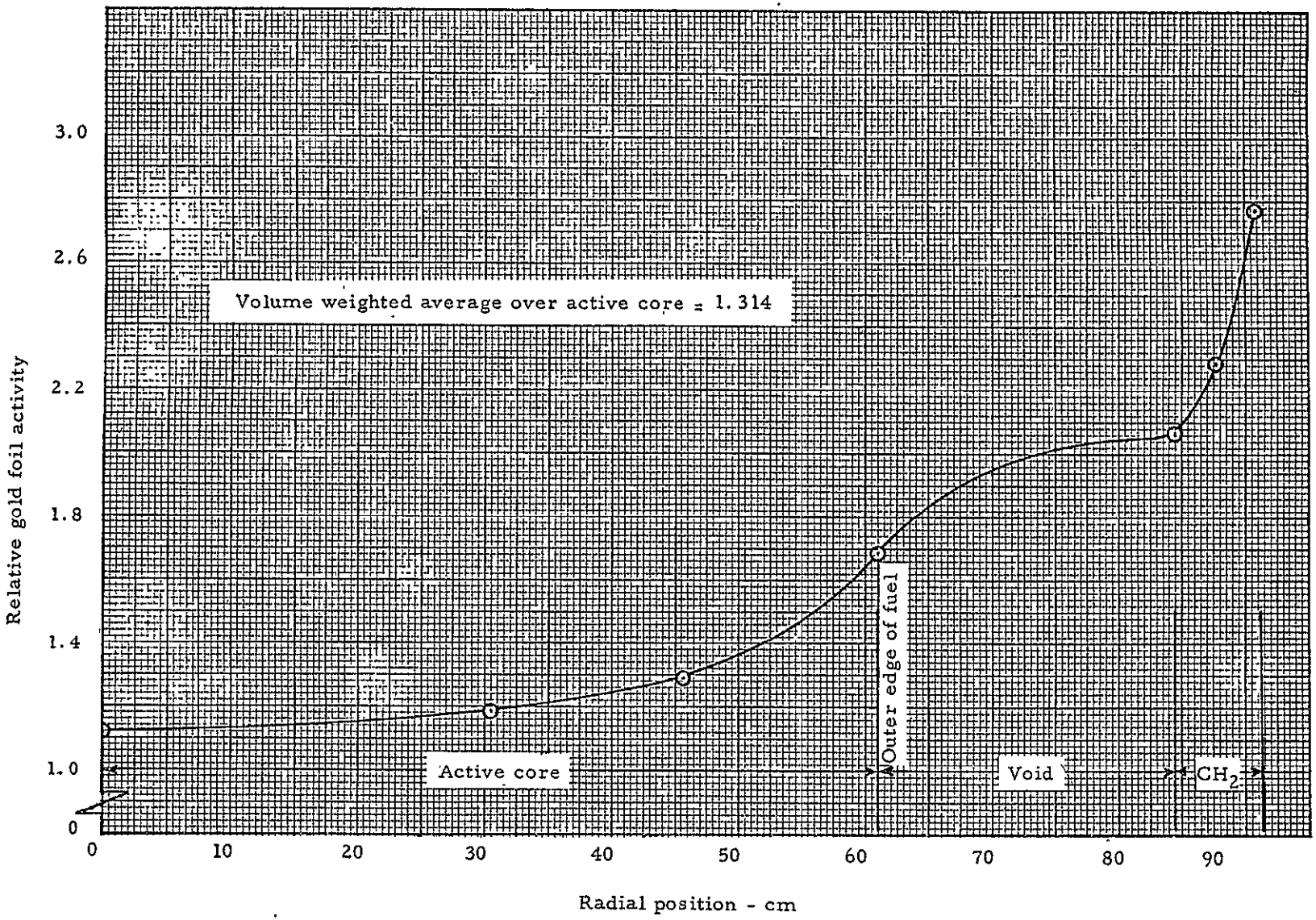

Fig. 5.9 Longitudinally averaged gold foil activity vs radius (cavity region)

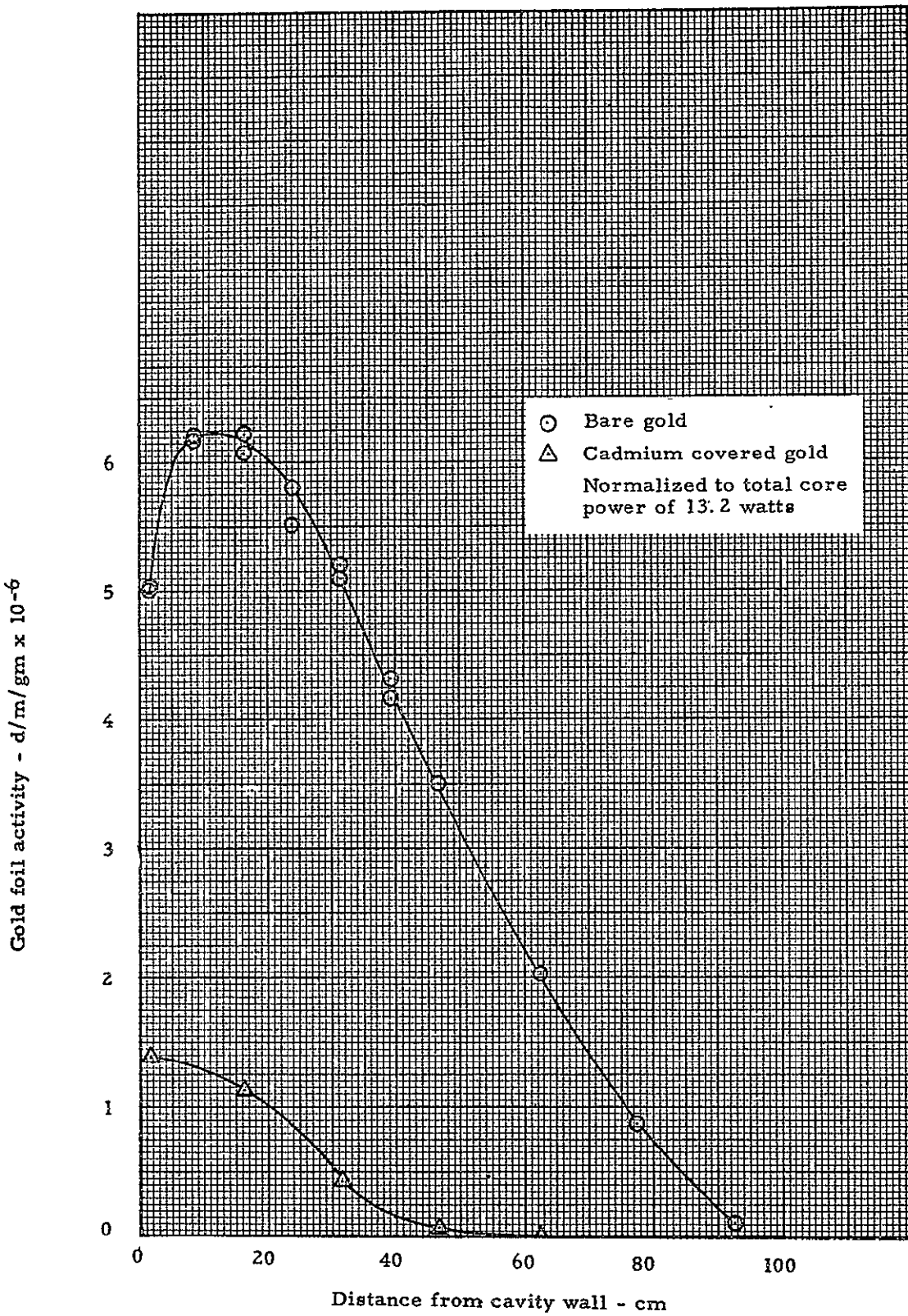

Fig. 5.10 Gold foil activity in the radial reflector (axial midplane)

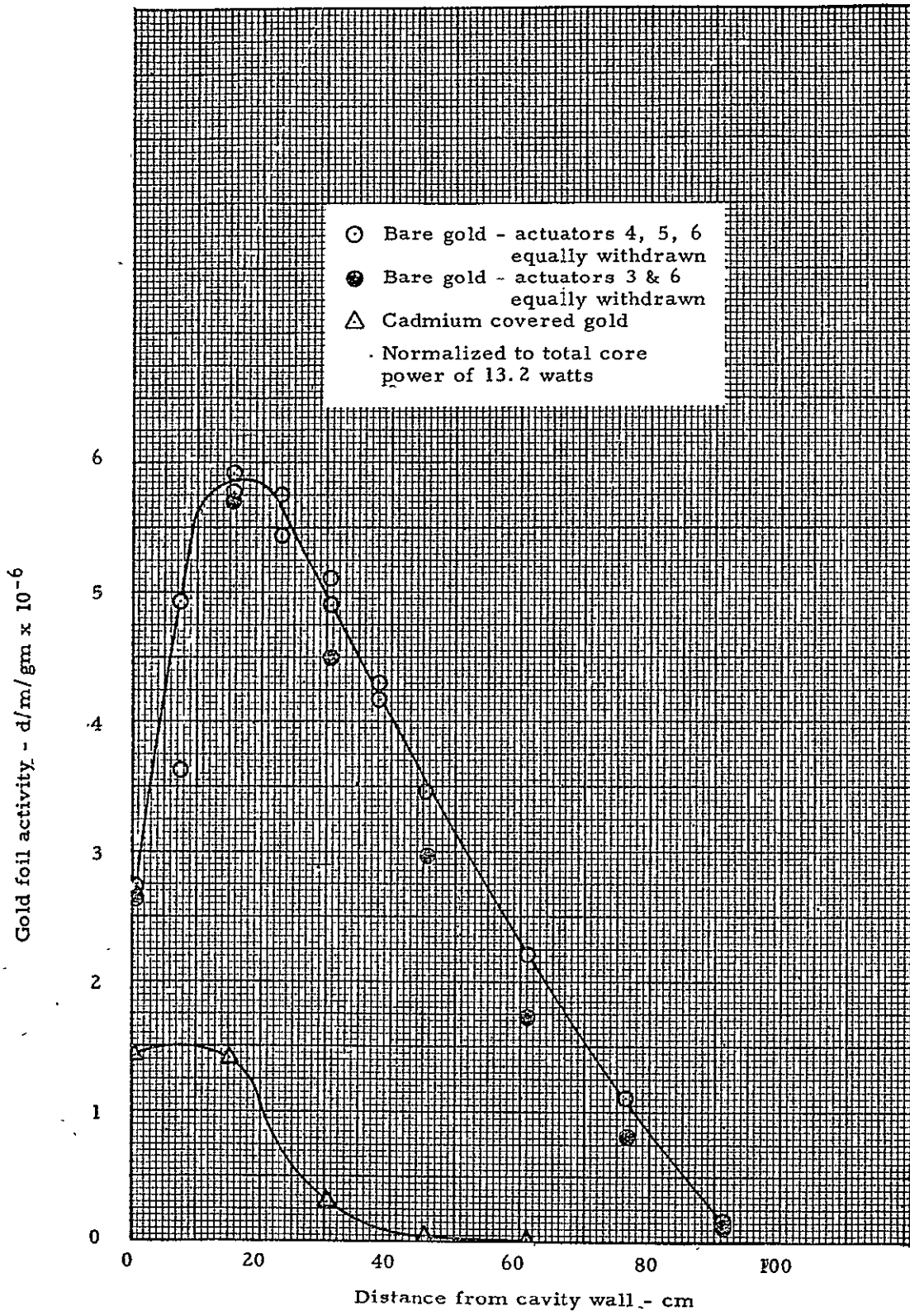

Fig. 5.11 Gold foil activity in the end reflector (axis)

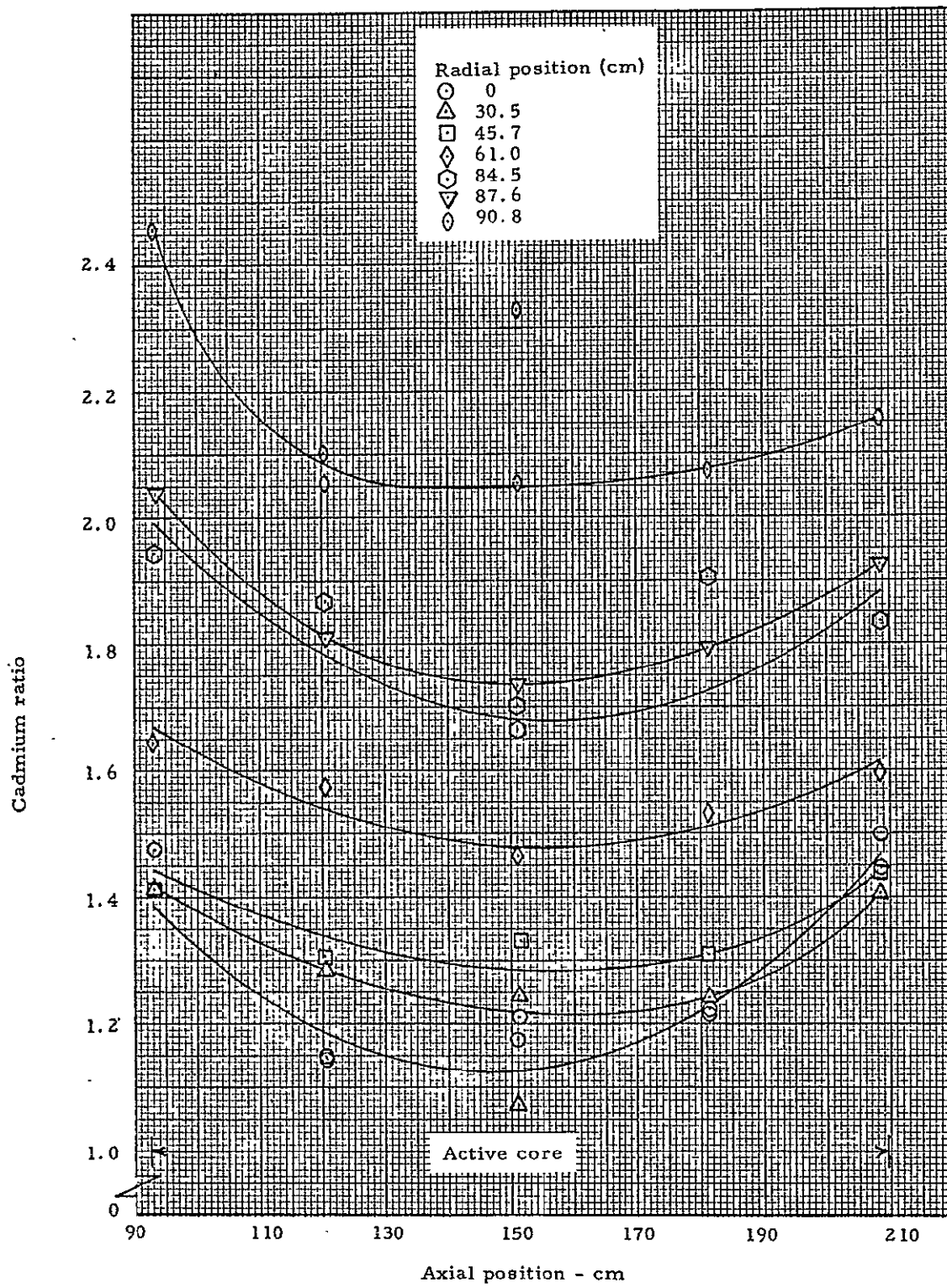

Fig. 5.12 Gold foil infinitely dilute cadmium ratios in cavity

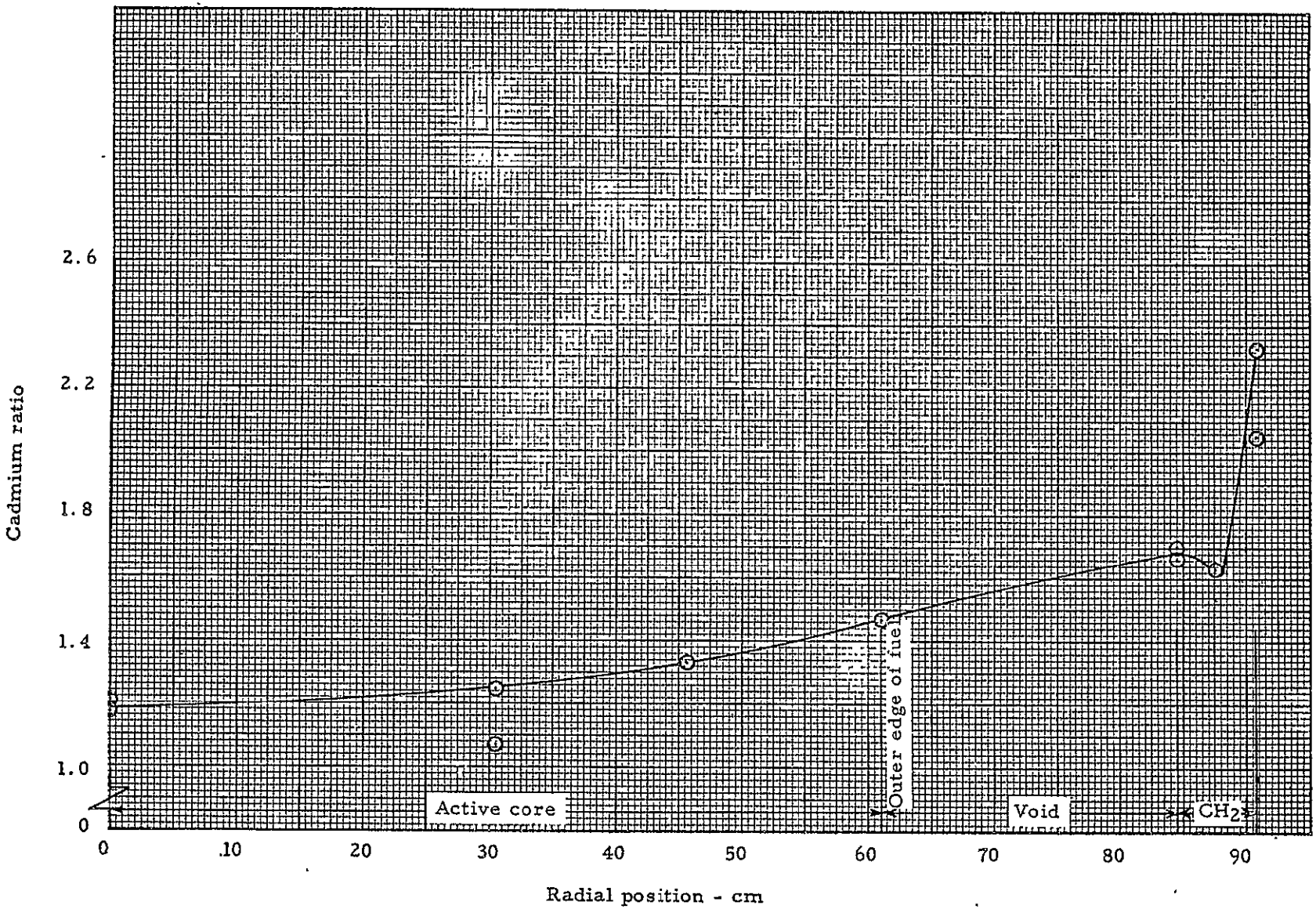

Fig. 5.13 Gold foil infinitely dilute cadmium ratios vs radius through axial midplane of cavity

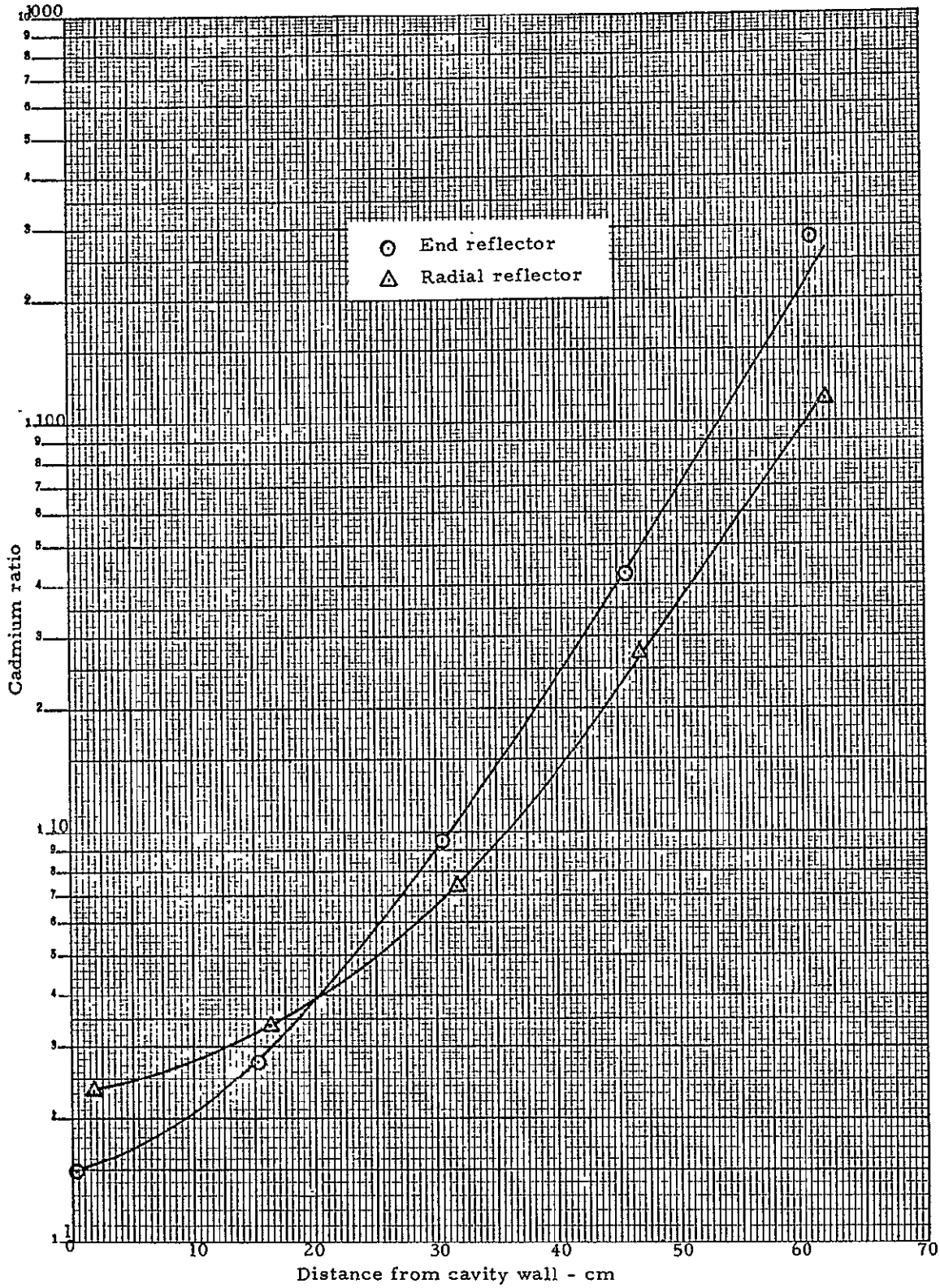

Fig. 5.14 Gold foil infinitely dilute cavity ratios in the reflector (end reflector, axis) (radial reflector axis)

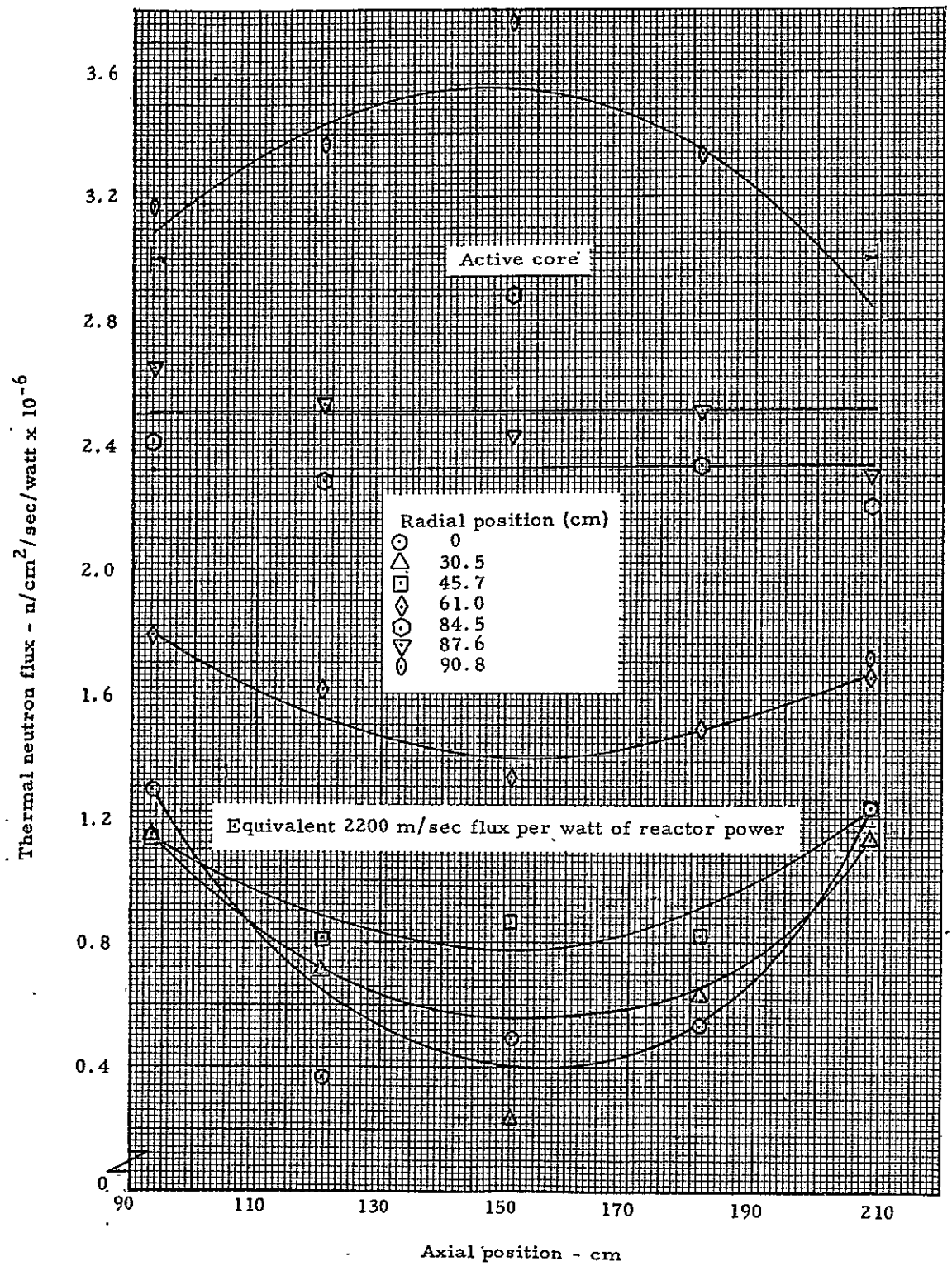

Fig. 5.15 Thermal neutron flux in cavity

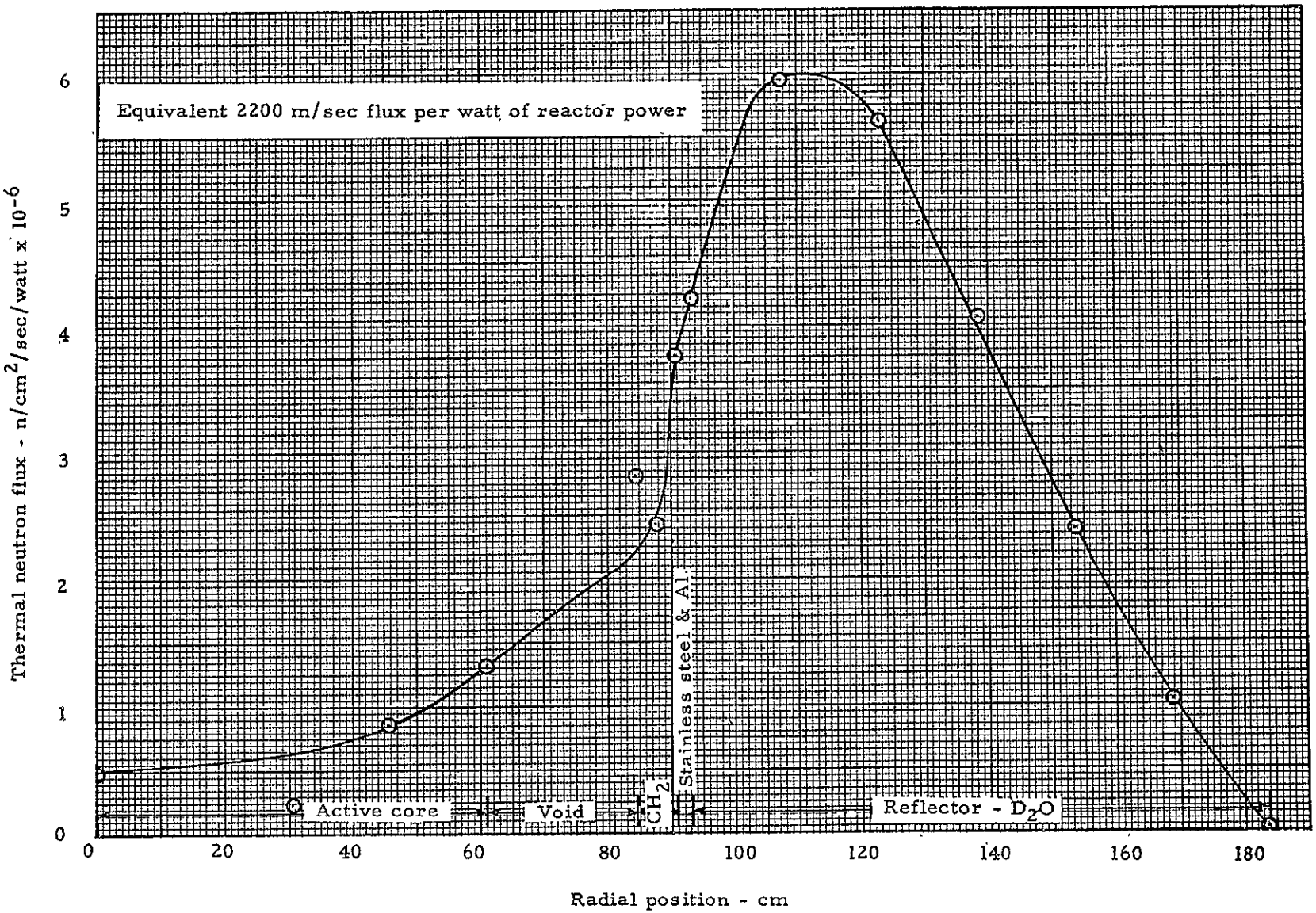

Fig. 5.16 Thermal neutron flux vs radius (axial midplane)

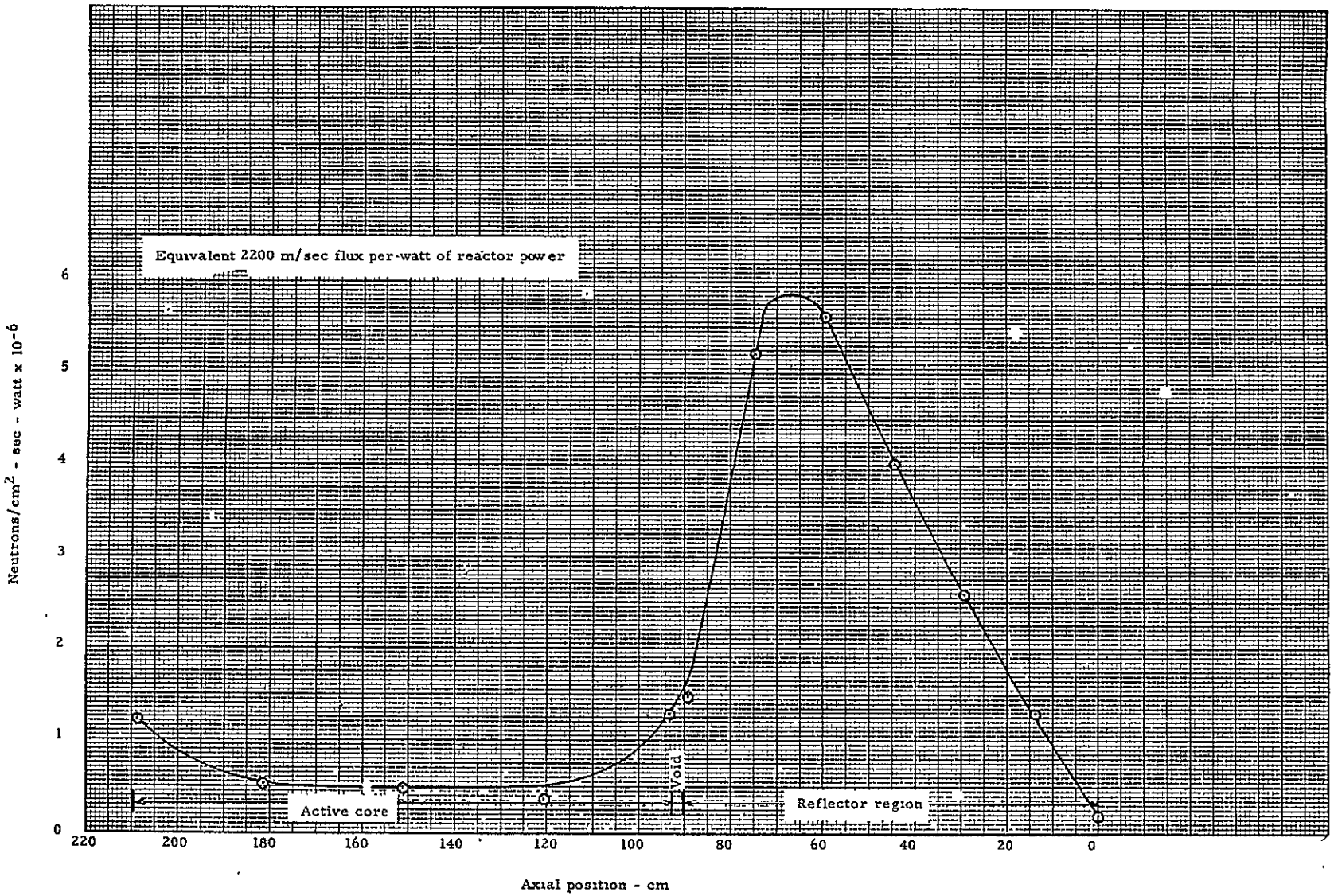

Fig. 5.17 Thermal neutron flux along axis

6.0 CONFIGURATION 2 (Three, 7.3 cm waves, fuel addition)

The fuel waves associated with Configuration 2 are shown in Figure 6.1. As noted from this figure, there were three waves and the reactivity worth of each was measured. These waves were a single stage of fuel (7.3 cm) square and formed an annulus around the active core. Special fuel elements were constructed to hold the fuel. These provided the same fuel dimensions as the normal fuel elements but differed in length and weight of structural material. The fuel for the single stage waves was placed in 14.6 cm long fuel elements with fuel occupying about half of the element. Three stage elements were also made for 22cm wave measurements. The fuel was loaded in the elements to the same number of sheets of fuel per stage as the normal core and with the three different fuel orientations. Thus, average fuel density was preserved in the fueled region. The short fuel elements component weights are as follows:

	14.6 cm long elements	22.1 cm long elements
Bare element	41.075 gm	55.87
Lid	8.75 gm	13.05
Each Spacer (4 per element)	3.46 gm (6 per element 3.46)	

Type 1100 aluminum was used for all of the fuel element parts.

The base core for these wave experiments was as described in Section 5.0. There were 30.5 kg of uranium in the active core.

6.1 Rod Worth Measurements

Several rod worth measurements were obtained during the course of the fuel wave experiments. Rather than present the rod worth measurements for each major configuration under individual sections, all the data will be given at this point. The test results were normally based on average rod worths where it was necessary to compute k-excess. Table 6.1 contains the rod worth data through Configuration 5.

6.2 Aluminum Worth

The fuel waves were created by placing fuel in short aluminum fuel elements, as has already been explained. It was necessary, therefore, to know the worth of aluminum in each of the waves so that the effect of the addition of uranium or the change in location of uranium could be determined. Several measurements were made to determine the worth of the short fuel elements at several axial locations corresponding to wave position. Both one and three stage wave measurements were obtained with and without the fuel spacer and lids in the fuel elements. These data are given in Table 6.2 and Figure 6.2. Some of the early measurements with the shortest elements, void of spacers or lids, gave values which were much more negative than later measurements at or near the same locations. No reason for this difference could be found.

The data also indicate the Al in the short fuel element without lids and spacers to be more negative than when the lids and spacers were in the element. This, however, was not observed with the larger wave configurations. When it was necessary to correct for the Al in the wave data, the curve through the data taken with a complete fuel element (fuel, lid, and spacer) was used.

Ideally, it would have been preferable to make the base measurements with empty cans in the wave positions, thus automatically correcting for aluminum worth. Though this method was employed on a few ocassions, in practice it was generally not practical, either because of shortage of aluminum cans or because in the alternation, there was excessive operational inefficiency in removing cans to the loading room for fuel additions while the reactor stands idle.

6.3 Reactivity Worth of Waves

The three waves shown in Figure 6.1, were designated Configurations 2A, 2B, and 2C. Each of these represent a wave at a different axial position as noted in Figure 6.1. In each case the complete wave was formed by placing fuel in the locations noted in Figure 6.3. There were 48 fuel elements in the wave with an average of 3.5 size 1.0 fuel sheets per element. Placing the wave around the active core added 441 gm of uranium to the cavity and resulted in the following increases in reactivity:

Configuration	Reactivity Worth (%Δk)
2A	0.725 ± 0.029
2B	0.525 ± 0.040
2C	0.524 ± 0.049

The highest value associated with Configuration 2A was at the location at the extreme end of the core were a larger number of neutrons from the end reflector could come in contact with the wave without passing through a portion of the normal active core.

TABLE 6.1

Rod Worths

Fuel Wave Experiments

	Actuator Combinations and Their Reactivity Worth (%Δk)			
Run No.	3 & 6 (6 rods)	1 to 6 (17 rods)	1 to 8 (23 rods)	1 to 12 (31 rods)
576	-1.2589			
578	-1.2469			
579	-1.2553			
580	-1.1995			
582	-1.2371			
583	-1.2324			
585	-1.2446			
586			-3.972	
587			-3.911	
589				-5.101
590				-5.010
591				-5.124
605	-1.2626			
606	-1.2556			
609	-1.2429			
615		-3.281		
616	-1.2441			
618	-1.2721			
619	-1.2898			
622	-1.2926			
624	-1.2710			
626	-1.2015			
630	-1.2176			
631	-1.2601			
633	-1.2300			
648			-4.281	
651			-4.114	
653				-5.162
654				-4.964
averages	-1.2481±0.0254	-3.281	-4.070±0.165	-5.072±0.082

TABLE 6.2

Aluminum Worth Measurements

Fuel Wave Experiments

Run No.	Distance From Separation Plane (cm)	Wave Location	Aluminum Weight (gm)	Reactivity Change (%Δk)	Aluminum Worth (%Δk/gm)x10^5
577	7.6	2A (6 in. boxes)	1807.3	-0.0544±0.007	-3.01±0.39
593	11.4	3A (9 in. boxes)	2793.5	-0.0475±0.007	-1.70±0.25
595	7.6	2A (6 in. boxes)	2382.4	-0.0538±0.007	-2.26±0.30
596	43.6	2B (6 in. boxes)	2382.4	-0.0742±0.007	-3.11±0.30
597	80.6	2C (6 in. boxes)	2382.4	-0.0776±0.007	-3.26±0.30
599	11.4	3A (9 in. boxes)	2458.3	-0.0408±0.007	-1.66±0.28
621	51.6, 109.6	4C (6 in. boxes)	3729.0	-0.1014±0.014	-2.72±0.38
622	51.6, 109.6	4C (6 in. boxes)	3284.0	-0.0842±0.014	-2.56±0.38
601	58.4	3B (9 in. boxes)	2178.9	-0.0510±0.007	-2.34±0.32
602	58.4	3B (9 in. boxes)	2458.3	-0.0590±0.007	-2.40±0.28
603	80.6	2C (6 in. boxes)	2382.4	-0.0835±0.007	-3.50±0.29
		Used base from previous day			
635	7.6	2A	2547.0	-0.0475±0.007	-1.864±0.274
636	25.6	Over stages 3 and 4	2547.0	-0.0485±0.007	-1.904±0.274
637	105.9	Over stages 14, 15	2547.0	-0.0674±0.007	-2.646±0.274
642	51.1	Over stages 7 and 8	994 (spacers & lids)	-0.0224±0.007	-2.25±0.70
643	51.1	Over stages 7 and 8	1807 (cans only)	-0.0484±0.007	-2.68±0.39
645	11.4	Over stages 1, 2, 3	3945	-0.0618±0.005	-1.57±0.14
646	11.4	Over stages 1, 2, 3	1487 (spacers & lids)	-0.0245±0.007	-1.65±0.49
647	11.4	Over stages 1, 2, 3	2458 (cans only)	-0.0373±0.005	-1.52±0.21

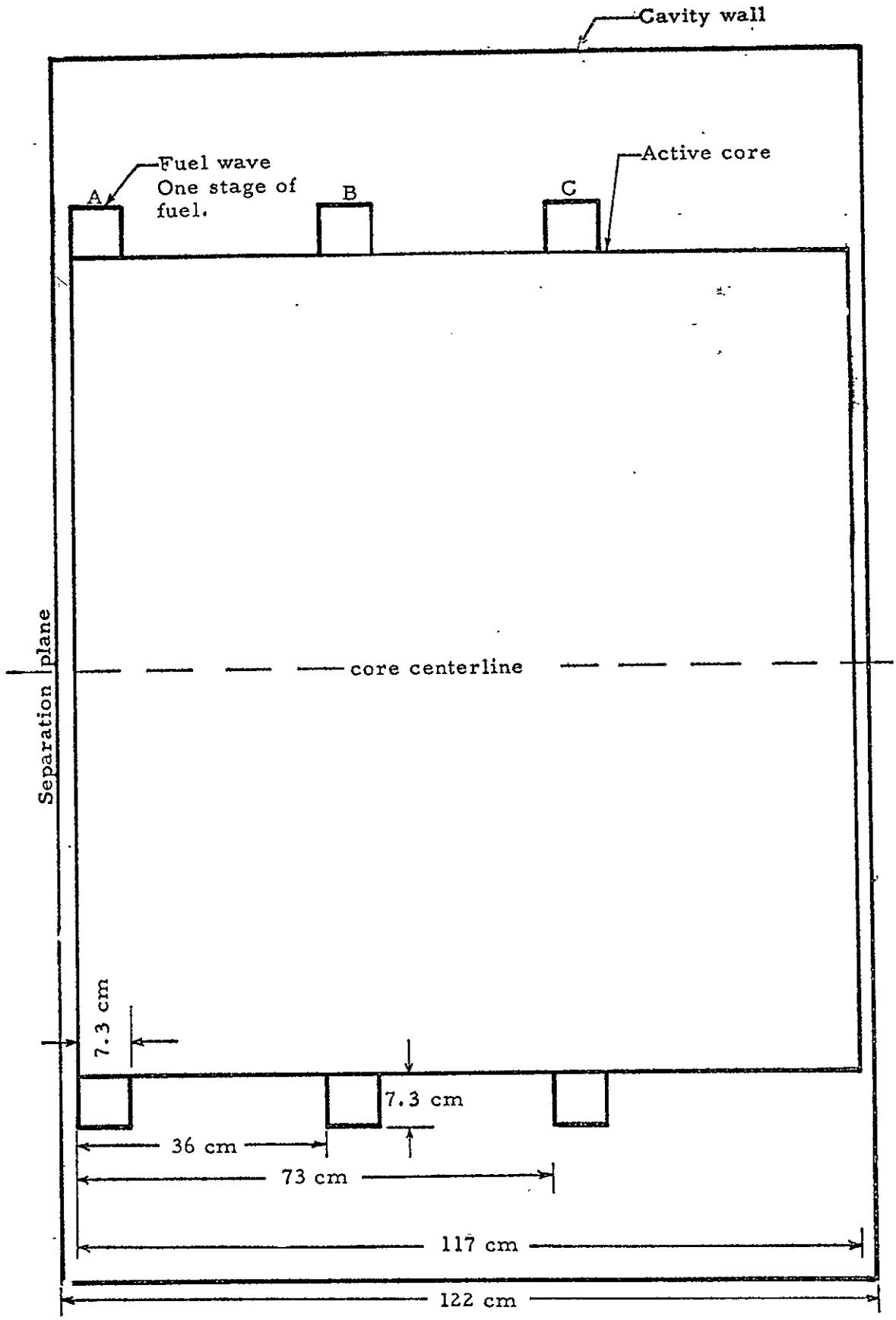

Fig. 6.1 Configuration two waves. 7.3 cm height, net fuel addition

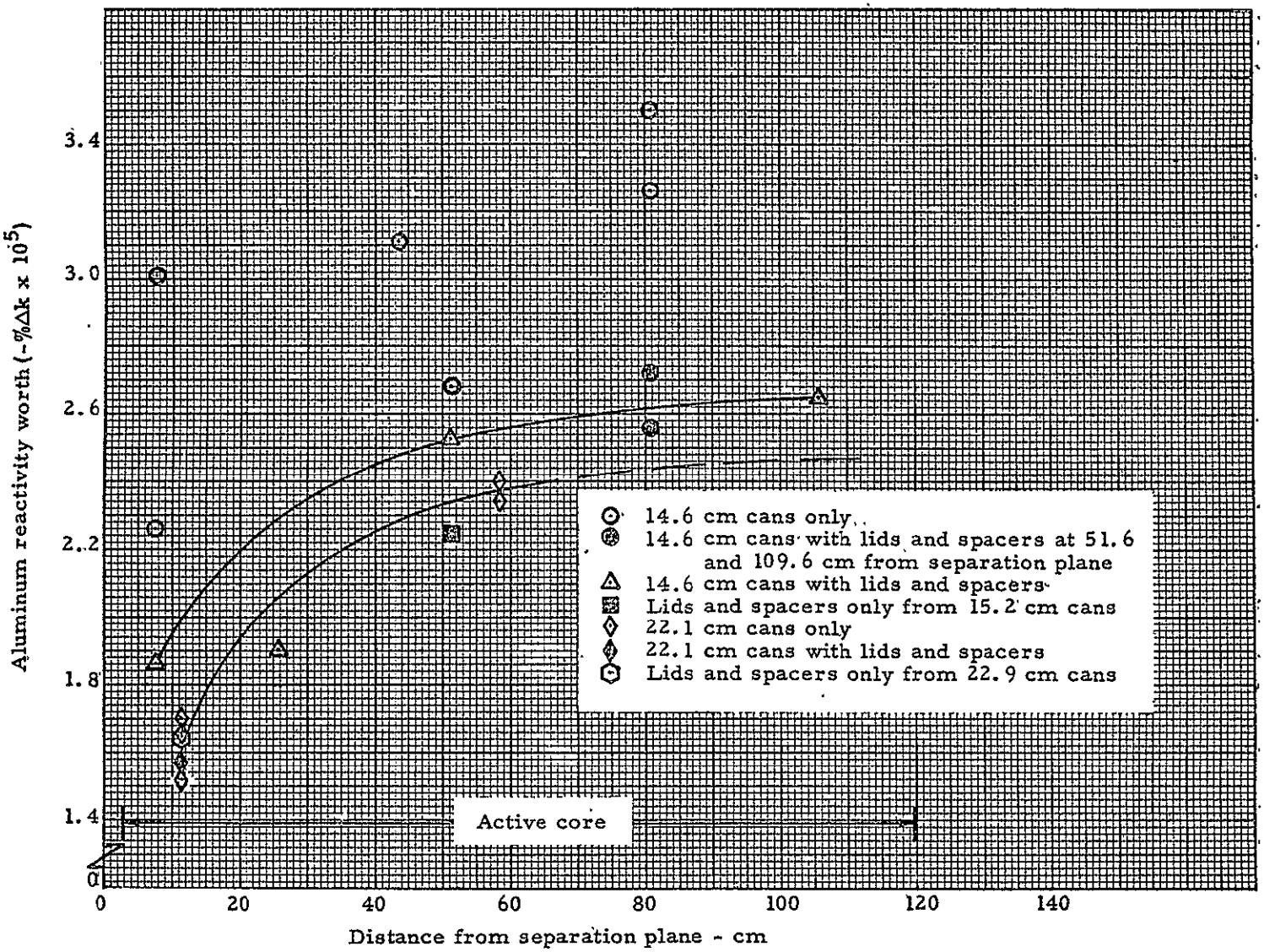

Fig. 6.2 Aluminum worth in cavity

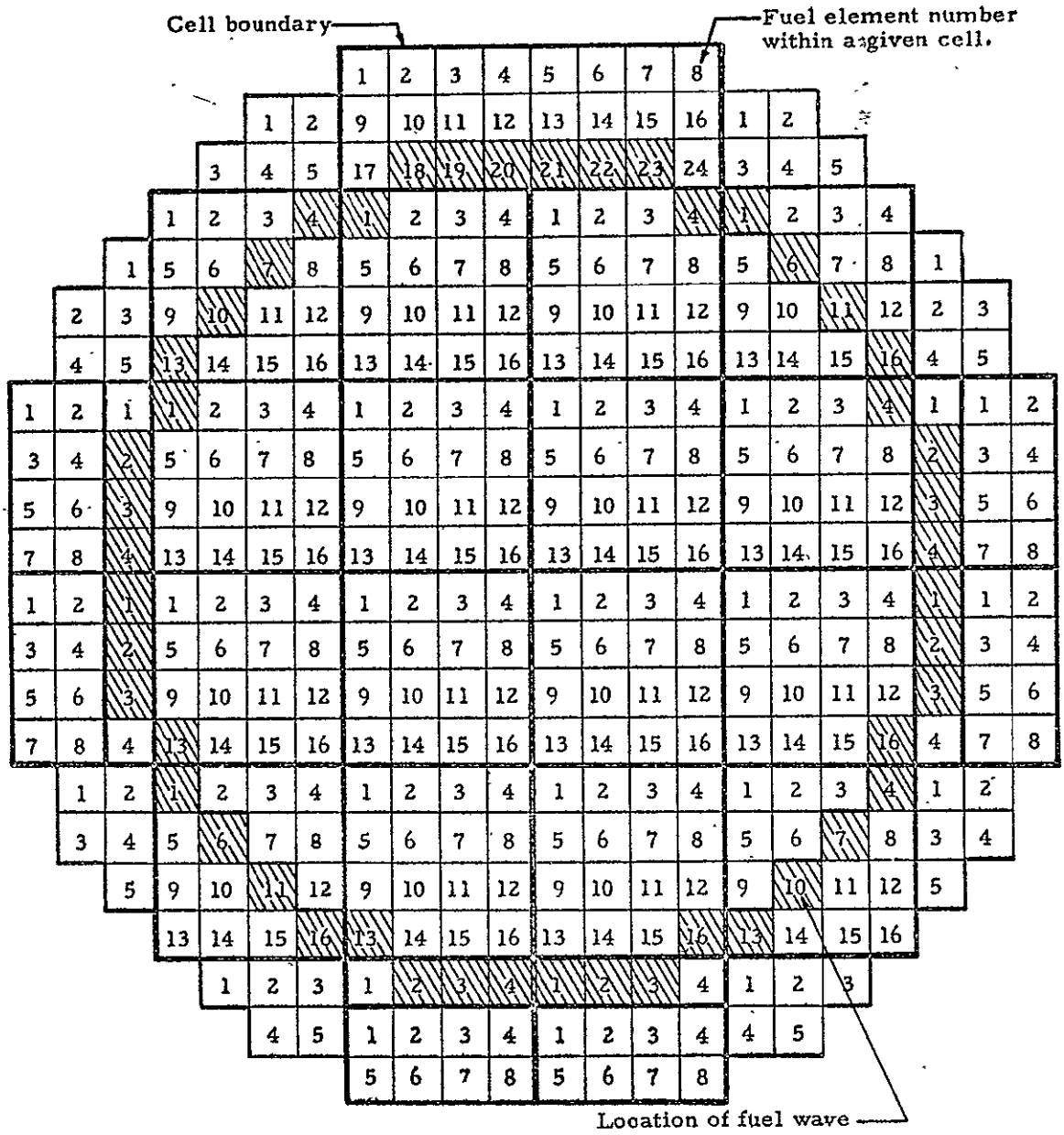

Fig. 6.3 Cross sectional view of wave - type 2 showing fuel element locations

7.0 CONFIGURATION 3 (Two, 22 cm waves, fuel addition)

Configuration 3 waves are shown in Figure 7.1. These waves were three stages square (21.9 cm) and the single wave was measured at two axial positions. Because of the large amount of fuel involved in adding the total wave and the limited worth of the control system, it was not feasible to add the complete wave. Half of the wave was added, however, and from this an extrapolation was made to the total wave. Measurements on 1/4 and 1/2 of the full wave showed essentially a linear dependence, and thus a linear extrapolation to a full wave is warranted. The positions of the fuel elements in the wave are shown in Figure 7.2. The worth of the complete 360° fuel waves were as follows:

Configuration	Reactivity Worth (%Δk)
3A	6.136 ± 0.159
3B	5.743 ± 0.126

These values are for a complete wave extrapolated linearly from the worth of 180 degrees of the waves. Each full wave represents an addition of 4.84 kg of uranium to the cavity region. The fuel elements were loaded with an average of 3.5 size 1.0 fuel sheets per stage. As noted earlier on the smaller waves, the worth of the wave is less near the center than at the end.

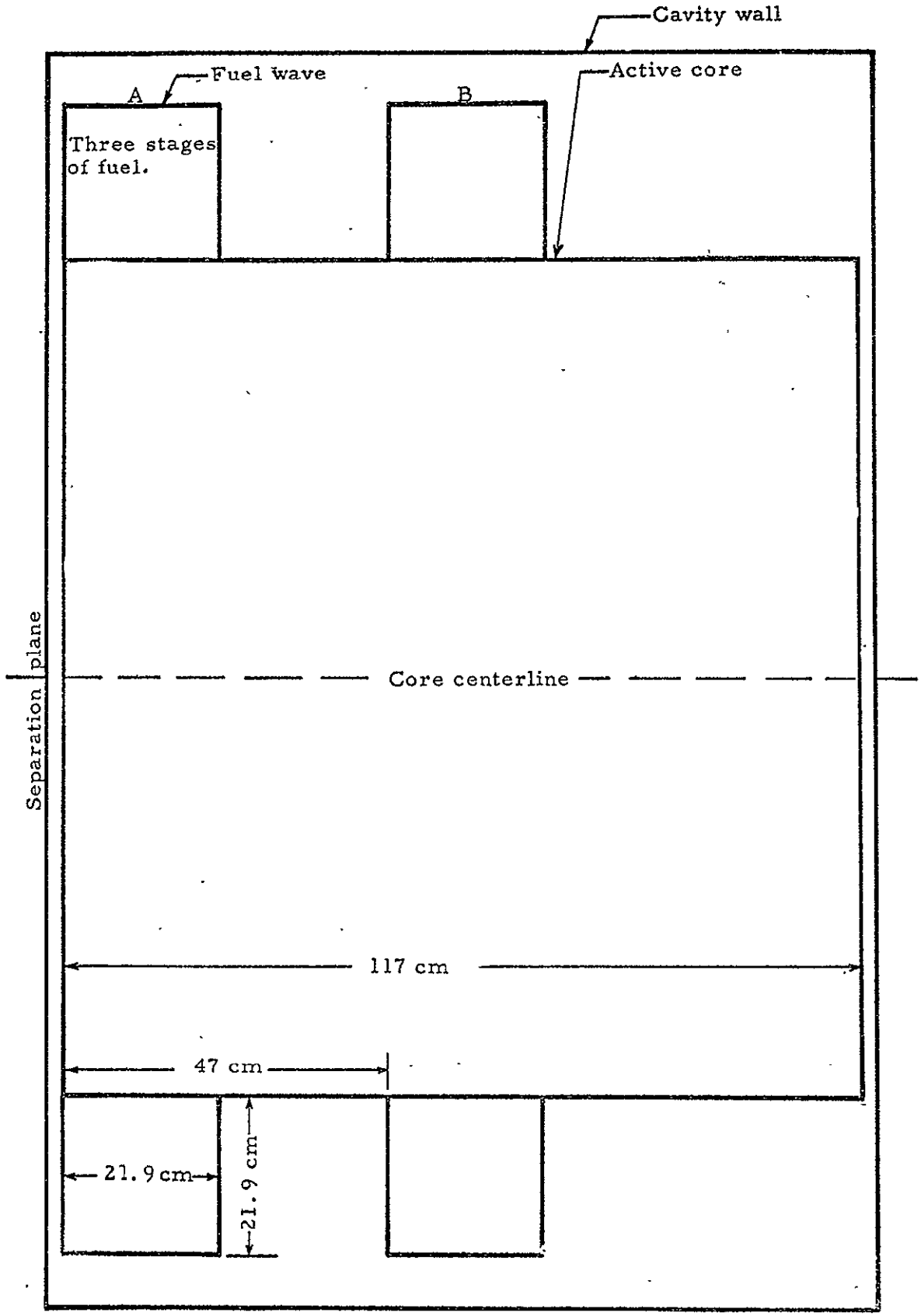

Fig. 7.1 Configuration 3 waves. 22 cm height; net fuel addition

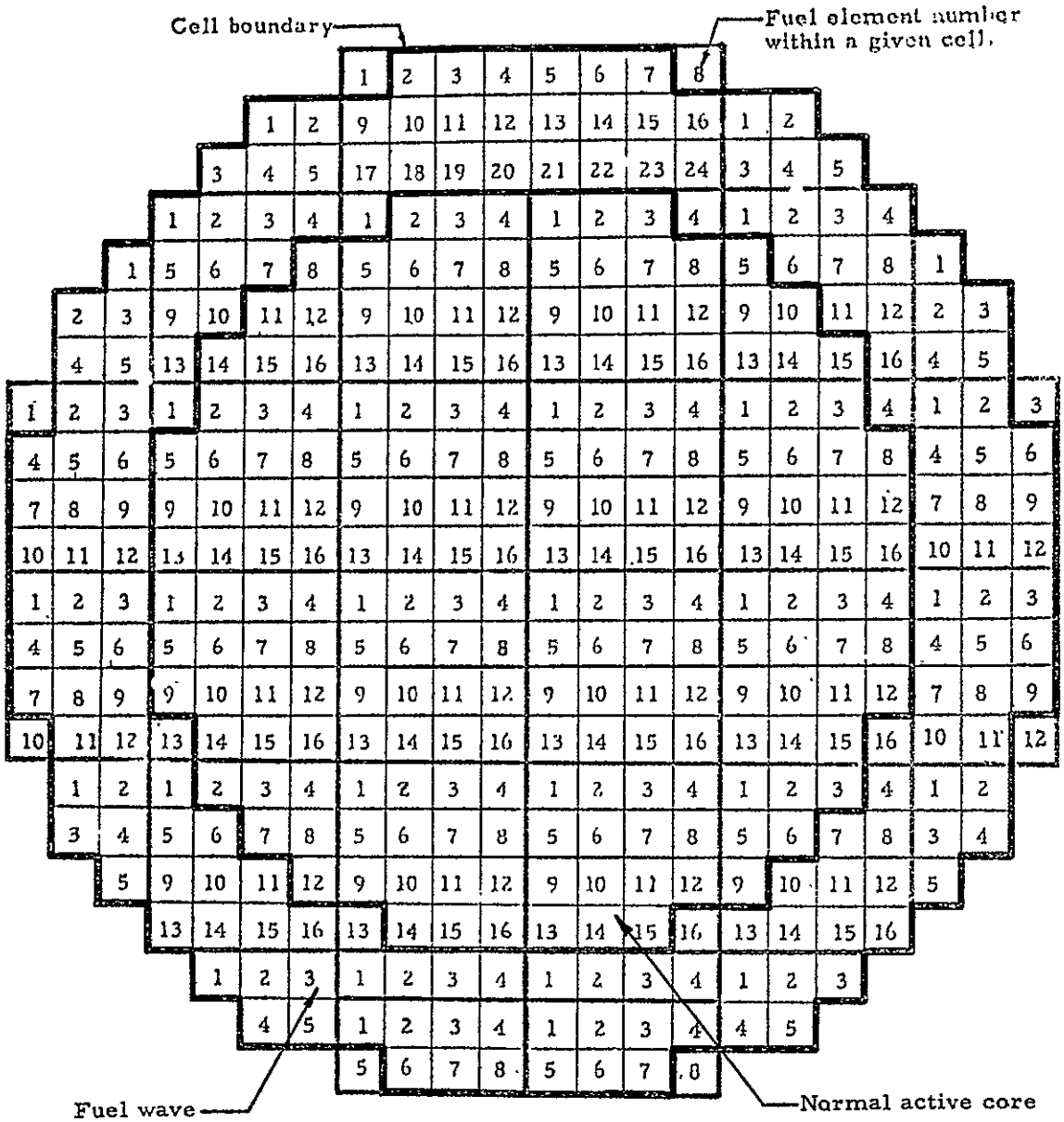

Fig. 7.2 Cross sectional view of wave - type 3 showing fuel element positions

8.0 CONFIGURATION 4 (7.3 cm waves, no addition of fuel)

8.1 Reactivity Measurements

The initial wave experiments required the addition of fuel to the outer boundary of the core which might occur in an operating reactor if the fuel were injected into the reactor near the outer portion of the active core. Another type of wave, which would be more likely to occur, is one with a crest and trough much the same as on the surface of water. As such a wave develops at the outer edge of the active core, the total fuel loading would be conserved. Configuration 4 waves, as shown in Figures 8.1 to 8.4, were designed to evaluate this type of wave where the crest and trough were each one stage of fuel square. Figure 8.5 shows the fuel element positions involved in the measurements. A single wave (Configuration 4A) required the relocation of 403 gm of fuel from just within the ordinary boundary of the active core to just outside this boundary. The double waves (Configurations 4B and 4C) relocated 806 gm of uranium and the triple wave (Configuration 4D) relocated 1209 gm of uranium.

The reactivity worth of these waves was as follows:

Configuration	Reactivity Worth (%Δk)
4A	0.243 ± 0.027
4B	0.433 ± 0.017
4C	0.222 ± 0.027
4D	0.532 ± 0.024

It will be noted here that there was a large difference between 4B and 4C and yet they were both double waves. In order to better understand what was happening, Configuration 4A was reversed so that the void within the active core was at the separation plane and the portion of the wave extending beyond the active core was over stage 2. This caused an increase in excess reactivity of 0.122 ± 0.017%Δk. This increase was only half the amount noted above for Configuration 4A and explains in part the difference between 4B and 4C. The center wave of Configuration 4D was also measured to be worth 0.214 ± 0.013%Δk.

The sum of the single waves do not equal the worth of the multiple waves. In each case where there were single waves to compare with, the worth of the multiple waves was always less than the sum of the individual waves.

It should also be noted from the above data that Configuration 4A was worth more than the center wave of 4D. This same relationship occurred for Configurations 2 and 3. Based on these results and the aluminum worths, it appears that the separation plane is a unique area and not like the other end of the core. Of course the reactor was not structural symmetrical with respect to the two ends. There was a 30.5 cm hole through the center of the end reflector at the separation plane end, while no such hole existed at the other

end of the reactor. There was also a gap of about 1.2 cm between the two tanks plus 540 kg of aluminum in the plates of the two tanks at the separation plane.

8.2 Power Distribution Measurements - Bare Catcher Foils

Configuration 4D was power mapped with both bare and cadmium covered catcher foils within the cavity region. These data are given in Table 8.1. Only a few cadmium covered foils were exposed and these are given at the end of Table 8.1 along with the resultant cadmium ratios.

Figures 8.6 and 8.7 show the axial and radial power profiles normalized to the center of the core. The axial profiles shown in Figure 8.6 were averaged and these averages were used to produce the radial profile in Figure 8.7. The volume weighted average for the active core was 1.99 with respect to the core center. Figure 8.6 distinctly shows the effects of the waves. The distribution at 53.3 cm from the center of the core was at the inner surface of the void region while the profile at 68.6 cm was at the outer surface of the portion of the wave extending beyond the normal active core boundary, which was at 61.0 cm from the center of the core. The catcher foils were nominally 1.43 cm in diameter and thus represent an integrated power over the foil cross section. Some portions of the waves show steep power gradients which are somewhat undefined because of the relatively large foils. However, finer resolution (use of smaller foils) to obtain better detail did not seem justified since the dispersal of fuel sheets in the waves is a significant factor affecting the observed power distribution. The importance of fine resolution of power distribution effects in an operating power reactor is not as great in a gaseous core as in a solid core since variations in temperature at or near the core boundary will likely have little effect on the temperature distribution in the structural material.

It is interesting to note that where the trough in the wave comes at the end of the core and the fuel wave crest follows in the next stage of the fuel element, there is a considerable depression in power over the void region. This does not occur on waves in which the reserve order of crest and trough exists, i.e., where the trough portion of the wave is in the second stage of fuel from end of the core, while the crest is at the very end at the separation plane. These observations accounts for part or all of the reactivity difference noted between Configuration 4A and its reverse wave.

The 823.2 gm of U^{235} in the radial reflector fuel annulus generated 2.09 watts of power or 0.136 of the total core power. Extrapolating to 1 kg of fuel in the annulus gives a power fraction of 0.160.

All of the power mapping was performed at an average D_2O temperature of 26°C. Actuators 1, 2, and 3 were fully withdrawn and Actuators 4, 5, and 6 were equally withdrawn 9.8 cm on the average.

8.3 Catcher Foil Cadmium Ratios

As stated in the previous section, cadmium covered catcher foil data were minimal and are given at the end of Table 8.1. These values were plotted in Figures 8.8 and 8.9. At the core center the ratio was 6.2 and this increased to 17.0 at the outer edge of the fuel (61.0 cm from the center of the core). It will be noted from Figure 8.8 that at the radial center of the reactor, the separation plane had a cadmium ratio of 15.2 while the opposite end of the core showed a ratio of 10.9. The hole in the center of the movable tank which simulates the exhaust nozzle allows additional thermal flux to reach the core and causes the higher cadmium ratio at the separation plane.

8.4 Resonance Detector Data - Bare Gold Foils

Both bare and cadmium covered gold foils (0.0005 cm thick) were exposed in the cavity and reflector regions of this reactor. The data were obtained in five exposures and each exposure was power normalized to the first run (Run 1143) as shown in Table 8.2.

All of the gold foil data are given in Table 8.3. Figures 8.10 and 8.11 show the relative bare gold foil distribution within the cavity. As with the catcher foils, the axial profiles were averaged and the averages were plotted to give the radial profile. The volume weighted average over the active core was 1.223 normalized to 1.0 at the center of the core. The gold foil detail around the waves was less than the detail with catcher foils since the power distribution was of the most interest.

Both the bare and cadmium covered gold foil distributions within the reflector regions are presented in Figures 8.12 and 8.13. The peak bare foil activity is about the same in the two reflectors.

8.5 Gold Foil Cadmium Ratios

The gold foil cadmium ratios are given in Table 8.4 and are plotted in Figures 8.14, 8.15, and 8.16. The values given here are based on infinitely dilute foil activities. In the cavity the data fall within 5% of a smooth curve but there is larger data scatter than this in the reflector regions because of the lower epi-thermal fluxes. No repeat measurements were made to resolve the points with apparent anomalous results.

8.6 Thermal Neutron Flux

Where both bare and cadmium covered gold foil data were available, thermal neutron flux was calculated and reduced to neutrons per cm^2 per second per watt of active core power. The power generation rate in the fuel annulus was not factored into the core power when normalizing the data. The calculated values are presented in Table 8.4 and Figures 8,17 and 8.18.

TABLE 8.1

Catcher Foil Data

Wave Configuration 4D

Foil No.	Type	Location Radial (cm)	Location Axial (cm)	Normalized Counts	Local to Foil (X)
Run 1143					
1	Bare	0	93.3	48740	2.083
2	Bare	0	105.3	40550	1.733
3	Bare	0	120.6	26629	1.138
4	Bare	0	135.8	24957	1.066
5	Bare	0	151.1	23403	1.000 (X)
6	Bare	0	166.3	25075	1.071
7	Bare	0	181.5	29214	1.248
8	Bare	0	196.8	35731	1.527
9	Bare	0	208.8	62799	2.683
10	Bare	30.5	93.3	56815	2.428
11	Bare	30.5	105.3	39189	1.675
12	Bare	30.5	120.6	31805	1.359
13	Bare	30.5	135.8	32206	1.376
14	Bare	30.5	151.1	30848	1.318
15	Bare	30.5	166.3	32959	1.408
16	Bare	30.5	181.5	32858	1.404
17	Bare	30.5	196.8	39789	1.700
18	Bare	30.5	208.8	56776	2.426
19	Bare	53.3	93.3	79222	3.385
20	Bare	53.3	96.3	70936	3.031
21	Bare	53.3	101.1	48624	2.078
22	Bare	53.3	105.3	56591	2.418
23	Bare	53.3	120.6	57769	2.468
24	Bare	53.3	135.8	49124	2.099
25	Bare	53.3	147.4	55203	2.359
26	Bare	53.3	141.1	51203	2.188
27	Bare	53.3	154.7	56947	2.433
28	Bare	53.3	166.3	49082	2.097
29	Bare	53.3	181.5	47516	2.030
30	Bare	53.3	198.5	68447	2.925
31	Bare	53.3	205.8	70600	3.017
32	Bare	53.3	208.8	70390	3.008
33	Bare	61.0	93.3	83322	3.560
34	Bare	61.0	96.3	85351	3.647
35	Bare	61.0	101.1	74289	3.174
36	Bare	61.0	105.3	68564	2.930
37	Bare	61.0	120.6	81362	3.477
38	Bare	61.0	135.8	81932	3.501
39	Bare	61.0	147.4	81434	3.480
40	Bare	61.0	151.1	71891	3.072

TABLE 8.1

(Continued)

Foil No.	Foil Type	Location Radial (cm)	Location Axial (cm)	Normalized Counts	Local to Foil (X)
Run 1143 (Cont'd)					
41	Bare	61.0	154.7	66271	2.832
42	Bare	61.0	166.3	72358	3.092
43	Bare	61.0	181.5	76950	3.288
44	Bare	61.0	198.5	79273	3.387
45	Bare	61.0	205.8	76775	3.281
46	Bare	61.0	208.8	79736	3.407
47	Bare	68.6	93.3	97868	4.182
48	Bare	68.6	96.3	97597	4.170
49	Bare	68.6	101.1	91939	3.929
50	Bare	68.6	105.3	83764	3.665
51	Bare	68.6	120.6	80572	3.443
52	Bare	68.6	135.8	81298	3.474
53	Bare	68.6	147.4	83480	3.567
54	Bare	68.6	151.1	82209	3.513
55	B re	68.6	154.7	84227	3.599
56	Bare	68.6	166.3	91828	3.924
57	Bare	68.6	181.5	83125	3.552
58	Bare	68.6	198.5	38545	1.647
59	Bare	68.6	205.8	86433	3.693
60	Bare	68.6	208.8	92471	3.951
Run 1146					
1	Bare	15.2	93.3	49751	2.126
2	Bare	15.2	105.3	32899	1.406
3	Bare	15.2	120.6	29144	1.245
4	Bare	15.2	135.8	26200	1.120
5	Bare	15.2	151.1	24725	1.056
6	Bare	15.2	166.3	24833	1.061
7	Bare	15,2	181.5	31713	1.355
8	Bare	15.2	196.8	34951	1.493
9	Bare	15.2	208.8	53050	2.267
10	Bare	45.7	93.3	62957	2.690
11	Bare	45.7	105.3	49432	2.112
12	Bare	45.7	120.6	44071	1.883
13	Bare	45.7	135.8	40980	1.751
14	Bare	45.7	151.1	46881	2.003
15	Bare	45.7	166.3	39795	1.700
16	Bare	45.7	181.5	41865	1.789
17	Bare	45.7	196.8	49665	2.122

TABLE 8.1

(Continued)

Foil No.	Type	Location Radial (cm)	Location Axial (cm)	Normalized Counts	Local to Foil (X)
Run 1146 (Cont'd)					
18	Bare	45.7	208.8	64747	2.767
19	Bare	76.2	93.3	101114	4.321
20	Bare	76.2	105.3	99756	4.263
21	Bare	76.2	120.6	96012	4.103
22	Bare	76.2	135.8	99977	4.272
23	Bare	76.2	151.1	95305	4.072
24	Bare	76.2	166.3	91963	3.930
25	Bare	76.2	181.5	98181	4.195
26	Bare	76.2	196.8	89018	3.804
27	Bare	76.2	208.8	94002	4.017
28	Bare	91.4	93.3	142711	6.098
29	Bare	91.4	105.3	147299	6.294
30	Bare	91.4	120.6	149283	6.379
31	Bare	91.4	135.8	162229	6.932
32	Bare	91.4	151.1	151059	6.455
33	Bare	91.4	166.3	159662	6.822
34	Bare	91.4	181.5	148893	6.362
35	Bare	91.4	196.8	128626	5.496
36	Bare	91.4	208.8	123030	5.257
Run 1147					
1	Bare	86.3	93.3	134967	5.767
2	Bare	86.3	105.3	124428	5.317
3	Bare	86.3	120.6	121660	5.199
4	Bare	86.3	135.8	125228	5.351
5	Bare	86.3	151.1	121477	5.191
6	Bare	86.3	166.3	133615	5.709
7	Bare	86.3	181.5	134114	5.731
8	Bare	86.3	196.8	114773	4.904
9	Bare	86.3	208.8	113833	4.864
10	Bare	111.1	128.2	260360	11.13
11	Bare	111.7	128.2	254862	10.89
12	Bare	111.1	151.1	268112	11.46
13	Bare	111.7	151.1	250379	10.70
14	Bare	111.1	174.0	239830	10.25
15	Bare	111.7	174.0	241664	10.33

TABLE 8.1

(Continued)

Foil No.	Foil Type	Location Radial (cm)	Location Axial (cm)	Normalized Counts	Local to Foil (X)
Run 1144					
1	Cd	0	93.3	4462	10.9
2	Cd	0	120.6	4084	6.5
3	Cd	0	151.1	3747	6.2
4	Cd	0	181.5	4129	7.1
5	Cd	0	208.8	4157	15.1
6	Cd	30.5	151.1	3904	7.9
7	Cd	61.0	151.1	4221	17.0
8	Cd	91.4	151.1	5063	29.8

TABLE 8.2

Power Normalization Factors

Configuration 4D

Run No.	Count Time	Decay Time (min)	Decay Factor	Counts per Minute	Corrected Counts per Minute	Norm. Factor
1143	1207.81	64.5	1.353	186290	252050	
	1209.81	66.5	1.406	178942	251592	
	1211.81	68.5	1.460	172902	252437	
					252026	1.000
1144	1453.23	60.5	1.258	199784	251328	
	1454.83	62.1	1.288	193392	249089	
	1457.23	64.5	1.353	184764	249986	
					250134	1.008
1145	1627.84	36.5	0.705	358046	252422	
	1629.84	38.5	0.746	337807	252004	
	1631.84	40.5	0.788	320312	252406	
					252277	0.999
1146	1105.09	69.0	1.473	170653	251372	
	1107.09	71.0	1.527	165366	252514	
	1109.09	73.0	1.580	161082	254510	
					252799	0.997
1147	1510.32	57.5	1.182	212188	250806	
	1512.32	59.5	1.232	203784	251062	
	154.32	61.5	1.284	195968	251623	
					251164	1.003

TABLE 8.3

Gold Foil Data

Configuration 4D

Foil No.	Foil Type	Location Radial (cm)	Location Axial (cm)	Foil Weight (gm)	Specific Activity d/m/gm x 10^{-6}	Local to Foil (X)
Run 1143						
1	Bare	0	89.4	0.0169	2.650 (1)	
2	Bare	0	74.9	0.01995	6.235	
3	Bare	0	59.6	0.0164	5.261	
4	Bare	0	44.4	0.0208	3.471	
5	Bare	0	29.1	0.0187	2.055	
6	Bare	0	13.9	0.0185	0.942	
7	Bare	0	0	0.0160	0.125	
8	Bare	93.2	151.1	0.0168	5.090 (1)	
9	Bare	107.7	151.1	0.0161	5.864	
10	Bare	123.0	151.1	0.0212	4.802	
11	Bare	138.2	151.1	0.0179	3.434	
12	Bare	153.5	151.1	0.0186	2.076	
13	Bare	168.7	151.1	0.0221	1.042	
14	Bare	183.9	151.1	0.0198	0.150	
Run 1144						
1	Cd Cov.	0	89.4	0.0168	1.422	
2	Cd Cov.	0	59.6	0.0181	0.306	
3	Cd Cov.	0	29.1	0.0173	0.008	
4	Cd Cov.	93.2	151.1	0.0169	1.683	
5	Cd Cov.	123.0	151.1	0.0133	0.440	
6	Cd Cov.	153.5	151.1	0.0172	0.010	
Run 1145						
1	Cd Cov.	30.5	151.1	0.0140	1.329	
2	Cd Cov.	45.7	151.1	0.0162	1.301	
3	Cd Cov.	61.0	151.1	0.0165	1.393	
4	Cd Cov.	76.2	151.1	0.0184	1.499	
5	Cd Cov.	91.4	151.1	0.0184	1.569	
6	Bare	86.3	93.3	0.0174	3.864	2.297
7	Bare	86.3	105.3	0.0206	4.024	2.392
8	Bare	86.3	120.6	0.0156	4.288	2.549
9	Bare	86.3	135.8	0.0158	4.399	2.615
10	Bare	86.3	166.3	0.0166	4.388	2.609
11	Bare	86.3	181.5	0.0182	4.092	2.433
12	Bare	86.3	196.8	0.0142	3.861	2.295

TABLE 8.3

(Continued)

Foil No.	Type	Location Radial (cm)	Location Axial (cm)	Foil Weight (gm)	Specific Activity d/m/gm x 10^{-6}	Local to Foil (X)
Run 1145 (Cont'd)						
13	Bare	86.3	208.8	0.0210	3.323	1.976
Run 1146						
1	Cd cov	0	74.9	0.01355	12.88	
2	Cd cov	0	44.4	0.0171	0.071	
3	Cd cov	107.7	151.1	0.0191	1.181	
4	Cd cov	138.2	151.1	0.0136	0.050	
5	Bare	0	93.3	0.0167	2.184	1.298
6	Bare	0	105.3	0.01975	1.737	1.033
7	Bare	0	120.6	0.01165	1.831	1.089
8	Bare	0	135.8	0.0156	1.654	0.983
9	Bare	0	151.1	0.139	1.682	1.000 (X)
10	Bare	0	166.3	0.0202	1.514	0.900
11	Bare	0	181.5	0.0189	1.709	1.016
12	Bare	0	196.8	0.0136	1.961	1.166
13	Bare	0	208.8	0.0163	2.332	1.386
14	Bare	30.5	93.3	0.0158	2.422	1.440
15	Bare	30.5	105.3	0.0171	1.906	1.133
16	Bare	30.5	120.6	0.0134	1.925	1.144
17	Bare	30.5	135.8	0.0196	1.717	1.021
18	Bare	30.5	151.1	0.0178	1.752	1.042
19	Bare	30.5	166.3	0.0190	1.721	1.023
20	Bare	30.5	181.5	0.0180	1.796	1.068
21	Bare	30.5	196.8	0.01625	1.954	1.162
22	Bare	30.5	208.8	0.0205	2.228	1.325
Run 1147						
1	Bare	0	82.5	0.0198	3.838	
2	Bare	0	67.2	0.0149	5.808	
3	Bare	0	52.0	0.0123	4.327	
4	Bare	100.1	151.1	0.0203	6.336	
5	Bare	155.4	151.1	0.0182	5.987	
6	Bare	130.6	151.1	0.0163	4.354	
7	Cd cov	0	93.3	0.0180	1.325	
8	Cd cov	0	120.6	0.0200	1.192	
9	Cd cov	0	151.1	0.0200	1.056	
10	Cd cov	0	181.5	0.0146	1.274	
11	Cd cov	0	208.8	0.0151	1.282	

TABLE 8.3

(Continued)

Foil No.	Foil Type	Location Radial (cm)	Location Axial (cm)	Foil Weight (gm)	Specific Activity d/m/gm x 10^{-6}	Local to Foil (X)
Run 1147 (Cont'd)						
12	Bare	45.7	93.3	0.0162	2.498	1.485
13	Bare	45.7	105.3	0.0175	2.145	1.275
14	Bare	45.7	120.6	0.0176	1.959	1.165
15	Bare	45.7	135.8	0.0155	1.953	1.161
16	Bare	45.7	151.1	0.0175	1.976	1.175
17	Bare	45.7	166.3	0.0157	2.018	1.200
18	Bare	45.7	181.5	0.0193	1.918	1.140
19	Bare	45.7	196.8	0.0185	2.132	1.268
20	Bare	45.7	208.8	0.0155	2.452	1.458
21	Bare	61.0	93.3	0.0164	2.890	1.718
22	Bare	61.0	105.3	0.0191	2.518	1.497
23	Bare	61.0	120.6	0.0184	2.597	1.544
24	Bare	61.0	135.8	0.0175	2.656	1.579
25	Bare	61.0	151.1	0.028	1.912	1.137
26	Bare	61.0	166.3	0.0159	2.625	1.561
27	Bare	61.0	181.5	0.0185	2.629	1.563
28	Bare	61.0	196.8	0.0136	2.744	1.631
29	Bare	61.0	208.8	0.0174	2.753	1.637
30	Bare	76.2	93.3	0.0159	3.252	1.933
31	Bare	76.2	105.3	0.0211	3.066	1.823
32	Bare	76.2	120.6	0.0182	3.217	1.913
33	Bare	76.2	135.8	0.0154	3.133	1.863
34	Bare	76.2	151.1	0.0172	3.218	1.913
35	Bare	76.2	166.3	0.0169	3.156	1.876
36	Bare	76.2	181.5	0.0166	3.162	1.880
37	Bare	76.2	196.8	0.0167	3.032	1.803
38	Bare	76.2	208.8	0.0167	2.998	1.782
39	Bare	91.4	93.3	0.0186	3.556	2.114
40	Bare	91.4	105.3	0.0152	4.009	2.383
41	Bare	91.4	120.6	0.0139	4.260	2.533
42	Bare	91.4	135.8	0.0187	4.324	2.571
43	Bare	91.4	151.1	0.0191	4.313	2.564
44	Bare	91.4	166.3	0.0192	4.264	2.535
45	Bare	91.4	181.5	0.0184	4.092	2.433
46	Bare	91.4	196.8	0.0175	3.769	2.241
47	Bare	91.4	208.8	0.0211	3.294	1.958

(1) These two values were interchanged as it was apparent that the foils were not properly identified. Interchanging these two foils results in good correlation with the other points.

TABLE 8.4

Gold Foil Cadmium Ratios and Thermal Flux

Configuration 4D

Location Radial (cm)	Axial (cm)	Cd Ratio	$n/cm^2/sec/watt$ ($\times 10^{-6}$)
0	29.1	144.539	2.391
0	44.4	28.005	3.977
0	59.6	9.923	5.775
0	74.9	3.409	5.962
0	89.4	1.490	1.433
93.2	151.1	2.143	3.966
107.7	151.1	3.119	5.395
123.0	151.1	7.151	5.170
138.2	151.1	42.147	3.958
153.5	151.1	117.130	2.414
30.5	151.1	1.238	0.613
45.7	151.1	1.312	0.828
61.0	151.1	1.312	0.892
76.2	151.1	1.617	1.967
91.4	151.1	1.967	3.229
0	93.3	1.344	0.963
0	120.6	1.182	0.476
0	151.1	1.246	0.568
0	181.5	1.252	0.632
0	208.8	1.496	1.264

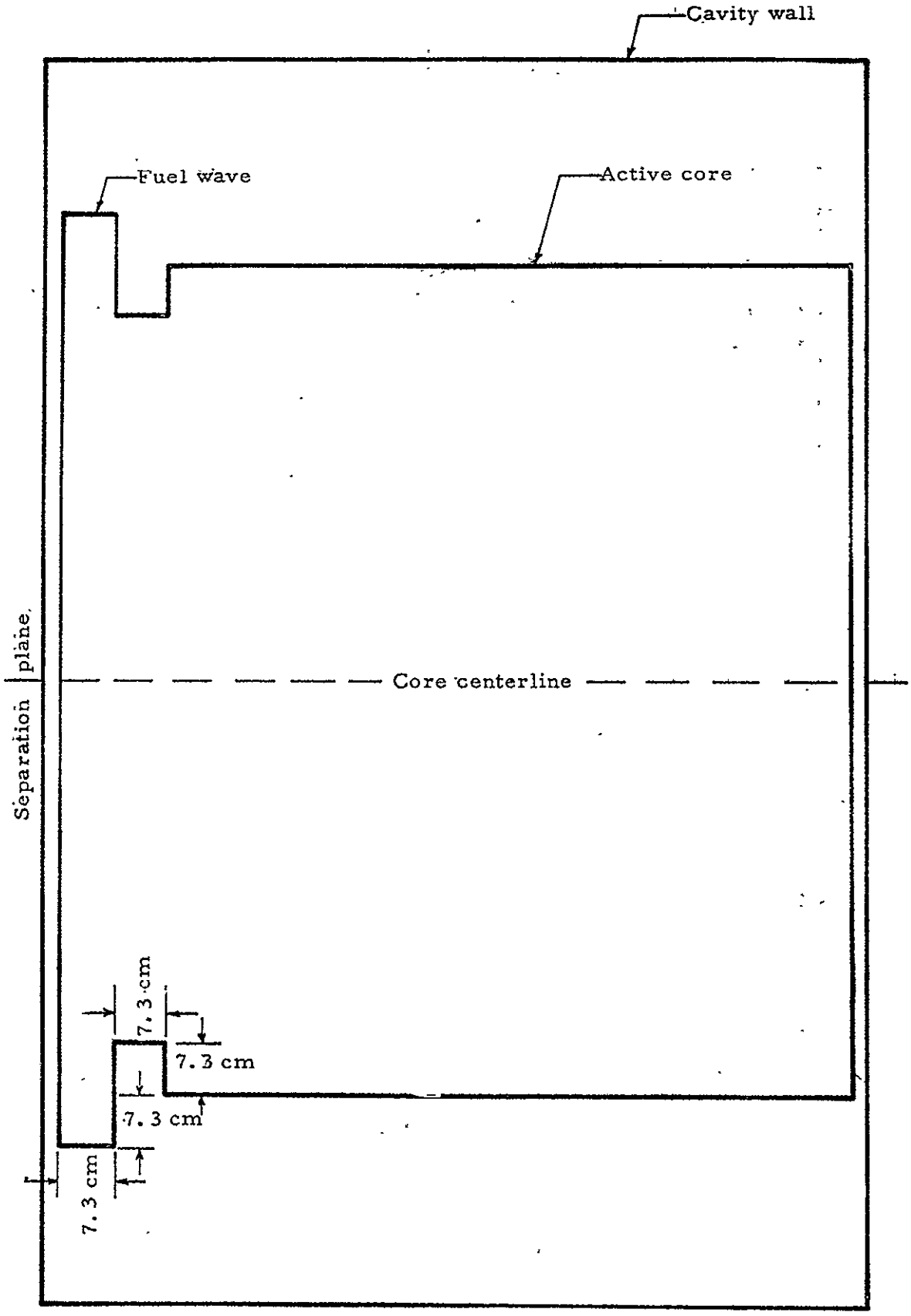

Fig. 8.1 Configuration 4A wave. 7.3 cm amplitude, no net fuel addition

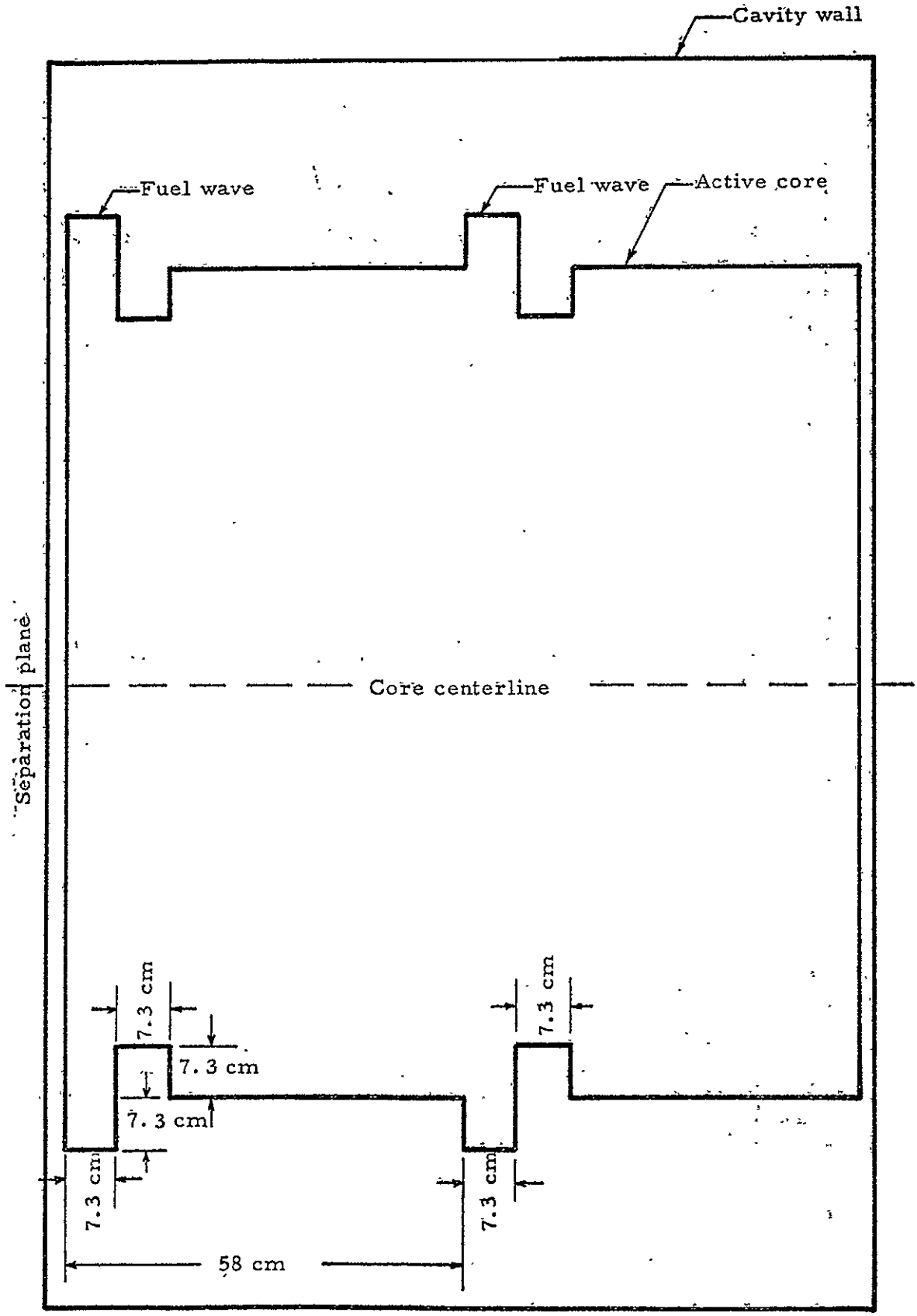

Fig. 8.2 Configuration 4B wave. 7.3 cm amplitude, no net fuel addition

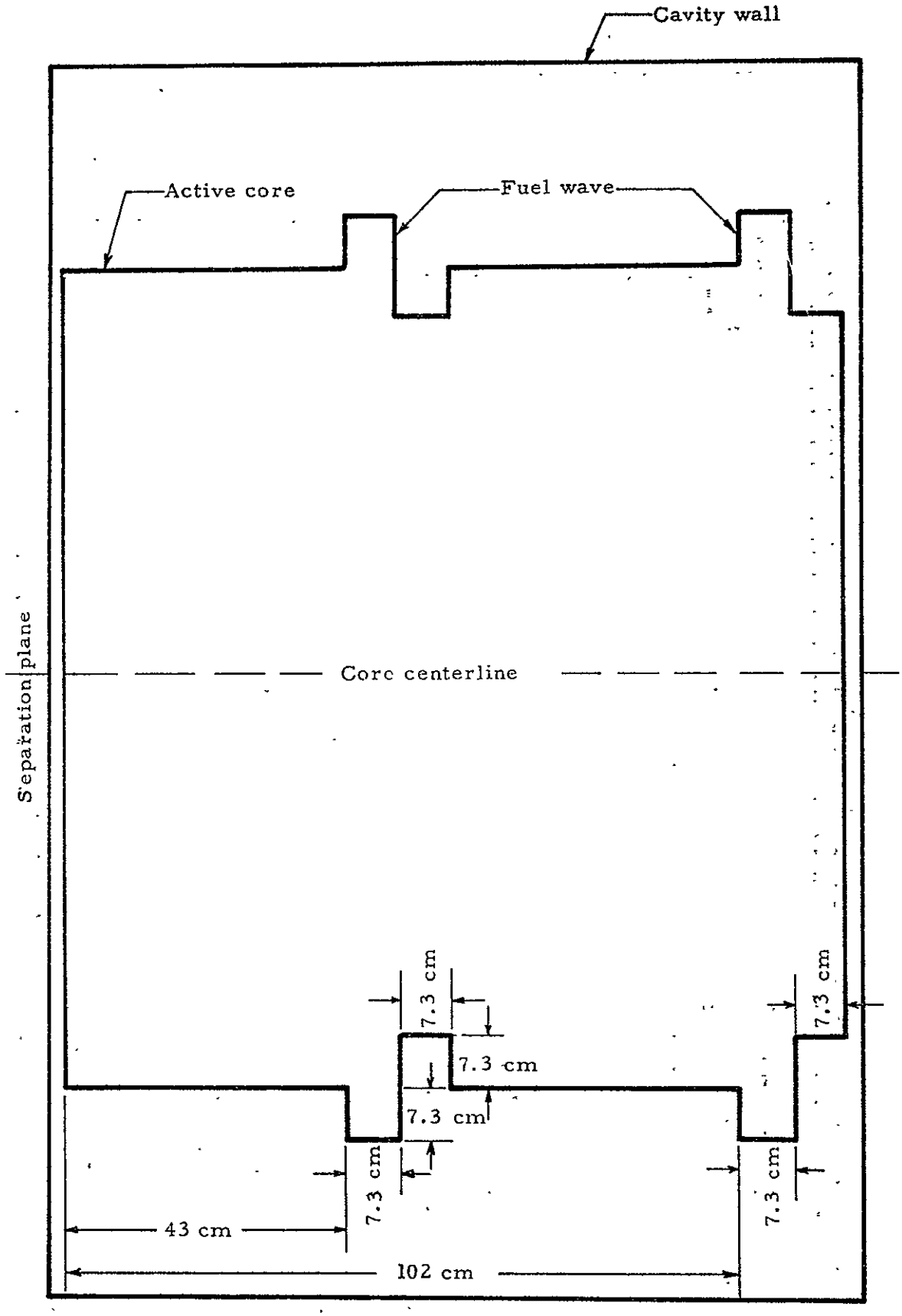

Fig. 8.3 Configuration 4C wave. 7.3 cm amplitude, no net fuel addition

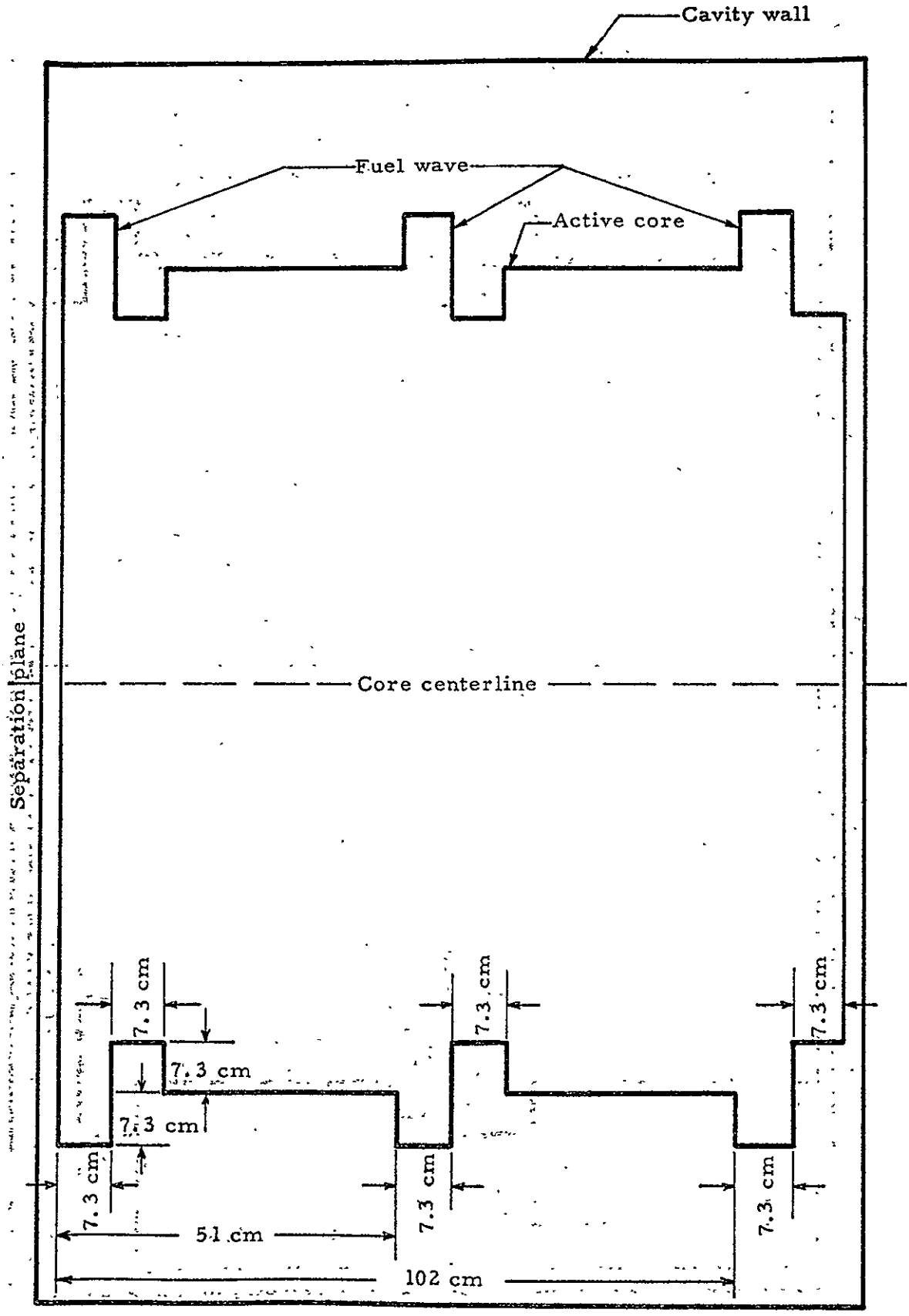

Fig. 8.4 Configuration 4D wave. 7.3 cm amplitude, no net fuel addition

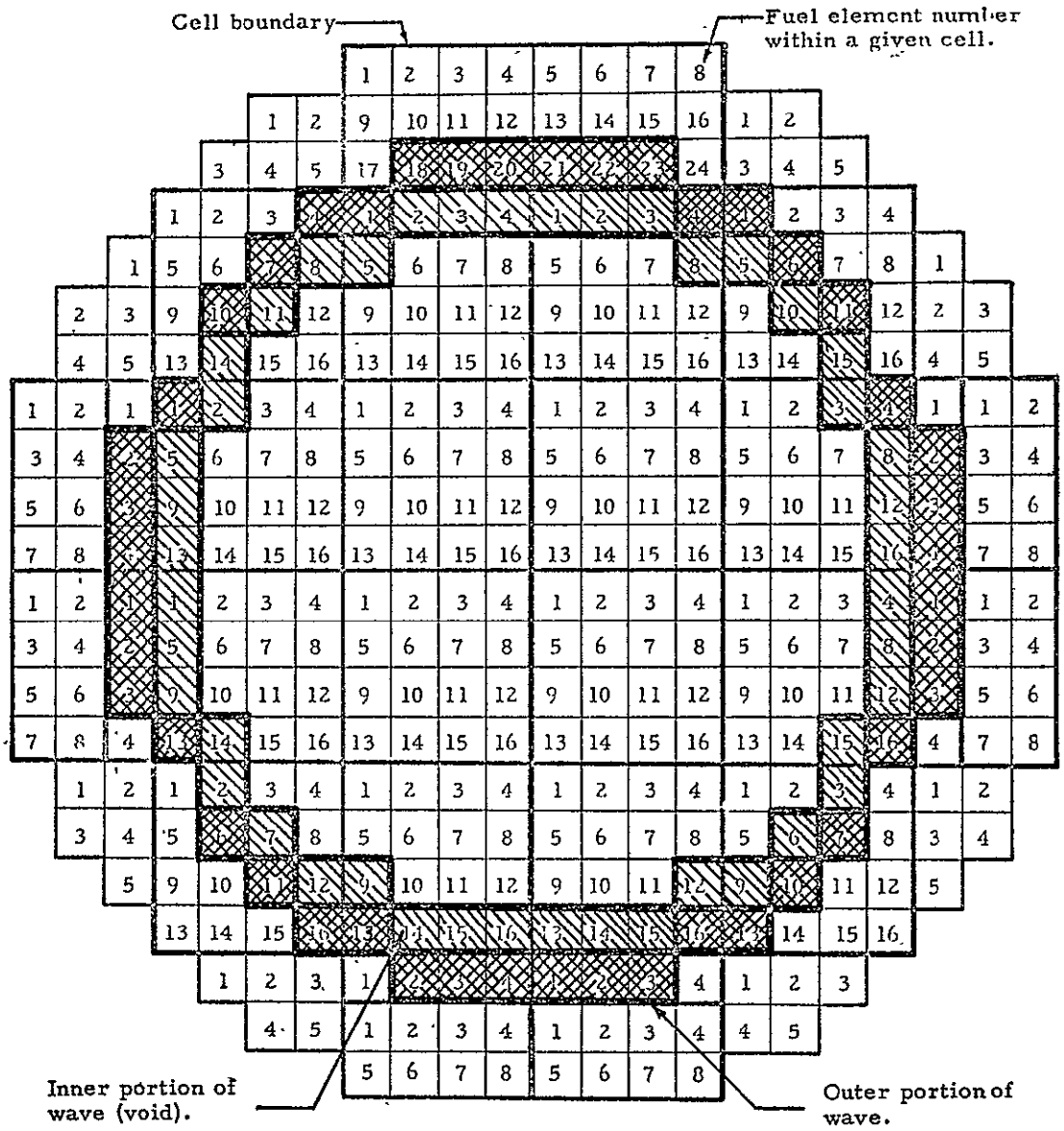

Fig. 8.5 Cross sectional view of wave - type 4 showing fuel element locations

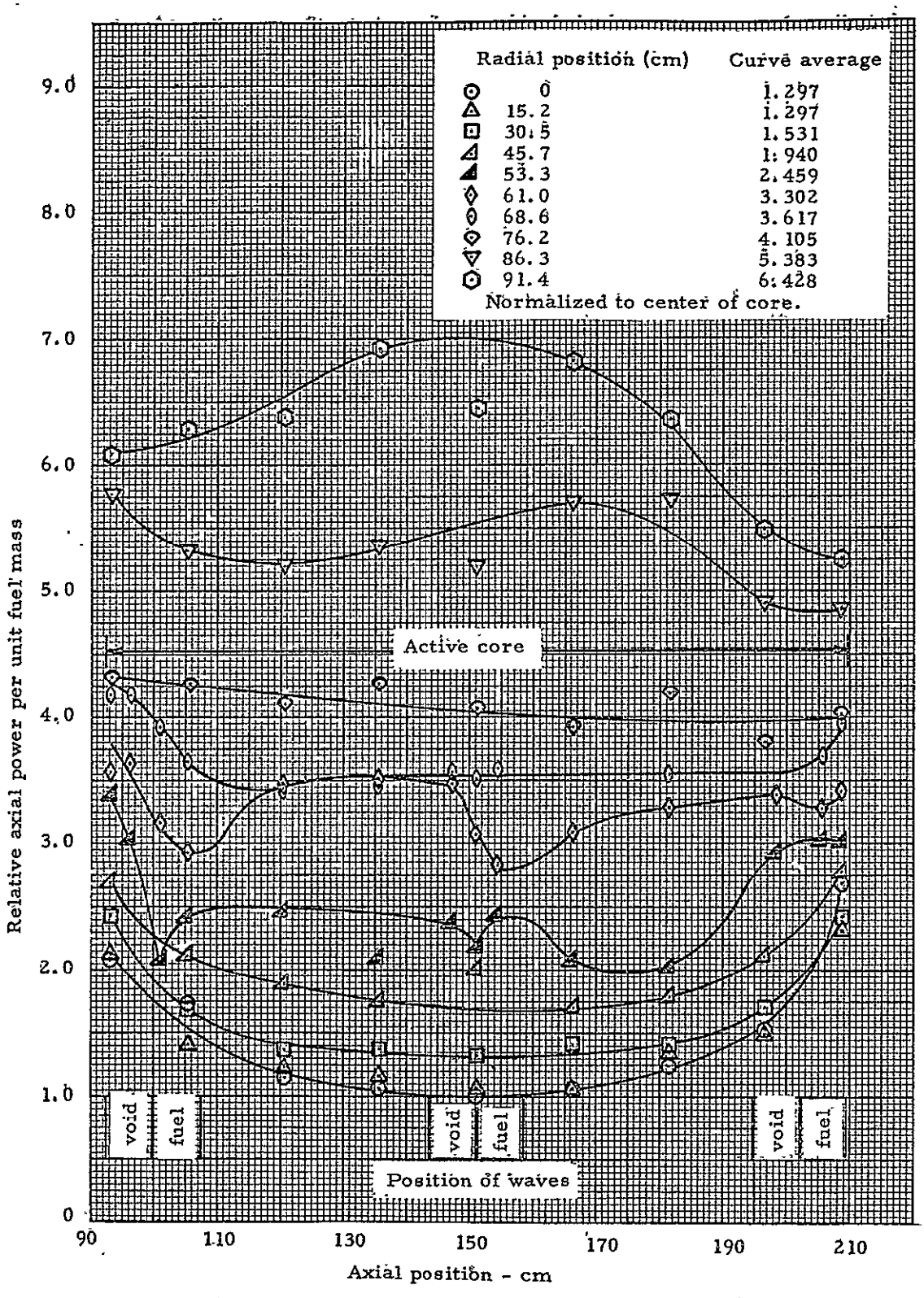

Fig. 8.6 Power distribution, configuration 4D (3 waves, 7.3 cm amplitude)

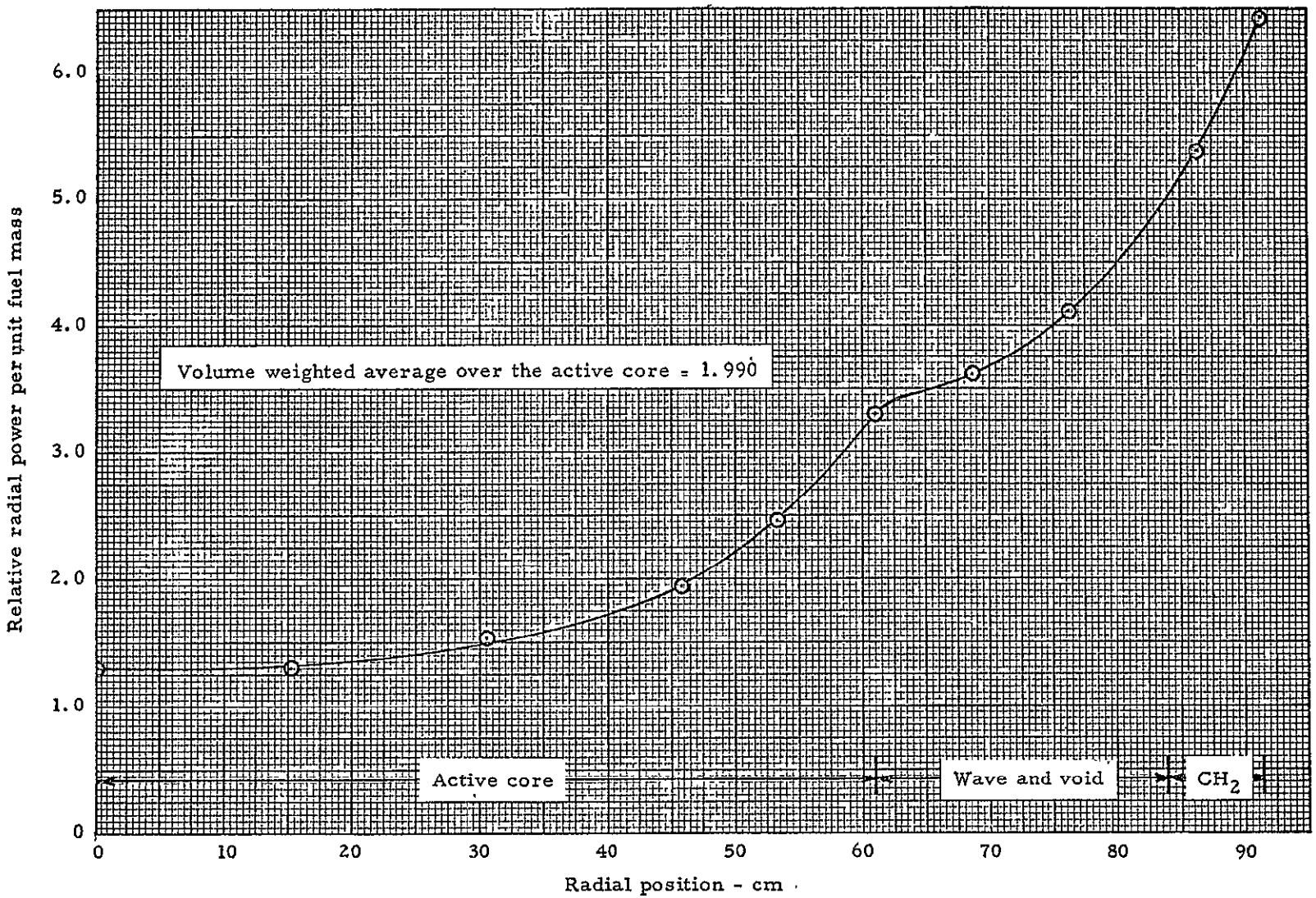

Fig. 8.7 Longitudinally averaged power distribution vs radius

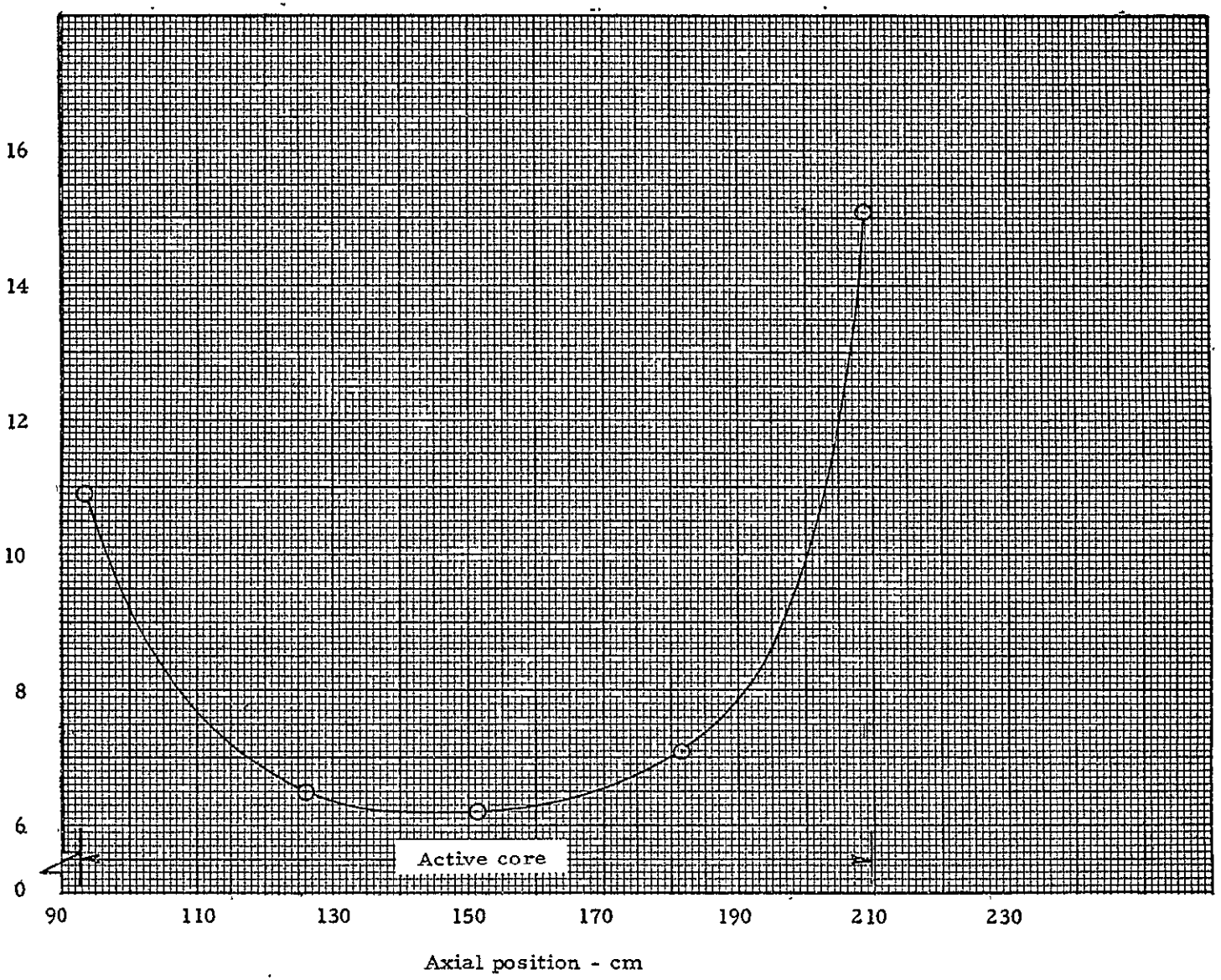

Fig. 8.8 U^{235} cadmium ratio along axis - configuration 4D

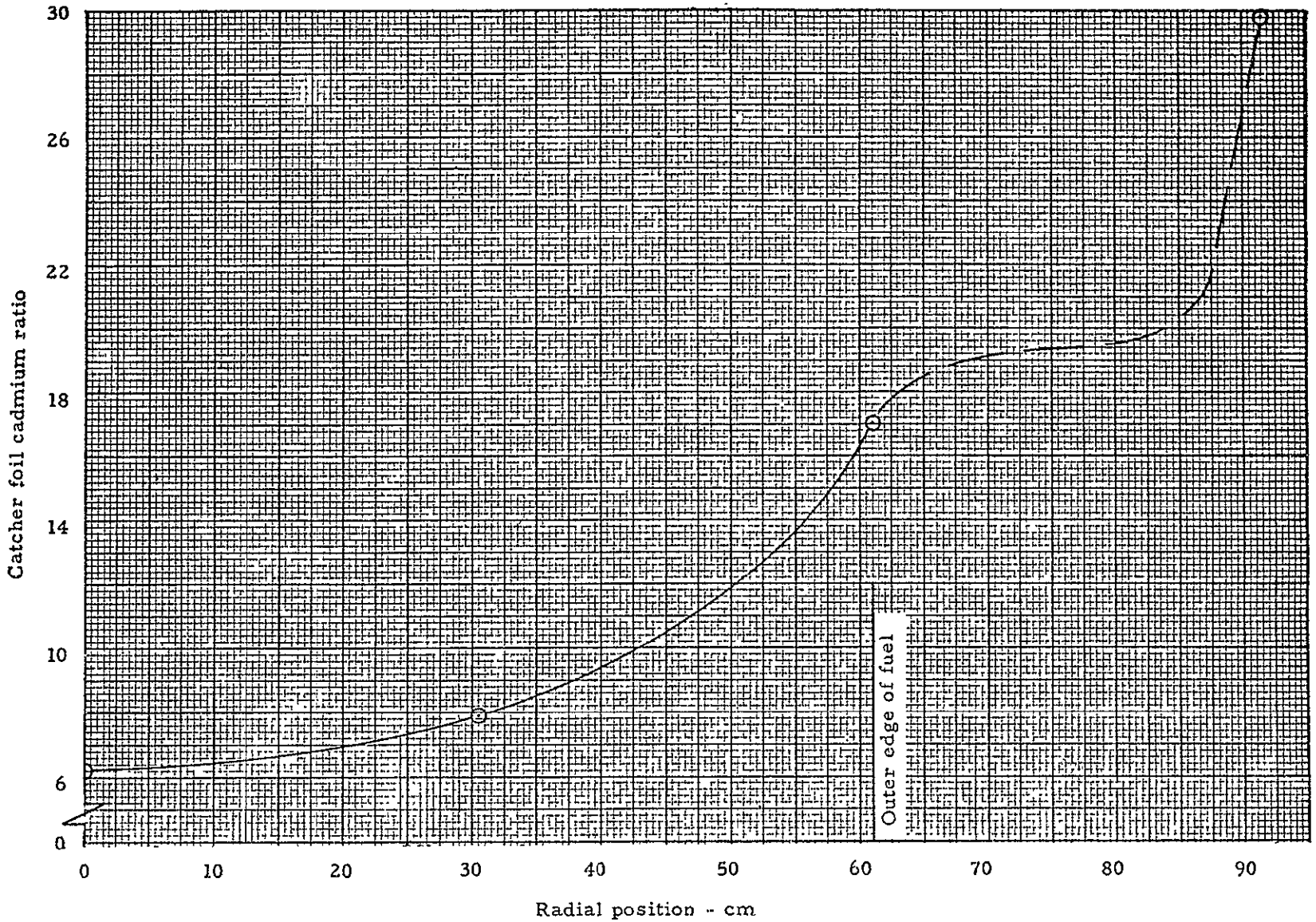

Fig. 8.9 U^{235} cadmium ratio vs radius, axial midplane in the cavity

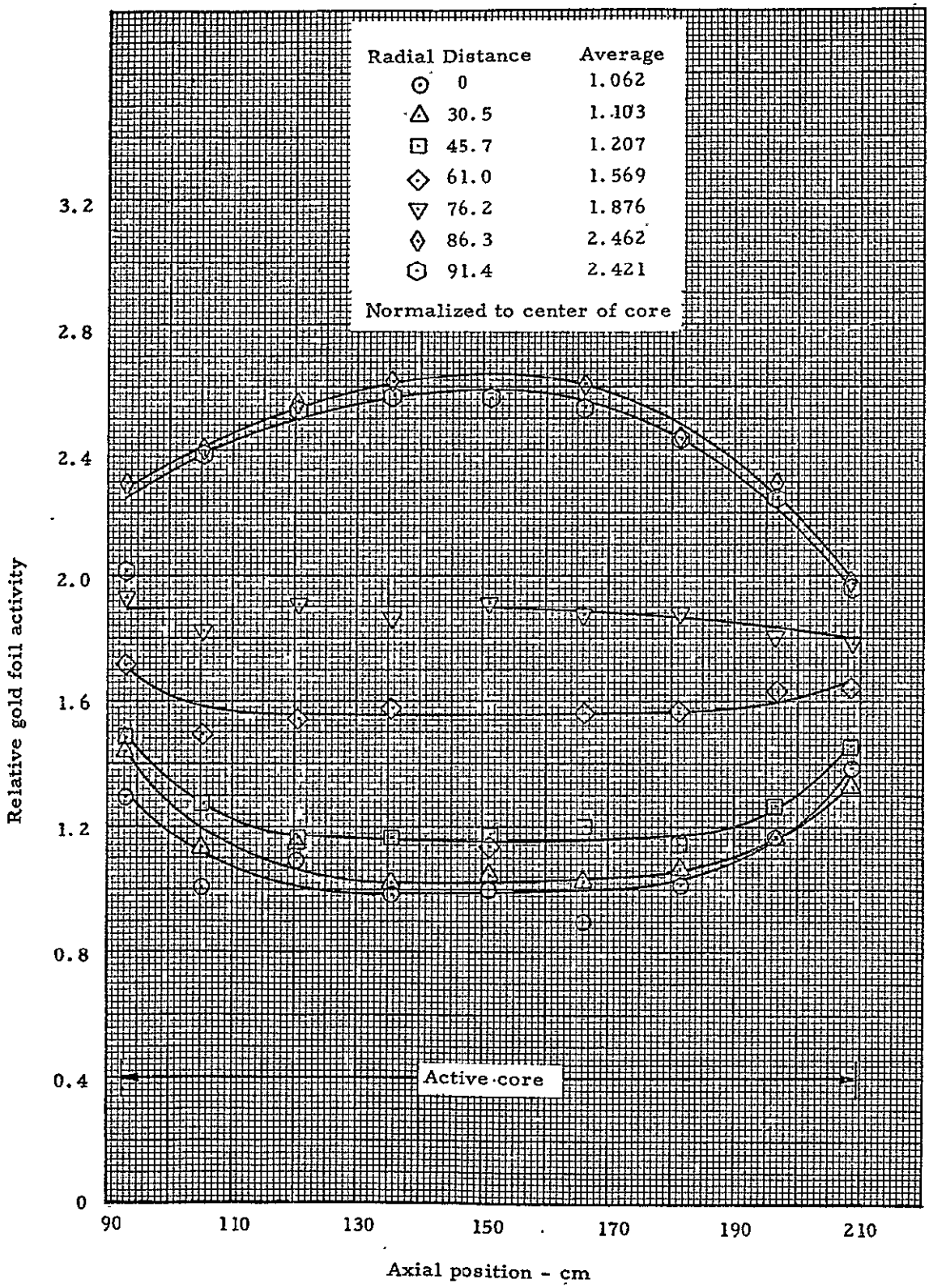

Fig. 8.10 Gold foil (0.0005 cm thick) activity in cavity

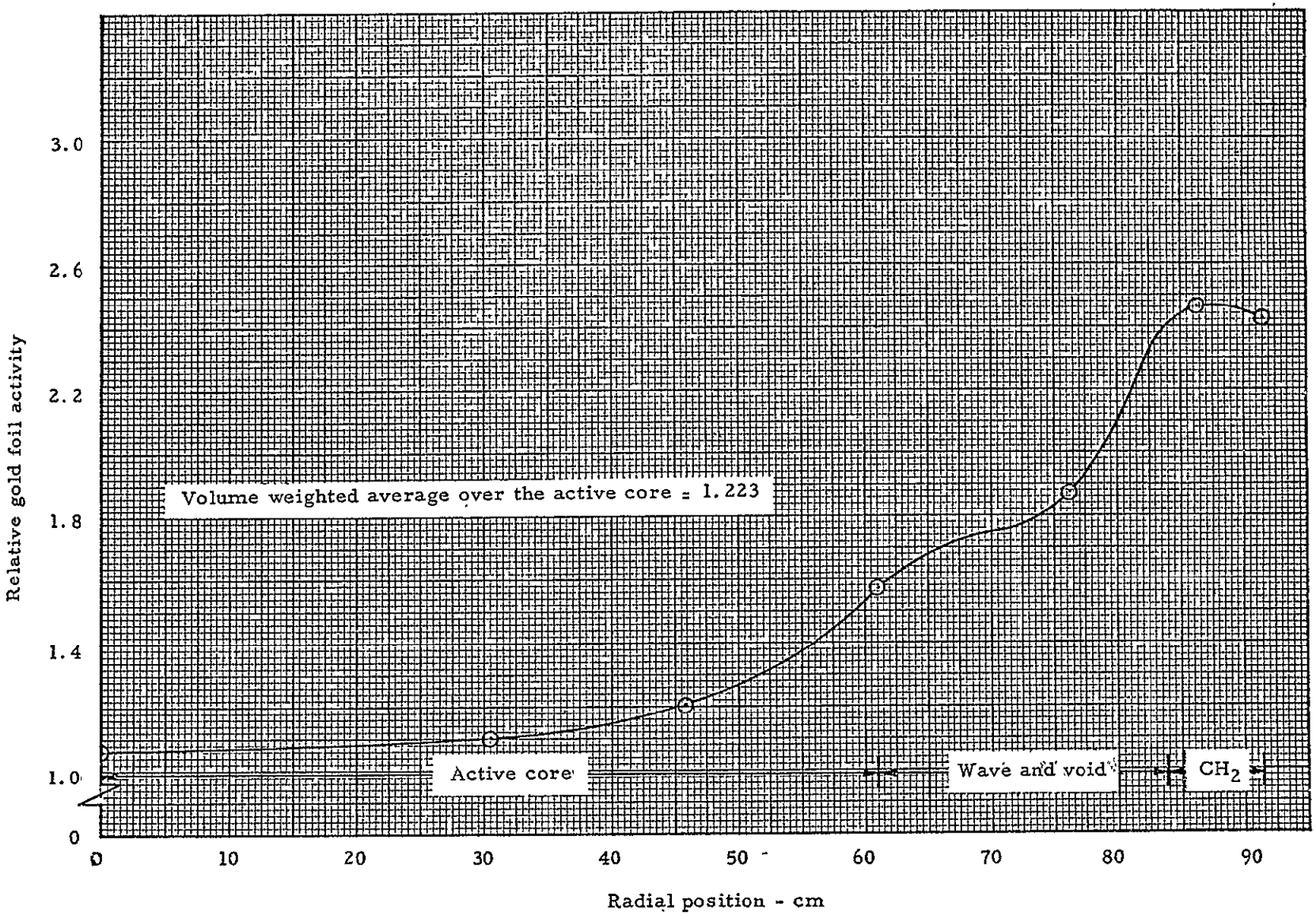

Fig. 8.11 Longitudinally averaged gold foil activity in cavity, configuration 4D

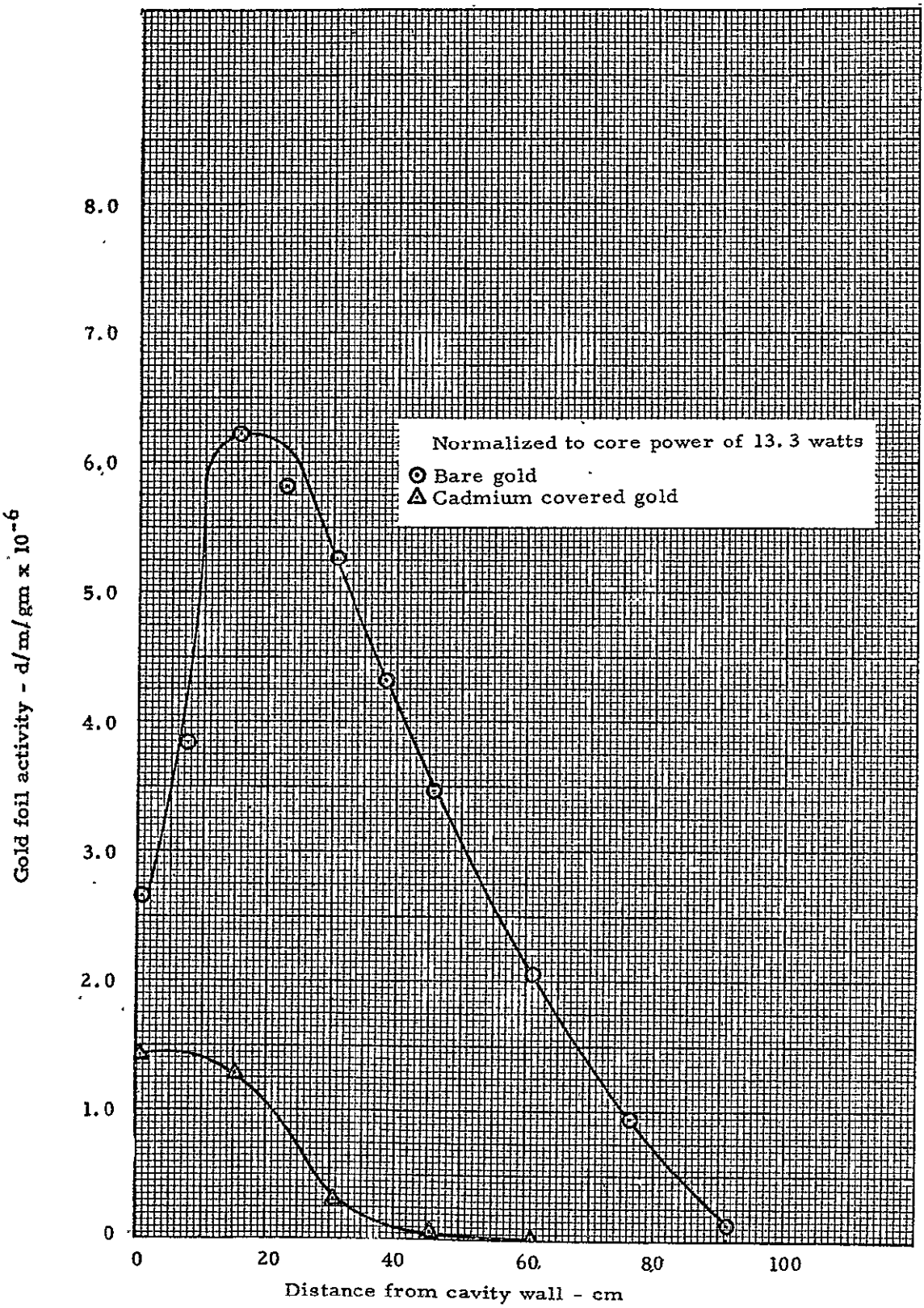

Fig. 8.12 Gold foil activity and reflector, along axis

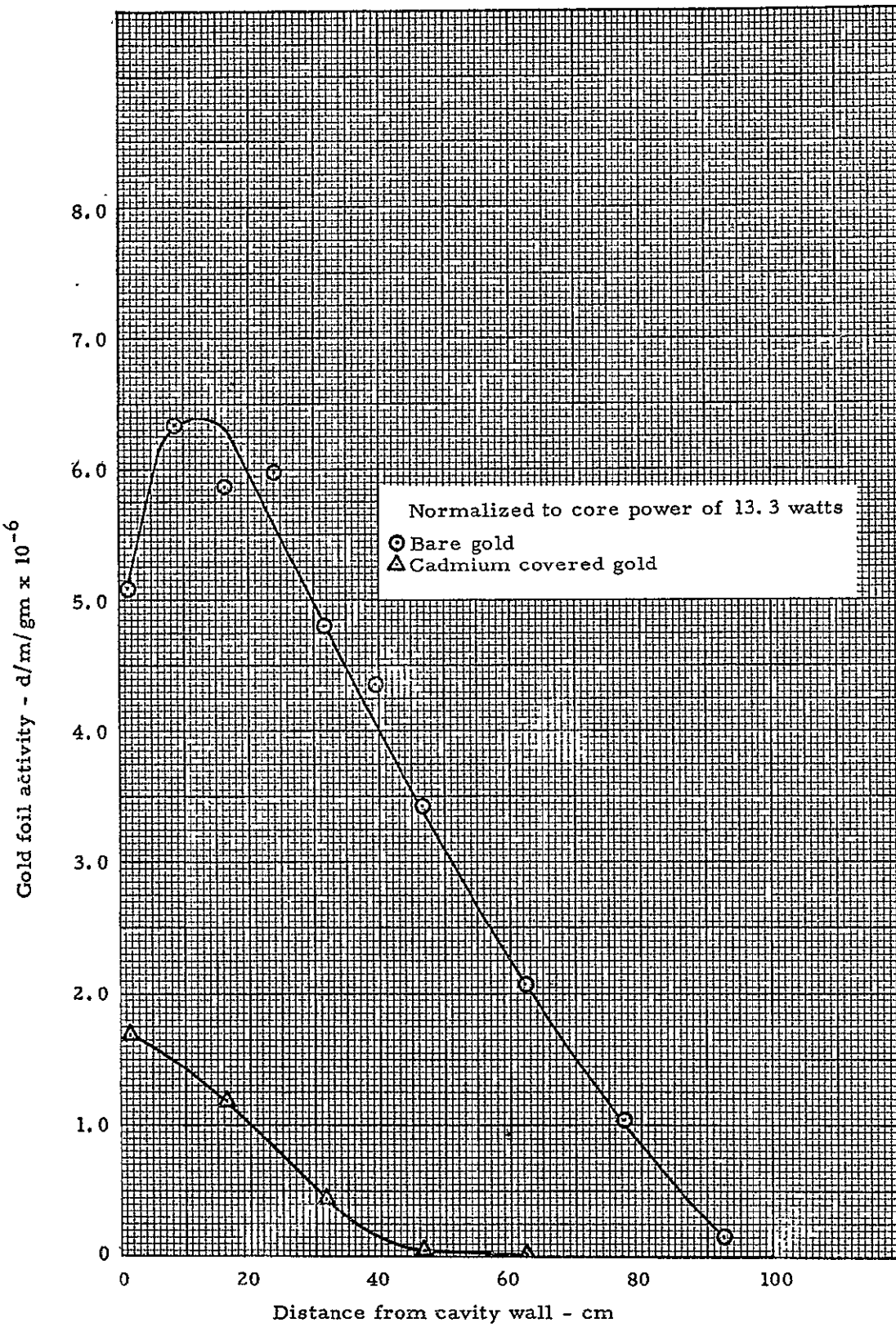

Fig. 8.13 Gold foil activity in radial reflector, axial midplane

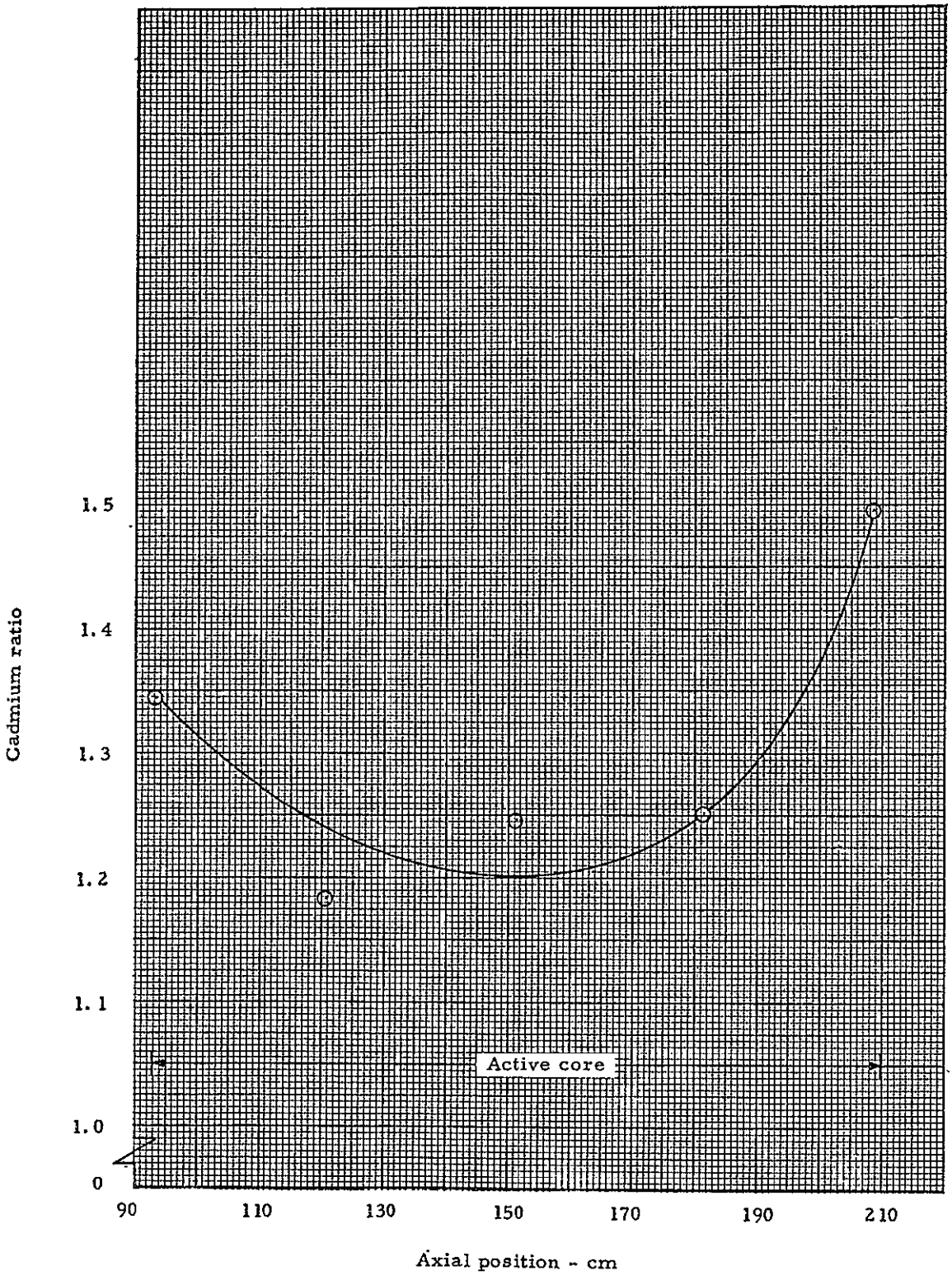

Fig. 8.14 Gold infinitely dilute cadmium ratio along axis in cavity - Configuration 4

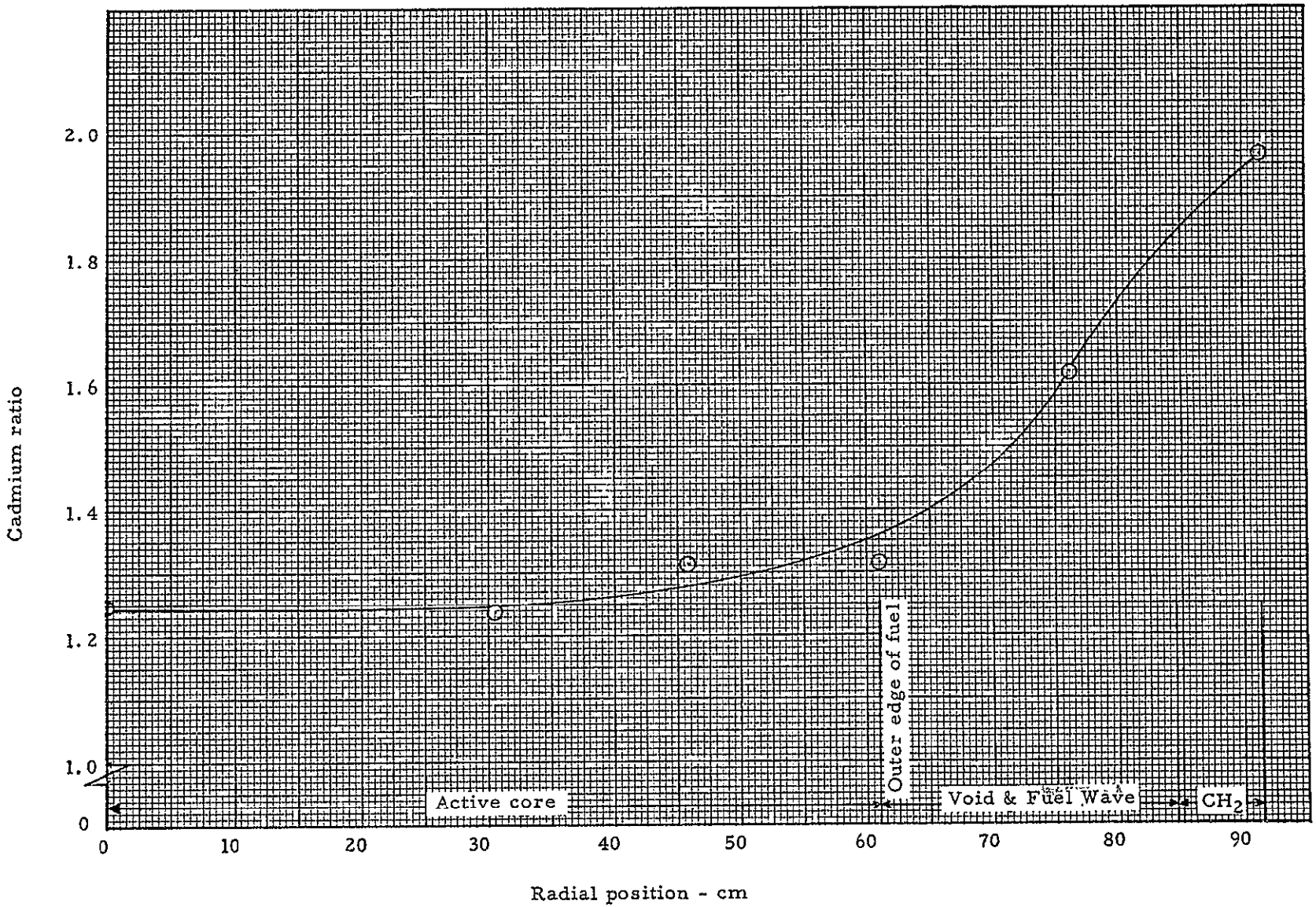

Fig. 8.15 Gold infinitely dilute cadmium ratio vs radius on axial midplane of cavity - configuration 4

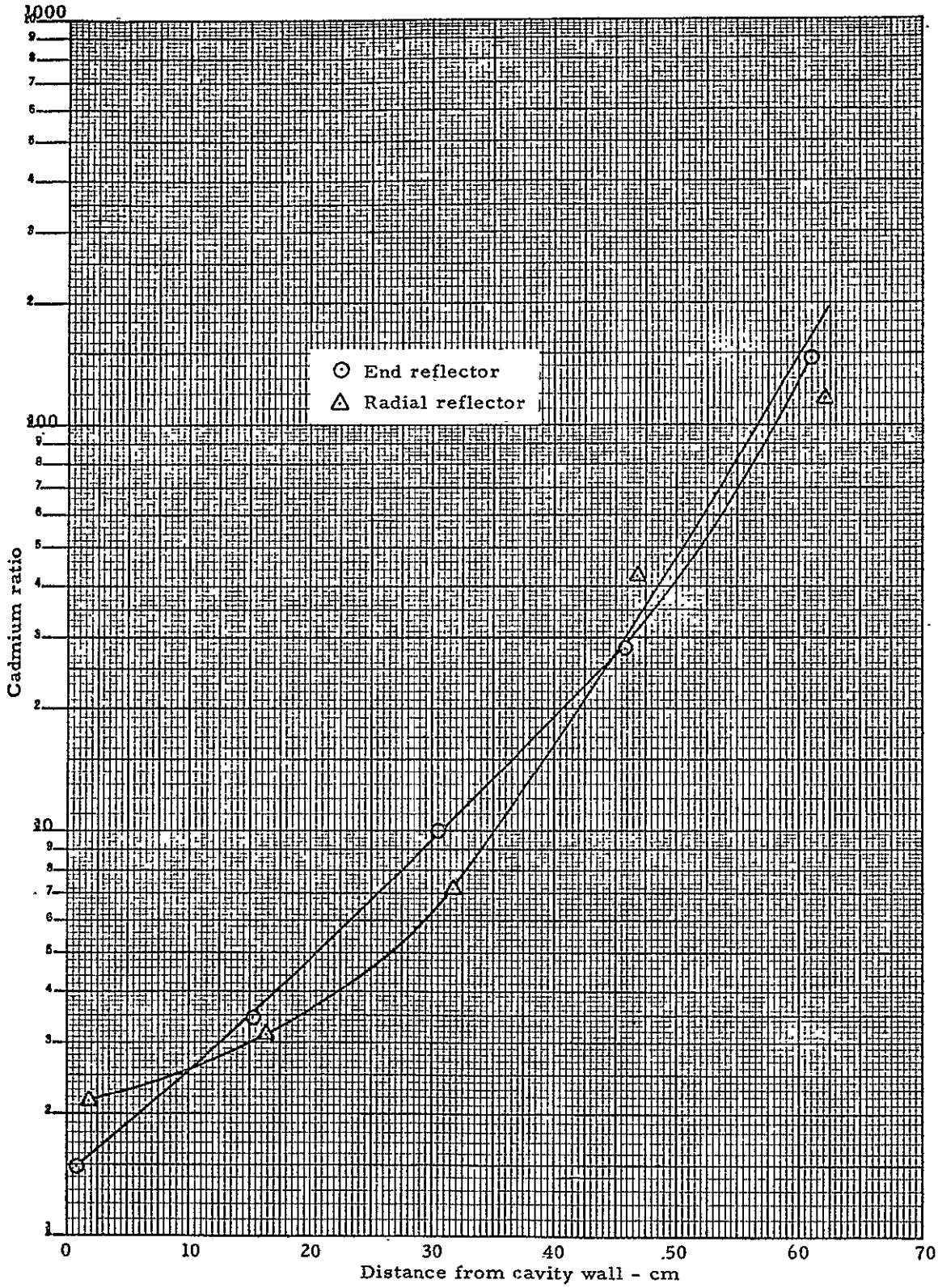

Fig. 8.16 Gold infinitely dilute cadmium ratios in the reflector - configuration 4

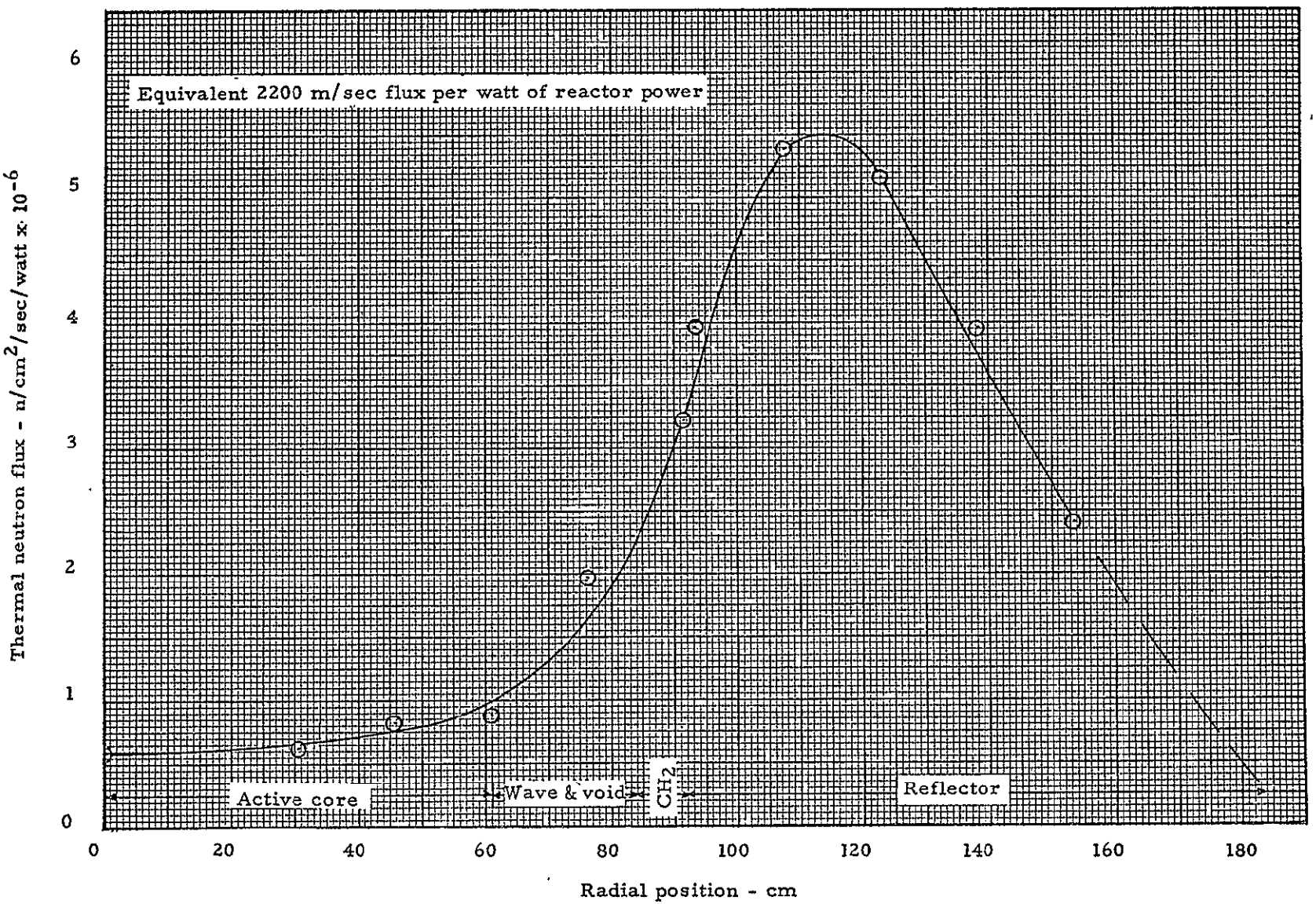

Fig. 8.17 Thermal neutron flux radial traverse at axial midplane

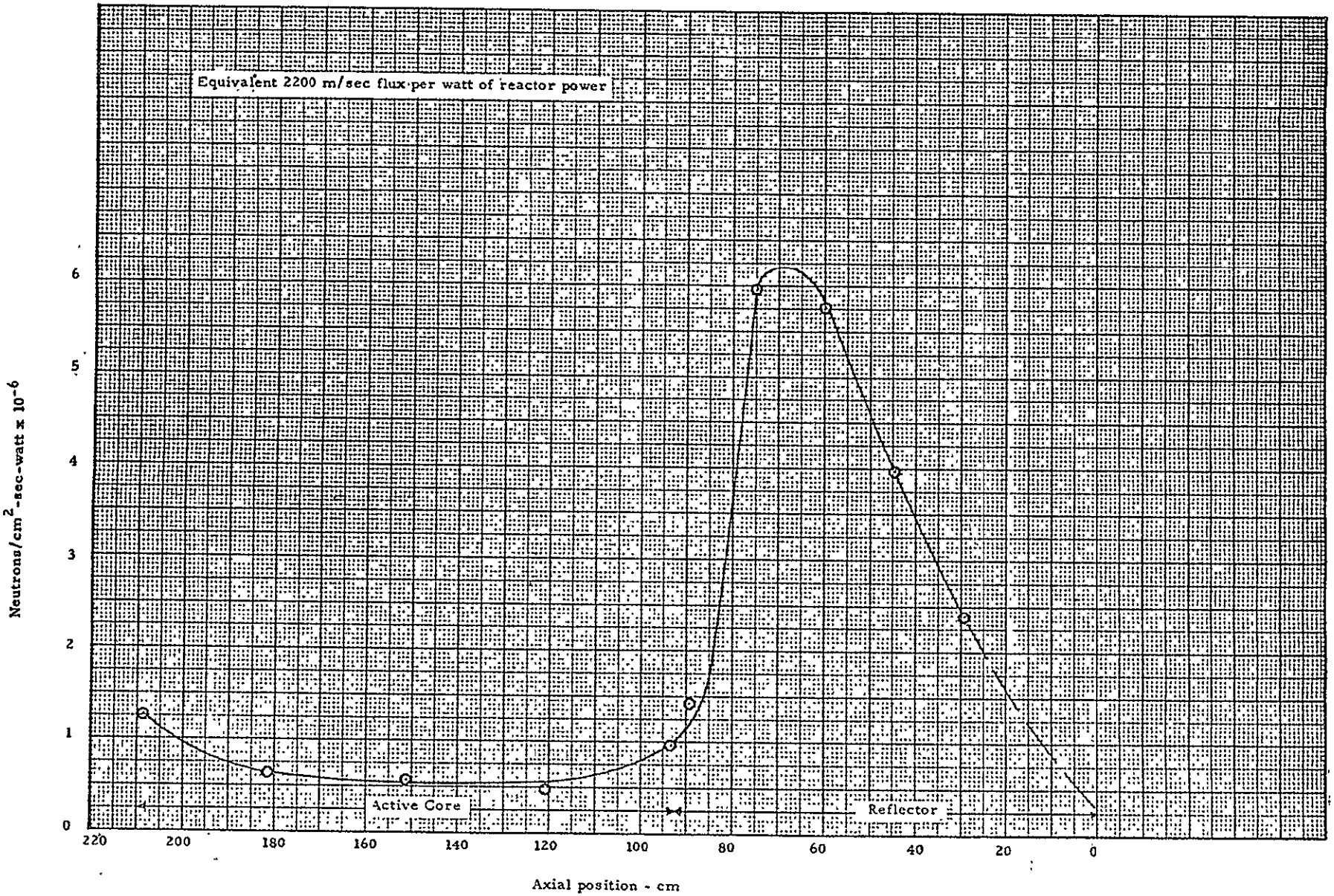

Fig. 8.18 Thermal neutron flux traverse along axis - configuration 4

9.0 CONFIGURATION 5 (22 cm waves, no addition of fuel)

Configuration 5 waves were three stages square and produced both single and double waves as shown in Figures 9.1, 9.2, and 9.3. As with Configuration 4 waves, the fuel in the reactor was conserved. Since, because of the different average radii, the volume in the portion of the wave extending beyond the core boundary was considerably more than that within the active core region, the fuel element cans containing the crests (fuel outside the normal active core boundary) were loaded with less density of uranium (less fuel per fuel element) than for those fuel element cans inside the active core boundary. Figure 9.4 shows the fuel element positions involved in the wave. The portion of the wave within the normal active core (the trough portion) affected 120 fuel elements while there were 176 positions in the outer portion (the crest) of the wave.

The total fuel shifted from within the normal active core to the region between the active core and the cavity wall was 3301 gm for Configuration 5A and 6602 gm for Configurations 5B and 5C. The wave for Configuration 5A was created first. It was necessary to add the wave in increments as follows:

1st increment, fuel removed from 21 fuel elements in the active core and 31 fuel elements added to the outer part of the wave.

Final k-excess	1.128 ± 0.015 %Δk
Initial k-excess	-0.668 ± 0.009%Δk
Gross change	0.460 ± 0.018%Δk
Worth of 2781 gm Al	+0.044 ± 0.007%Δk
Net change	0.504 ± 0.019%Δk

2nd increment (1/2 of Configuration 5A wave)

Final k-excess	1.879 ± 0.066%Δk
Initial k-excess	-0.599 ± 0.021%Δk
Gross change	1.280 ± 0.069%Δk
Worth of 7893 gm of Al	+0.126 ± 0.019%Δk
Net change	1.406 ± 0.072%Δk

The first increment extrapolates to a total wave worth of 2.891 ± 0.109%Δk while the half wave extrapolates to a total wave worth of 2.812 ± 0.144%Δk. The two values are the same within the experimental error. The portions of the wave added in the two increments are shown in Figure 9.5. Since the two measurements extrapolated to essentially the same wave worth, the total wave was not measured.

It will be noted that the initial k-excess values given above were different for the two increments. Prior to establishing any portion of the wave, the base k-excess was measured for two different rod patterns, one with Actuators 3 and 6 in the reactor and all others withdrawn, and one with all rods equally inserted. The necessity for using all rods banked was anticipated because of the large increases in reactivity due to the waves. It had been noted earlier

in the experiments that k-excess differed slightly with large changes in rod pattern. This, however, did not jeopardize the data as long as the reactivity changes were based on k-excess values using the same rod pattern.

Configuration 5B required the addition of two waves with the wave from Configuration 5A as one of the waves. The measurement was, therefore, performed by retaining Configuration 5A and adding the second wave.

The second wave was added in two increments. The first increment was 1/4 of the wave and this plus the correction for aluminum increased k-excess 0.522 ± 0.077%Δk. This value times 4 (extrapolating to the full wave) plus the worth of the other wave of 2.812 ± 0.144%Δk gives a total worth of 4.900 ± 0.340%Δk. One half of the second wave was worth 1.013 ± 0.089%Δk. The total extrapolated worth of Configuration 5B, based on this result and the worth of the first wave of 2.812 ± 0.144%Δk, was 4.838 ± 0.230%Δk. Here again the two extrapolations are about the same.

Configuration 5C required the wave from 5B to be moved back from the separation plane 14.6 cm or two stages of fuel. This was done in two equal steps. The first step caused a net decrease of 0.142 ± 0.094 %Δk. This represented 1/4 of the wave being moved from the 5B to 5C position, thus the extrapolated total decrease over Configuration 5B would be 0.568 ± 0.376%Δk and this subtracted from the worth of Configuration 5B of 4.838 ± 0.230%Δk would give a net worth of 4.270 ± 0.431%Δk. The second increment completed moving the 180 degree portion of Configuration 5C into place. The total difference between the 180 degree portions of Configurations 5B and 5C was -0.321 ± 0.102%Δk. Extrapolating to the total difference between the two waves and subtracting from 4.838 ± 0.230%Δk gives a net worth of Configuration 5C of 4.196 ± 0.279%Δk.

In each of the above waves, the addition was made in increments and in each case the extrapolated total wave worth was slightly (approximately 2%) lower for the second increment. Although within the indicated standard error of the measurement, it appears that the consistency of the results implies a non-linearity of the extrapolated values of about 2%. The following summarizes these values:

Configuration	Wave Worths (%Δk)	
	1st Increment	2nd Increment
5A	2.891 ± 0.109	2.812 ± 0.144
5B	4.900 ± 0.340	4.838 ± 0.230
5C	4.270 ± 0.431	4.196 ± 0.279

On the average, the extrapolation from the second increment was less than 2% below the extrapolation from the first increment. It is concluded that the values measured for a 180 degree sector of the waves can be extrapolated to the total with a small possible error (approximately 2%) but well within the experimental errors quoted.

Configuration 5C showed a significant decrease over 5B for the same reason the reverse of Configuration 4A decreased in worth. Creating the void (trough) at the ends of the core and moving the fuel to the outside of the active core (the crest) at a position not at the ends of the core consistently give less increase in reactivity than when the crest of the wave occurred at the end of the core. This is a logical effect since the fuel within the active core is worth more at the outer surface and removing fuel where more outer surface is involved would cause a smaller change in reactivity for the wave such as Configuration 5C.

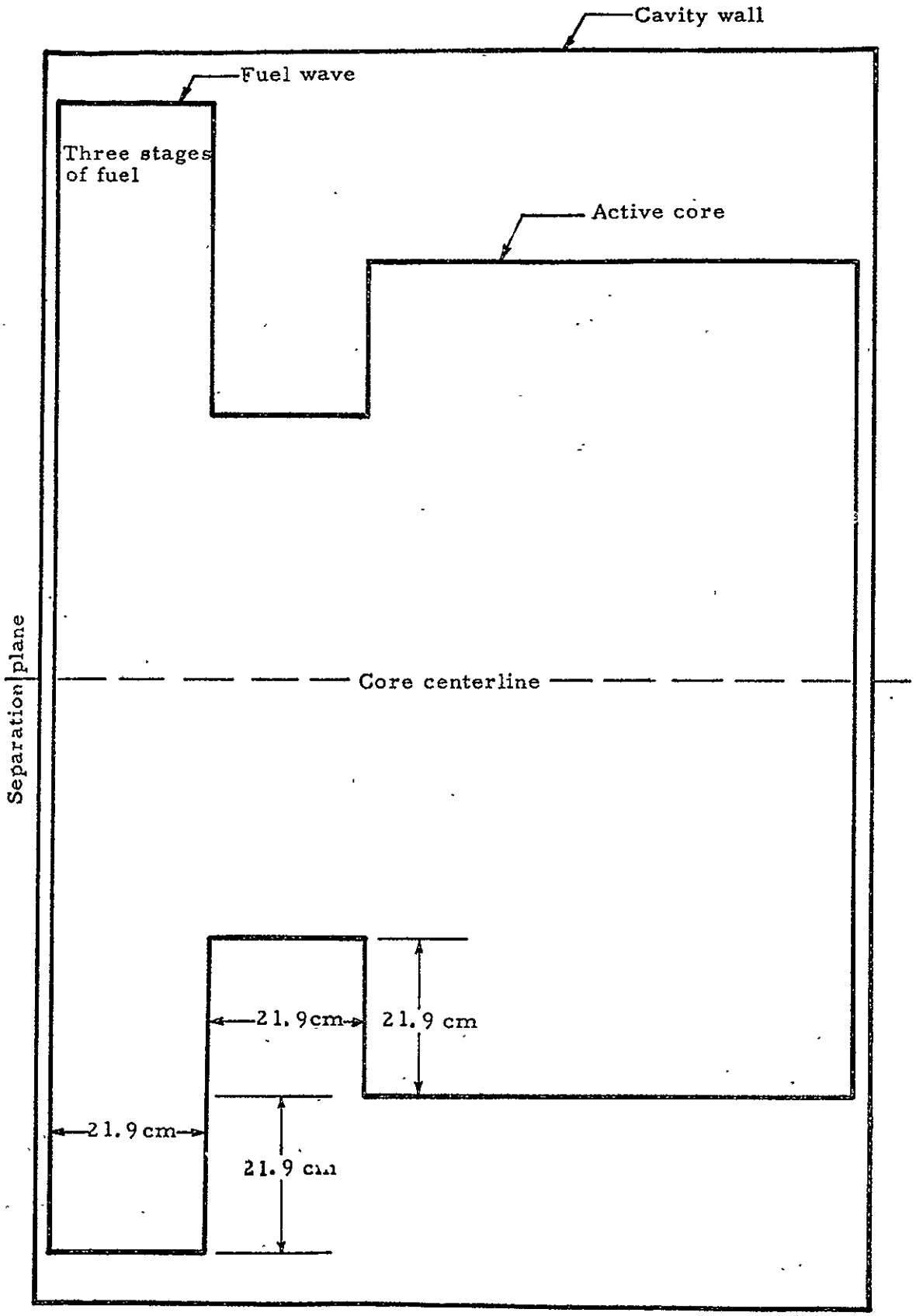

Fig. 9.1 Configuration 5A wave. 22 cm amplitude, no net fuel addition

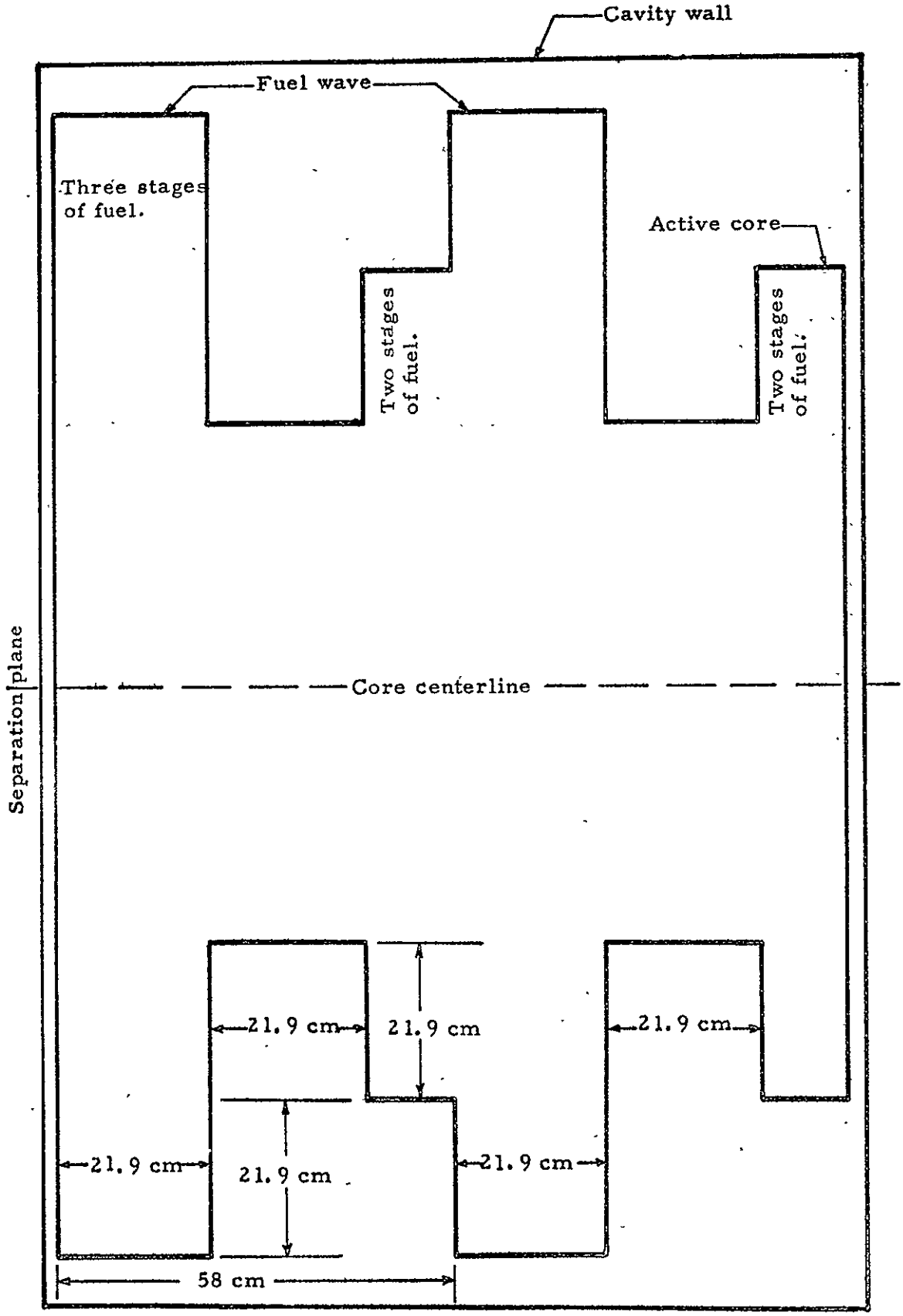

Fig. 9.2 Configuration 5B wave. 22 cm amplitude, no net fuel addition

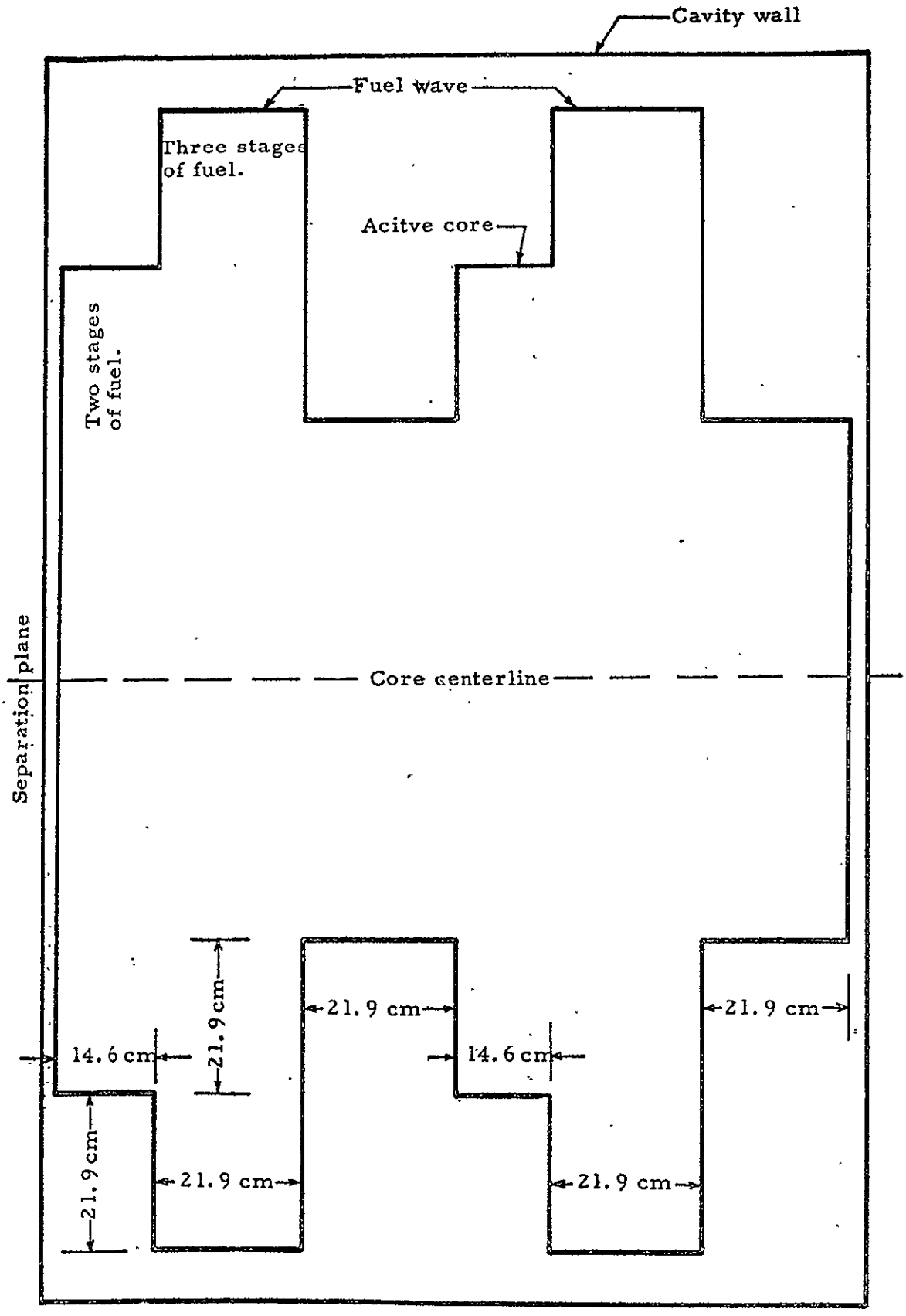

Fig. 9.3 Configuration 5C wave. 22 cm amplitude, no net fuel addition

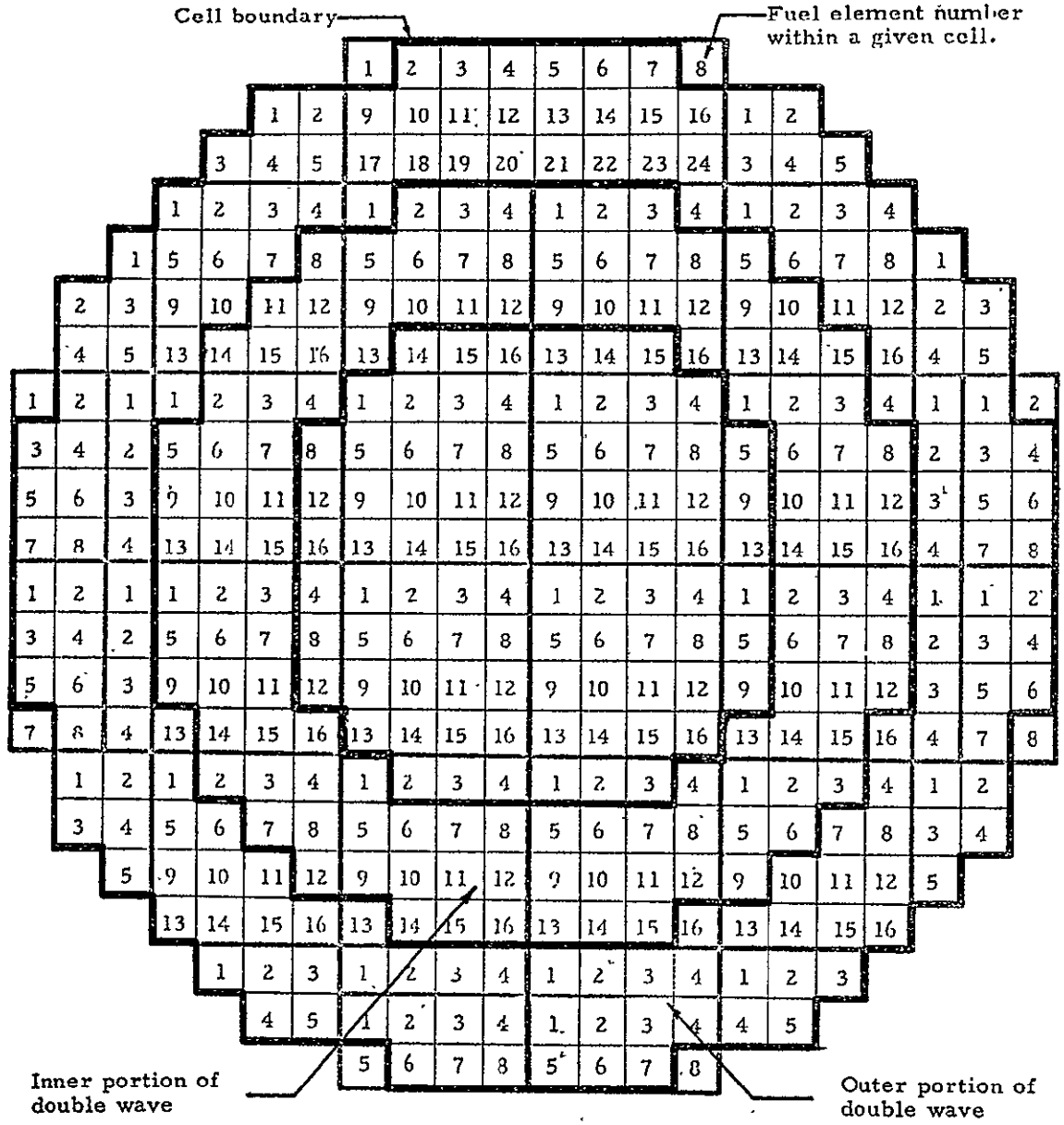

Fig. 9.4 Cross sectional view of wave - type 5 showing fuel element positions

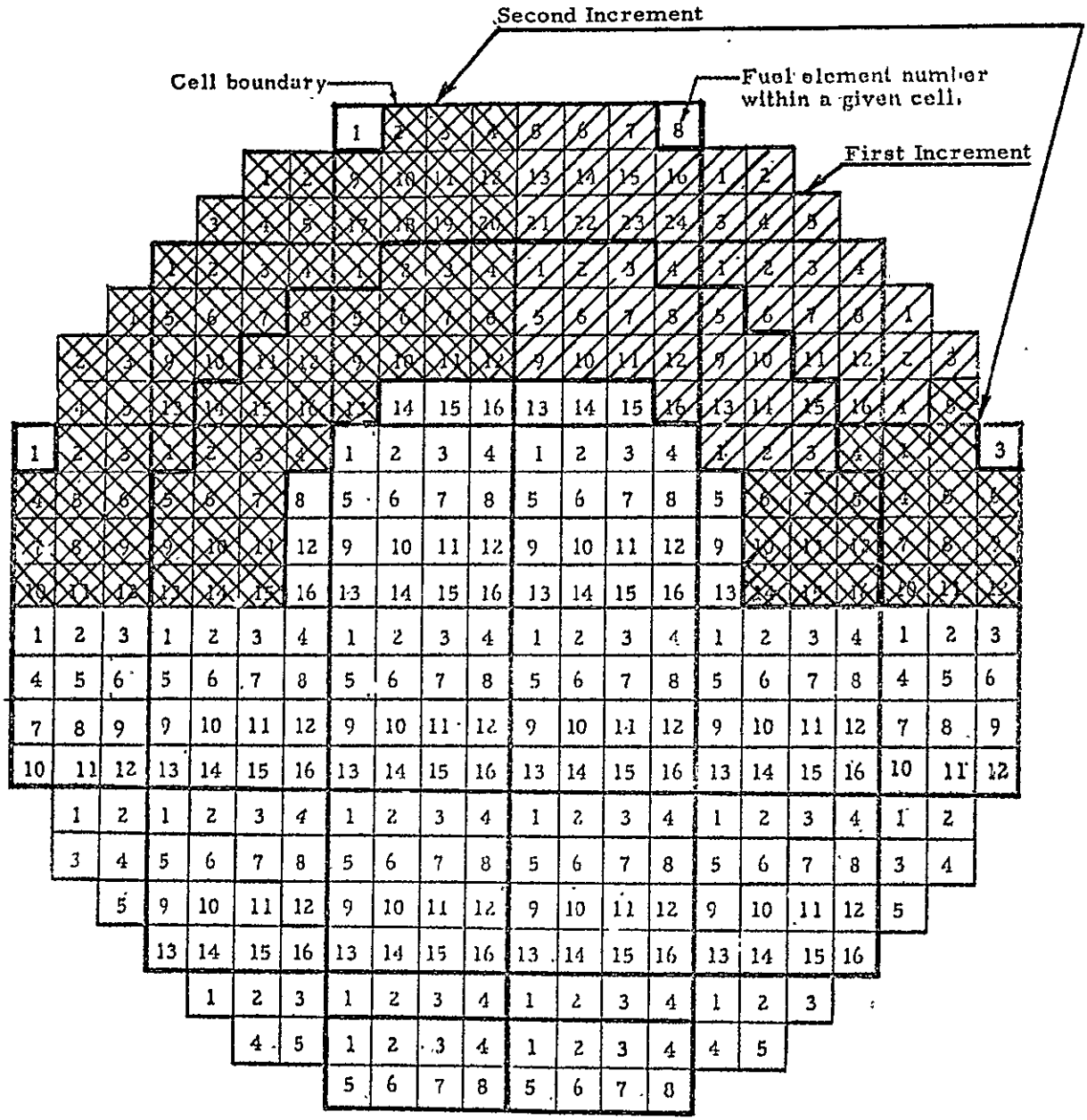

Fig. 9.5 Cross sectional view of wave showing increments. That wave was added to the core

10.0 CONFIGURATION 6

Configuration 6 waves were the small, one stage waves and required the fuel to be moved directly opposite the void as shown in Figure 10.1. This configuration more nearly represents a spalling off of fuel rather than the development of a wave. Four such "waves" were measured as shown in the above figures and the results were as follows:

Configuration	Worth of Wave (%Δk)
6A	0.160 ± 0.028
6B	0.167 ± 0.019
6C	0.206 ± 0.013
6D	0.579 ± 0.026

Configuration 6D was the sum of the other three configurations and it will be noted that its worth was higher than the sum of 6A, 6B, and 6C by 0.046 ± 0.044%Δk. This was the first case in the wave measurements where the combination of two or more waves was ostensibly worth more than the sum of the worths of the individual waves. There is no obvious explanation for such an effect, but the 68% confidence limit error is essentially as large as the effect. Therefore, it is concluded that with such small "waves," the sum of the parts (the individual waves) equals the whole.

It is also noted that there is a difference in the worth of a wave depending on whether the fuel was removed from in front or beneath the wave. Configuration 4A gave a worth of 0.243±0.027%Δk, with the fuel removed from in front while configuration 6A resulted in only 0.160± 0.028%Δk for the same wave size but located directly over the voided region. In Configuration 4A the fuel is removed from a position of less importance to a position of greater importance along the axis.

Configuration 6D as compared to Configuration 4D both with 3 equal sized waves shows a higher worth of fuel 0.579±0.026%Δk versus 0.532±0.024%Δk for 4D.

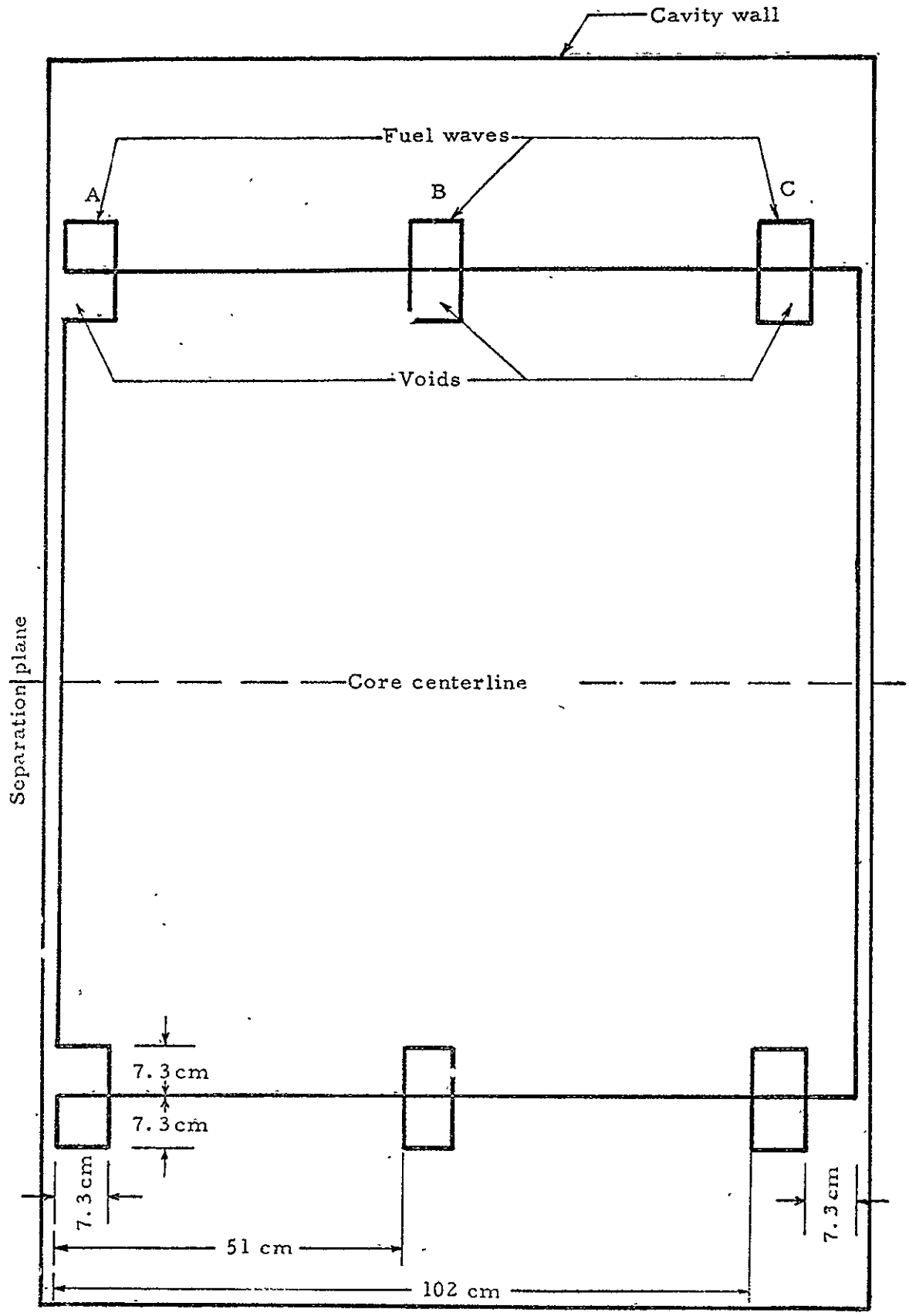

Fig. 10.1 Configuration 6 type waves (7.3 cm fuel displacement from core edge)

11.0 CONFIGURATION 8 (3-zoned core, different radii)

This reactor required a complete reloading of the fuel elements in order to mockup an active core with a uniform fuel density but a variable (stepped) fuel radius. The fuel radius decreased towards the exhaust nozzle thus simulating the active core geometry expected to exist under conditions of flow and power. Figure 11.1 shows the layout of the cavity region and the radial variations. Region 1 had the normal core radius used for most of the previously operated reactors. The ratio of the fuel radius to cavity radius for Regions 1, 2, and 3 was 0.68, 0.59, and 0.51, respectively. As will be noted from the figure, Region 1 was six-stages long while Regions 2 and 3 were each five stages long. The exact fuel loading was as follows:

Region	Fuel Fraction	Fuel Mass (kg of U)	Number of Fuel Sheets
1	0.476	17.1	6516
2	0.304	10.9	4159
3	0.220	7.9	3014
	1.000	35.9	13689

The fuel elements were loaded according to the recipe given in Figure 11.2. The active core boundaries for the three regions are shown in Figures 11.3, 11.4, and 11.5. The cross sectional boundaries are irregular, but give the equivalent cylindrical diameters shown in Figure 11.1 for each of the three regions. There were 208 fuel element positions in Region 1, 160 in Region 2, and 116 in Region 3. All of the fuel elements extended through all regions and were 116.8 cm (46 inches) long. The outer fuel elements were fueled only in Region No. 1; the second layer of fuel (108.8 cm outer diameter) extended over Regions 1 and 2; and the inner cylinder (92.5 cm outer diamter) was fueled over the full core length. Figures 11.1, 11.2, and 11.7 shows this arrangement.

There were 32.9 of polyethylene (CH_2) in the outer 8 cm of the cavity on the radial wall. The 0.0965 cm thick stainless steel liner (83.1 kg) was on the cavity wall and the fuel annulus containing 823.2 kg of U^{235} was 19 cm from the cavity wall in the radial reflector.

11.1 Initial Loading

Initial loading of Configuration 8, which will be referred to as Configuration 8A so as to distinguish it from the wave measurements to follow, began on September 26, 1968, with a completely unloaded core. The normal incremental loading procedure was used to load the fuel elements in the reactor. Three count rate channels were used to record multiplication and the results are given in Table 11.1 and Figure 11.6. It was found that the reactor was about 0.5%Δk subcritical with all the fuel in the reactor so it was necessary to remove some of the polyethylene, as shown in Table 11.1. With 6.08 kg of CH_2 removed, (leaving 26.82 kg in the reactor) k-excess was 0.203%Δk.

The layout of the types of fuel elements in each of the core positions for the fully loaded reactor can be seen in Figure 11.7. The following aluminum masses were in the cavity region:

1.	Core structure	84.09 kg
2.	Fuel elements	108.33 kg
3.	Lids	6.16 kg
4.	Fuel sheet spacers	18.70 kg
5.	Fuel element spacers (front end)	2.57 kg

All of the aluminum was type 1100 except for 15.15 kg of type 6061 in the support structure.

11.2 Rod Worth Measurements

Three rod worth measurements were obtained with Actuators 3 and 6 equally inserted in the reactor and all others withdrawn. The average worth was -1.3710 ± 0.0091%Δk. A single measurement of Actuators 1 to 10 containing 27 control rods gave a worth of -6.030%Δk. The worth of Actuators 3 and 6 was about 10% higher than was measured on the previous wave experiments (Table 6.1). Although an exact comparison cannot be made with the worth of 27 rods because the same number of rods was not measured on the earlier experiments, it appears that their worth was in the order of 20% higher for this reactor configuration. The increase in reactivity appears to be due to the fact that a larger percentage of the fuel was in the end of the cavity nearest the control rods. This increase is rod worth was also noted on similar reactor configurations reported in Reference 3, p. 292 and 309.

During the operation of Configuration 8, a rod worth curve was measured (27 rods) for all rods by using an inverse reactor kinetics technique. See Reference 4. A computer program entitled, "LUNCH" developed by the Argonne National Laboratories was used to reduce the data. The measurement was made with all of the rods in the withdrawn position and the reactor leveled at a power of about 10 watts. In order to level on an infinite period and still have the rods in the withdrawn position, the table was separated slightly thus reducing the multiplication factor to 1.0. The rods were then inserted as a bank by activating the shutdown switch. The input data for the computer program was taken from one of the linear channel traces. The results of this measurement is shown in Figure 11.8. This is essentially the same curve as the subcritical all rods worth curve measured early in the cavity reactor experiments and reported in Reference 3, p. 94.

The above measurement also results in a total rod worth. The correlation between the rod worths obtained by rod bumps and the calculated values have been within ±10% or less. Both measurements depends on the fission delayed and photo neutron delayed information, neutron

lifetime and source level. The inverse kinetics method is a sensitive indicator of the compatibility of the delayed neutron and source level input data. For instance, incorrect delayed neutron parameters or source level will destroy the asymptotic reactivity with all rods inserted, and instead indicate a varying reactivity. Appropriate adjustment of the parameters can correct this. But if the delayed neutrons are changed by 20% the resultant rod worth changes by 9%. However, the delayed neutron parameters are known within ±3%, and the photo neutron parameters are only about 12% of the total value of the dollar. The source level is difficult to measure because it is at or below the normal noise level of the detectors or in the range of 10^{-12} ampere on the picoammeters. The source level is important and if properly measured can result in a reliable calculation of rod worth. Thus, reliable results from the inverse kinetics method require reliable input data from all the parameters, and a result that gives an asymptotic reactivity. The latter serves as an indicator of reliability of these parameters.

In the case of rod bump extrapolations, the questions of space mode effects and additive effects of small reactivities to give large effects arise. The ±10% or less typical deviations that occur between the rod bumps and inverse kinetic methods cannot be assigned exclusively to either one of the methods.

11.3 Reactivity Measurements

While removing the polyethylene, its worth was measured to be -0.12 ± 0.01%Δk/kg. The critical loading required to give a multiplication of 1.00 can, therefore, be extrapolated to 35.9kg of uranium and 28.51 kg of polyethylene with the other reactor components as described above. Fuel worth measurements were not obtained on this reactor so the fuel loading adjustment was not attempted in extrapolating to the critical loading.

The wave configurations which were measured on this reactor are shown in Figures 11.9 to 11.12. The waves were formed by moving a stage of fuel within the active core to the next fuel element location just outside the core. The locations involved are shown in Figure 8.5 for Region 1 and Figures 11.13 and 11.14 for Regions 2 and 3, respectively.

The results of the wave measurements are given in Table 11.2. The sum of the individual wave worths equals 0.791%Δk which is 5.3% higher than the worth of all three waves together.

TABLE 11.1

Initial Loading - Configuration 8A

Increment	Sheets of Fuel in Reactor	Channel No. 1 CPM	Channel No. 1 CRo/CR	Channel No. 2 CPM	Channel No. 2 CRo/CR	Channel No. 3 CPM	Channel No. 3 CRo/CR	Avg.	Rod Positions
0	0	345	1.000	279	1.000	265	1.000	1.000	In
0	0	391	1.000	309	1.000	297	1.000	1.000	Out
1	1852	747	0.462	588	0.474	551	0.481	0.472	In
1	1852	924	0.423	751	0.411	685	0.434	0.423	Out
1	1852	809	0.427	584	0.478	553	0.479	0.461	In
1	1852	956	0.409	744	0.415	690	0.430	0.418	Out
2	2655	927	0.372	748	0.373	687	0.386	0.377	In
2	2655	1204	0.325	965	0.320	910	0.326	0.324	Out
3	4143	1372	0.246	1066	0.256	986	0.264	0.255	In
3	4143	1903	0.201	1487	0.204	1381	0.211	0.205	Out
4	5733	1817	0.1897	1455	0.1917	1372	0.1931	0.1915	In
4	5733	2724	0.1434	2236	0.1382	2088	0.1422	0.1413	Out
Corrected CRo		338		273		260			In
		383		303		291			Out
5 Added	7666	2574	0.1339	2146	0.1301	1958	0.1353	0.1331	In
5 1933	7666	4899	0.0798	3753	0.0823	3423	0.0868	0.0830	Out
6 1347	9013	3207	0.1054	2734	0.0999	2463	0.1056	0.1036	In
6 1347	9013	6620	0.0579	5479	0.0553	4978	0.0585	0.0572	Out
7 1357	10370	4151	0.0814	3361	0.0812	3113	0.0835	0.0820	In
7 1357	10370	10121	0.0378	8408	0.0360	7714	0.0377	0.0372	Out
8 1313	11683	5664	0.0591	4286	0.0632	3905	0.0658	0.0627	In
8 1313	11683	19764	0.0192	15243	0.0197	13438	0.0214	0.0201	Out
Corrected CRo		335		271		257			In
		379		300		288			Out
9	13068	6708	0.0499	5149	0.0526	4826	0.0533	0.0519	In
9	13068	41567	0.0091	32399	0.0093	28345	0.0102	0.0095	Out
10	13689	7242	0.0463	5735	0.0473	5142	0.0500	0.0479	In
10	13689	72996	0.0052	56399	0.0053	49829	0.0058	0.0054	Out

TABLE 11.1

(Continued)

Increment	Sheets of Fuel in Reactor	Channel No. 1 CPM	Channel No. 1 CRo/CR	Channel No. 2 CPM	Channel No. 2 CRo/CR	Channel No. 3 CPM	Channel No. 3 CRo/CR	Avg.	Rod Positions
11 Removed	13689	9076	0.0369	6017	0.0450	5420	0.0474	0.0431	In
11 2050 gm CH_2	13689	151901	0.0025	98700	0.0030	84670	0.0034	0.0030	Out
12 Removed	13689	9514	0.0352	6306	0.0430	5714	0.0450	0.0411	In
12 2041 gm CH_2	13689	775125	0.00049	373275	0.00080	304297	0.00095	0.00075	Out

TABLE 11.2

Configuration 8 Fuel Wave Measurements

Configuration	Uranium Mass Interchanged (gm)	Wave Worth (%Δk)
8B (wave in Region 1)	576	0.341 ± 0.007
8C (wave in Region 2)	558	0.261 ± 0.007
8D (wave in Region 3)	453	0.189 ± 0.006
8E (all 3 waves)	1587	0.751 ± 0.022

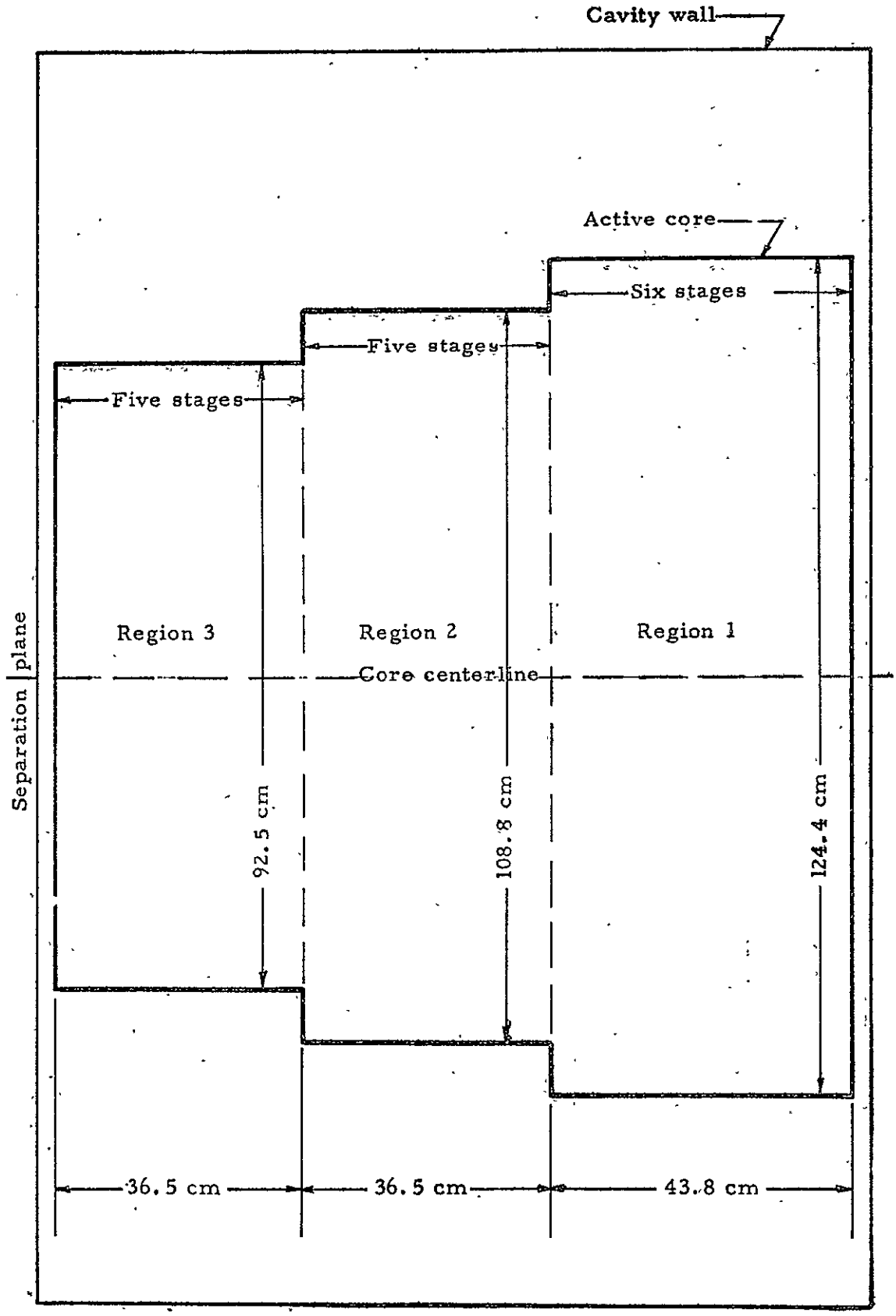

Fig. 11.1 Configuration 8 core cross section

TYPE 1 Fuel Element

1	2	3	4	5	6	7	8	9	10	11	12	13	14	15	16	← Stage number
1	2	3	1	2	3	1	2	3	1	2	3	1	2	3	1	← Fuel orientation
6	5	6	5	6	5	6	5	6	5	6	6	5	6	5	6	← Number of fuel sheets per stage

TYPE 2 Fuel Element

1	2	3	4	5	6	7	8	9	10	11	12	13	14	15	16	← Stage number
2	3	1	2	3	1	2	3	1	2	3	1	2	3	1	2	← Fuel orientation
5	6	5	5	5	5	5	5	5	5	5	5	5	5	5	5	← Number of fuel sheets per stage

TYPE 3 Fuel Element

1	2	3	4	5	6	7	8	9	10	11	12	13	14	15	16	← Stage number
3	1	2	3	1	2	3	1	2	3	1	2	3	1	2	3	← Fuel orientation
5	5	5	5	5	5	5	5	5	5	5	5	5	5	5	5	← Number of fuel sheets per stage

Region 1 | Region 2 | Region 3

The following number and types of fuel elements will be required for each region:

Region	Type 1	Type 2	Type 3	Totals
1	69	69	70	208 (1)
2	53	53	54	160
3	38	39	39	116

(1) 116 of these fuel elements will be fully loaded over the 16 stages, 44 will be loaded over Regions 1 and 2, and 48 will be loaded over Region 1 only.

Fig. 11.2 Configuration 8 fuel element loading pattern

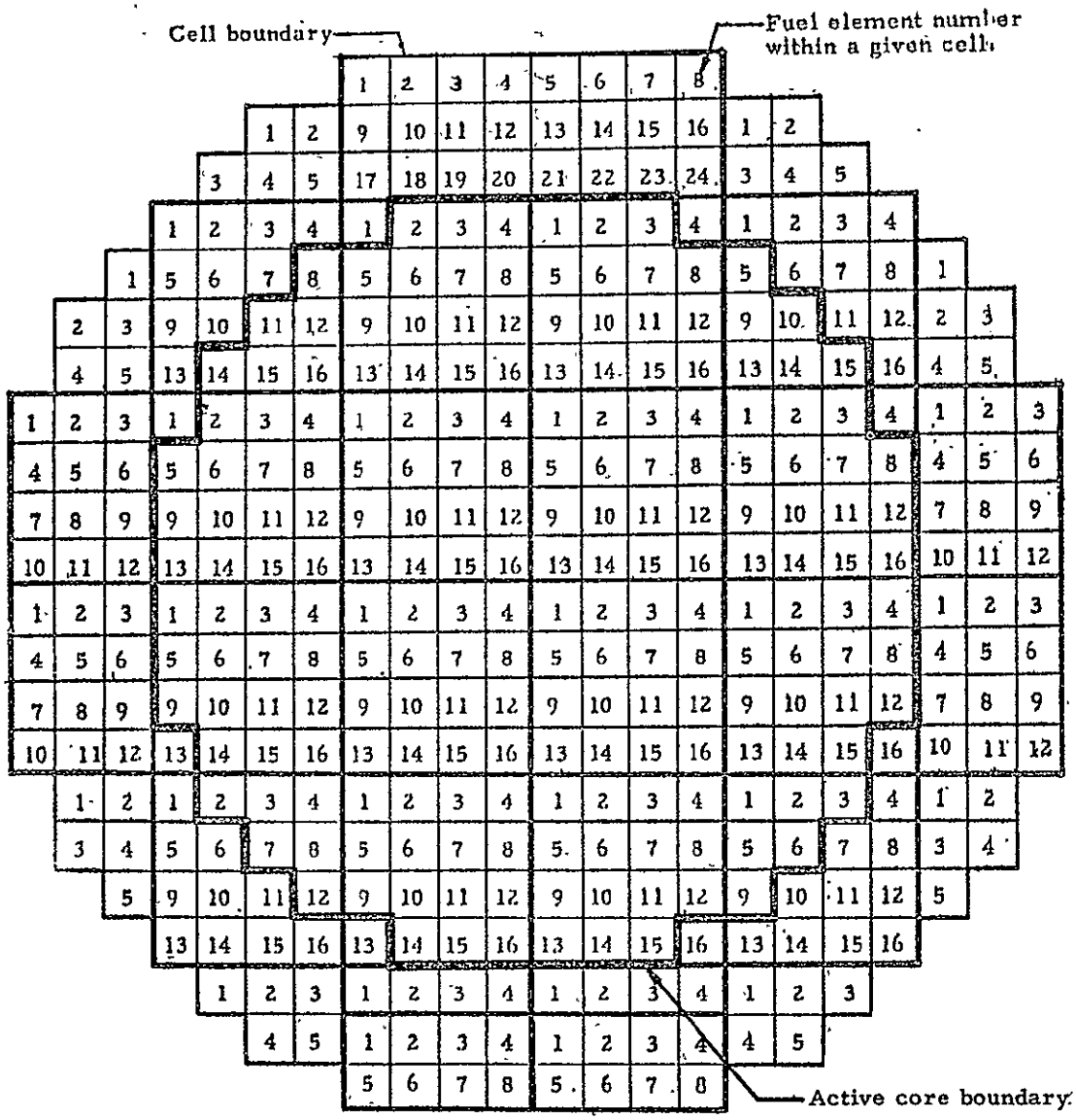

Fig. 11.3 Active core boundary region 1 - Configuration 8

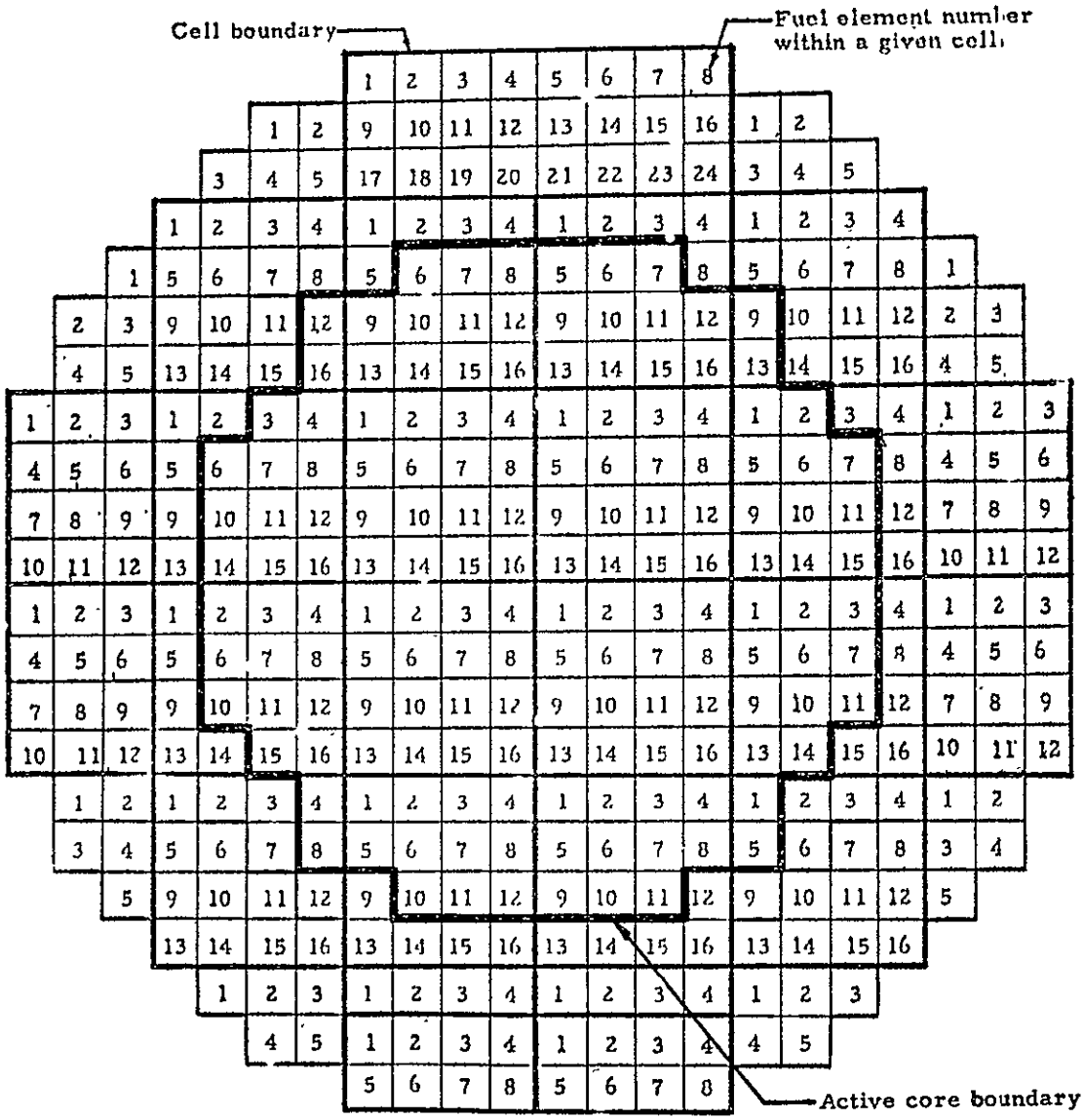

Fig. 11.4 Active core boundary region 2 - Configuration 8

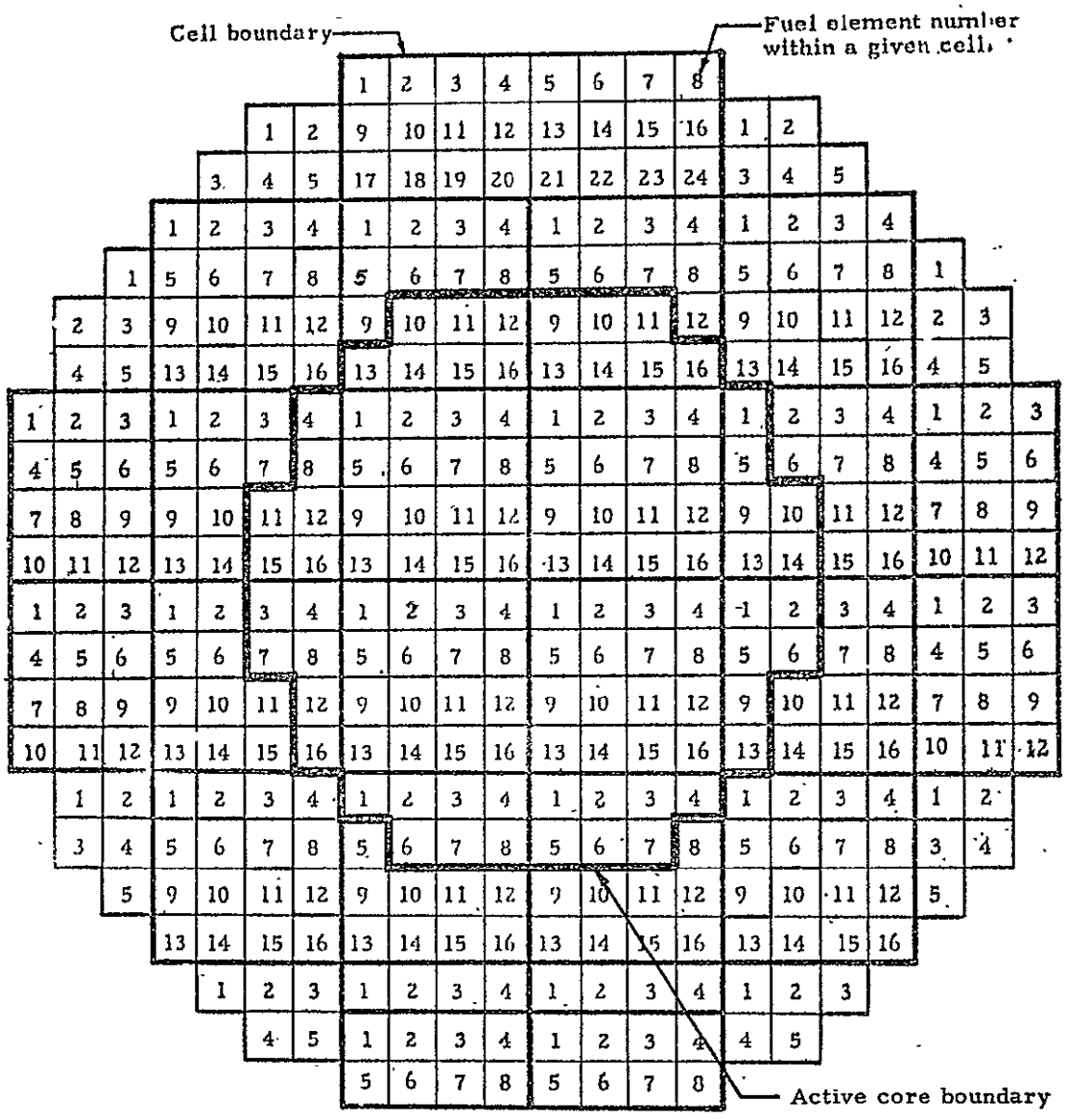

Fig. 11.5 Active core boundary region 3, - Configuration 8

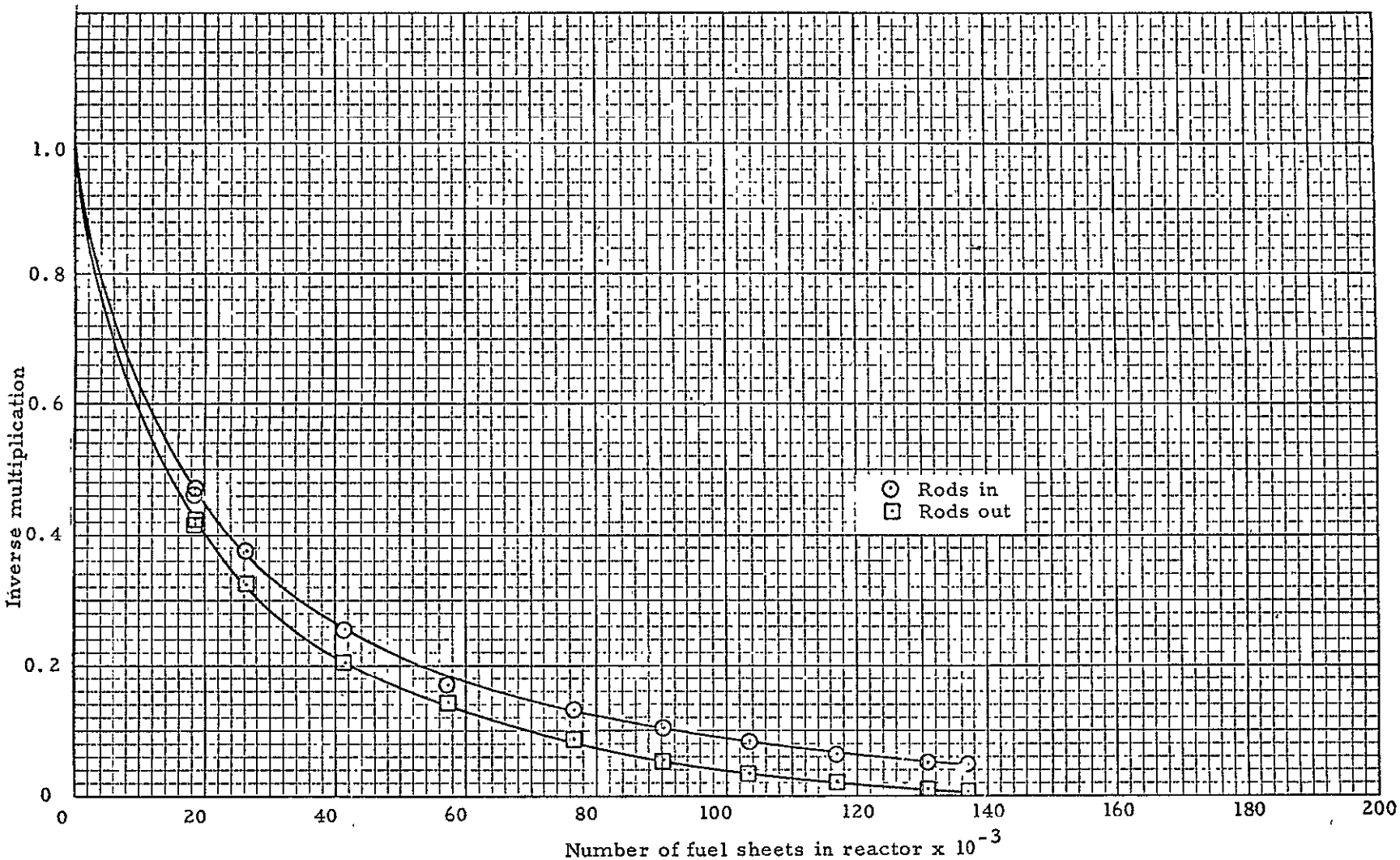

Fig. 11.6 Inverse multiplication curve for configuration 8

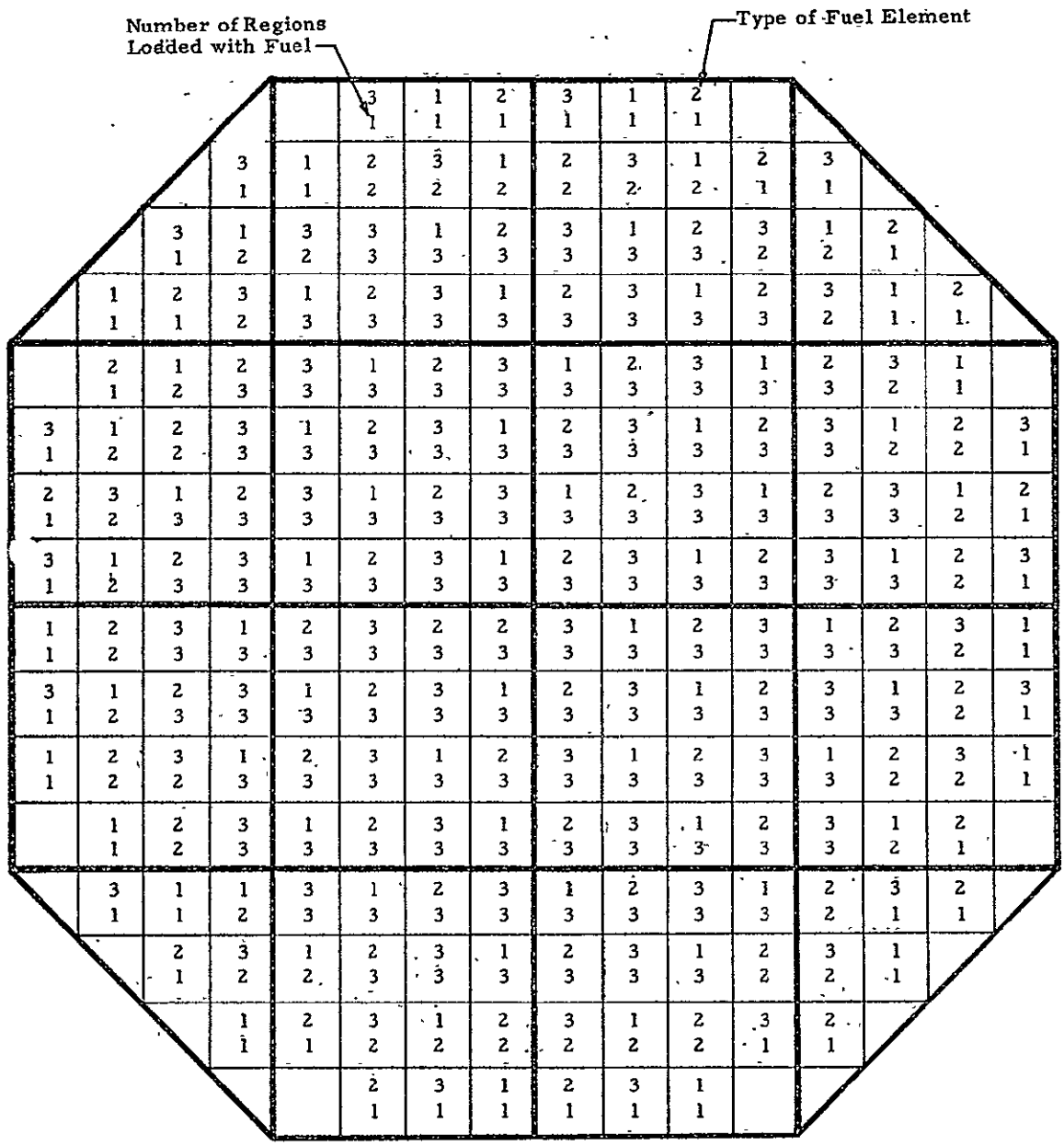

Fig. 11.7 Cross section of core showing fuel element types and locations for configuration 8

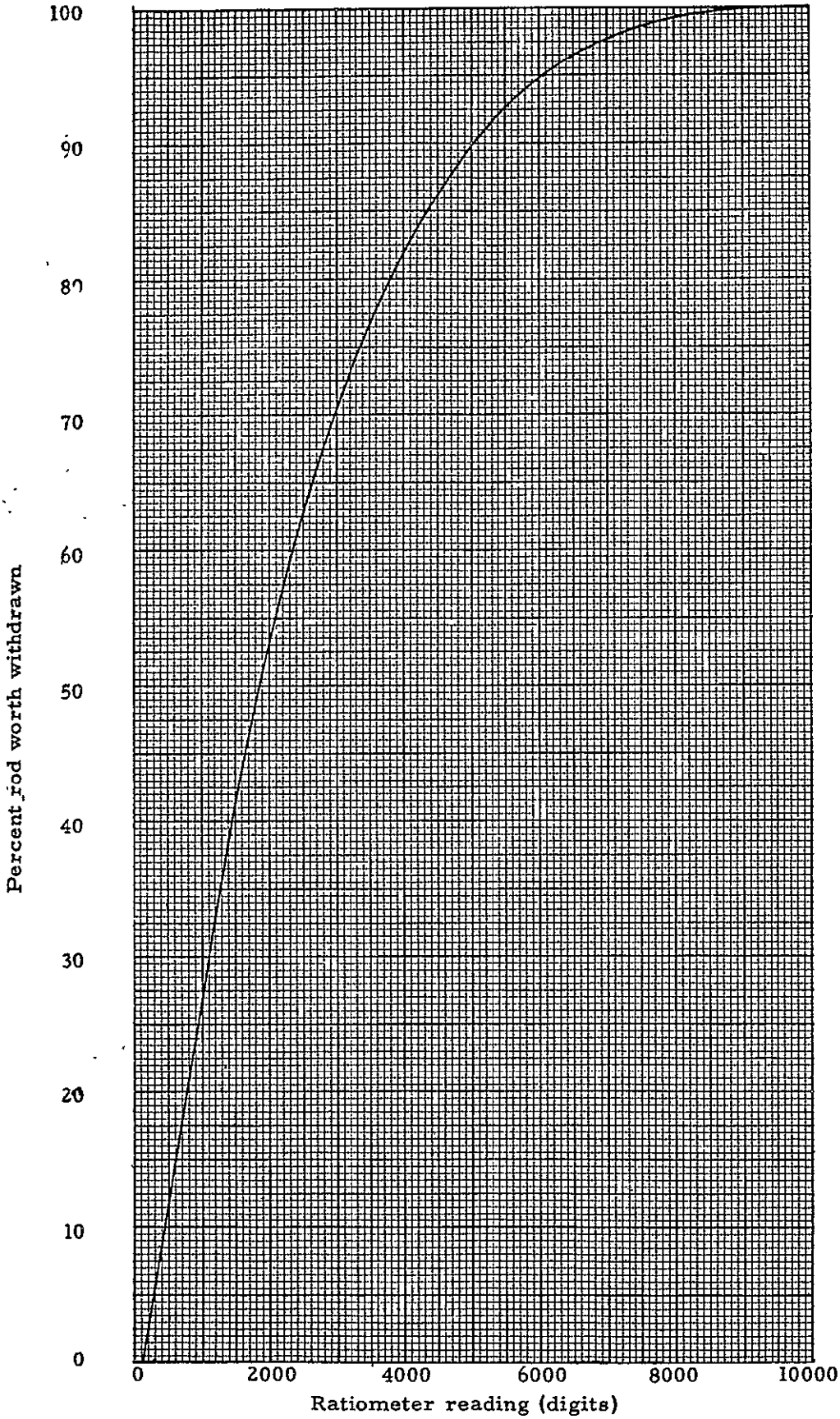

Fig. 11.8 Control rod shape curve - configuration 8

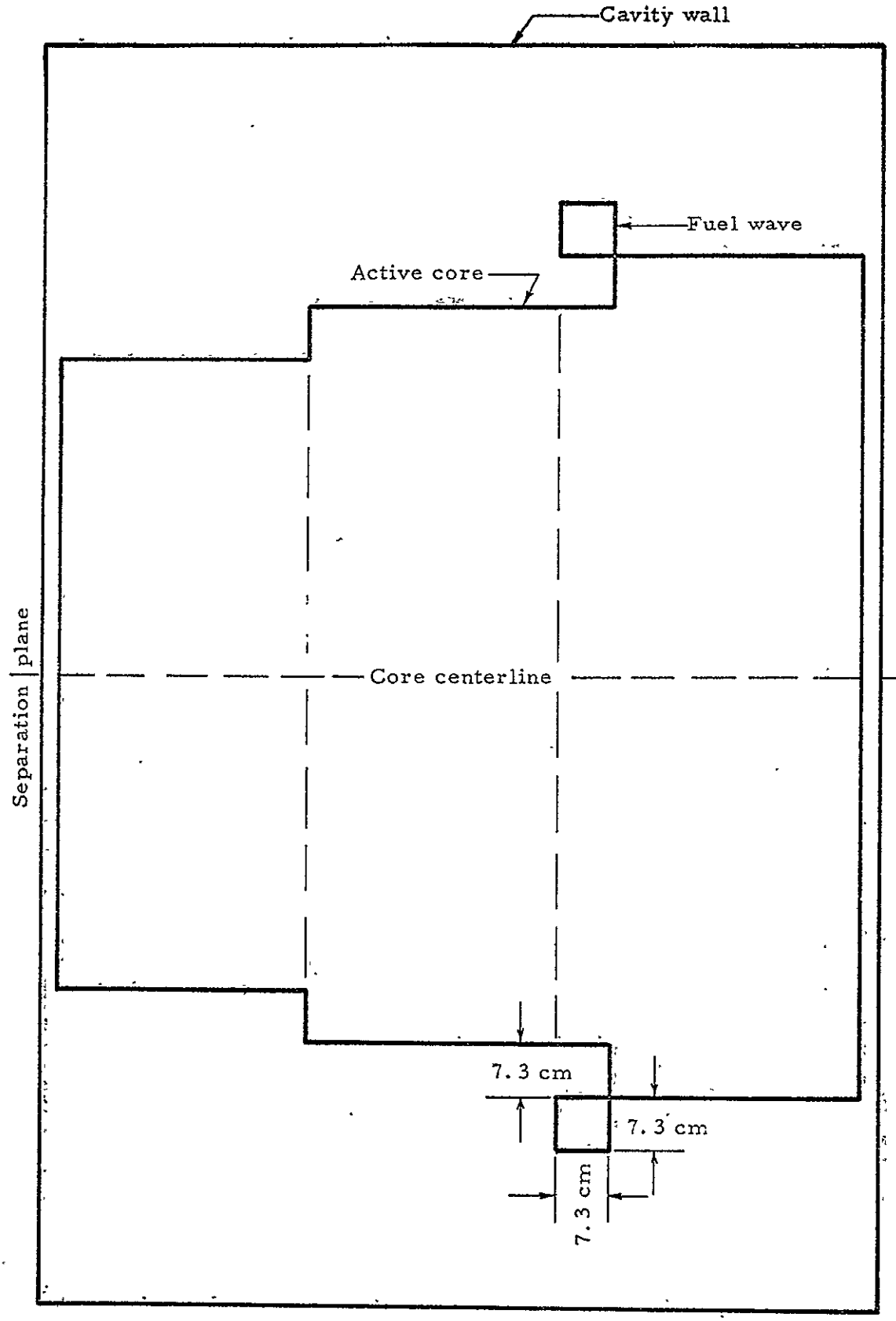

Fig. 11.9 Configuration 8B wave

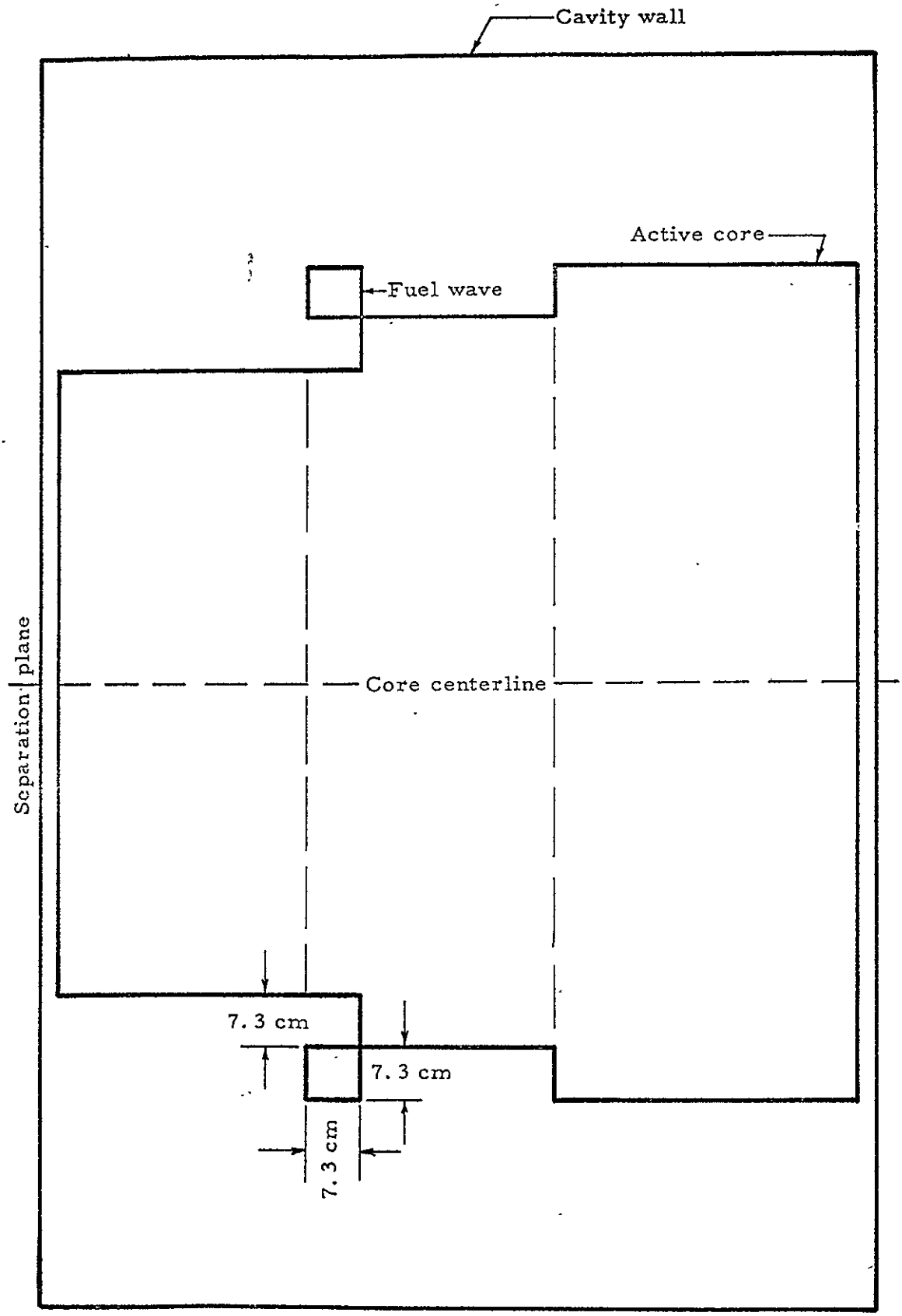

Fig. 11.10 Configuration 8C wave

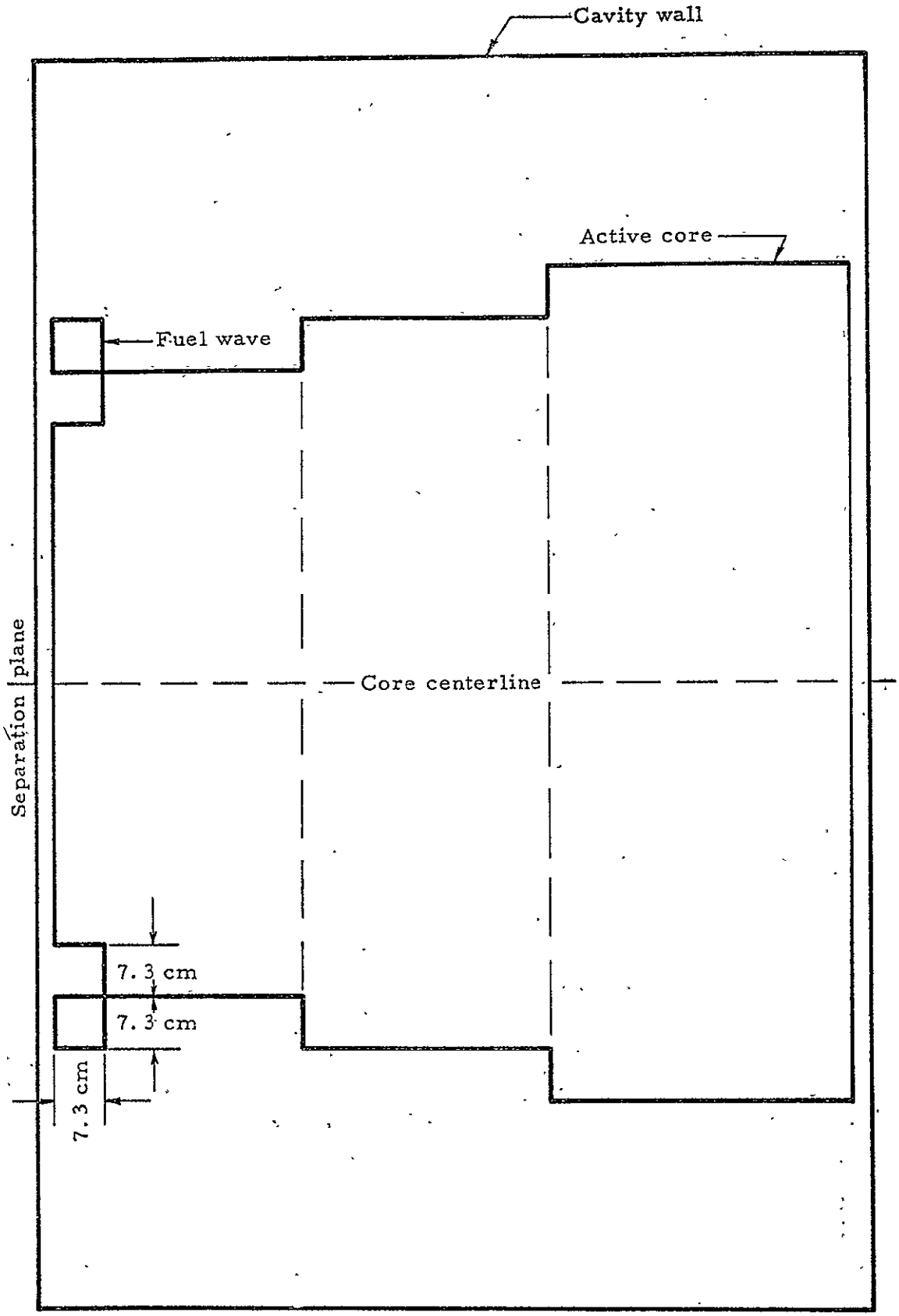

Fig. 11.11 Configuration 8D wave

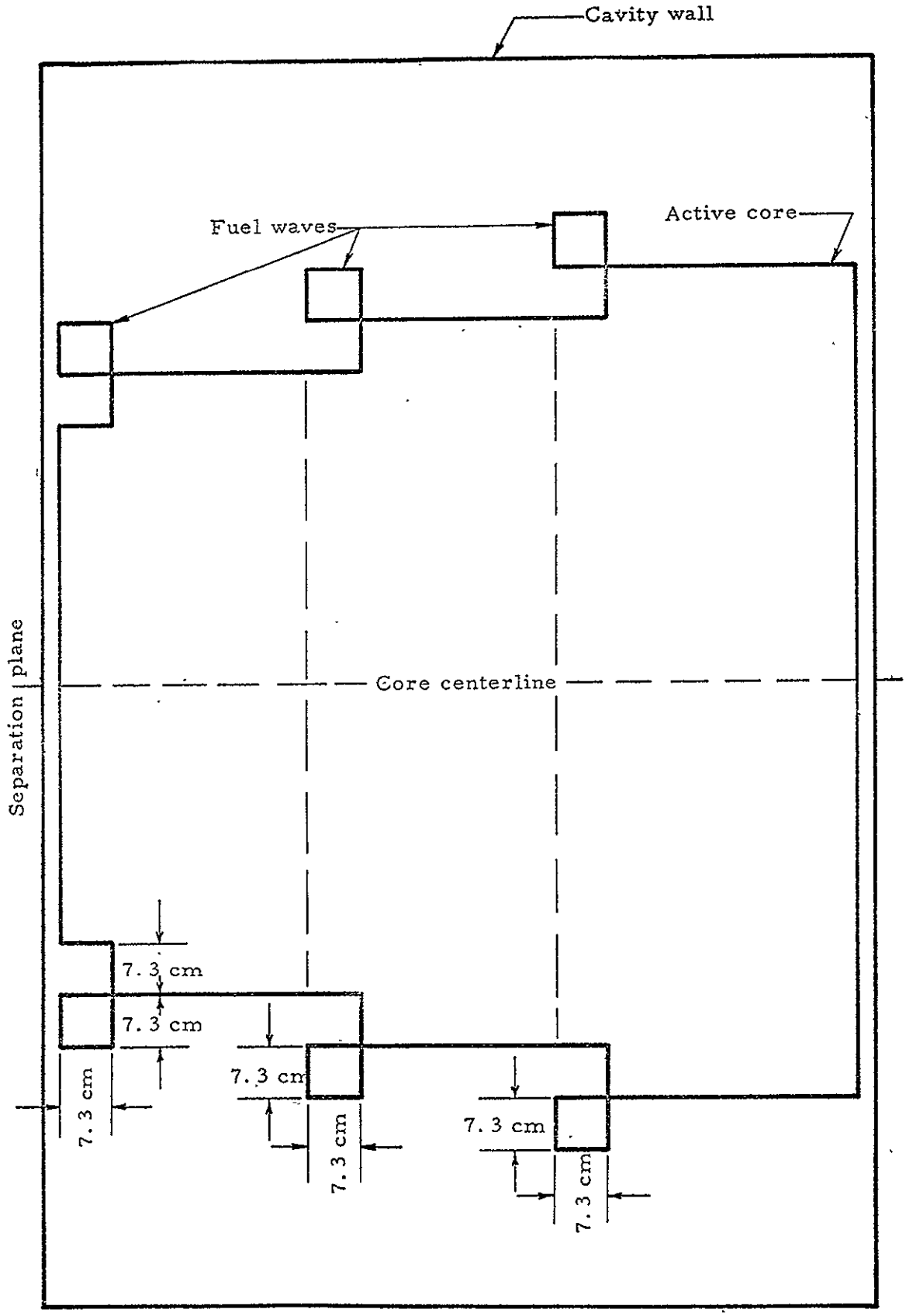

Fig. 11.12 Configuration 8E wave

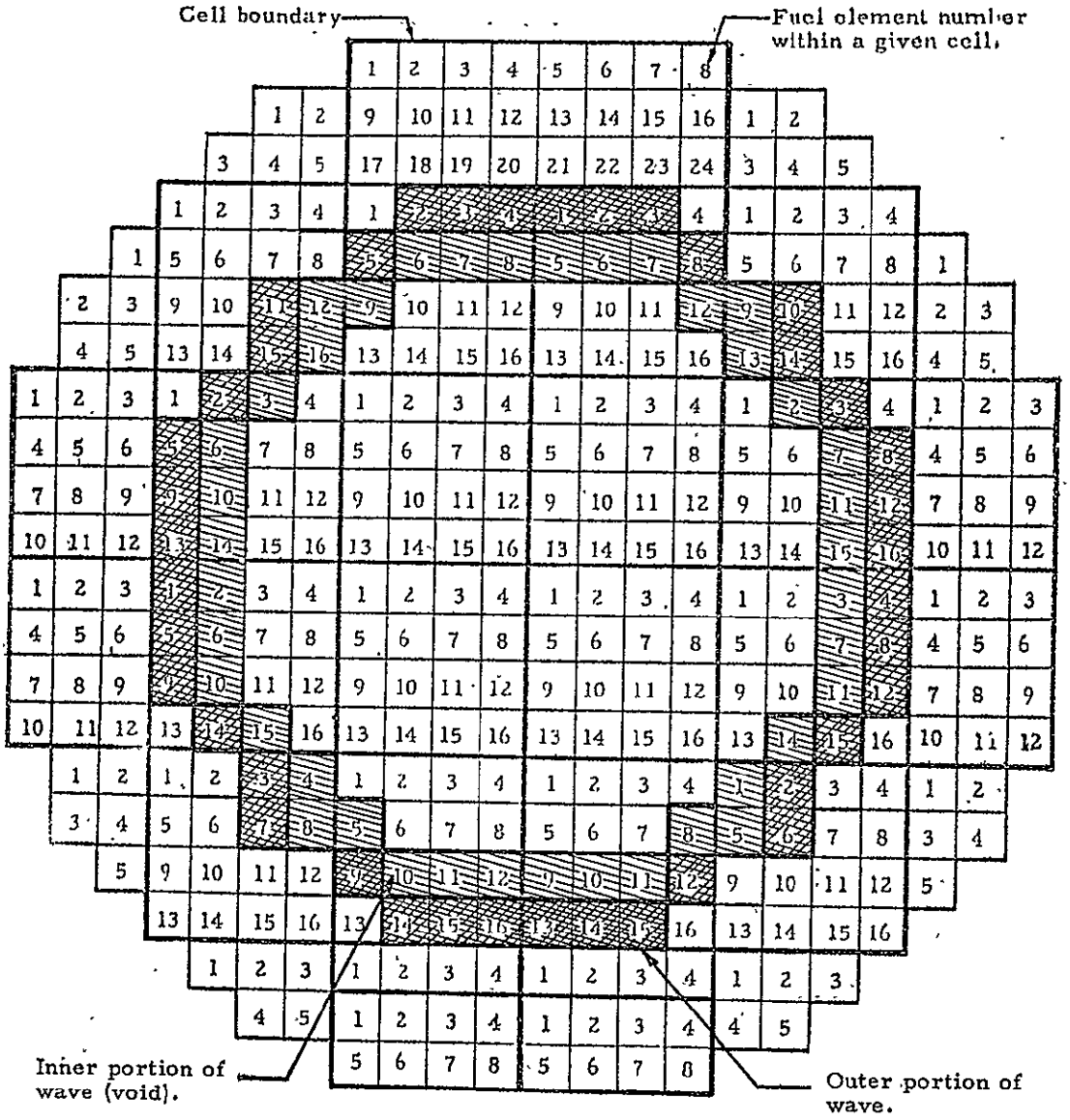

Fig. 11.13 Cross sectional view of configuration 8C wave

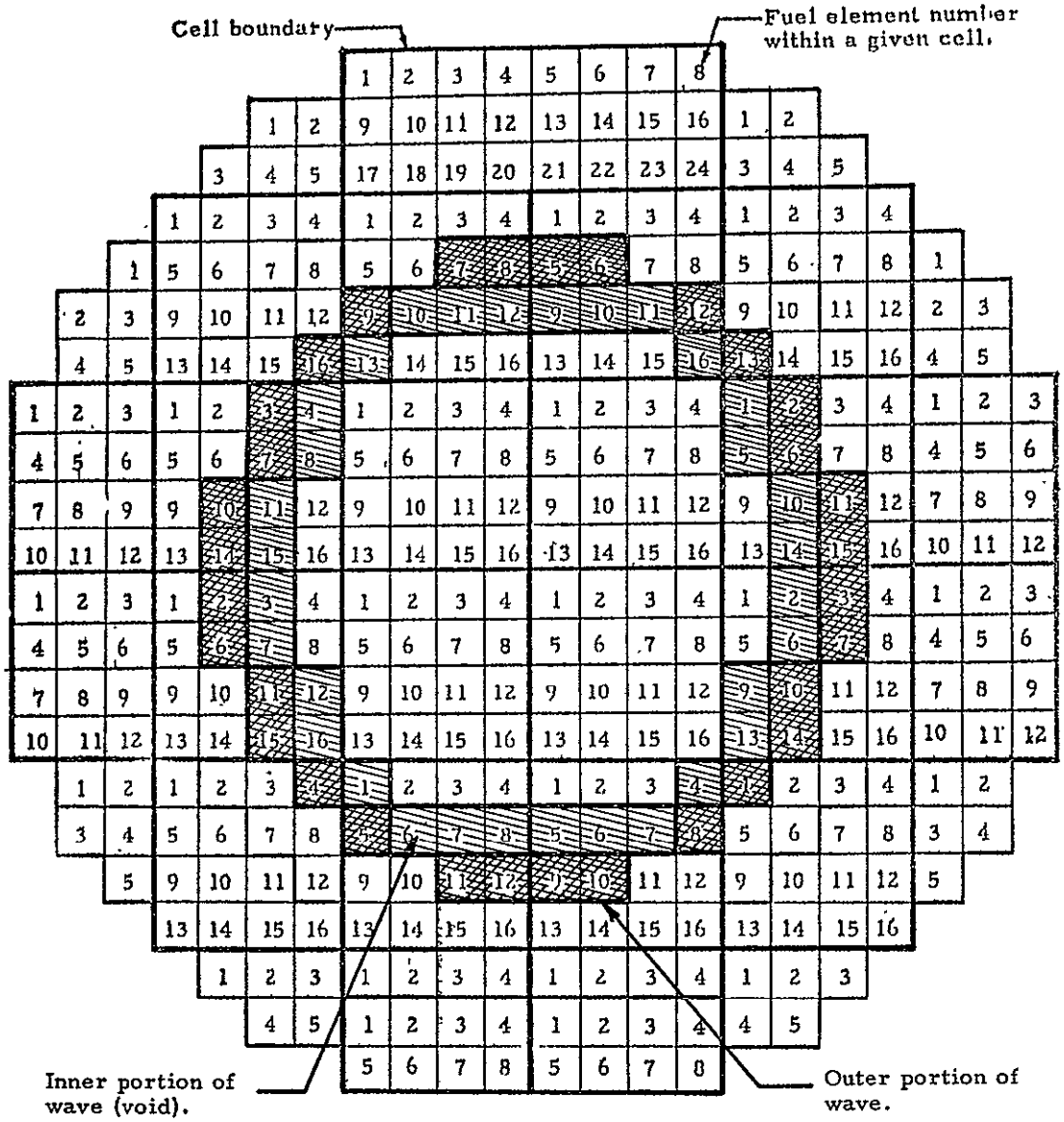

Fig. 11.14 Cross sectional view of configuration 8D wave

12.0 CONFIGURATION 9 (3-zoned core, different radii, variable densities)

Configuration 9 was a variable fuel density, variable fuel radius core. The core layout was exactly the same as Configuration 8 (Figure 11.1) as far as the three regions and fuel radii were concerned. The fuel loading, however, was of several different fuel densities, the density varied from region to region with the heaviest density in Region 1 and the lightest density in Region 3. The fuel density was uniform within each region. The following gives the core loading information

Region	Fuel Fraction	Fuel Mass (kg of U)	Number of Fuel Sheets	Fuel Density gm/cc
1	0.658	29.07	11094	0.0546
2	0.244	10.76	4106	0.0317
3	0.098	4.36	1664	0.0178
Totals	1.000	44.18	16864	

The exact loading recipe for each of the three types of fuel elements is given in Figure 12.1.

The hardware within the active core and reflector regions was the same as Configuration 8 except for the polyethylene in the outer 8 cm between the core support structure and cavity wall. The total mass of CH_2 was increased to 32.9 kg.

12.1 Initial Loading

A different loading procedure was used in establishing configuration 9. The reactor initially contained Configuration 8E prior to the changeover. One quarter of the core (52 fuel elements) was converted to Configuration 9 and k-excess increased 0.49%Δk. The next step was to add 7115 gm of CH_2 to the cavity (giving total polyethylene mass of 32.9 kg) to remove all of the fuel wave in Region 1, and to change an additional 72 fuel elements. These changes resulted in a loss in k-excess of 0.84%Δk. The remaining fuel elements were then converted to Configuration 9 which completed the changeover. The final excess reactivity was 0.56%Δk.

12.2 Rod Worth Measurements

A single all rods worth measurement was made after Configuration 9 was established. A total of 27 rods were involved and then were worth -5.407%Δk. All of the reactivity measurements were made with Actuators 3 and 6 equally withdrawn and the remaining rods withdrawn all the way. The worth of Actuators 3 and 6 was assumed to be -1.3710 ± 0.0091%Δk, which was the measured value for Configuration 8.

12.3 Reactivity Measurements

It was stated in Section 12.1 that k-excess was 0.56%Δk when the reactor was fully loaded. Since fuel worth measurements were not made on this configuration, the critical mass of uranium could not be accurately

extrapolated but the worth of CH_2 was known from Configuration 8 so the amount of CH_2 could easily be adjusted to give a multiplication of 1.00. Assuming CH_2 to be worth -0.12%Δk/kg, 0.56%Δk would be equal to 4.67 kg of CH_2. Thus, for criticality of k = 1.00, the total CH_2 would be 37.57 kg, the fuel loading 44.18 kg of uranium, and the other components as previously described.

The test program required the measurement of a single set of waves the same as Configuration 8E (Figure 11.12) which we will refer to as Configuration 9E. However, because of operational restrictions, Configuration 9E could not be established in a single increment based on the worth of Configuration 8 waves. Therefore, a single wave was first measured at the end of Region 1, the same as Configuration 8B, Figure 11.9. A total of 1037.5 gm of uranium was interchanged in the wave and k-excess increased 0.559 ± 0.010%Δk. The addition of the other two waves, one at the end of Region 2 and one at the end of Region 3 (Figure 11.12), increased k-excess and additional 0.303± 0.012%Δk and involved the interchange of 775.5 gm of uranium. The total reactivity increase due to creating the three waves in Configuration 9E was, therefore, 0.862 ± 0.016%Δk.

12.4 Power Distribution Measurements - Catcher Foil Data

Power distribution measurements were made on both Configuration 9A (no waves in the reactor) and Configuration 9E (three waves in the reactor). Only bare catcher foils were exposed in the cavity region and on the fuel annulus in the D_2O to determine power distribution. However, both bare and cadmium covered gold foils were exposed in the cavity and reflector regions to determine the thermal neutron flux. The D_2O temperature was 19.4°C during all foil exposures and all rods were withdrawn except Actuators 4, 5, 6, and 7 which were withdrawn 27.8 cm and 12.2 cm for Configuration 9A and 9E, respectively.

12.4.1 Configuration 9A

The catcher foil data were obtained in two foil exposures, the results of which are given in Table 12.1. The axial distributions in the cavity region are shown in Figures 12.2 and 12.3 along with the integrated average for each curve. These axial averages were plotted to show the radial power profile in Figure 12.4. Because of the variable loading in the reactor, it was decided to determine the axial curve averages over each region and then plot these averages to produce the radial profile over each of the three axial regions. These results are given in Figure 12.5. The volume weighted average was then calculated for each of these three curves as shown in Figure 12.5. These weighted averages were 1.852, 2.233, and 3.519 for Regions 1, 2, and 3, respectively. All of the catcher foil results are normalized to the point at the center of the core, so all values are relative to 1.0 at the core center.

The power generated in the various regions was calculated to be as follows:

Region	Power (watts)	Percent of Total Power
1	7.91	51.2
2	3.39	21.9
3	2.17	14.0
Fuel Annulus	1.99	12.9
Total	15.46	100.0

12.4.2 Configuration 9E

The catcher foil data obtained on the wave Configuration 9E are given in Table 12.2. These data were plotted the same as for Configuration 9A and are shown in Figures 12.6 to 12.9. The significant changes occurred, of course, in the region of the fuel waves and where the fuel was relocated. In order to compare the data for the two configurations the axial averages were first compared as shown in Table 12.3. It will be noted here that there is a general tendency for the wave configuration to have lower averages than the bare core. However, another factor needs to be considered before making this comparison. It will be noted from Runs 1148 and 1151 that there was a 4.5% difference in the normalized counts at the core center with Configuration 9E having the highest count. This is the count to which other data on the specific run are normalized before plotting the relative power distribution. Besides the normal statistical uncertainty, these data can be affected by actual changes in the flux at the core center relative to the flux at the location of the power normalization foils. The power normalization foils are located at the separation plane in the reflector region. This region is normally not sensitive to small changes in the core, but in this case it is concluded that there was a neutron flux increase in the center of the core and a general flattening of the power distribution in the fueled region relative to the reflector flux levels. This amounted to about 4.5% out to a fuel radius of 53 cm. The outer edge of Region 1 shows a 12 to 15% lower axial average for Configuration 9E than Configuration 9A.

The power generated in each cavity region as well as in the fuel annulus in the radial reflector is as follows:

Region	Power (watts)	Percent of Total Power
1	8.14	52.3
2	3.36	21.6
3	2.08	13.4
Fuel Annulus	1.97	12.7
Total	15.55	100.0

12.5 Resonance Detector Data - Bare Gold Foils

12.5.1 Configuration 9A

Gold foils were exposed in both cavity and reflector regions to determine neutron flux distributions. The gold foils were power normalized to Run 1148 and these normalization factors are given in Table 12.4.

The gold data, including both bare and cadmium covered foils, are presented in Table 12.5. The bare gold within the cavity region was normalized to the center of the core, as was done with the bare catcher foils, and the relative axial distributions of the foil activities were then plotted as shown in Figure 12.10. Since it was necessary to treat each axial region of the active core as a separate unit to produce meaningful radial flux profiles, the axial distributions were averaged over each of the three regions and these data were plotted as shown in Figure 12.11. The volume weighted average was then calculated for each of the three regions over the fueled portion of the core. These averages are given in Figure 12.11 as 1.303, 1.351, and 1.665 for Regions 1, 2, and 3, respectively, all with respect to 1.0 specific power at the core center.

The distributions of both bare and cadmium covered gold foil activities within the reflector regions are given in Figures 12.12 and 12.13. These are the foil activities at the active core power level of 13.5 watts. The power in the fuel annulus was not considered here because all previously reported gold foil activities in the reflector regions have been referenced to active core power only. The most noticeable difference between the two reflector regions is near the cavity reflector interface. In this region the bare foil activity was considerably higher in the radial reflector than in the end reflector. This difference is caused primarily by the polyethylene on the radial wall of the cavity which acts as a flux trap and reflects neutrons back into the radial reflector thus enhancing the thermal flux near the cavity wall. The data compare very well with that obtained from the base core configuration for the wave measurements and presented in Section 5.4 of this report.

12.5.2 Configuration 9E

Gold foils were exposed in the same locations for this configuration as for Configuration 9A so that direct comparisons could be made. The tabulated data are found in Table 12.6 and the base foil data within the cavity region are plotted in Figure 12.14. The axial profiles were averaged over each region and these averages are shown in Figure 12.15. The volume weighted averages for each region from the center of the core to the outer surface of the fuel were 1.298, 1.382, and 1.665 for Regions 1, 2, and 3, respectively, all with respect to 1.0 at the core center.

A comparison of the axial averages for the base configuration (9A) and this wave Configuration (9E) is shown in Table 12.7. The five axial averages over the full length of the core showed no differences within less than ±1.0%. The averages over the three regions also indicated no differences within the standard error on the values of ±1.5%.

The gold foil data in the reflector regions are shown graphically in Figures 12.16 and 12.17. These results are compared with Configuration 9A on a point by point basis in Table 12.8. The bare gold data in the end reflector show a 3.3 ± 3.4% decrease for Configuration 9E over 9A which was due to the control rods being further inserted into the end reflector on Configuration 9E. This was necessary because of the higher k-excess for Configuration 9E. The bare data in the radial reflector indicated no measurable change within the experimental error. The cadmium covered gold foil data in the end reflector show a decrease of about the same magnitude as the

bare data noted above for Configuration 9E over Configuration 9A. However, the radial reflector shows a definite increase in the cadmium activity of about 17 ± 12%, on the average for Configuration 9E compared to Configuration 9A. The reason for this is not known.

12.6 Resonance Detector Data - Cadmium Ratios

12.6.1 Configuration 9A

The gold foil cadmium ratios for Configuration 9A are listed in Table 12.9. Figure 12.18 shows the cadmium ratio axial profile down the center of the core while Figure 12.19 presents the radial profiles at three axial locations. No unusual values were observed within the active core. At the core center the cadmium ratio was 1.130 and this increased to 1.965 at the cavity wall. At the outer surfaces of Region 1, 2, and 3, the cadmium ratio was about 1.6.

Figure 12.20 shows the cadmium ratios in the reflector regions. The presence of fuel in radial reflector along with the polyethylene on the cavity wall cause a crossover in the cadmium ratio results in the end and side reflectors at a location near 20 cm from the cavity wall as noted from Figure 12.20. This also occurred with the base reactor for the wave experiments as noted in Figure 5.14.

12.6.2 Configuration 9E

The gold foil cadmium ratios for Configuration 9E are given in Table 12.10 and the resulting distributions are shown in Figures 12.21, 12.22, and 12.23. The values were much the same as observed for Configuration 9A as will be noted from Table 9.11. If the point at 153.5 cm from the core center in the radial reflector is ignored, the overall difference is negligible between the two configurations.

12.7 Thermal Neutron Flux

12.7.1 Configuration 9A

Where both bare and cadmium covered gold foil data were obtained, the thermal neutron flux was calculated. The procedures used to calculate neutron flux are given in Reference 3, p. 69. The values thus calculated are given in Table 12.12. A plot of the radial distribution through the axial centerline of the core as well as a plot of the axial distribution through the radial centerline of the core are given in Figures 12.24 and 12.25. All of these data were normalized to a watt of cavity core power only. The power in the fuel annulus in the radial reflector was not included in the core power since most of the previously reported data did not include fuel in the D_2O. Inclusion of the power in the fuel annulus would reduce the above neutron flux values by about 13%.

12.7.2 Configuration 9E

Table 12.13 contains the thermal neutron flux values from Configuration 9E. The same positions were flux mapped for both Configurations 9A and 9E so that a direct comparison could be made between the two. This comparison is shown in Table 12.13 as the ratio of the values between Configurations 9E to 9A. The overall average ratio was 0.976 ± 0.066 which indicates a slight but yet uncertain decrease in flux with respect to core power on Configuration 9E. The flux values for Configuration 9E are plotted in Figures 12.26 and 12.27.

TABLE 12.1

Catcher Foil Data

Configuration 9A

Foil No.	Type	Location Radial (cm)	Location Axial (cm)	Normalized Counts	Ratio of Local to Core Center (Foil No. (X)
Run 1148					
1	Bare	0	93.3	34542	2.050
2	Bare	0	105.3	14135	0.839
3	Bare	0	120.6	11126	0.660
4	Bare	0	135.8	13929	0.827
5	Bare	0	151.1	16842	1.000 X
6	Bare	0	166.3	22566	1.339
7	Bare	0	181.5	34998	2.078
8	Bare	0	196.8	44512	2.642
9	Bare	0	208.8	67041	3.980
10	Bare	15.2	93.3	37639	2.234
11	Bare	15.2	105.3	16969	1.007
12	Bare	15.2	120.6	11349	0.673
13	Bare	15.2	135.8	14544	0.863
14	Bare	15.2	151.1	20488	1.216
15	Bare	15.2	166.3	26126	1.551
16	Bare	15.2	181.5	38073	2.260
17	Bare	15.2	196.8	48736	2.893
18	Bare	15.2	208.8	68105	4.043
19	Bare	30.5	93.3	40245	2.389
20	Bare	30.5	105.3	18176	1.079
21	Bare	30.5	120.6	15323	0.909
22	Bare	30.5	135.8	18836	1.118
23	Bare	30.5	151.1	24272	1.441
24	Bare	30.5	166.3	29611	1.758
25	Bare	30.5	181.5	43663	2.592
26	Bare	30.5	196.8	57081	3.389
27	Bare	30.5	208.8	67130	3.985
28	Bare	45.7	93.3	48053	2.853
29	Bare	45.7	105.3	24817	1.473
30	Bare	45.7	120.6	24765	1.470
31	Bare	45.7	135.8	32245	1.914
32	Bare	45.7	151.1	40759	2.420
33	Bare	45.7	166.3	52493	3.116
34	Bare	45.7	172.9	56165	3.334
35	Bare	45.7	177.2	66936	3.974
36	Bare	45.7	181.5	71701	4.257
37	Bare	45.7	196.8	83042	4.930
38	Bare	45.7	208.8	89123	5.291

TABLE 12.1

(Continued)

Foil No.	Foil Type	Location Radial (cm)	Location Axial (cm)	Normalized Counts	Ratio of Local to Core Center (Foil No. (X)
Run 1148 (Cont'd)					
39	Bare	53.3	93.3	57664	3.423
40	Bare	53.3	105.3	39917	2.370
41	Bare	53.3	120.6	35179	2.088
42	Bare	53.3	131.5	44730	2.655
43	Bare	53.3	135.8	49279	2.925
44	Bare	53.3	140.1	63096	3.746
45	Bare	53.3	151.1	75371	4.475
46	Bare	53.3	166.3	79784	4.737
47	Bare	53.3	169.6	89368	5.306
48	Bare	53.3	172.9	89408	5.308
49	Bare	53.3	177.2	90485	5.372
50	Bare	53.3	181.5	91345	5.423
51	Bare	53.3	196.8	98047	5.821
52	Bare	53.3	208.8	99305	5.896
53	Bare	61.0	93.3	85725	5.089
54	Bare	61.0	105.3	84074	4.991
55	Bare	61.0	120.6	75492	4.482
56	Bare	61.0	131.5	83349	4.948
57	Bare	61.0	140.1	87115	5.172
58	Bare	61.0	151.1	88159	5.234
59	Bare	61.0	166.3	100076	5.942
60	Bare	61.0	181.5	97562	5.792
61	Bare	61.0	196.8	110837	6.580
62	Bare	61.0	208.8	103965	6.172
63	Bare	61.0	135.8	88124	5.232
Run 1149					
1	Bare	0	93.3	34778	1.887
2	Bare	0	105.3	14752	0.800
3	Bare	0	120.6	11305	0.613
4	Bare	0	135.8	13485	0.732
5	Bare	0	151.1	18422	1.000 X
6	Bare	0	166.3	23228	1.260
7	Bare	0	181.5	34995	1.899
8	Bare	0	196.8	46609	2.530
9	Bare	0	208.8	77199	4.190
10	Bare	76.2	93.3	117996	6.405
11	Bare	76.2	105.3	105524	5.728
12	Bare	76.2	120.6	100879	5.476

TABLE 12.1

(Continued)

Foil No.	Type	Location Radial (cm)	Location Axial (cm)	Normalized Counts	Ratio of Local to Core Center (Foil No. (X)
Run 1149 (Cont'd)					
13	Bare	76.2	135.8	101787	5.525
14	Bare	76.2	151.1	104898	5.694
15	Bare	76.2	166.3	103605	5.623
16	Bare	76.2	181.5	108663	5.898
17	Bare	76.2	196.8	109450	5.941
18	Bare	76.2	208.8	111523	6.053
19	Bare	91.4	93.3	157479	8.548
20	Bare	91.4	105.3	159818	8.675
21	Bare	91.4	120.6	162911	8.843
22	Bare	91.4	135.8	168040	9.121
23	Bare	91.4	151.1	169460	9.198
24	Bare	91.4	166.3	169214	9.185
25	Bare	91.4	181.5	160580	8.716
26	Bare	91.4	196.8	148200	8.044
27	Bare	91.4	208.8	121338	6.586
28	Bare	111.1	128.2	273337	14.837
29	Bare	111.7	128.2	279422	15.167
30	Bare	111.1	151.1	276474	15.007
31	Bare	111.7	151.1	265240	14.398
32	Bare	111.1	174.0	266707	14.477
33	Bare	111.7	174.0	248059	13.465

TABLE 12.2

Catcher Foil Data

Configuration 9E

Foil No.	Type	Location Radial (cm)	Location Axial (cm)	Normalized Counts	Local to Center of Core (Foil (X)
Run 1151					
1	Bare	0	93.3	36954	2.099
2	Bare	0	105.3	14384	0.817
3	Bare	0	120.6	10778	0.612
4	Bare	0	135.8	13293	0.755
5	Bare	0	151.1	17605	1.000 (X)
6	Bare	0	166.3	23435	1.331
7	Bare	0	181.5	34230	1.944
8	Bare	0	196.8	49025	2.785
9	Bare	0	208.8	69832	3.966
10	Bare	15.2	93.3	40152	2.281
11	Bare	15.2	105.3	18185	1.033
12	Bare	15.2	120.6	11790	0.670
13	Bare	15.2	135.8	13581	0.771
14	Bare	15.2	151.1	19074	1.083
15	Bare	15.2	166.3	24493	1.391
16	Bare	15.2	181.5	38938	2.212
17	Bare	15.2	196.8	44737	2.541
18	Bare	15.2	208.8	65137	3.700
19	Bare	30.5	93.3	41823	2.376
20	Bare	30.5	105.3	19294	1.096
21	Bare	30.5	120.6	14395	0.818
22	Bare	30.5	135.8	19858	1.128
23	Bare	30.5	151.1	25774	1.464
24	Bare	30.5	166.3	33207	1.886
25	Bare	30.5	181.5	45299	2.573
26	Bare	30.5	196.8	56239	3.194
27	Bare	30.5	208.8	69059	3.923
28	Bare	45.7	93.3	47521	2.699
29	Bare	45.7	105.3	23563	1.338
30	Bare	45.7	120.6	25044	1.422
31	Bare	45.7	135.8	29972	1.702
32	Bare	45.7	151.1	41799	2.374
33	Bare	45.7	166.3	51837	2.944
34	Bare	45.7	181.5	75257	4.275
35	Bare	45.7	196.8	83873	4.764
36	Bare	45.7	201.9	78986	4.486
37	Bare	45.7	205.7	81618	4.636
38	Bare	45.7	208.8	75760	4.303

TABLE 12.2

(Continued)

Foil No.	Foil Type	Location Radial (cm)	Location Axial (cm)	Normalized Counts	Local to Center of Core (Foil (X)
Run 1151 (Cont'd)					
39	Bare	53.3	93.3	56069	3.185
40	Bare	53.3	105.3	39512	2.244
41	Bare	53.3	120.6	35670	2.026
42	Bare	53.3	128.2	47911	2.721
43	Bare	53.3	135.8	56609	3.215
44	Bare	53.3	151.1	76102	4.323
45	Bare	53.3	166.3	73488	4.174
46	Bare	53.3	170.1	67279	3.821
47	Bare	53.3	173.9	76327	4.335
48	Bare	53.3	181.5	83994	4.771
49	Bare	53.3	196.8	92022	5.227
50	Bare	53.3	201.9	93725	5.324
51	Bare	53.3	208.8	94454	5.365
52	Bare	61.0	93.3	84492	4.799
53	Bare	61.0	105.3	77236	4.387
54	Bare	61.0	120.6	66921	3.801
55	Bare	61.0	128.2	63664	3.616
56	Bare	61.0	132.0	62239	3.535
57	Bare	61.0	135.8	61118	3.472
58	Bare	61.0	151.1	88286	5.015
59	Bare	61.0	166.3	90082	5.117
60	Bare	61.0	170.1	90623	5.147
61	Bare	61.0	173.9	89134	5.063
62	Bare	61.0	181.5	93701	5.322
63	Bare	61.0	196.8	97650	5.547
64	Bare	61.0	208.8	104131	5.915
Run 1152					
1	Bare	0	93.3	35637	1:985
2	Bare	0	105.3	14996	0.835
3	Bare	0	120.6	11559	0.644
4	Bare	0	135.8	13475	0.750
5	Bare	0	151.1	17957	1.000 (X)
6	Bare	0	166.3	22153	1.234
7	Bare	0	181.5	35864	1.997
8	Bare	0	196.8	47299	2.634
9	Bare	0	208.8	79016	4.400
10	Bare	68.6	93.3	101980	5.679
11	Bare	68.6	105.3	93781	5.223

TABLE 12.2

(Continued)

Foil No.	Foil Type	Location Radial (cm)	Location Axial (cm)	Normalized Counts	Local to Center of Core (Foil (X)
Run 1152 (Cont'd)					
12	Bare	68.6	120.6	90106	5.018
13	Bare	68.6	128.2	82322	4.585
14	Bare	68.6	132.0	88317	4.918
15	Bare	68.6	135.8	90458	5.038
16	Bare	68.6	151.1	96369	5.367
17	Bare	68.6	166.3	102579	5.713
18	Bare	68.6	181.5	101473	5.651
19	Bare	68.6	196.8	102168	5.690
20	Bare	68.6	208.8	100829	5.615
21	Bare	76.2	93.3	107896	6.009
22	Bare	76.2	105.3	99286	5.529
23	Bare	76.2	120.6	83980	4.677
24	Bare	76.2	135.8	103196	5.747
25	Bare	76.2	151.1	98324	5.477
26	Bare	76.2	166.3	108232	6.027
27	Bare	76.2	181.5	104401	5.814
28	Bare	76.2	196.8	105890	5.897
29	Bare	76.2	208.8	110677	6.164
30	Bare	91.4	93.3	165893	9.239
31	Bare	91.4	105.3	174830	9.736
32	Bare	91.4	120.6	168253	9.370
33	Bare	91.4	135.8	169320	9.429
34	Bare	91.4	151.1	160447	8.935
35	Bare	91.4	166.3	167121	9.307
36	Bare	91.4	181.5	170562	9.499
37	Bare	91.4	196.8	144061	8.024
38	Bare	91.4	208.8	123107	6.856
39	Bare	111.1	128.2	261620	14.57
40	Bare	111.7	128.2	290901	16.20
41	Bare	111.1	151.1	263534	14.68
42	Bare	111.7	151.1	261726	14.58
43	Bare	111.1	174.0	249067	13.87
44	Bare	111.7	174.0	265834	14.80

TABLE 12.3

Comparison of Axial Averages

Catcher Foil Data

Configuration 9

Radial Location of Axial Profile	Axial Average Configuration 9A	Configuration 9E	9E/9A
0	1.473	1.431	0.971
15.2	1.633	1.513	0.927
30.5	1.866	1.852	0.992
45.7	2.904	2.734	0.941
53.3	4.104	3.774	0.920
61.0	5.470	4.713	0.862
76.2	5.728	5.704	0.996
91.4	8.758	9.113	1.041
	Comparison by Regions		
	Region 1		
0	0.880	0.865	0.983
15.2	1.015	0.981	0.967
30.5	1.135	1.163	1.025
45.7	1.675	1.535	0.916
53.3	2.440	2.447	1.003
61.0	4.780	4.042	0.846
	Region 2		
0	1.115	1.096	0.983
15.2	1.232	1.173	0.952
30.5	1.545	1.595	1.032
45.7	2.680	2.466	0.920
53.3	4.450	4.099	0.921
61.0	5.525	4.718	0.854
	Region 3		
0	2.615	2.477	0.947
15.2	2.850	2.493	0.875
30.5	3.125	2.970	0.950
45.7	4.710	4.444	0.944
53.3	5.844	5.068	0.867
61.0	6.225	5.468	0.878

TABLE 12.4

Power Normalization Factors

Run	Time	Decay Time (min)	Decay Factor	Activity (CPM)	Corrected Activity (CPM)	Normalization Factor
1148	1351.57	66.50	1.406	161065	226457	
	1353.57	68.50	1.460	155301	226739	
	1355.57	70.50	1.500	149683	224524	
					225907	1.000
1149	1350.50	85.94	1.925	119347	229743	
	1352.50	87.94	1.978	115659	228774	
	1354.50	89.94	2.031	112797	229091	
					229203	0.986
1150	1555.38	19.50	0.394	572077	225398	
	1557.38	21.50	0.427	527616	225292	
	1559.38	23.50	0.461	489770	225784	
					225491	1.002
1151	1408.17	51.50	1.035	214210	221707	
	1410.17	53.50	1.083	204351	221312	
	1412.17	55.50	1.132	195616	221437	
					221485	1.020
1152	1226.43	47.50	0.942	239836	225926	
	1228.03	49.10	0.979	230885	226036	
	1229.93	51.00	1.023	220931	226012	
					225991	1.000
1153	1517.22	41.00	0.798	283793	226467	
	1519.22	43.00	0.841	269006	226234	
	1521.22	45.00	0.886	255448	226327	
					226343	0.998

TABLE 12.5

Gold Foil Data

(0.0005 cm thick)

Configuration 9A

Foil No.	Foil Type	Position Radial (cm)	Position Axial (cm)	Foil Weight (gm)	d/m/gm at S.D. x 10^{-6}	Norm to Center of Core
Run 1148						
1	Bare	0	89.4	0.0211	2.166	
2	Bare	0	74.9	0.0175	5.654	
3	Bare	0	59.6	0.0184	4.939	
4	Bare	0	44.4	0.0192	3.413	
5	Bare	0	29.1	0.0191	2.111	
6	Bare	0	13.9	0.0187	1.119	
7	Bare	0	0	0.0139	0.156	
8	Bare	93.2	151.1	0.0152	5.048	
9	Bare	107.7	151.1	0.0186	5.995	
10	Bare	123.0	151.1	0.0167	4.724	
11	Bare	138.2	151.1	0.0158	3.483	
12	Bare	153.5	151.1	0.0166	1.980	
13	Bare	168.7	151.1	0.0169	0.835	
14	Bare	183.9	151.1	0.0172	0.124	
Run 1149						
1	Cd cov	0	89.4	0.0136	1.283	
2	Cd cov	0	59.6	0.0174	0.330	
3	Cd cov	0	29.1	0.0159	0.011	
4	Cd cov	93.2	151.1	0.0211	1.444	
5	Cd cov	123.0	151.1	0.0182	0.360	
6	Cd cov	153.5	151.1	0.0154	0.010	
1	Bare	0	93.3	0.0185	1.650	1.327
2	Bare	0	105.3	0.0159	1.166	0.938
3	Bare	0	120.6	0.0208	1.051	0.845
4	Bare	0	135.8	0.0164	1.106	0.890
5	Bare	0	151.1	0.0175	1.243	1.000
6	Bare	0	166.3	0.0184	1.379	1.109
7	Bare	0	181.5	0.0191	1.599	1.286
8	Bare	0	196.8	0.0155	1.839	1.479
9	Bare	0	208.8	0.0185	2.268	1.824
10	Bare	15.2	93.3	0.0193	1.572	1.264
11	Bare	15.2	120.6	0.0157	1.083	0.871
12	Bare	15.2	151.1	0.0175	1.289	1.036
13	Bare	15.2	181.5	0.0155	1.643	1.321

TABLE 12.5

(Continued)

Foil No.	Foil Type	Position Radial (cm)	Position Axial (cm)	Foil Weight (gm)	d/m/gm at S.D. x 10^{-6}	Norm. to Center of Core
Run 1149 (Cont'd)						
14	Bare	15.2	208.8	0.0176	2.107	1.695
15	Bare	30.5	93.3	0.0175	1.782	1.433
16	Bare	30.5	105.3	0.0162	1.302	1.047
17	Bare	30.5	120.6	0.0151	1.167	0.939
18	Bare	30.5	135.8	0.0146	1.306	1.051
19	Bare	30.5	151.1	0.0176	1.434	1.153
20	Bare	30.5	166.3	0.0200	1.565	1.258
21	Bare	30.5	181.5	0.0180	1.842	1.481
22	Bare	30.5	196.8	0.0163	2.076	1.669
23	Bare	30.5	208.8	0.0182	2.331	1.875
24	Bare	61.0	93.3	0.0203	2.466	1.983
25	Bare	61.0	105.3	0.0123	2.449	1.970
26	Bare	61.0	120.6	0.0149	2.339	1.881
27	Bare	53.3	135.8	0.0198	1.857	1.493
28	Bare	53.3	151.1	0.0205	2.246	1.806
29	Bare	53.3	166.3	0.0163	2.437	1.960
30	Bare	45.7	181.5	0.0180	2.320	1.866
31	Bare	45.7	196.8	0.0190	2.531	2.036
32	Bare	45.7	208.8	0.0178	2.640	2.123
33	Bare	76.2	93.3	0.0196	3.032	2.438
34	Bare	76.2	120.6	0.0134	2.976	2.394
35	Bare	76.2	151.1	0.0171	3.070	2.469
36	Bare	76.2	181.5	0.0158	3.105	2.497
37	Bare	76.2	208.8	0.0163	2.889	2.323
38	Bare	91.4	93.3	0.0136	4.035	3.245
39	Bare	91.4	120.6	0.0189	4.095	3.293
40	Bare	91.4	151.1	0.0202	3.964	3.188
41	Bare	91.4	181.5	0.01395	3.868	3.111
42	Bare	91.4	208.8	0.0156	3.186	2.562
Run 1150						
1	Cd cov	0	93.3	0.01165	1.221	
2	Cd cov	0	120.6	0.01975	0.910	
3	Cd cov	0	151.1	0.0167	1.024	
4	Cd cov	0	181.5	0.0135	1.083	
5	Cd cov	0	208.8	0.0191	1.112	
6	Cd cov	30.5	151.1	0.0171	0.625	
7	Cd cov	45.7	181.5	0.01355	1.250	
8	Cd cov	53.3	151.1	0.0210	1.137	

TABLE 12.5

(Continued)

Foil No.	Foil Type	Position Radial (cm)	Position Axial (cm)	Foil Weight (gm)	d/m/gm at S.D. x 10^{-6}	Norm. to Center of Core
Run 1150 (Cont'd)						
9	Cd cov	61.0	120.6	0.0142	1.215	
10	Cd cov	91.4	151.1	0.0182	1.460	
11	Cd cov	0	74.9	0.0166	1.261	
12	Cd cov	0	44.4	0.0158	0.060	
13	Cd cov	107.7	151.1	0.0156	1.140	
14	Cd cov	138.2	151.1	0.0206	0.066	

TABLE 12.6

Gold Foil Data

(0.0005 cm thick)

Configuration 9E

Foil No.	Type	Position Radial (cm)	Position Axial (cm)	Foil Weight (gm)	d/m/gm at S.D. x 10^{-6}	Norm. to Center of Core x 10^{-6}
Run 1151						
1	Bare	0	89.4	0.0174	2.206	
2	Bare	0	74.9	0.0184	5.607	
3	Bare	0	59.6	0.0184	4.839	
4	Bare	0	44.4	0.0165	3.191	
5	Bare	0	29.1	0.0162	2.050	
6	Bare	0	13.9	0.0140	1.073	
7	Bare	0	0	0.0172	0.143	
8	Bare	93.2	151.1	0.0133	5.298	
9	Bare	107.7	151.1	0.0169	5.999	
10	Bare	123.0	151.1	0.0173	5.145	
11	Bare	138.2	151.1	0.0181	3.440	
12	Bare	153.5	151.1	0.0198	1.640	
13	Bare	168.7	151.1	0.0198	0.844	
14	Bare	183.9	151.1	0.0221	0.120	
Run 1152						
1	Bare	0	93.3	0.0186	1.614	1.290
2	Bare	0	105.3	0.0179	1.175	0.939
3	Bare	0	120.6	0.0212	1.015	0.811
4	Bare	0	135.8	0.0161	1.193	0.954
5	Bare	0	151.1	0.0169	1.251	1.000
6	Bare	0	166.3	0.0160	1.384	1.106
7	Bare	0	181.5	0.0185	1.597	1.277
8	Bare	0	196.8	0.0187	1.860	1.487
9	Bare	0	208.8	0.0208	2.210	1.767
10	Bare	15.2	93.3	0.0164	1.748	1.397
11	Bare	15.2	120.6	0.01995	1.073	0.858
12	Bare	15.2	151.1	0.0168	1.324	1.058
13	Bare	15.2	181.5	0.0189	1.636	1.308
14	Bare	15.2	208.8	0.0104	2.122	1.696
15	Bare	30.5	93.3	0.0148	1.854	1.482
16	Bare	30.5	105.3	0.0145	1.341	1.072
17	Bare	30.5	120.6	0.0185	1.111	0.888
18	Bare	30.5	135.8	0.0157	1.300	1.039

TABLE 12.6

(Continued)

Foil No.	Type	Position Radial (cm)	Position Axial (cm)	Foil Weight (gm)	d/m/gm at S.D. x 10^{-6}	Norm. to Center of Core x 10^{-6}
Run 1152 (Cont'd)						
19	Bare	30.5	151.1	0.0161	1.445	1.155
20	Bare	30.5	166.3	0.0201	1.495	1.195
21	Bare	30.5	181.5	0.0163	1.806	1.444
22	Bare	30.5	196.8	0.0172	2.134	1.706
23	Bare	30.5	208.8	0.0130	2.420	1.934
24	Bare	61.0	93.3	0.0144	2.495	1.994
25	Bare	61.0	105.3	0.0183	2.399	1.918
26	Bare	61.0	120.6	0.0187	2.042	1.632
27	Bare	53.3	135.8	0.0153	2.042	1.632
28	Bare	53.3	151.1	0.0174	2.428	1.941
29	Bare	53.3	166.3	0.0153	2.370	1.894
30	Bare	45.7	181.5	0.0141	2.387	1.908
31	Bare	45.7	196.8	0.0161	2.509	2.006
32	Bare	45.7	208.8	0.0169	2.665	2.130
33	Bare	76.2	93.3	0.0164	3.064	2.449
34	Bare	76.2	120.6	0.0160	2.973	2.376
35	Bare	76.2	151.1	0.0161	3.090	2.470
36	Bare	76.2	181.5	0.0163	3.024	2.417
37	Bare	76.2	208.8	0.0199	2.874	2.297
38	Bare	91.4	93.3	0.0177	3.760	3.006
39	Bare	91.4	120.6	0.0175	4.173	3.336
40	Bare	91.4	151.1	0.0179	4.095	3.273
41	Bare	91.4	181.5	0.0189	3.882	3.103
42	Bare	91.4	208.8	0.0210	2.961	2.367
43	Cd cov	0	89.4	0.0143	1.266	
44	Cd cov	0	59.6	0.0131	0.346	
45	Cd cov	0	29.1	0.0177	0.010	
46	Cd cov	93.2	151.1	0.0129	1.764	
47	Cd cov	123.0	151.1	0.0139	0.423	
48	Cd cov	153.5	151.1	0.0177	0.013	
Run 1153						
1	Cd cov	0	74.9	0.0152	1.239	
2	Cd cov	0	44.4	0.0133	0.055	
3	Cd cov	107.7	151.1	0.0176	1.118	
4	Cd cov	138.2	151.1	0.0158	0.076	
5	Cd cov	0	93.3	0.0209	1.043	

TABLE 12.6

(Continued)

Foil No.	Foil Type	Position Radial (cm)	Position Axial (cm)	Foil Weight (gm)	d/m/gm at S.D. x 10^{-6}	Norm. to Center of Core x 10^{-6}
Run 1153 (Cont'd)						
6	Cd cov	0	120.6	0.0172	0.921	
7	Cd cov	0	151.1	0.0153	1.020	
8	Cd cov	0	181.5	0.0211	1.026	
9	Cd cov	0	208.8	0.0177	1.107	
10	Cd cov	30.5	151.1	0.0163	1.073	
11	Cd cov	61.0	120.6	0.0141	1.261	
12	Cd cov	53.3	151.1	0.0159	1.200	
13	Cd cov	45.7	181.5	0.0199	1.136	
14	Cd cov	91.4	151.1	0.0187	1.412	

TABLE 12.7

Comparison of Axial Averages

Gold Foil Data

Configuration 9

Radial Location of Axial Profile	Axial Average Configuration 9A	Configuration 9E	9E/9A
0	1.113	1.104	0.992
15.2	1.145	1.153	1.007
30.5	1.256	1.263	1.006
76.2	2.442	2.417	0.990
91.4	3.155	3.165	1.003
	Comparison by Region		
	Region 1		
0	0.947	0.927	0.979
15.2	0.973	0.991	1.018
30.5	1.047	1.051	1.004
61.0	1.921	1.867	0.972
76.2	2.407	2.391	0.993
91.4	3.260	3.258	0.999
	Region 2		
0	1.013	1.024	1.011
15.2	1.063	1.078	1.014
30.5	1.184	1.186	1.002
53.3	1.826	1.878	1.028
76.2	2.472	2.468	0.998
91.4	3.233	3.259	1.008
	Region 3		
0	1.440	1.422	0.988
15.2	1.449	1.438	0.992
30.5	1.620	1.611	0.994
45.7	1.970	1.975	1.003
76.2	2.444	2.378	0.973
91.4	2.922	2.900	0.992

TABLE 12.8

Comparison of Gold Foil Data in Reflector Regions

Configuration 9

Location			Gold Foil Activity (d/m/gm x 10^{-6})		
Radial (cm)	Axial (cm)	Type	Configuration 9A	Configuration 9E	9E/9A
0	89.4	Bare	2.166	2.206	1.018
0	74.9	Bare	5.654	5.607	0.992
0	59.6	Bare	4.939	4.839	0.980
0	44.4	Bare	3.413	3.191	0.935
0	29.1	Bare	2.111	2.050	0.971
0	13.9	Bare	1.119	1.073	0.959
0	0	Bare	0.156	0.143	0.917
93.2	151.1	Bare	5.048	5.298	1.050
107.7	151.1	Bare	5.995	5.999	1.001
123.0	151.1	Bare	4.724	5.145	1.089
138.2	151.1	Bare	3.483	3.440	0.988
153.5	151.1	Bare	1.980	1.640	0.828
168.7	151.1	Bare	0.835	0.844	1.011
183.9	151.1	Bare	0.124	0.120	0.968
0	89.4	Cd	1.283	1.266	0.987
0	74.9	Cd	1.261	1.239	0.983
0	59.6	Cd	0.330	0.346	1.048
0	44.4	Cd	0.060	0.055	0.917
0	29.1	Cd	0.011	0.010	0.909
93.2	151.1	Cd	1.444	1.764	1.222
107.7	151.1	Cd	1.140	1.118	0.981
123.0	151.1	Cd	0.360	0.423	1.175
138.2	151.1	Cd	0.066	0.076	1.152
153.5	151.1	Cd	0.010	0.013	1.300

TABLE 12.9

Gold Foil Cadmium Ratios

Configuration 9A

Location		Infinitely Dilute Foil Activity (d/m/gm x 10^{-6})		Cadmium
Radial (cm)	Axial (cm)	Bare Foil	Cadmium Covered Foil	Ratio
0	89.4	3.174	2.113	1.502
0	74.9	6.632	2.217	2.992
0	59.6	5.205	0.598	8.829
0	44.4	3.461	0.104	33.36
0	29.1	2.120	0.019	111.2
93.2	151.1	6.192	2.761	2.242
107.7	151.1	6.884	1.963	3.507
123.0	151.1	5.006	0.653	7.665
138.2	151.1	3.536	0.125	28.26
153.5	151.1	6.987	0.017	115.9
0	93.3	2.517	1.918	1.312
0	120.6	1.857	1.699	1.093
0	151.1	2.039	1.804	1.130
0	181.5	2.414	1.780	1.357
0	208.8	3.195	2.052	1.557
30.5	151.1	2.253	1.850	1.217
45.7	181.5	3.239	2.056	1.575
53.3	151.1	3.270	2.171	1.506
61.0	120.6	3.172	2.029	1.563
91.4	151.1	5.206	2.649	1.965

TABLE 12.10

Gold Foil Cadmium Ratios

Configuration 9E

Location		Infinitely Dilute Foil Activity (d/m/gm x 10^{-6})		Cadmium
Radial (cm)	Axial (cm)	Bare Foil	Cadmium Covered Foil	Ratio
0	89.4	3.139	2.119	1.481
0	74.9	6.561	2.115	3.102
0	59.6	5.093	0.563	9.043
0	44.4	3.230	0.090	35.91
0	29.1	2.058	0.018	114.5
93.2	151.1	6.408	2.858	2.243
107.7	151.1	6.870	2.005	3.427
123.0	151.1	5.453	0.702	7.773
138.2	151.1	3.499	0.131	26.63
153.5	151.1	1.651	0.023	70.67
0	93.3	2.514	1.988	1.265
0	120.6	1.798	1.639	1.097
0	151.1	2.009	1.745	1.152
0	181.5	2.484	1.962	1.266
0	208.8	3.154	1.989	1.585
30.5	151.1	2.242	1.875	1.196
45.7	181.5	3.237	2.127	1.522
53.3	151.1	3.343	2.079	1.608
61.0	120.6	3.219	2.101	1.532
91.4	151.1	5.248	2.586	2.029

TABLE 12.11

Comparison of Gold Foil Cadmium Ratios (Infinitely Dilute)

Configurations 9A and 9E

Location		Cadmium Ratios		
Radial (cm)	Axial (cm)	Configuration 9A	Configuration 9E	9E/9A
0	89.4	1.502	1.481	0.986
0	74.9	2.992	3.102	1.037
0	59.6	8.829	9.043	1.024
0	44.4	33.36	35.91	1.076
0	29.1	111.2	114.5	1.030
93.2	151.1	2.242	2.243	1.000
107.7	151.1	3.507	3.427	1.977
123.0	151.1	7.664	7.773	1.014
138.2	151.1	28.26	26.63	0.942
153.5	151.1	115.9	70.67	0.610
0	93.3	1.312	1.265	0.964
0	120.6	1.093	1.097	1.004
0	151.1	1.130	1.152	1.019
0	181.5	1.357	1.266	0.933
0	208.8	1.557	1.585	1.018
30.5	151.1	1.217	1.196	0.983
45.7	181.5	1.575	1.522	0.966
53.3	151.1	1.506	1.608	1.066
61.0	120.6	1.563	1.532	0.980
91.4	151.1	1.965	2.029	1.033

TABLE 12.12

Thermal Neutron Flux

Configuration 9A

Location		Thermal Neutron Flux
Radial (cm)	Axial (cm)	n/cm^2-sec-watt x 10^{-6}
0	89.4	1.221
0	74.9	5.081
0	59.6	5.311
0	44.4	3.863
0	29.1	2.417
93.2	151.1	3.947
107.7	151.1	5.663
123.0	151.1	5.009
138.2	151.1	3.925
153.5	151.1	2.267
0	93.3	0.689
0	120.6	0.182
0	151.1	0.271
0	181.5	0.730
0	208.8	1.316
30.5	151.1	0.463
45.7	181.5	1.360
53.3	151.1	1.265
61.0	120.6	1.315
91.4	151.1	2.942

TABLE 12.13

Thermal Neutron Flux

Configuration 9E

Location			
Radial (cm)	Axial (cm)	Thermal Neutron Flux n/cm^2 sec watt x 10^{-6}	Configuration 9E / Configuration 9A
0	89.4	1.165	0.954
0	74.9	5.078	0.999
0	59.6	5.174	0.974
0	44.4	3.586	0.928
0	29.1	2.330	0.964
93.2	151.1	4.056	1.028
107.7	151.1	5.558	0.981
123.0	151.1	5.428	1.084
138.2	151.1	3.847	0.980
153.5	151.1	1.859	0.820
0	93.3	0.602	0.874
0	120.6	0.182	1.000
0	151.1	0.302	1.114
0	181.5	0.596	0.816
0	208.8	1.330	1.011
30.5	151.1	0.420	0.907
45.7	181.5	1.268	0.932
53.3	151.1	1.444	1.142
61.0	120.6	1.277	0.971
91.4	151.1	3.040	1.033
		Average	0.976 ± 0.066

TYPE 1 Fuel Element

1	2	3	4	5	6	7	8	9	10	11	12	13	14	15	16	← Stage number
1	2	3	1	2	3	1	2	3	1	2	3	1	2	3	1	← Fuel orientation
9	8	9	8	9	9	6	5	6	5	5	3	2	3	2	3	← Number of fuel sheets per stage

TYPE 2 Fuel Element

1	2	3	4	5	6	7	8	9	10	11	12	13	14	15	16	← Stage number
2	3	1	2	3	1	2	3	1	2	3	1	2	3	1	2	← Fuel orientation
9	9	9	9	9	9	5	5	5	5	5	3	3	3	3	3	← Number of fuel sheets per stage

TYPE 3 Fuel Element

1	2	3	4	5	6	7	8	9	10	11	12	13	14	15	16	← Stage number
3	1	2	3	1	2	3	1	2	3	1	2	3	1	2	3	← Fuel orientation
9	9	9	9	9	9	5	5	5	5	5	3	3	3	3	3	← Number of fuel sheets per stage

Region 1 | Region 2 | Region 3

The following number and types of fuel elements will be required for each region:

Region	Type 1	Type 2	Type 3	Totals
1	69	69	70	208 (1)
2	53	53	54	160
3	38	39	39	116

(1) 116 of these fuel elements will be fully loaded over the 16 stages, 44 will be loaded over Regions 1 and 2, and 48 will be loaded over Region 1 only.

Fig. 12.1 Fuel element loading pattern for configuration 9A

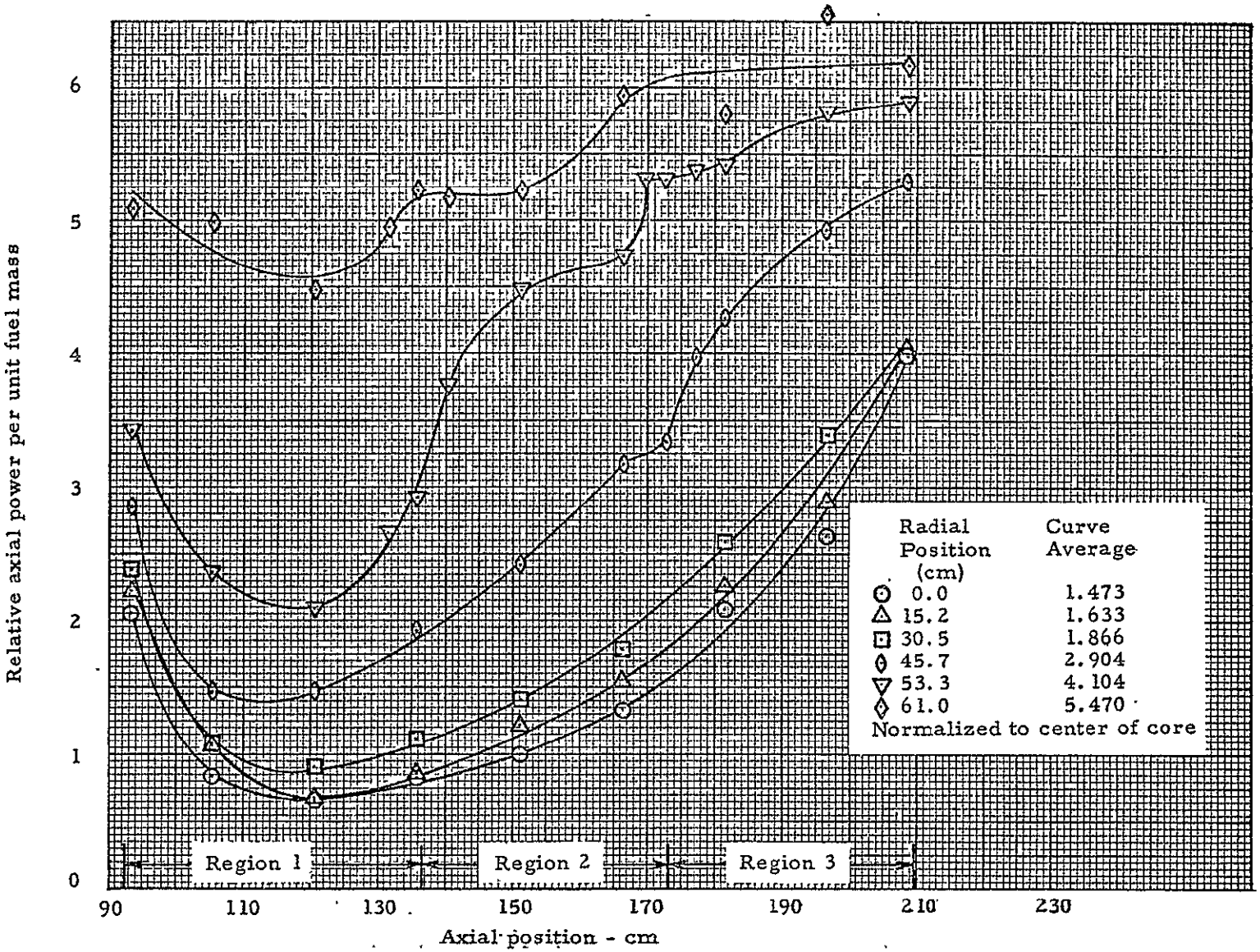

Fig. 12.2 Power distribution in core of configuration 9A

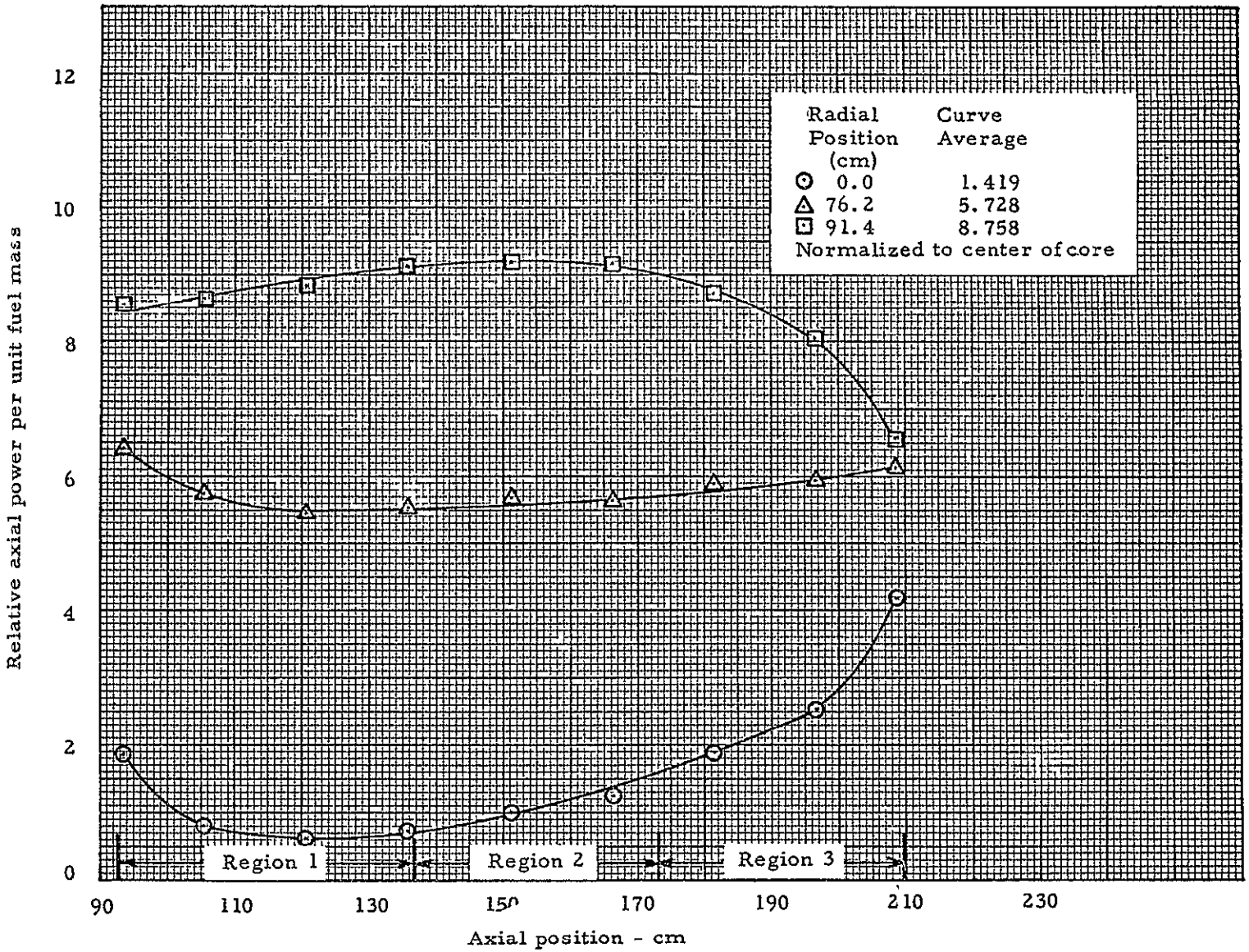

Fig. 12.3 Specific power distribution in cavity of configuration 9A

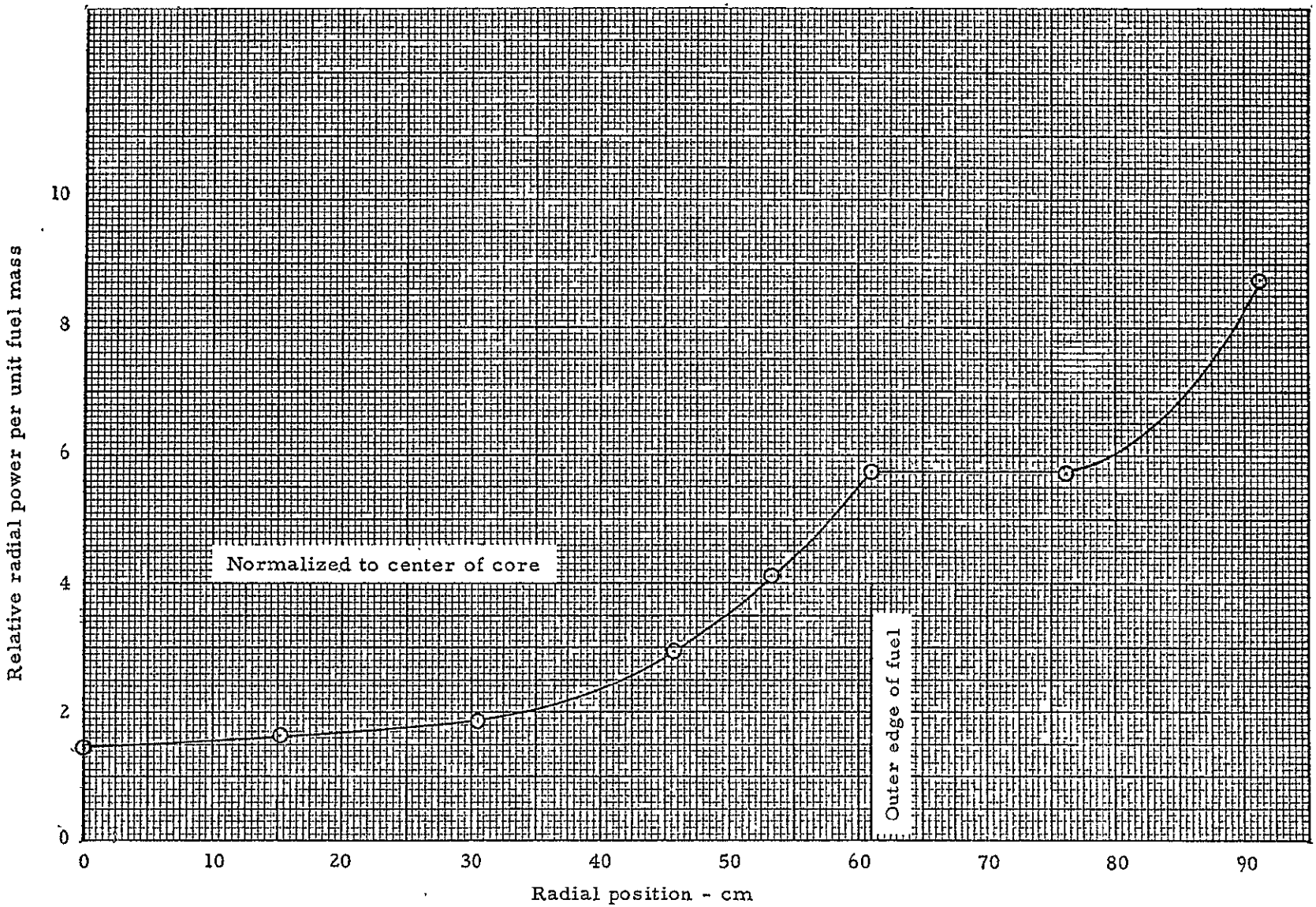

Fig. 12.4 Longitudinally averaged power distribution vs radius - configuration 9A

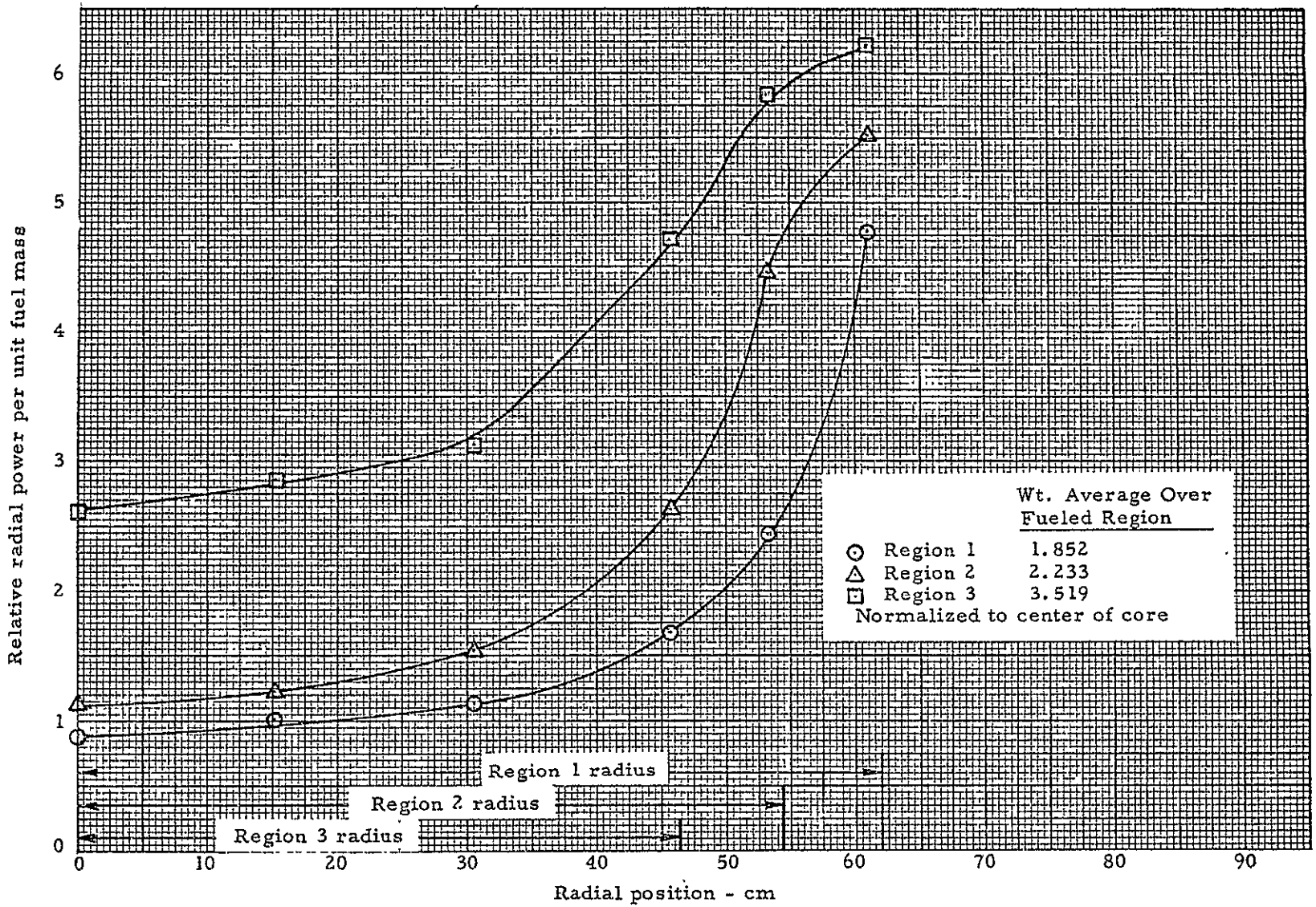

Fig. 12.5 Relative radial power distribution from axial averages over each region - configuration 9A

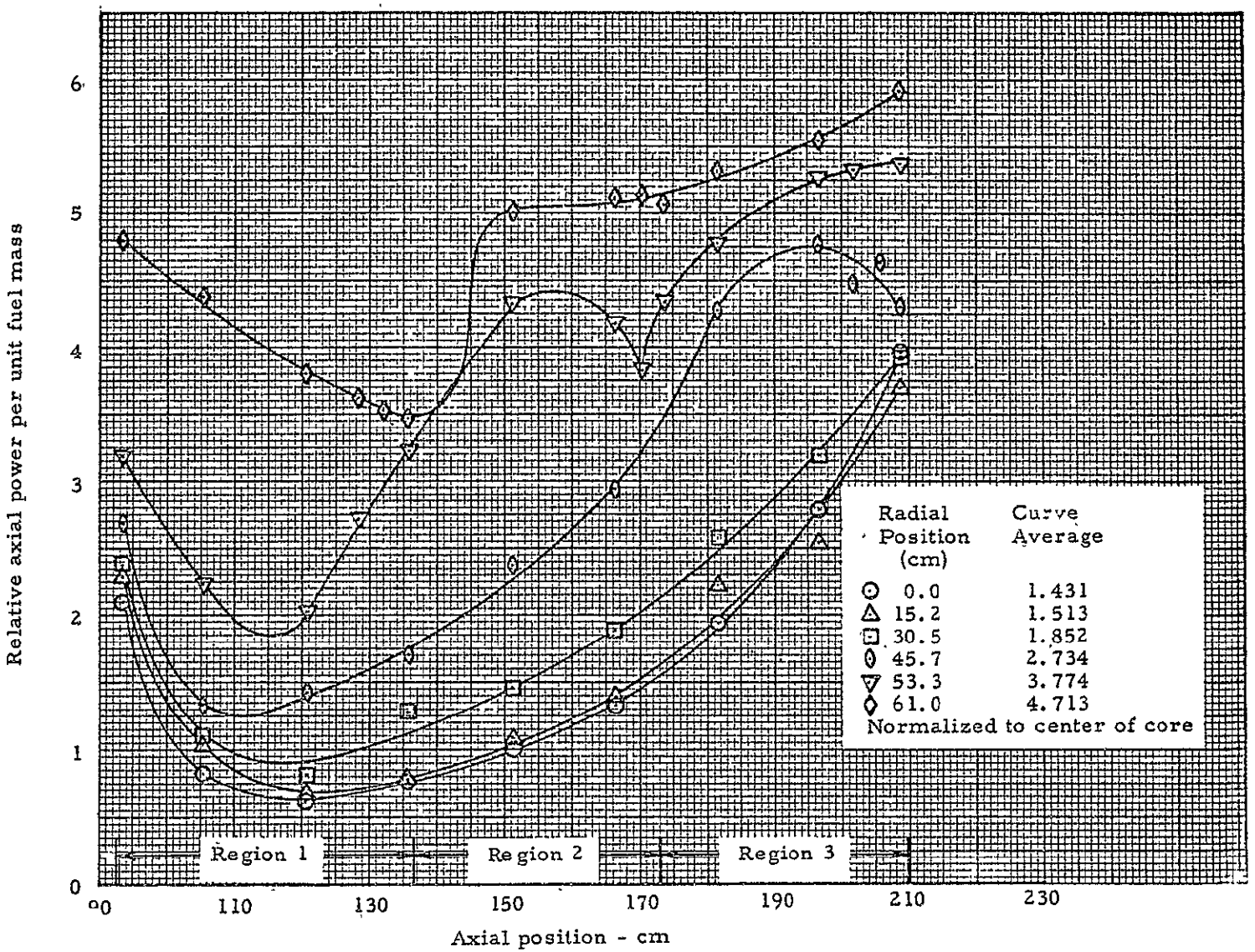

Fig. 12.6 Relative axial power distribution from bare catcher foils - configuration 9E

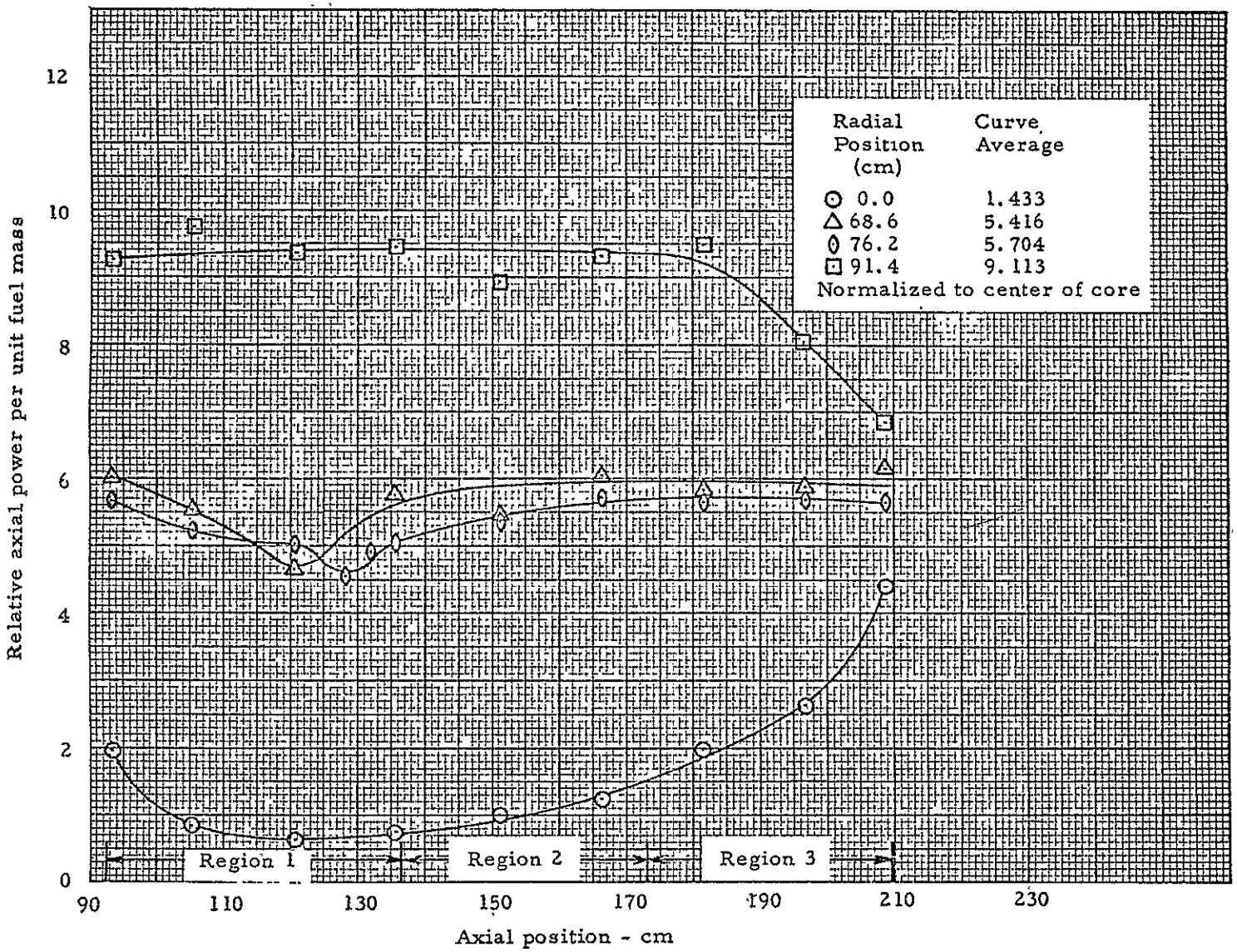

Fig. 12.7 Relative axial power distribution from bare catcher foils - configuration 9E

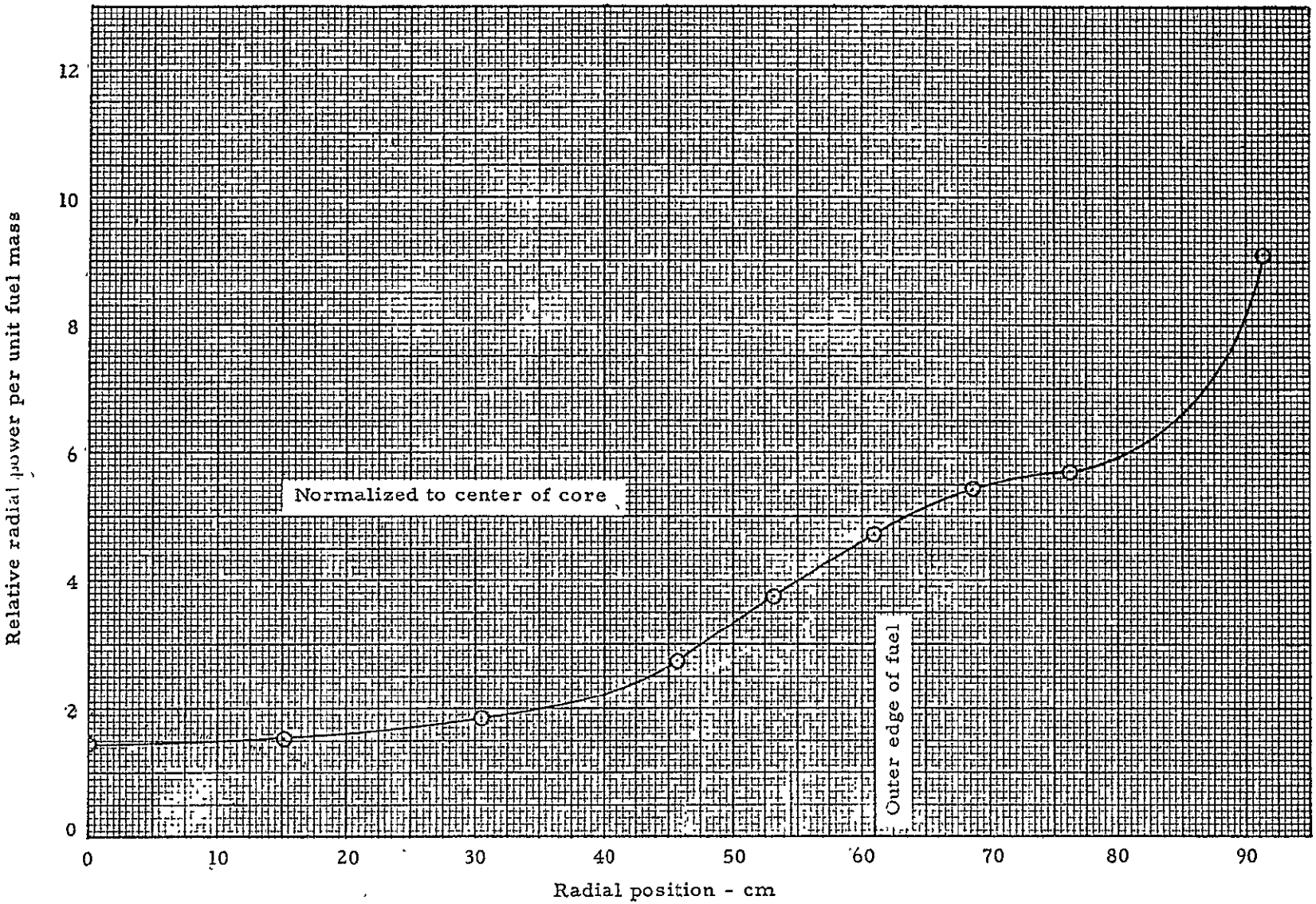

Fig. 12.8 Relative radial power distribution longitudinally averaged over full core length - configuration 9E

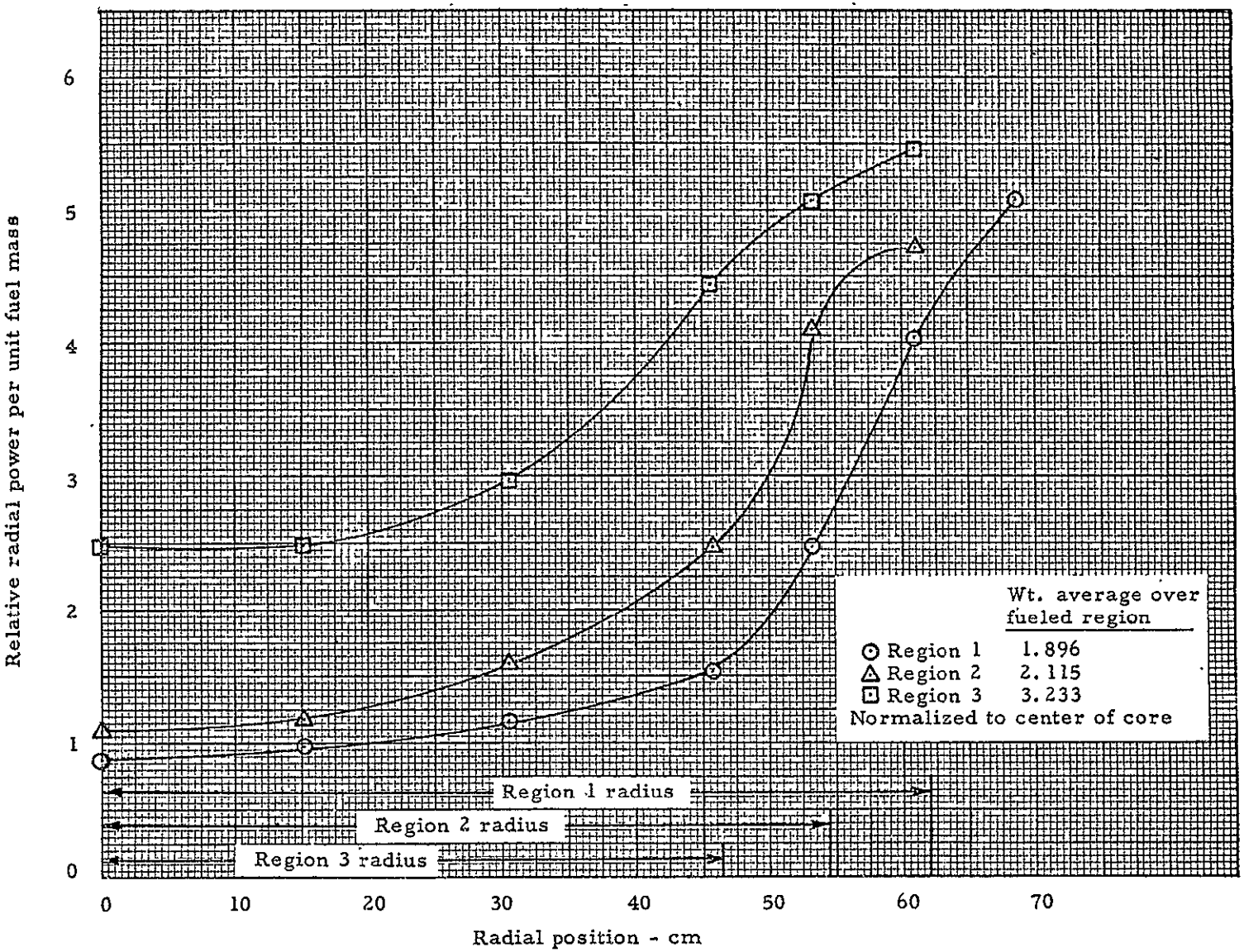

Fig. 12.9 Relative radial power distribution from axial averages over each region - configuration 9E

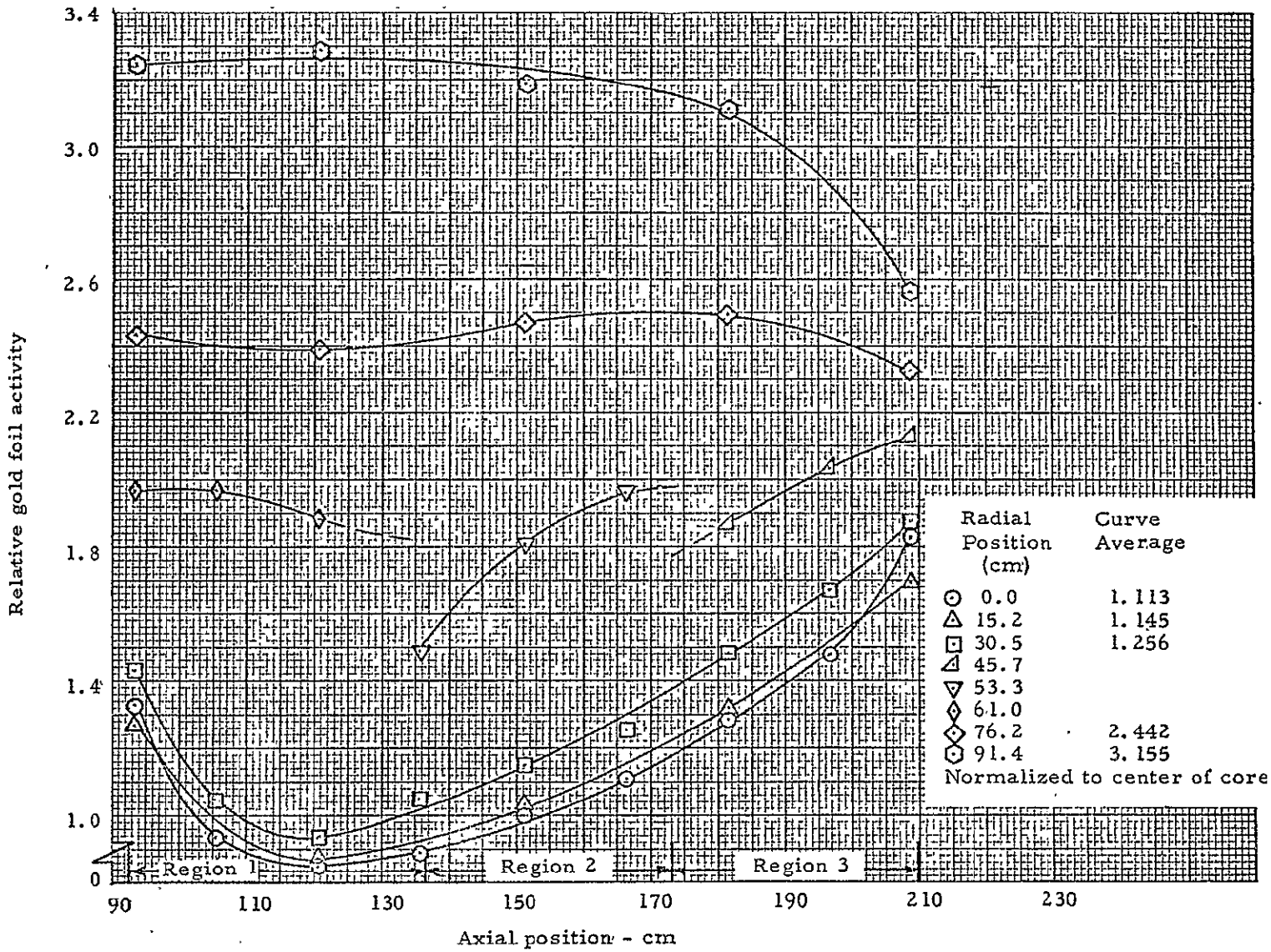

Fig. 12.10 Relative axial distribution of bare gold foil activity - configuration 9A

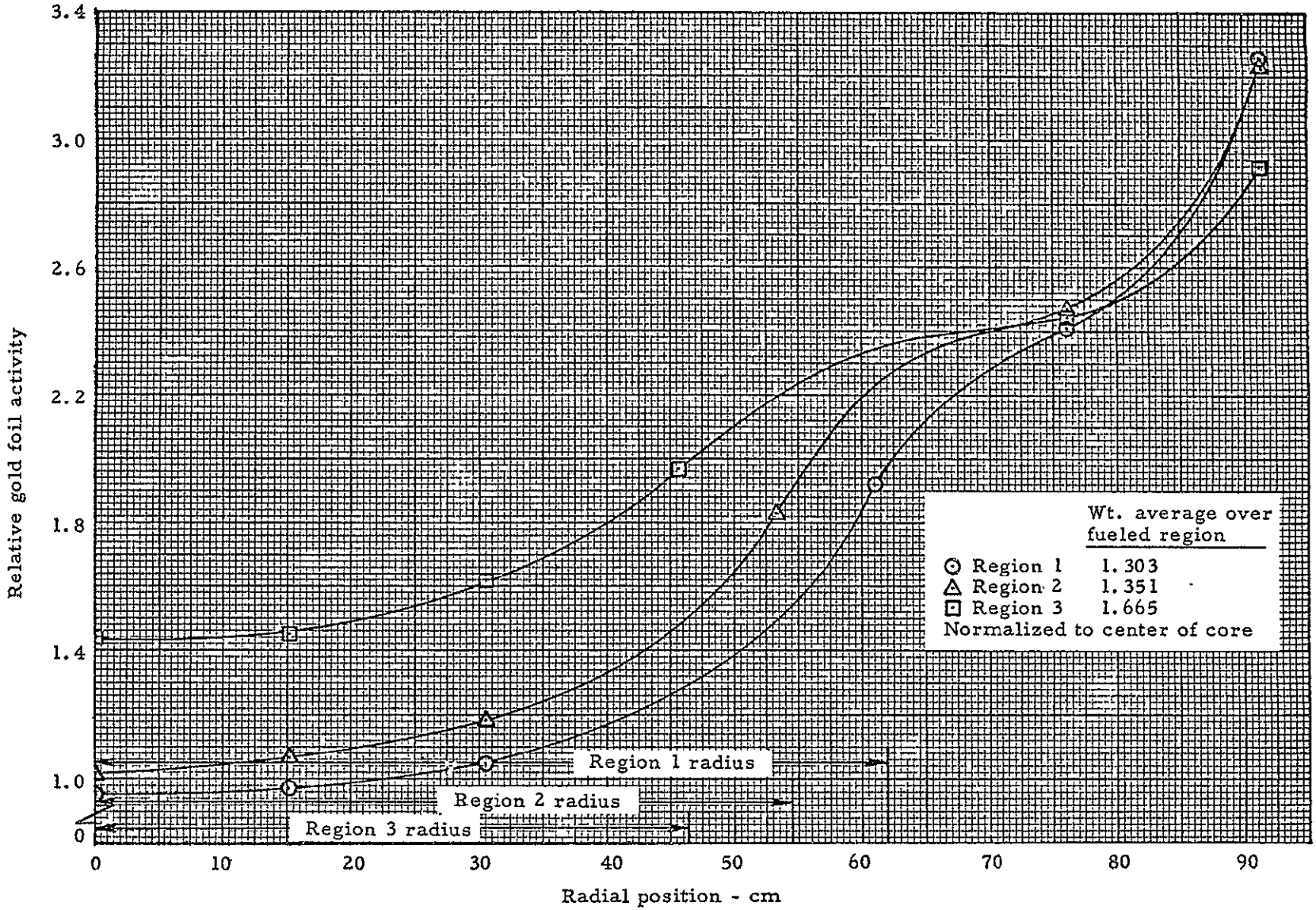

Fig. 12.11 Relative radial distribution of bare gold foil activity from axial averages over each region - configuration 9A

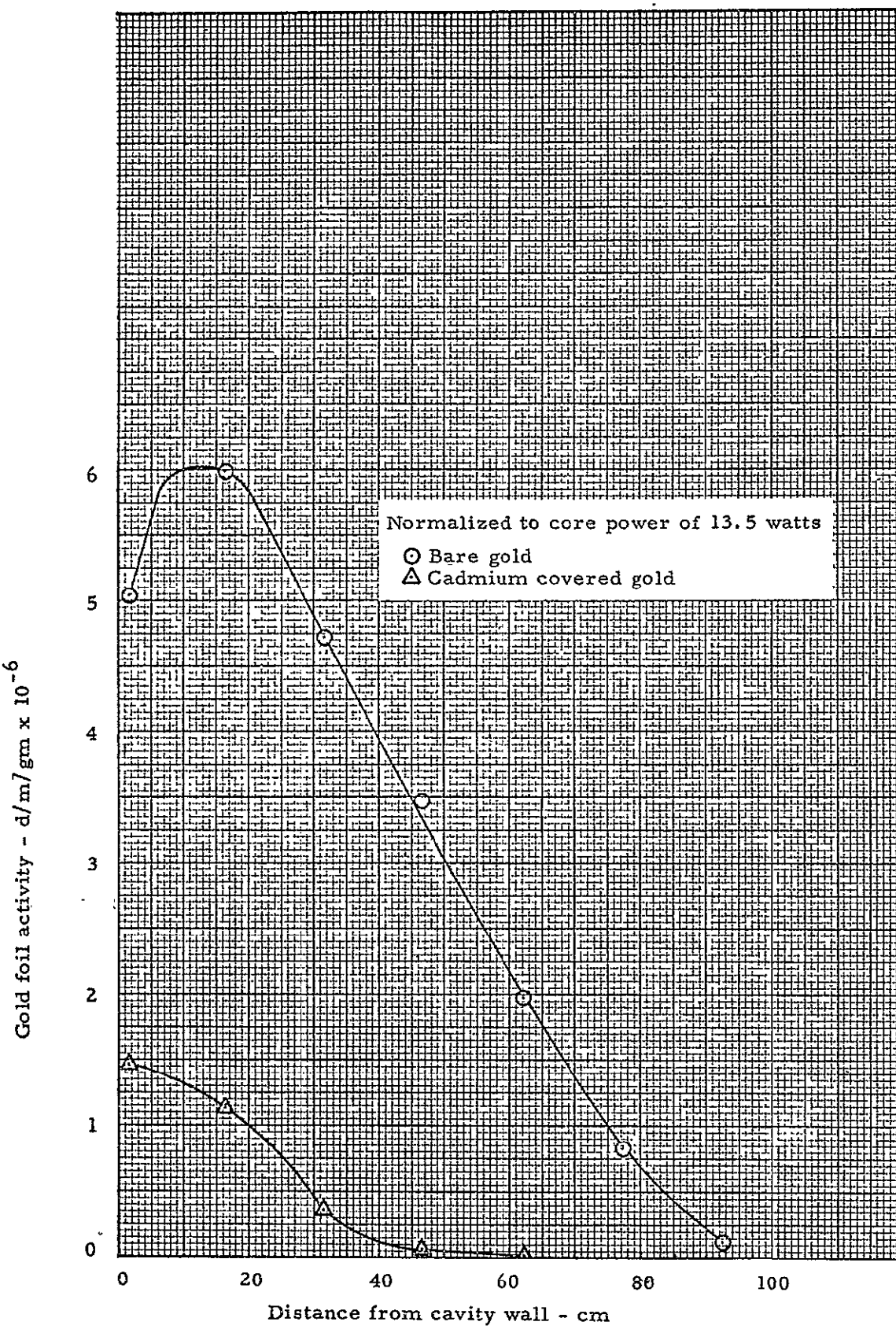

Fig. 12.12 Distribution of bare and cadmium covered gold foil activity in the radial reflector - configuration 9A

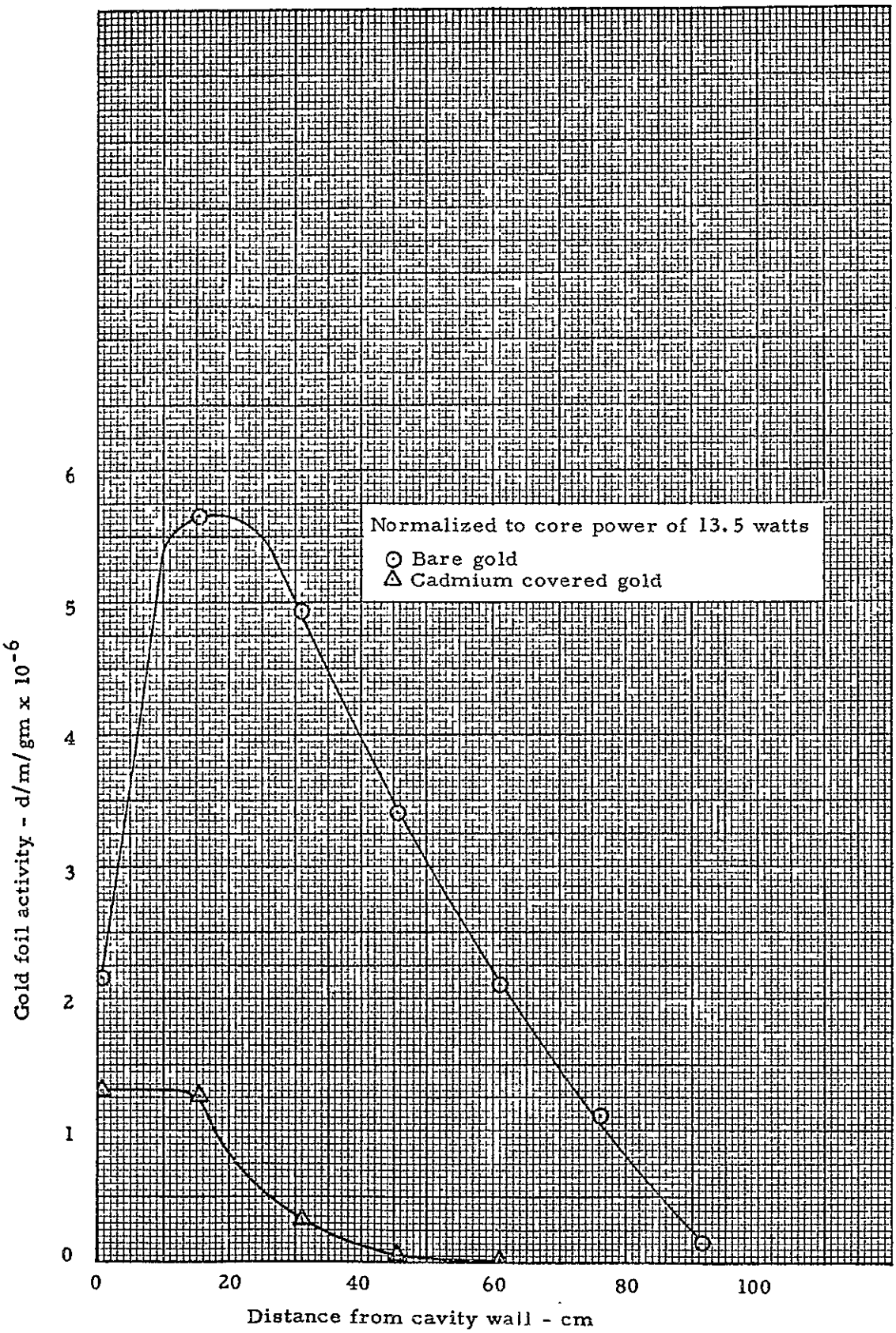

Fig. 12.13 Distribution of bare and cadmium covered gold foil activity in the end reflector - configuration 9A

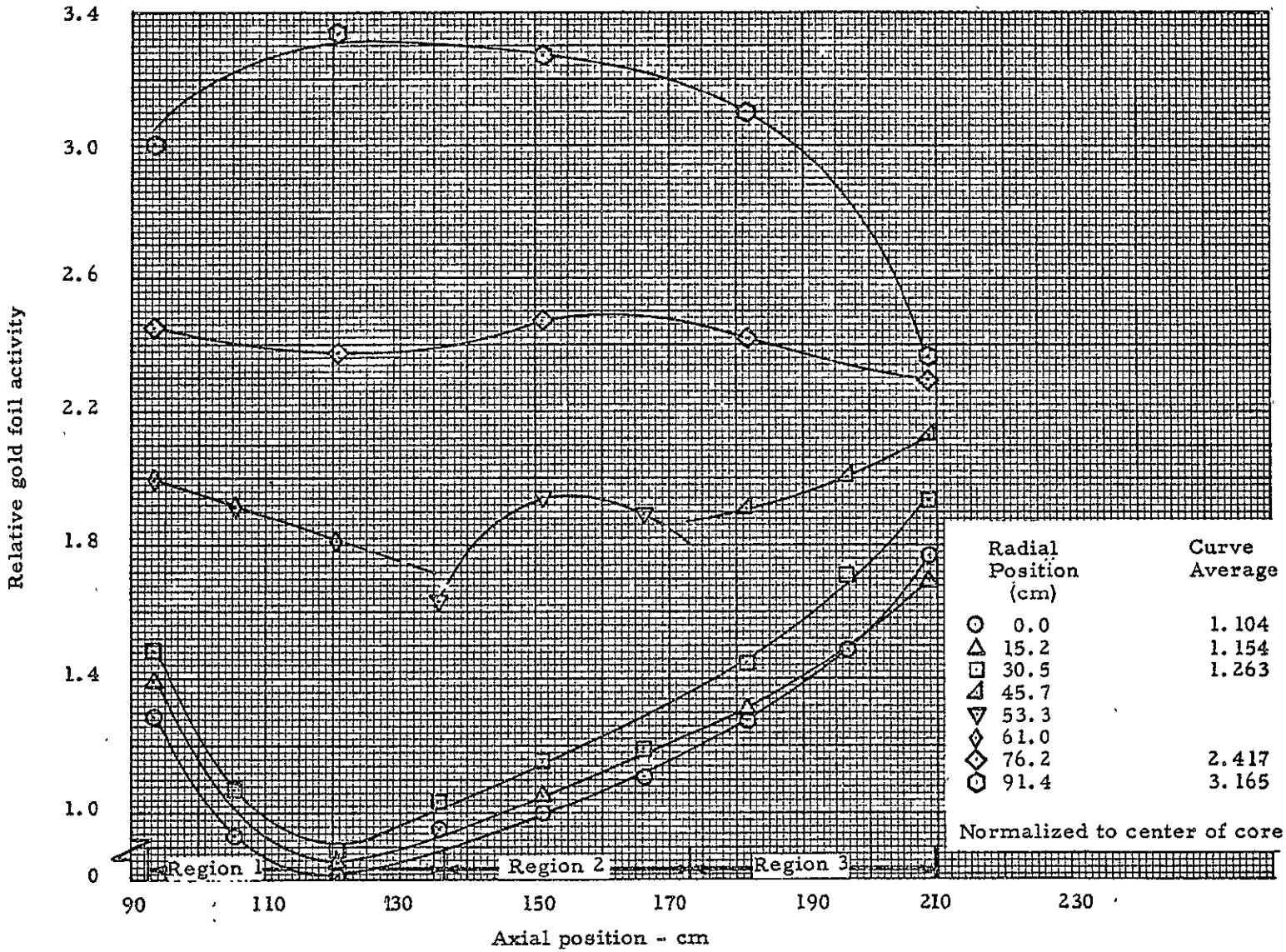

Fig. 12.14 Gold foil activity in cavity of configuration 9E

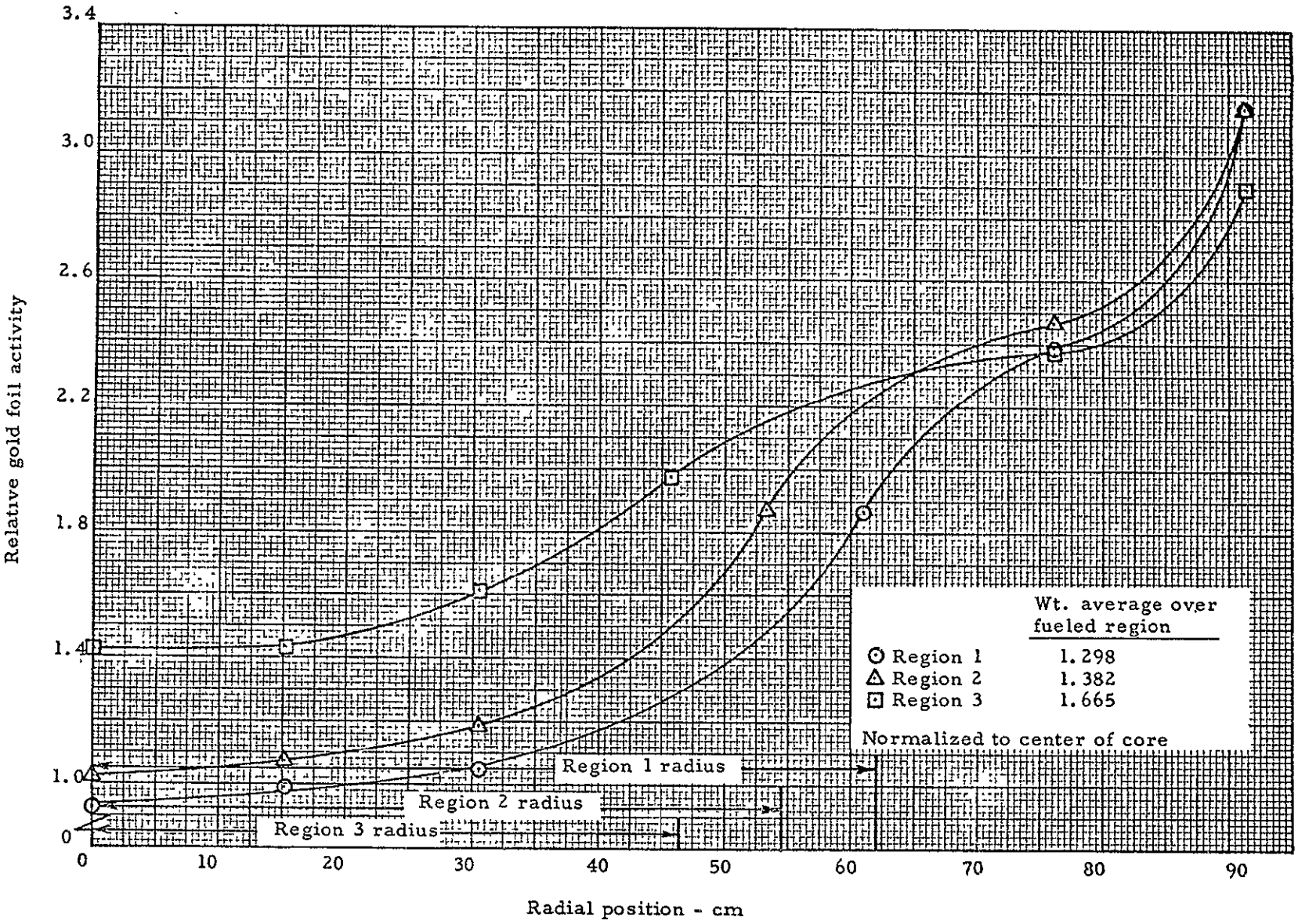

Fig. 12.15 Longitudinally averaged gold foil activity vs radius - configuration 9E

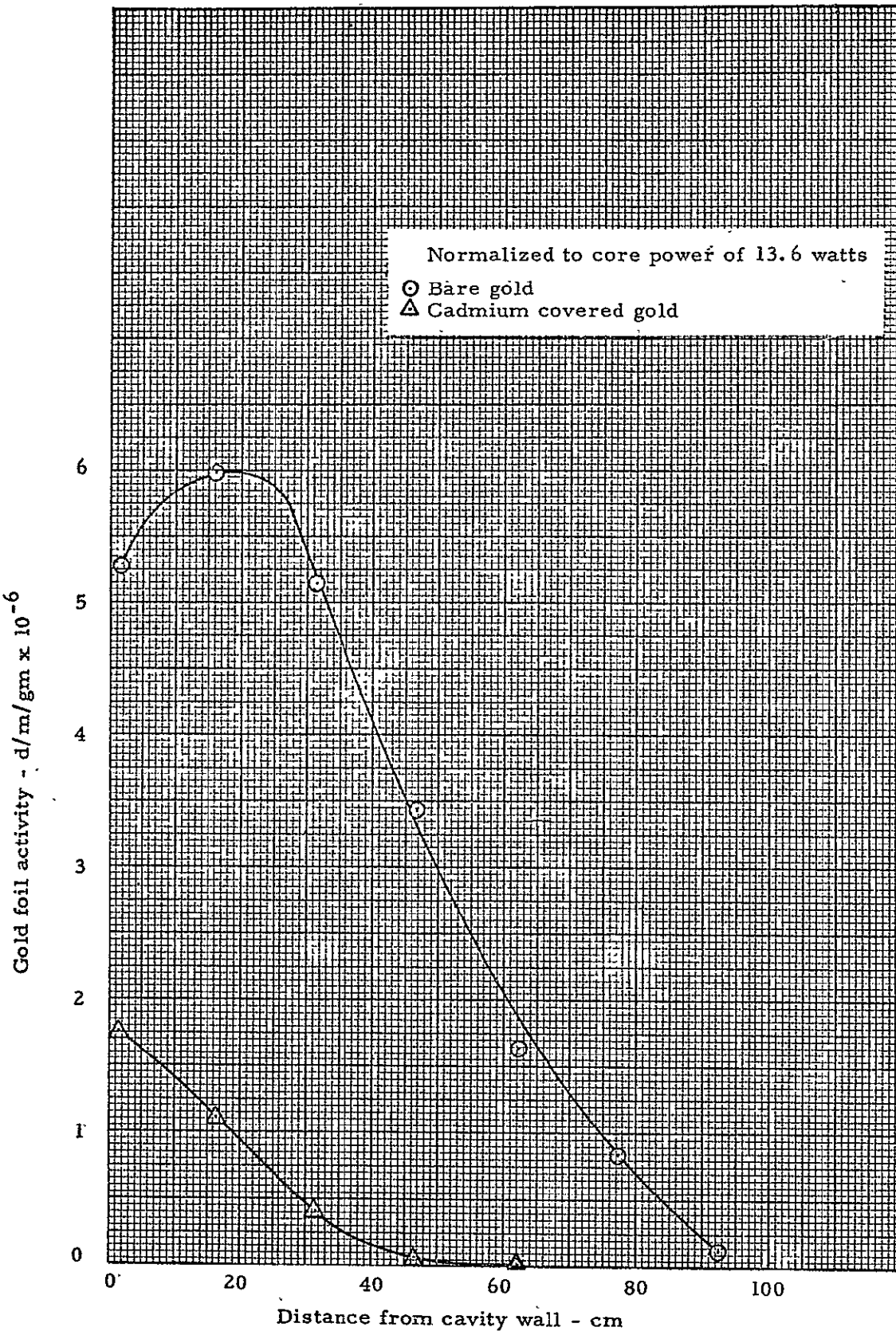

Fig. 12.16 Gold foil activity in radial reflector at axial midplane - configuration 9E

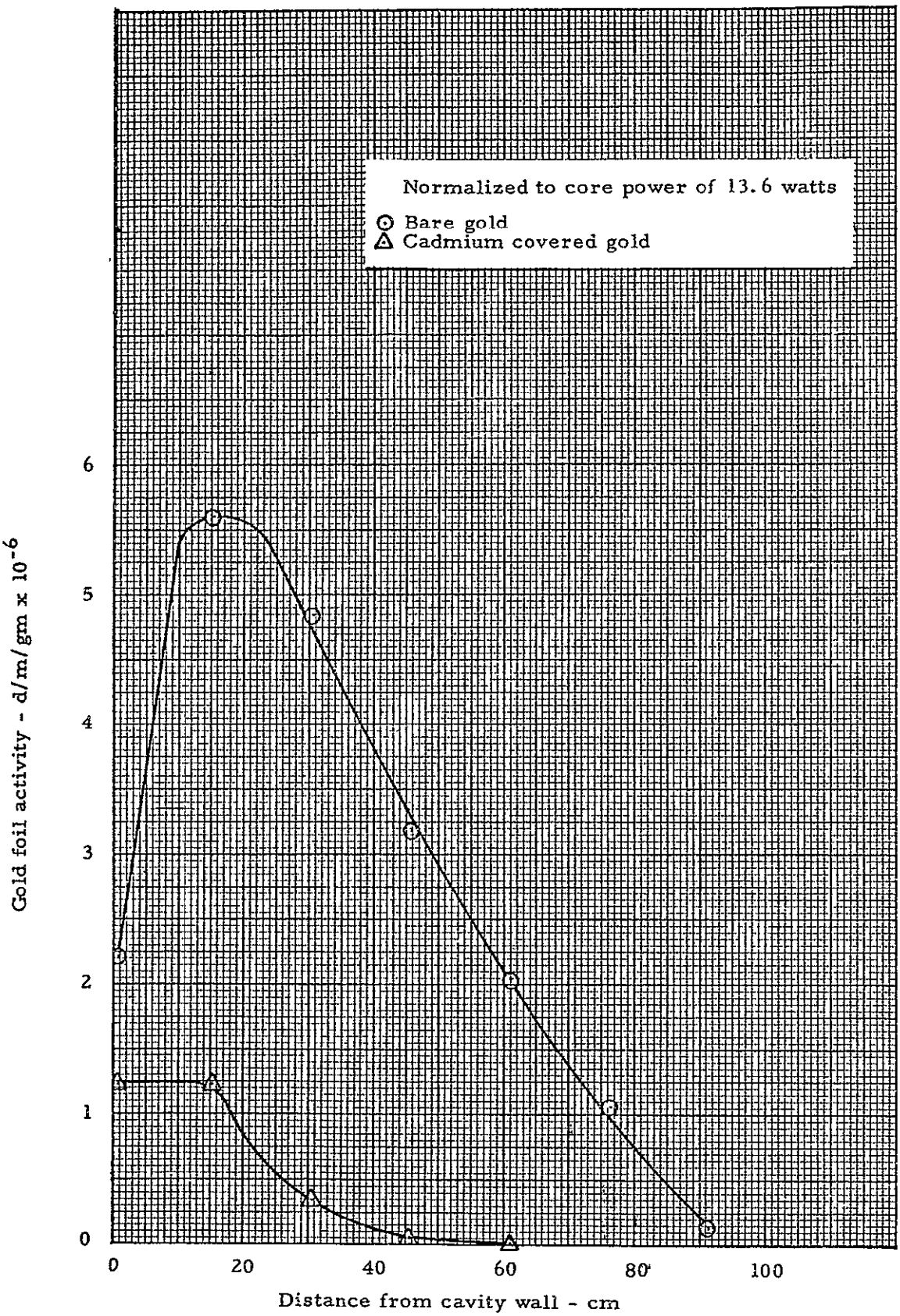

Fig. 12.17 Gold foil activity on axis at end reflector - configuration 9E

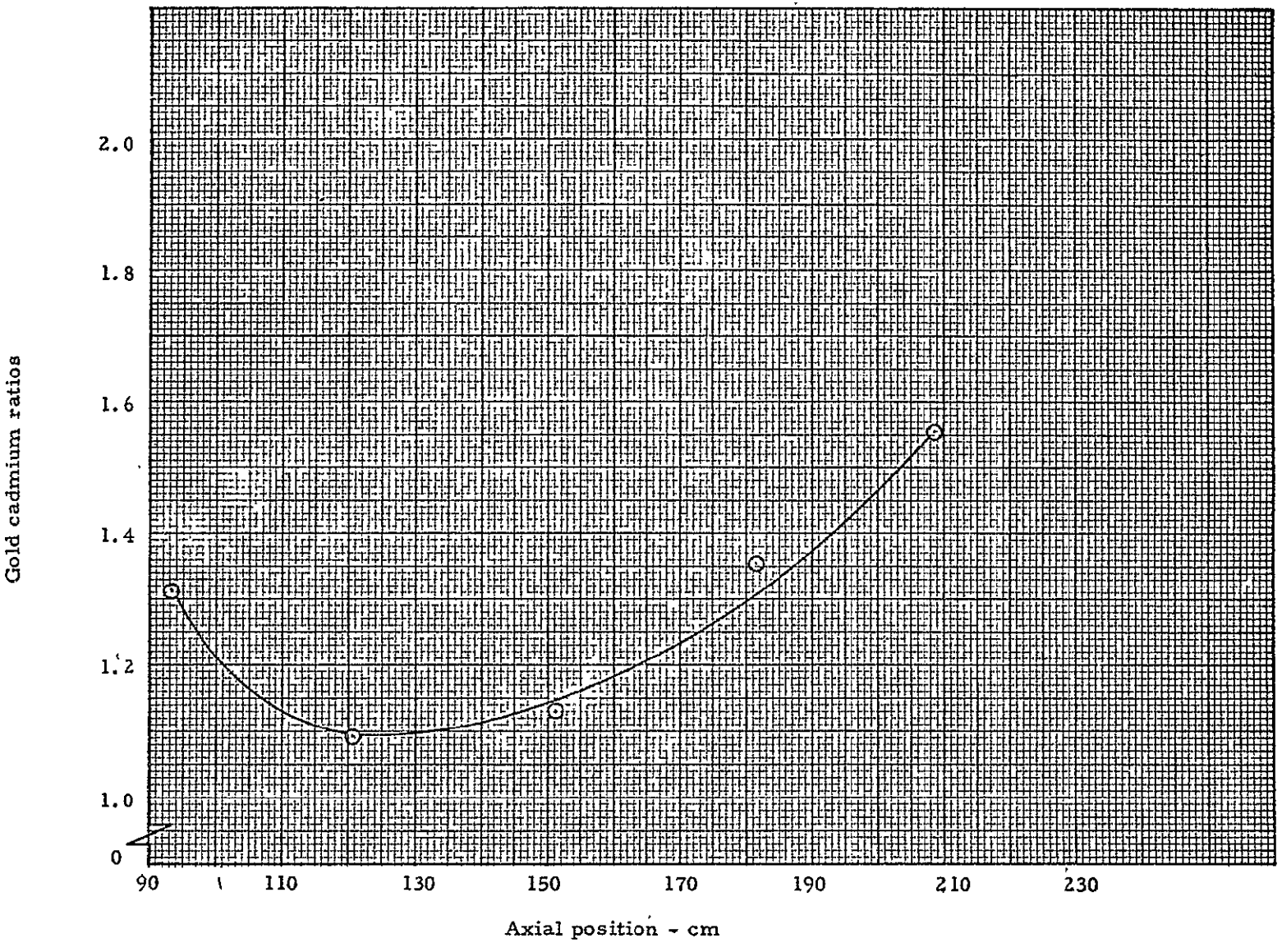

Fig. 12.18 Axial distribution of gold foil cadmium ratios at the core center - configuration 9A

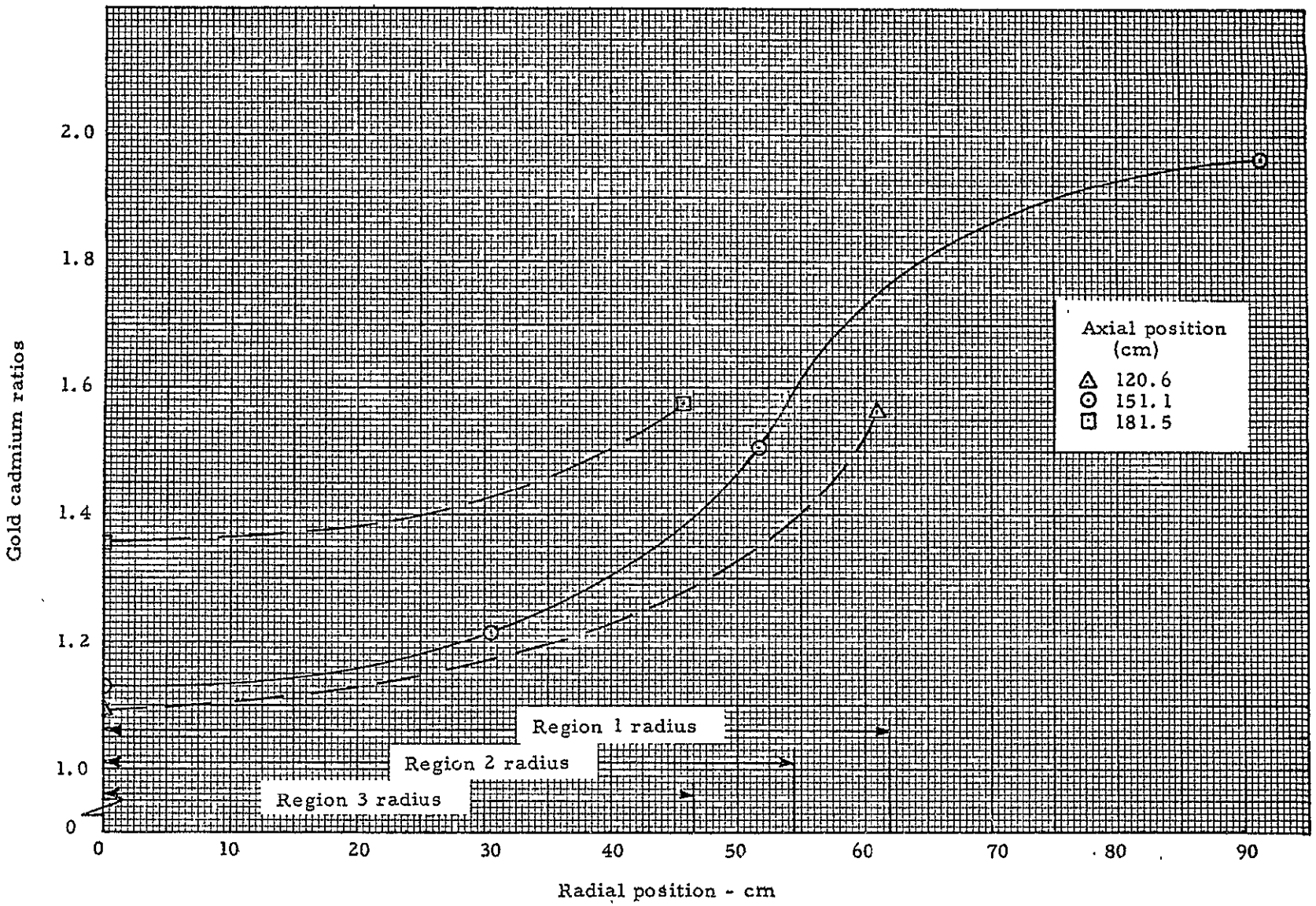

Fig. 12.19 Radial distribution of gold foil cadmium ratios - configuration 9A

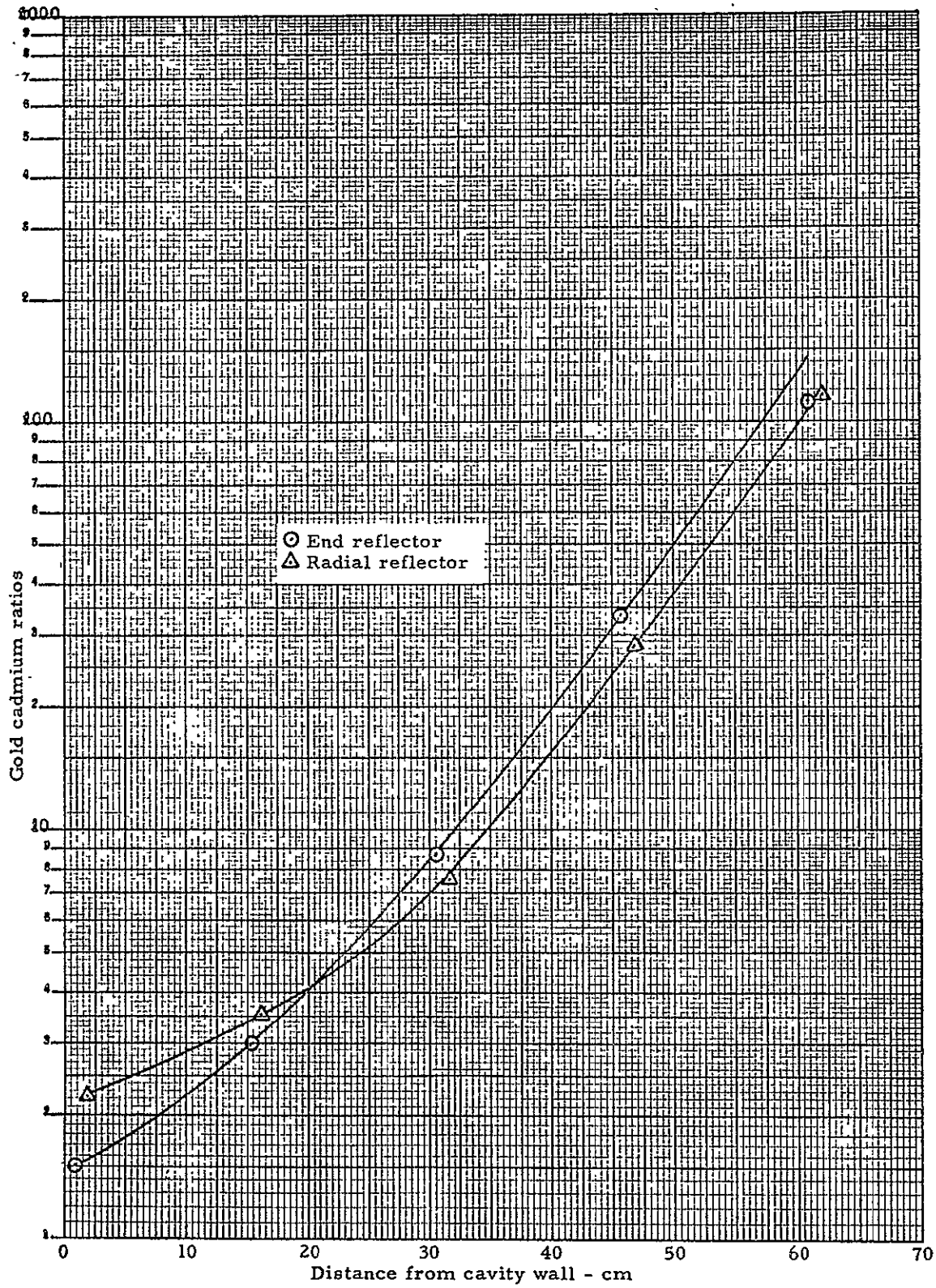

Fig. 12.20 Gold foil cadmium ratio distribution in the reflector regions - configuration 9A

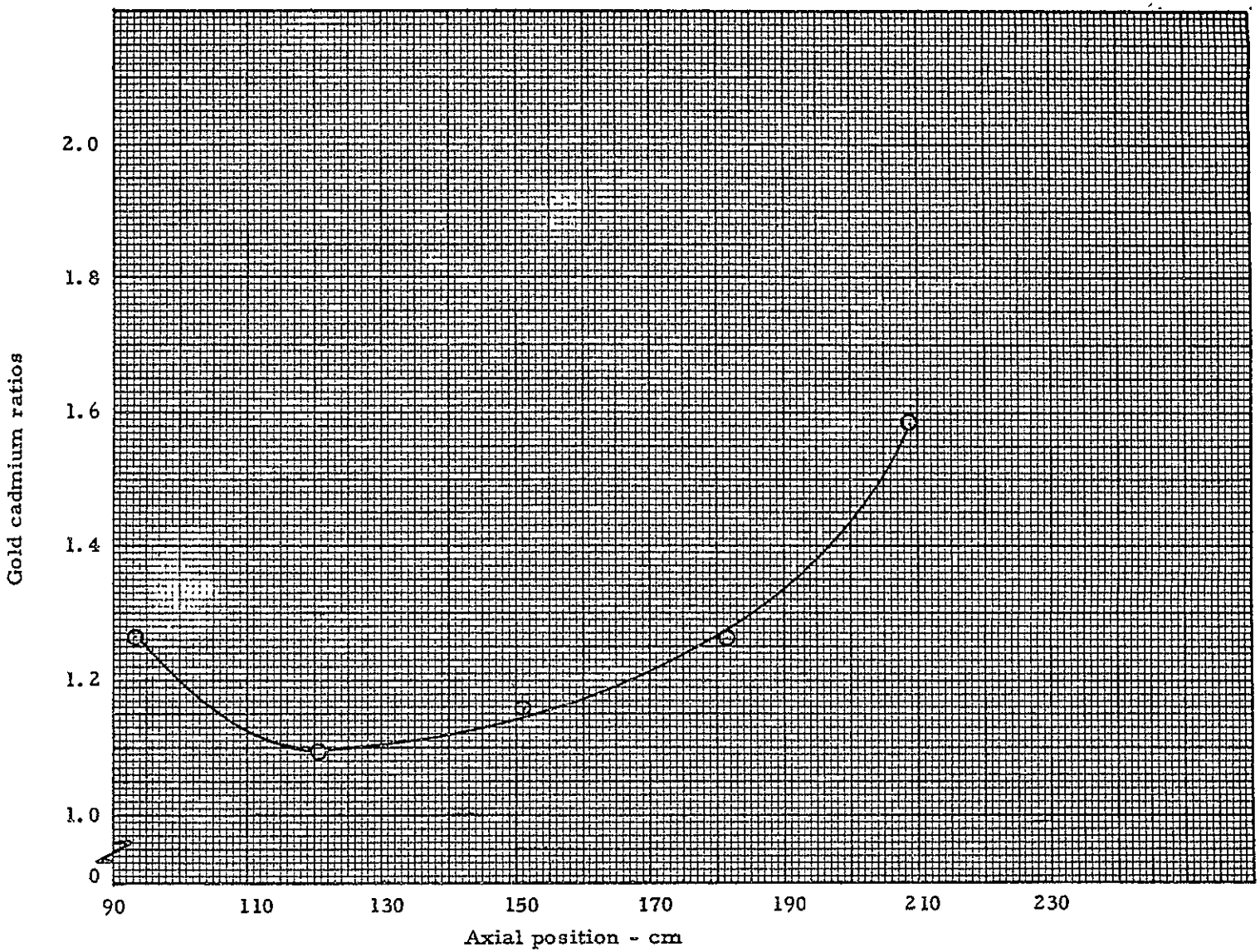

Fig. 12.21 Gold infinitely dilute cadmium ratios along core axis - configuration 9E

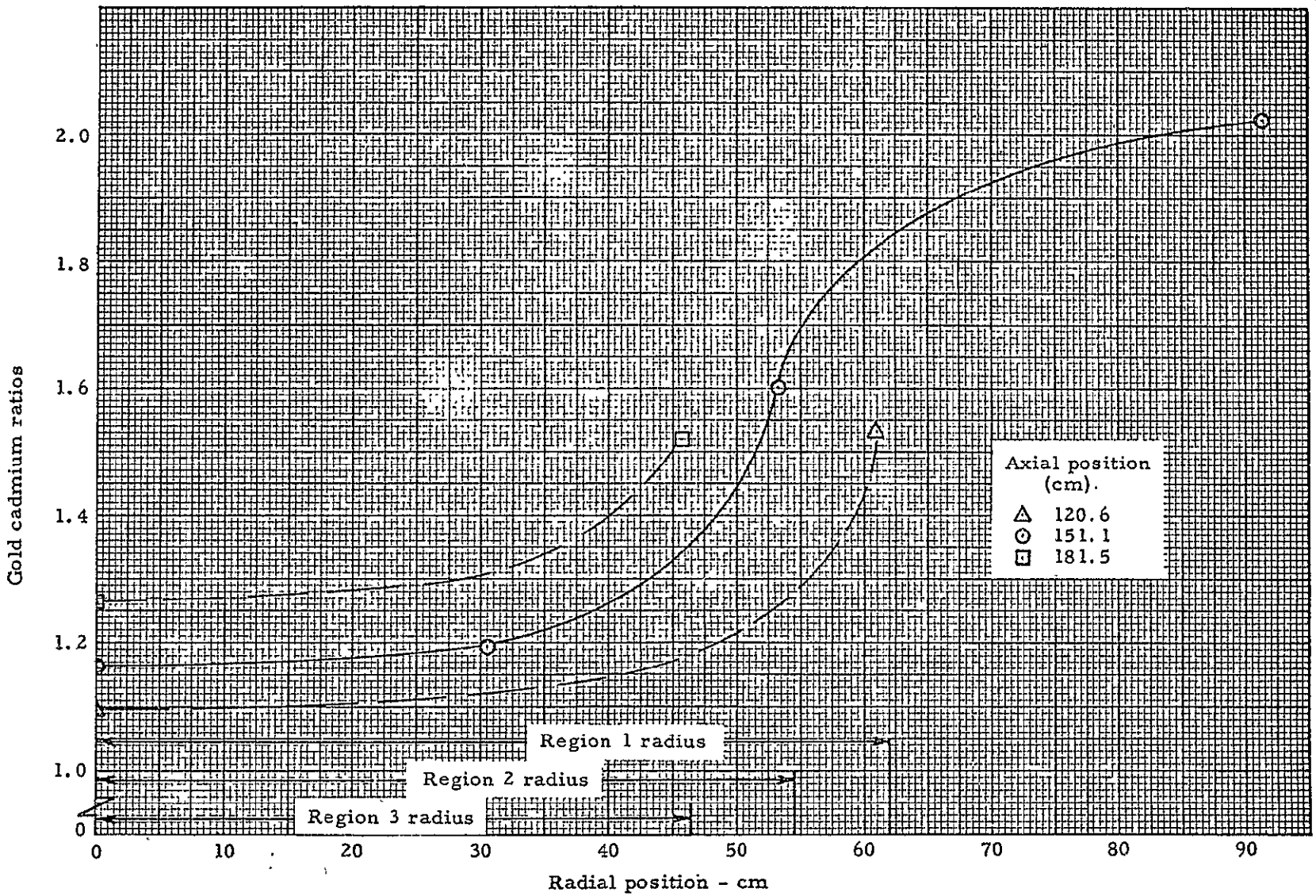

Fig. 12.22 Gold infinitely dilute cadmium ratios in the core - configuration 9E.

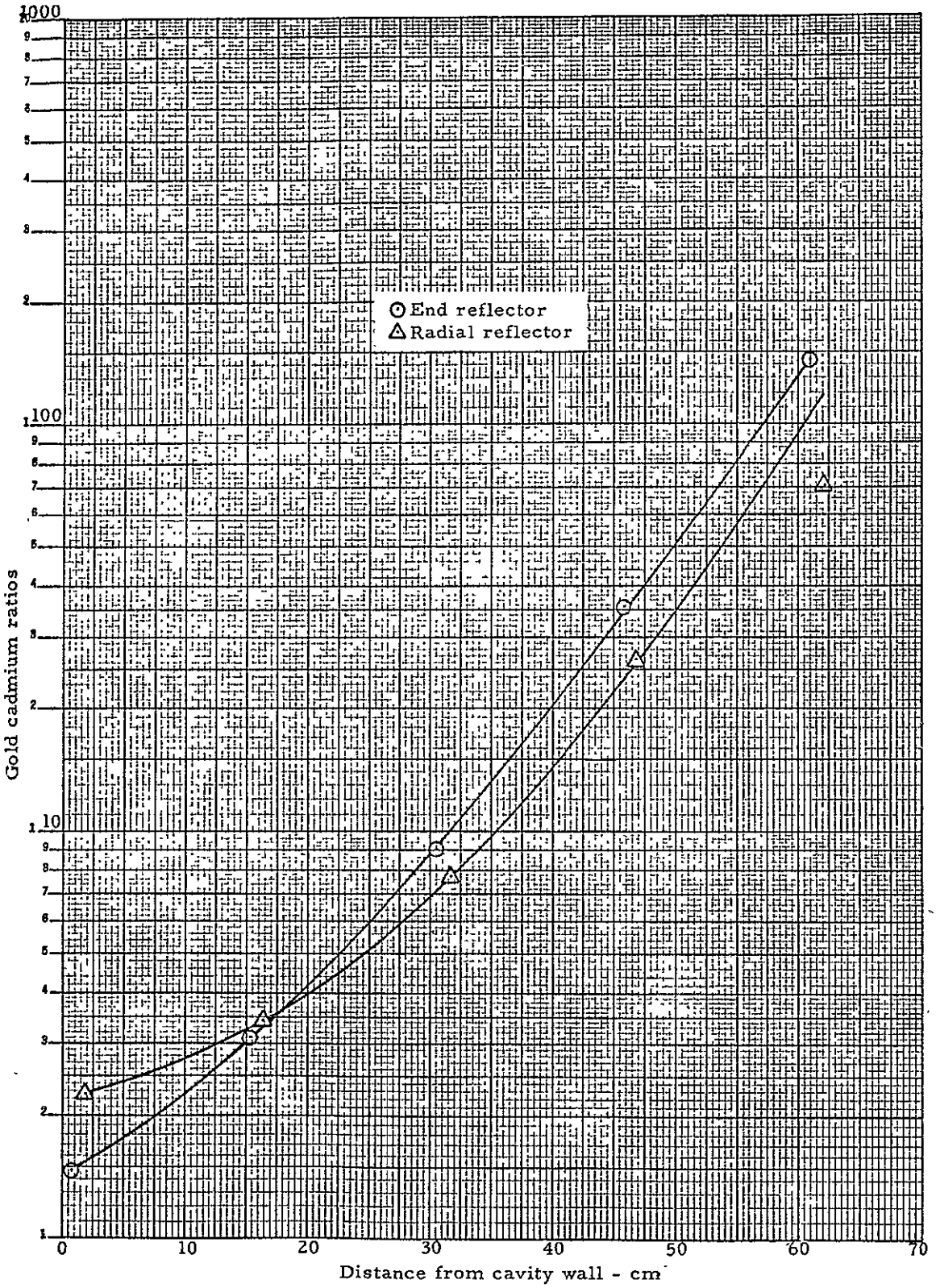

Fig. 12.23 Gold infinitely dilute cadmium ratios in the reflector - configuration 9E

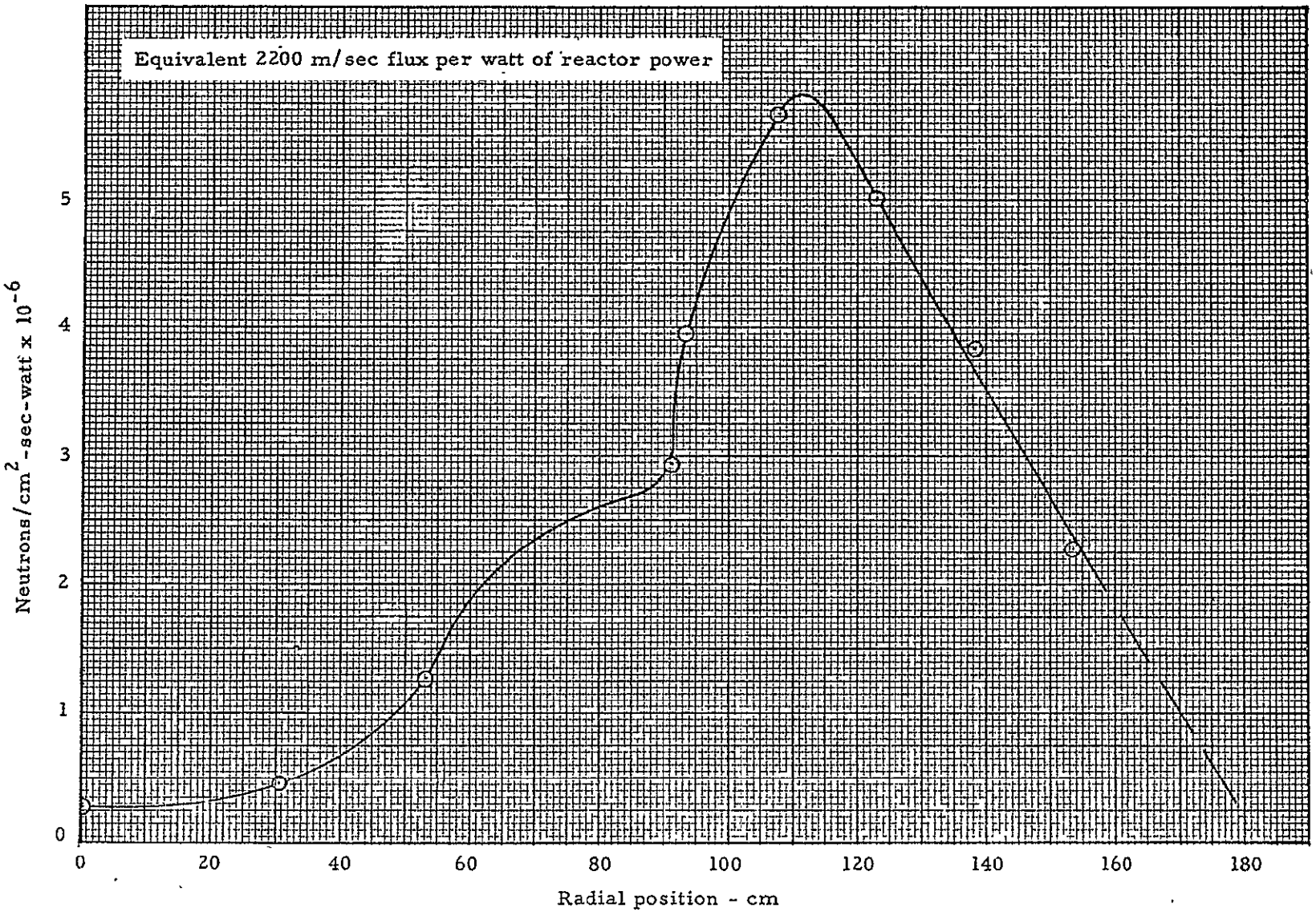

Fig. 12.24 · Radial distribution of thermal flux at axial midplane - configuration 9A

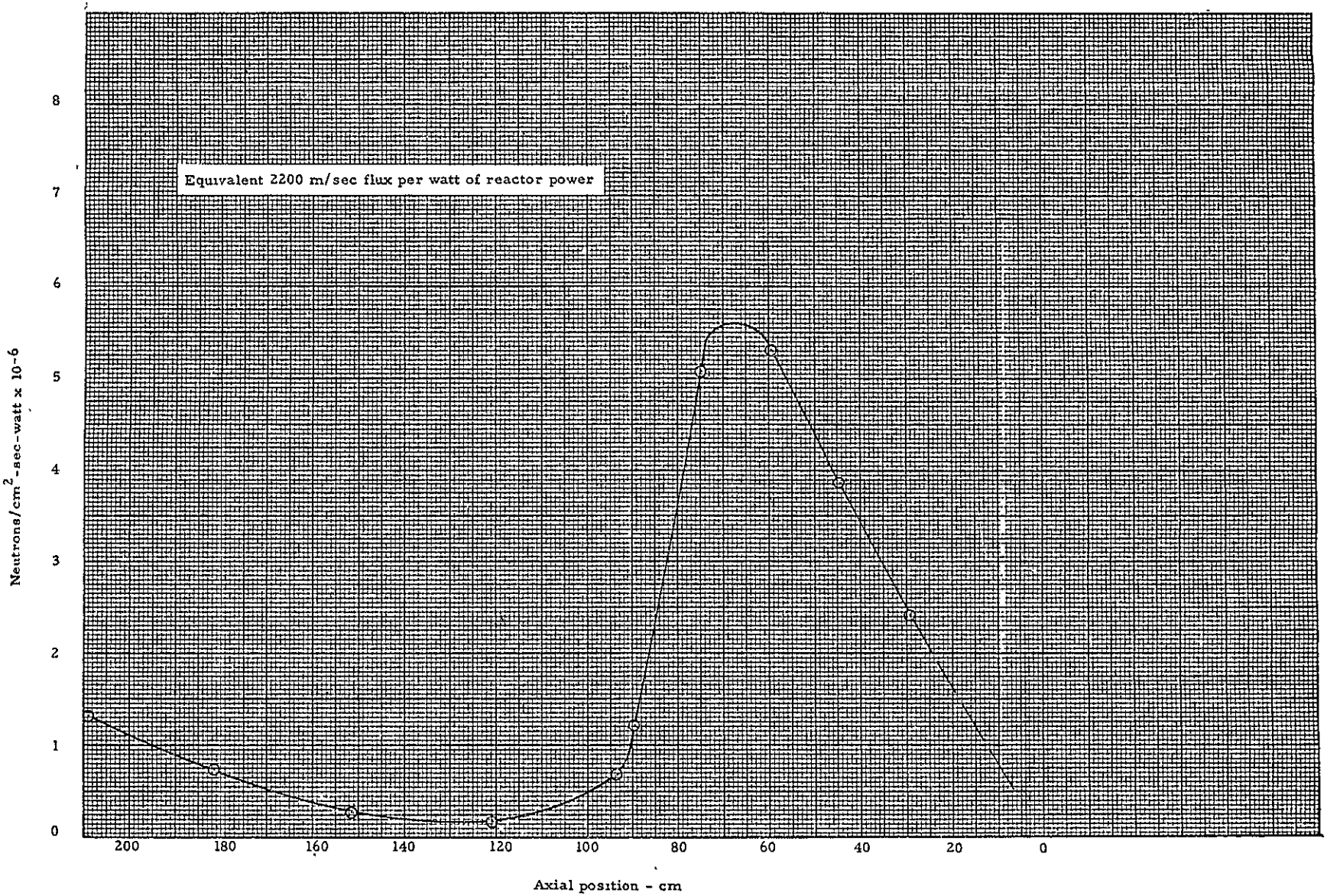

Fig. 12.25 Longitudinal distribution of thermal flux along axis of configuration 9A

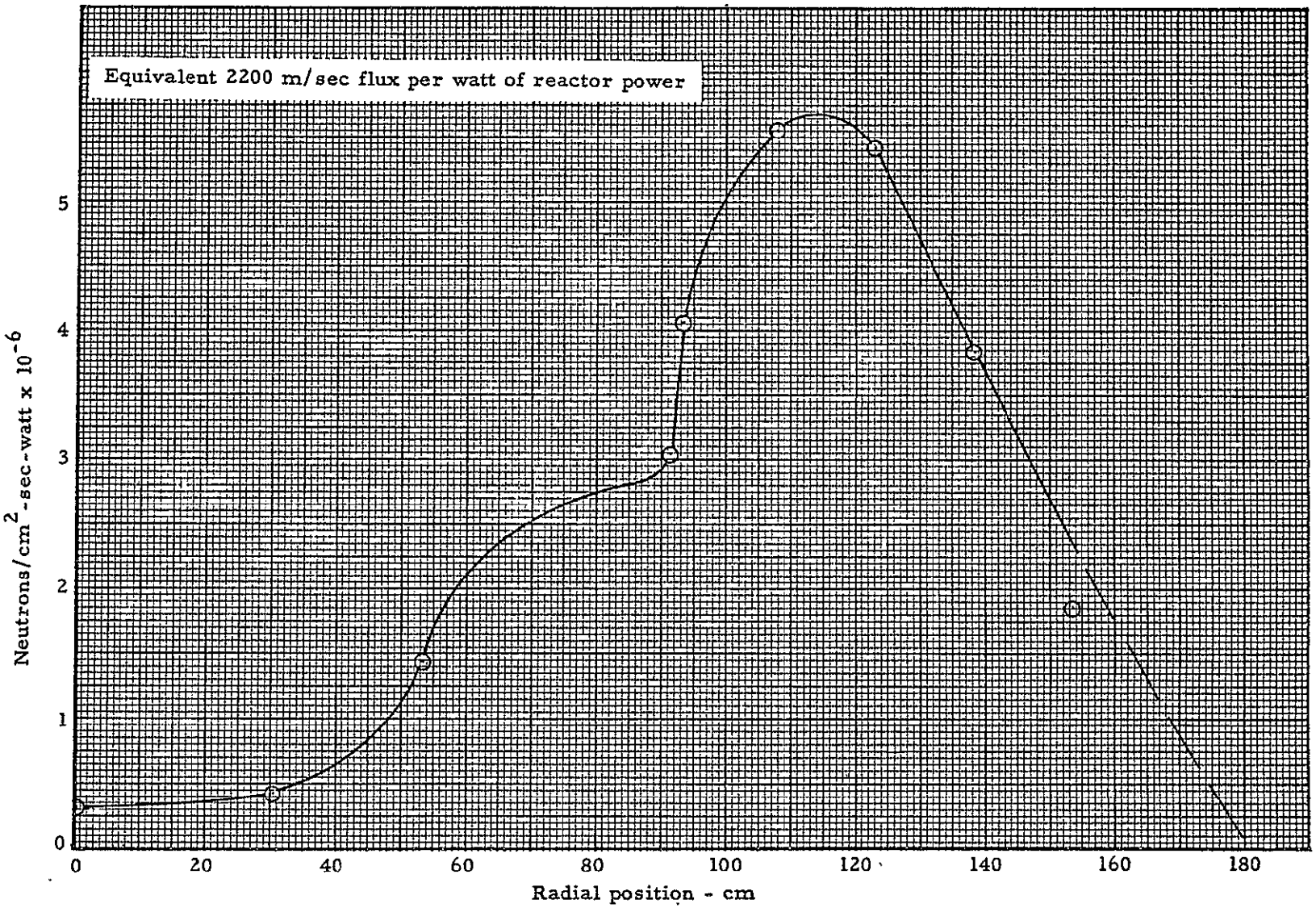

Fig. 12.26 Radial distribution of thermal flux at axial midplane - configuration 9A

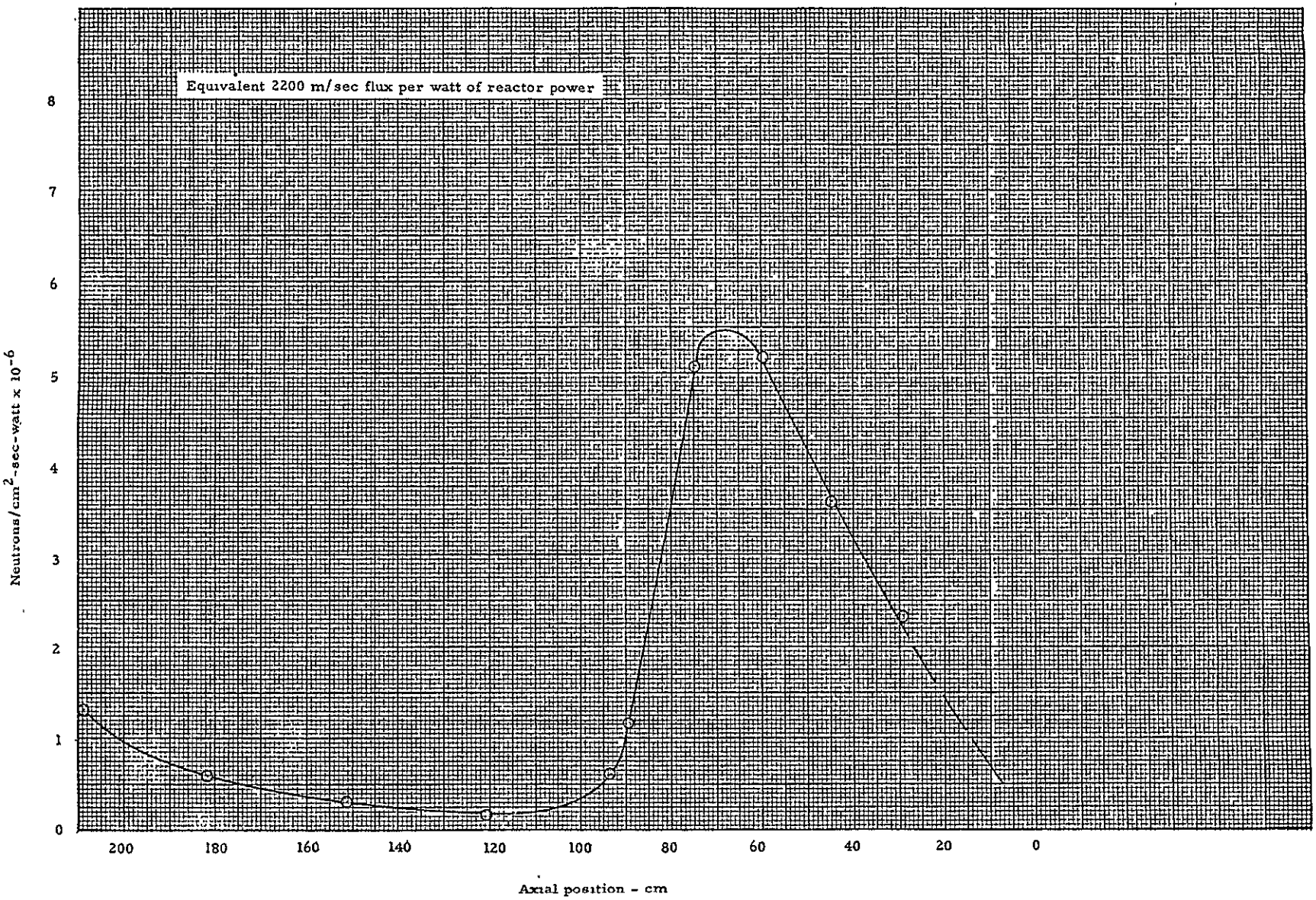

Fig. 12.27 Longitudinal distribution of thermal flux along axis of configuration 9A

13.0 CORE ROUNDING MEASUREMENTS

The cavity reactor, under power operation, will not have a sharp boundary at the ends of the core. This is particularly true at the exhaust end of a cylindrical reactor. The shape of the fueled region at the inlet end of the core will depend on the geometry of the fuel and coolant injection system. Because of these considerations, measurements were performed on Configuration 9A (this configuration is described in Section 12.0) to determine the reactivity penalty due to rounding the outer portion of the fueled region at both ends of the core. In addition, a single stage of fuel was removed from the inlet end to measure the effect of shortening the core.

13.1 Rod Worth Measurements

Several rod worth measurements were obtained during the course of the experiment and the results are given in Table 13.1. These values are based on previously measured rod worth curves which are given in Reference 1, p. 26 and 27. After removing the fuel in the rounding measurements and all of the fuel on stage 1 at the end of the core opposite the separation plane, rod worth curve measurements were repeated to determine if the curve shapes had changed. Inverse kinetic techniques (Reference 4) were used to generate the curves which are shown in Figures 13.1 and 13.2. There were 20 rods connected to seven actuators for the all-rods curve and the single actuator curve was generated from Actuator 5 containing three rods located in the outer ring of actuators. The points for the previous all rods curve were obtained from the subcritical curve data given in Reference 3, p. 94. The points on the single actuator curve were from a measurement of Actuator 6 and reported in Reference 1, p. 69.

There were some differences in the old and new curves so the new curves were reduced to tabular form as shown in Tables 13.2 and 13.3. The new data were subsequently used to evaluate rod worths and k-excess for the shorter core. The changes in rod worth are noted in Table 13.1. The all-rods value showed a 16% decrease in worth due to shortening the core while the worth of Actuators 3 and 6 decreased by only 4.4%.

13.2 Reactivity Measurements

13.2.1 Core Average Fuel Worth Measurements

The reactivity worth of uranium was measured in each of the three regions of Configuration 9 before performing the rounding measurements. Prior to starting these measurements, the exhaust nozzle tank filled with D_2O was placed in the end reflector (center of the movable tank) to increase k-excess. This filled the 30.5 cm diameter hole in the end reflector, and simulated the condition without an exhaust nozzle in the cavity reactor. This tank of D_2O was worth $0.459 \pm 0.042\%\Delta k$. A previous measurement on a core with substantially lighter loading (14 kg) gave a tank worth of $0.698 \pm 0.088\%\Delta k$ (Reference 3, p. 162).

The fuel worth measurements were made over a 1/4 sector of each of the three regions. Only one region was measured at a time and the results are shown in Table 13.4. The core average fuel worth is readily obtained by multiplying the fuel fraction in each region by the average fuel worth for that region and then summing the three products. This average was 0.293%Δk/kg, as shown in the table.

The worth of fuel was also measured in the regions next to the polyethylene where dilute amounts of fuel were added to the reactor to increase k-excess for the rounding measurements. The fuel was placed in the reactor in short, 2-stage fuel elements and they were positioned near the axial midplane of the reactor to minimize any possible effect on the desired rounding measurements. The average of two measurements gave a uranium worth of 1.713 ± 0.025%Δk/kg, but with no correction being made for the aluminum in the fuel elements (nominally 5% of the total effect).

13.2.2 Core Rounding

The rounding measurements were performed in increments as shown in Figure 13.3. The locations of the fuel elements in the three outer rings involved in these measurements are given in Figure 13.4 for the end of the core nearest the separation plane and Figure 13.5 for the back end of the core or that end opposite the separation plane.

Table 13.5 contains the results of these rounding measurements. The first increment at the separation plane was removed in three steps as shown in the Table 13.5. It was determined by the removal of this single stage of fuel that a sector of the rounding measurement could be extrapolated quite accurately to the total worth of the complete increment, within the experimental error, so the subsequent rounding measurements at the separation plane were limited to a 180° sector. The same procedure was followed at the back end of the core as at the separation plane except that more steps were taken. The three steps used to remove increment 1 showed more variation than at the separation plane, so additional steps were taken for increments 2 and 3 to determine if the variation observed in increment 1 was simply data scatter. The existence of data scatter was confined by the results. With the exception of the first increment, fuel removal was again limited to 180° of the core. The estimated error (68% confidence limit) on these data is ±5% or less. The fuel mass was based on the number of fuel sheets removed and an average uranium mass of 2.62 grams per sheet so part of the data variation could be due to slight differences in fuel mass.

The rounding measurement results show that uranium at the separation plane in Region 3 is about twice the worth of uranium at the other end of the core (Region 1). This is due primarily to the differing fuel concentrations in the two regions although the difference in the fuel radii would also have some effect. The relative fuel density in Region 3 was 0.325 of the fuel density in Region 1, so there would be much less self-shielding of neutron flux in Region 3 than in Region 1. Before performing the rounding measurements at the back end of the core the fuel was restored at the separation plane end to the normal configuration.

However, the fuel was not restored at the opposite end of the core at the completion of the rounding measurements. After removing increment 3 at that end (inlet end), the core was shortened one stage by removing the remaining stage 1 fuel sheets. (The first stage of fuel is next to the cavity wall. There were 16 stages with stage 16 being at th separation plane.) Sixty stage 1 fuel elements already had their fuel removed in a 180° sector as a result of the rounding measurements. There were a total of 208 fuel elements over Region 1 so there were still 44 fuel elements containing stage 1 over the 180° sector where increments 2 and 3 had been removed. Removal of these 44 stages reduced k-excess 0.3865%Δk and involved the removal of 396 sheets of fuel or 1037.5 grams of uranium. The next step was to remove the first stage over the remaining 180°. It will be noted from Table 13.5 that increment 1 had been previously removed over a 180° sector at the inlet end of the core. The next step taken was to remove 22 of the 104 first stages in the 180° sector. These were worth -0.4265%Δk. The remaining 82 stage 1's were removed and they reduced k-excess 0.9615%Δk. The total removal of stage 1 over 180° sector was, therefore, worth -1.388%Δk so the effect of shortening the core one stage (7.3 cm) and removing the fuel (4.90 kg) over that stage would reduce k-excess by 2.776%Δk.

All of the above measurements were intended to deduce the reactivity penalty between the more easily analyzable, "squared off" cores and the cores more like those that would exist in a flowing gas experiment. Besides the rounding of the "square corners," the fuel would not be allowed to approach the cavity wall as close as stage 1 fuel does. Therefore, the reactivity effects measured in these experiments should be interpreted as a total anticipated penalty, and can be transformed into the necessary critical fuel mass addition.

TABLE 13.1

Rod Worth Measurements

During Rounding Experiment

Run No.	Actuator Combinations and Reactivity Worth (%Δk) 3 and 6 (6 rods)	1 and 3 (6 rods)	5 (3 rods)	1 to 7 (20 rods)
676				-4.322
677	-1.415			
679	-1.318			
682	-1.404			
683	-1.320			
687		-1.451		
689	-1.388			
694		-1.513		
704			0.578	
Averages	-1.369 ± 0.047	-1.482 ± 0.044	-0.578	-4.322
	After removal of Stage 1			
706	-1.300			
709				-3.730
714				-3.709
715				-3.713
Averages	-1.300			-3.717 ± 0.011
	After removal of Stage 1 from new rod worth curves			
706	-1.309			
709				-3.715
714				-3.531
715				-3.616
Averages	-1.309			-3.621 ± 0.092

TABLE 13.2

Seven Actuator Tabular Rod Worth Curve

One Stage of Fuel Removed at Control Rod End

	0	100	200	300	400	500	600	700	800	900
0	100.00	100.00	98.40	96.60	94.46	91.96	89.06	85.76	82.23	78.73
1000	75.38	72.16	69.06	66.08	63.22	60.45	57.82	55.30	52.88	50.56
2000	48.33	46.19	44.14	42.16	40.26	38.44	36.69	35.01	33.40	31.85
3000	30.37	28.93	27.55	26.21	24.92	23.68	22.49	21.34	20.24	19.18
4000	18.15	17.17	16.23	15.33	14.45	13.63	12.83	12.07	11.35	10.66
5000	10.00	9.37	8.77	8.20	7.66	7.15	6.67	6.21	5.78	5.38
6000	5.00	4.64	4.30	3.98	3.68	3.40	3.14	2.89	2.66	2.44
7000	2.24	2.05	1.87	1.70	1.53	1.38	1.24	1.11	0.98	0.86
8000	0.75	0.65	0.55	0.46	0.38	0.31	0.24	0.18	0.13	0.09
9000	0.06	0.04	0.02	0.01	0.00					

	0	100	200	300	400	500	600	700	800	900
0	0	0	1.60	1.80	2.14	2.50	2.90	3.30	3.53	3.50
1000	3.35	3.22	3.10	2.98	2.86	2.77	2.63	2.52	2.42	2.32
2000	2.23	2.14	2.05	1.98	1.90	1.82	1.75	1.68	1.61	1.55
3000	1.48	1.44	1.38	1.34	1.29	1.24	1.19	1.15	1.10	1.06
4000	1.03	0.98	0.94	0.90	0.87	0.83	0.80	0.76	0.72	0.69
5000	0.66	0.63	0.60	0.57	0.54	0.51	0.48	0.46	0.43	0.40
6000	0.38	0.36	0.34	0.32	0.30	0.28	0.26	0.25	0.23	0.22
7000	0.20	0.19	0.18	0.17	0.17	0.15	0.14	0.13	0.13	0.12
8000	0.11	0.10	0.10	0.09	0.08	0.07	0.07	0.06	0.05	0.04
9000	0.03	0.02	0.02	0.01	0.01	0				

TABLE 13.3

Actuator 5 Tabular Rod Worth Curve

Stage 1 Removed - % Worth Inserted

	0	100	200	300	400	500	600	700	800	900
0	100.00	100.00	99.40	98.26	96.66	94.45	91.58	88.08	84.48	80.88
1000	77.34	73.96	70.76	67.72	64.82	62.05	59.41	56.86	54.42	52.10
2000	49.85	47.68	45.58	43.56	41.62	39.75	37.95	36.23	34.57	32.97
3000	31.34	29.97	28.56	27.20	25.90	24.65	23.45	22.32	21.22	20.17
4000	19.16	18.17	17.23	16.33	15.46	14.62	13.82	13.04	12.29	11.57
5000	10.87	10.20	9.56	8.96	8.37	7.80	7.36	6.74	6.24	5.77
6000	5.32	4.90	4.50	4.12	3.76	3.42	3.10	2.80	2.52	2.26
7000	2.02	1.80	1.59	1.40	1.22	1.06	0.91	0.77	0.64	0.53
8000	0.43	0.34	0.26	0.19	0.13	0.08	0.04	0.01	0	
9000										

Difference Table

	0	100	200	300	400	500	600	700	800	900
0	0	0	0.60	1.14	1.60	2.20	2.88	3.50	3.60	3.60
1000	3.54	3.38	3.20	3.04	2.90	2.77	2.64	2.55	2.44	2.32
2000	2.25	2.17	2.10	2.02	1.94	1.87	1.80	1.72	1.66	1.60
3000	1.53	1.47	1.41	1.36	1.30	1.25	1.19	1.14	1.10	1.05
4000	1.01	0.99	0.94	0.90	0.87	0.84	0.80	0.78	0.75	0.72
5000	0.70	0.67	0.64	0.60	0.59	0.57	0.54	0.52	0.50	0.47
6000	0.45	0.42	0.40	0.38	0.36	0.34	0.32	0.30	0.28	0.26
7000	0.24	0.22	0.21	0.19	0.18	0.16	0.15	0.14	0.13	0.11
8000	0.10	0.09	0.08	0.07	0.06	0.05	0.04	0.03	0.02	0.01
9000	0.00									

TABLE 13.4

Fuel Worth Measurements

Configuration 9 With Exhaust Nozzle Tank in Reactor

Region	Mass of U Added (gm)	Reactivity Increase (%Δk)	Uranium Worth (%Δk/kg)
1	817.4	0.1850	0.226
2	524.0	0.1678	0.320
3	379.9	0.2562	0.674
Core average			0.293

Note: Estimated standard error on the fuel worth is ±5% or less.

TABLE 13.5

Fuel Rounding Measurements on Configuration 9

Location	Sector (degrees)	Uranium Mass Removed (gm)	Sector Worth (%Δk)	Worth of 360 (%Δk)	U Worth (%Δk/kg)
Separation Plane					
Increment 1	90	62.88	-0.1022	-0.4088	1.625
Increment 1	90	62.88	-0.0968	-0.3872	1.539
Increment 1	180	125.76	-0.1952	-0.3904	1.552
Increment 2	180	220.08	-0.2849	-0.5698	1.295
Increment 3	180	317.02	-0.3795	-0.7590	1.197
Inlet End of Core					
Increment 1	90	259.38	-0.2412	-0.9648	0.930
Increment 1	180	516.14	-0.4265	-0.8530	0.826
Increment 1	90	259.38	-0.2060	-0.8240	0.794
Increment 2	90	489.94	-0.3082	-1.233	0.629
Increment 2	90	489.94	-0.3134	-1.254	0.640
Increment 3	90	694.30	-0.4089	-1.636	0.589
Increment 3	90	691.68	-0.4328	-1.731	0.626
Stage 1 completely removed	180	2452.32	-1.3880	-2.776	0.566

Note: Estimated standard error on the uranium worths is ±5% or less

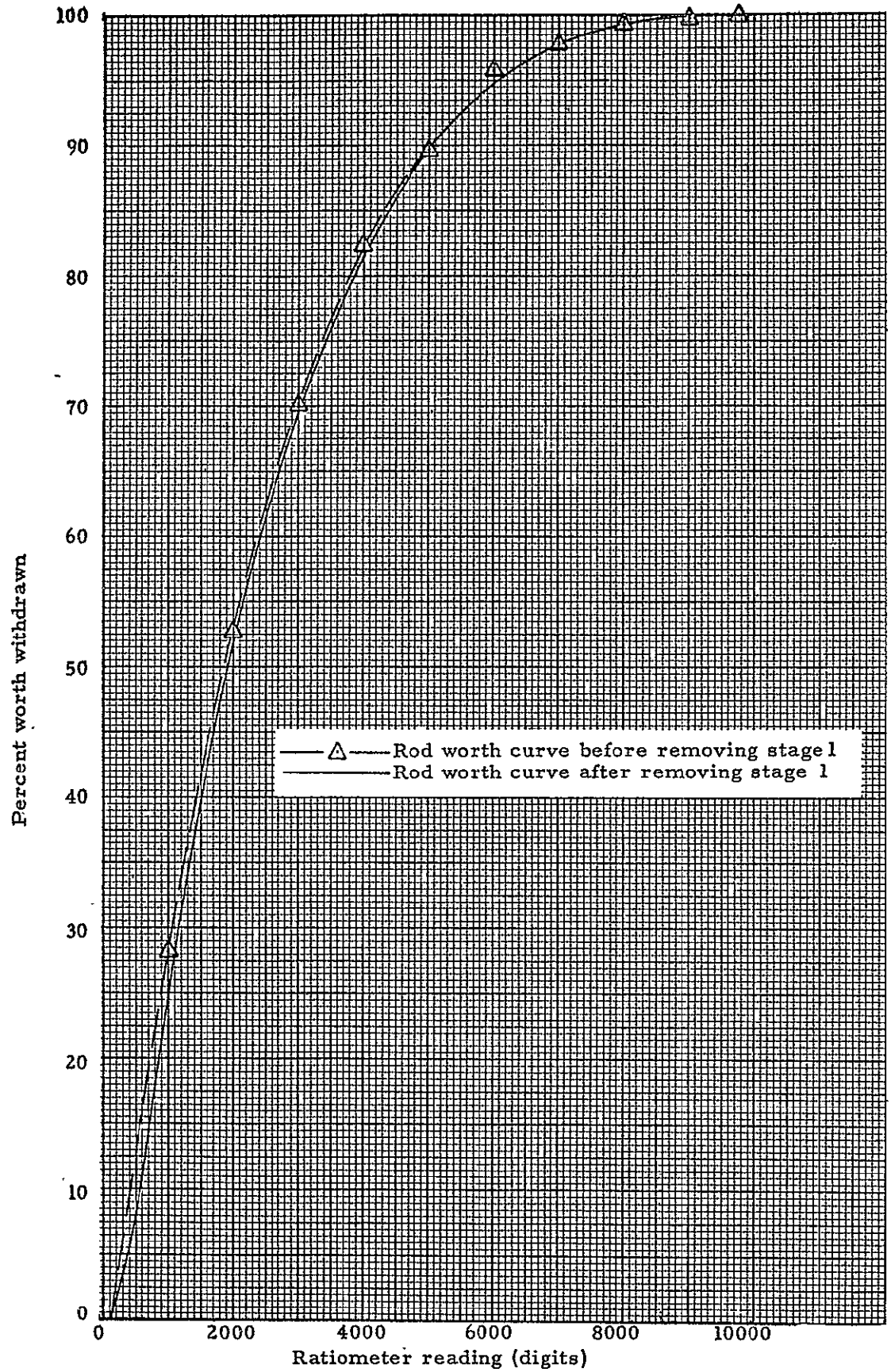

Fig. 13.1 Comparison of control rod shape curves, all rods (20)

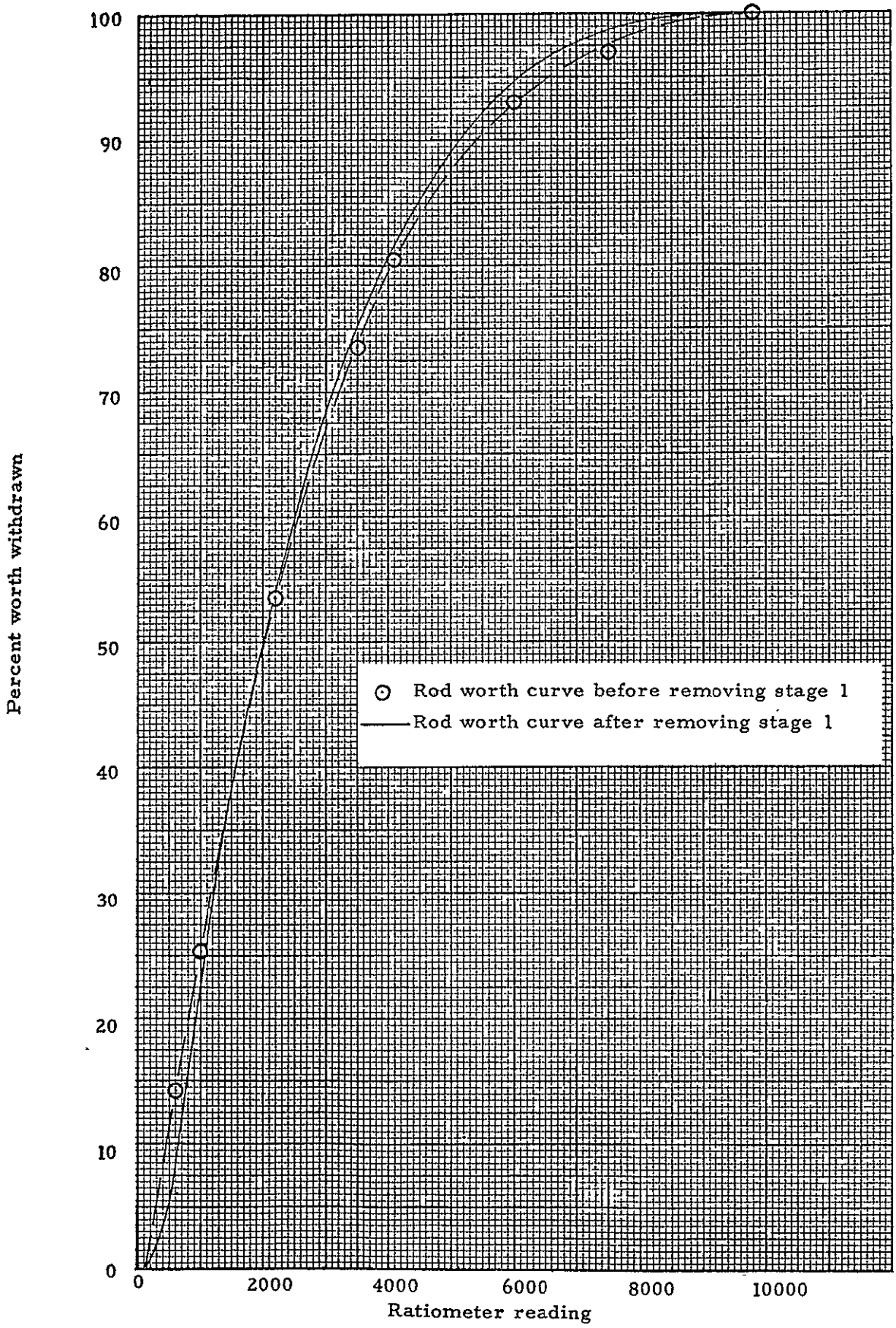

Fig. 13.2 Comparison of control rod shape curves, single rod (No. 5)

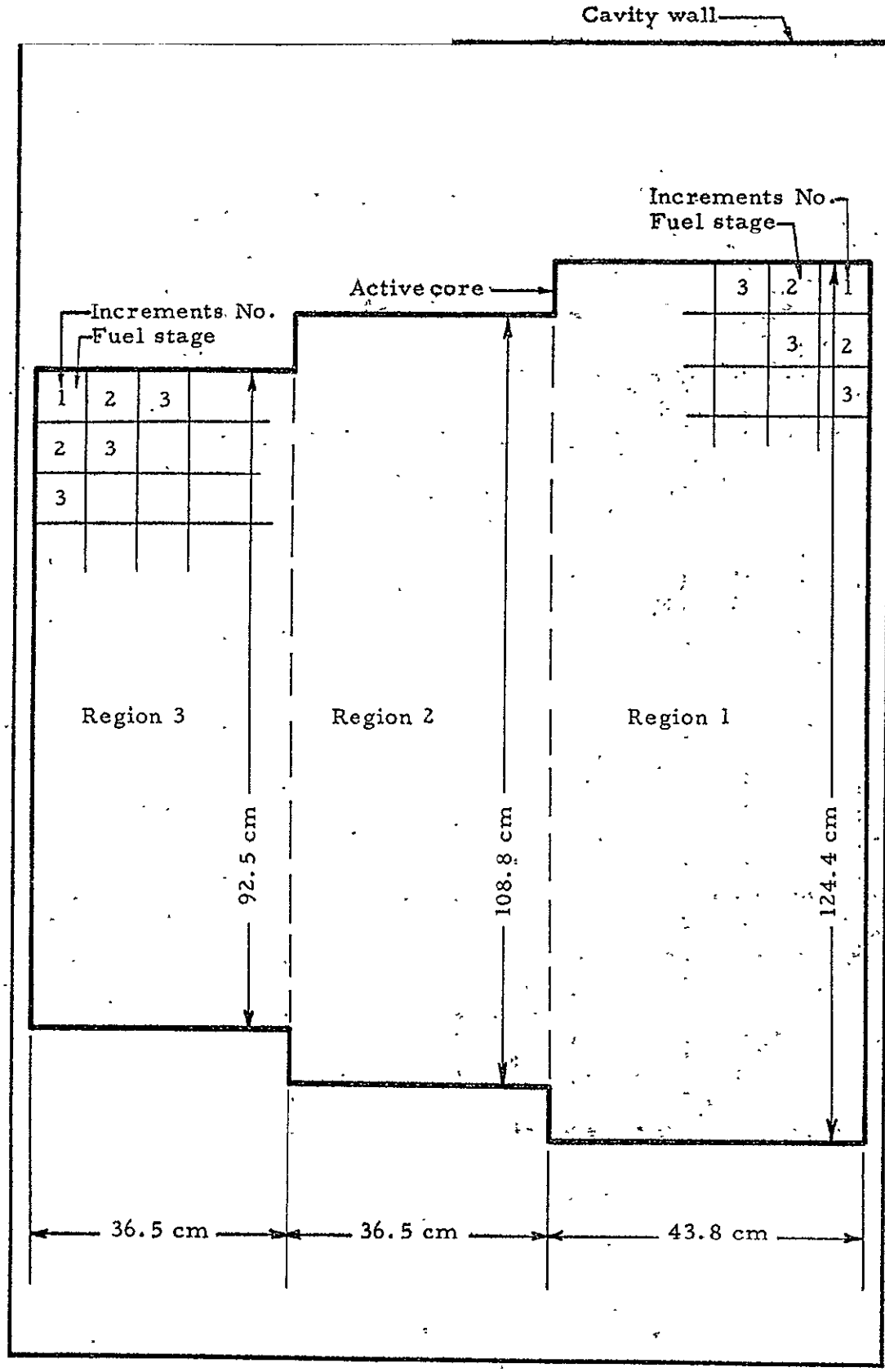

Fig. 13.3 Core - rounding increments

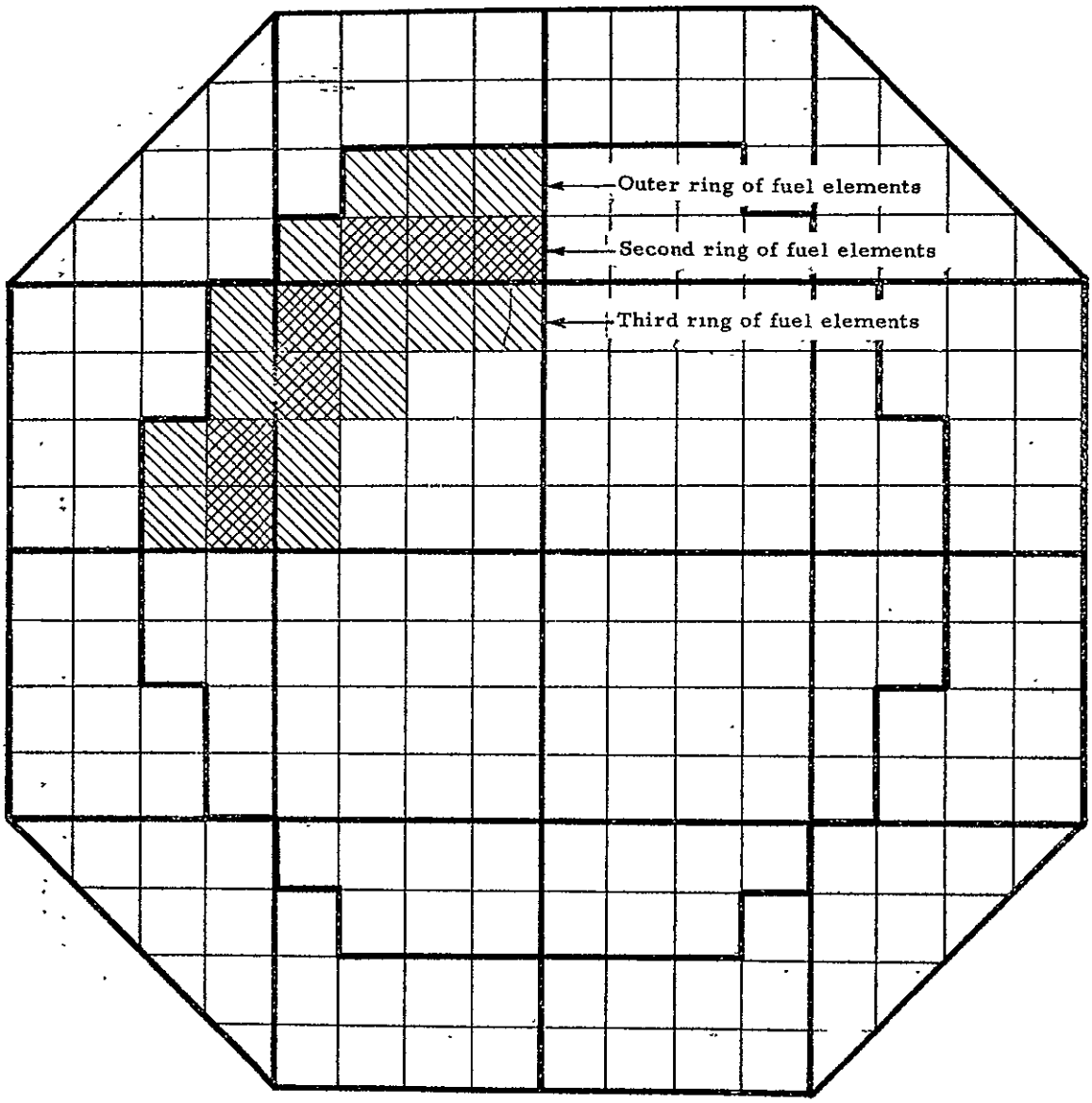

Fig. 13.4 Cross sectional view showing core - rounding increments small end of core

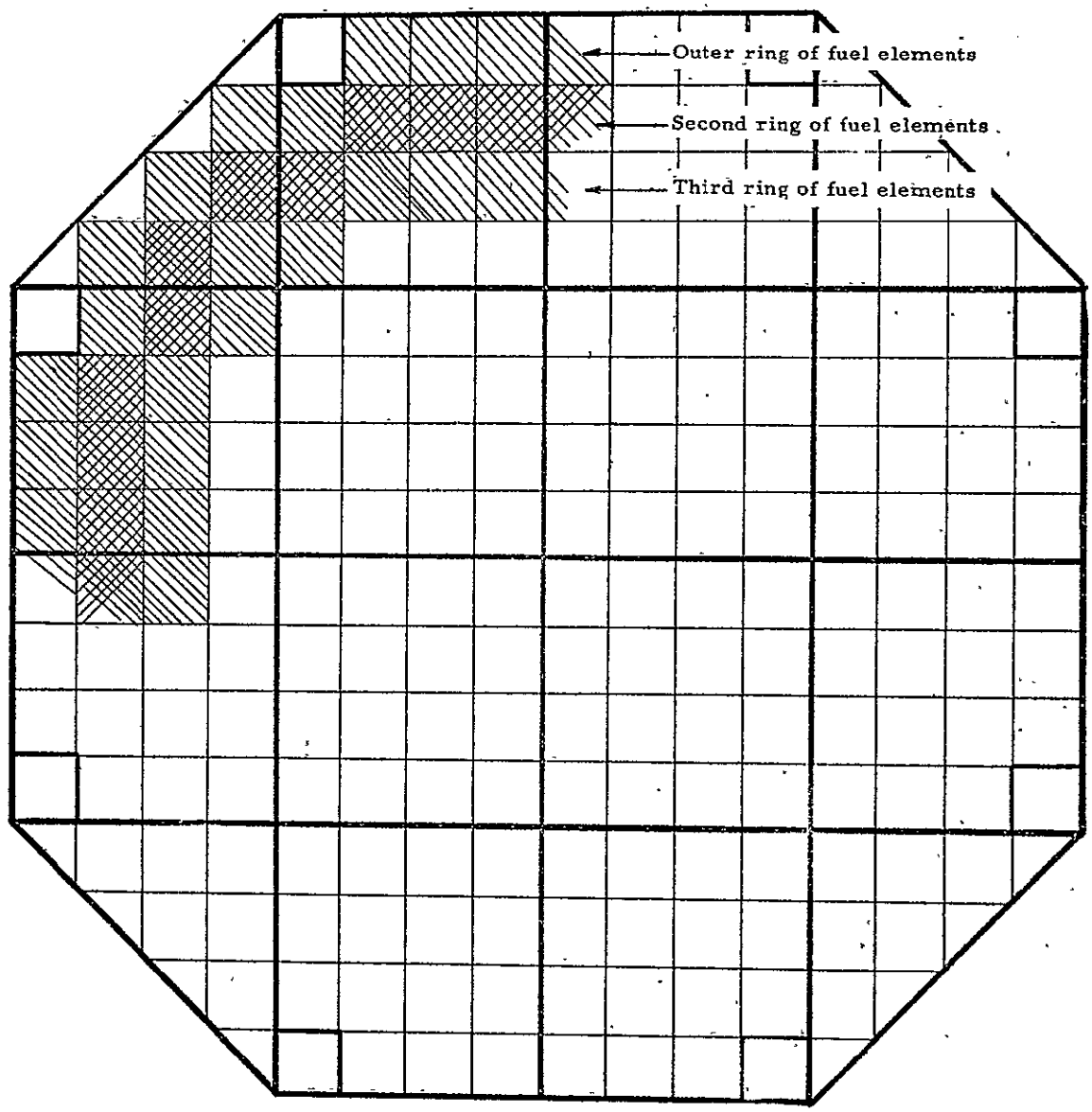

Fig. 13.5 Cross sectional view showing core - rounding increments large end of core

14.0 CONTROL MEASUREMENTS

The control measurements were performed immediately following the rounding measurements. The fuel over stage 1 was still out of the reactor as well as the fuel over the 180° sector involved in the rounding measurements at the end of the core opposite the separation plane. Also, some fuel had been placed between the active core and cavity wall in order to maintain a critical assembly. The reactor was further modified by removing a sector of the fuel annulus in the radial reflector so that control measurements could be made near the cavity wall. To compensate for the reactivity loss by the removal of this fuel from the reflector, additional uranium was placed in the region between the active core and cavity wall. All of the extra fuel in the region between the core and cavity wall was evenly distributed over the length of the core and was restricted to the void regions on either side of the active core thus leaving the top and bottom portion of the normal void region clear of extra fuel. This was done so as to maintain the usual core cavity configuration along the vertical axis in anticipation of power mapping measurements which were to follow. The total fuel loading in the cavity region was 41.5 kg of uranium, 37.8 kg of which was in the normal active core region while the remainder was in the void region between the active core and cavity wall. Despite the many compromises in the core from that of a normal core configuration, the measurement of control methods in the reflector would not be compromised. These measurements were made at the top of the core and hence on the vertical axis which was essentially unperturbed.

14.1 Reactivity

All reactivity measurements obtained during this phase of the experiment were evaluated from the rod worth curves given in Section 13.1 for the short core. The rod worths which were used are given in Table 13.1 after removal of stage 1 and were -1.309%Δk for Actuators 3 and 6 and -3.621%Δk for Actuators 1 to 7 (all rods).

The first group of measurements were made to evaluate a sector of a poison sleeve which could be moved axially from within the end reflector until it surrounded the cavity region. A plate of cadmium 30.5 cm wide, 61.0 cm long, and 0.051 cm thick was fastened to an aluminum positioning wand. The long dimension of the cadmium plate was placed parallel to the length of the cavity as shown in Figure 14.1. The cadmium weighed 877 grams. Two traverses were made from the axial midplane of the cavity into the end reflector, each traverse at a different radial distance from the cavity wall, as shown in Table 14.1 and Figure 14.2. The traverse which began at a radial spacing of 5.7 cm from the cavity wall had to be altered to 10.1 cm when positioning the plate at the end of the cavity region because of structural hardware interference. It was also necessary to shift the plate to one side by 21.6 cm because of a beam, which extended vertically from the cavity tank to the outer D_2O tank wall. The points at 51.9 and 72.2 cm were missed on the first measurements because the cadmium plate position was maintained directly over the tank and the vertical beam at the end of the cavity prevented measurements at these locations. The curve

shapes at the three radial distances were similar, and the poison was worth the most at the radial location nearest the cavity wall, and not at the flux peak (nominally 20 cm) as might apriori be expected.

Since only a small sector of complete cadmium sleeve was measured, measurements were made to determine how well the data might be expected to extrapolate to a full sleeve. The cadmium plate was cut in half with the cut being made in the long direction of the plate. One piece contained 427 grams and the other 450 grams after the cut. It will be noted from Table 14.1 that 49% of the cadmium mass was worth 54% of the total plate worth. This measurement was repeated with the cadmium on the cavity wall, for more precise reproducibility of position. (Actually the cadmium was placed between the polyethylene and stainless steel liner in the cavity.) The small half of the plate was removed first and it was worth 44% of the total worth. Then the second half (51% of the total Cd plate) was removed and it was worth 56% of the total worth. It is obvious from these data that there is a loss in specific poison worth as the plate size increases. A complete sleeve of cadmium of the same length and thickness as the above plate positioned 5.7 cm from the cavity wall would contain about 20 times more mass than the above plate. From the data taken thus far, it would be impossible to extrapolate to a total sleeve worth with any certainty. It can be concluded, however, that a large amount of control, certainly much greater than -5.0%Δk, could be attained with a poison sleeve control system.

Measurements were also made to determine poison worth vs nuclear absorption thickness, $\Sigma_a X$. The poison plates for these measurements were 22.1 cm wide by 40.0 cm long and were placed 7.5 cm from the cavity wall in the radial reflector centered over the axial midplane of the cavity. The results are given in Table 14.2 and Figure 14.3. It will be noted from these data that when increasing from a $\Sigma_a X$ of 0.048 to 0.118, a factor of 2.46, the poison worth changed only by a factor of 1.78, indicating a non-linearity of flux perturbation effects over these small values of mean free path lengths. It will also be observed from the curve that little or no advantage would be gained by using a material thickness greater than about 6 mean free paths. Note, no advantage was found with theborated stainless steel. Neither its epithermal cross section for absorption nor the slowing down migration length were significant enough to show any appreciable differences over a purely thermal absorber such as cadmium.

The next set of measurements were concerned with a control drum such as shown in Figure 14.4. The same cadmium plate was used as for the sleeve measurements. The poison plate was fastened to an aluminum drum 76 cm in diameter and the drum rested on the cavity wall. The long dimension of the cadmium plate was placed parallel to the axial plane of the cavity as was done with the sleeve measurements. The cadmium plate was first positioned so that it was farthest from the cavity wall or in its least effective position. It was then manually rotated in 45° increments until it had been rotated 180° to its most poisonous position. The results are given in Table 14.3 and Figure 14.5. The data show no peaking in worth at the thermal flux peak, which occurs around 20 cm from the

cavity wall. The cadmium was most effective on the cavity wall and at this point was worth -2.05%Δk/kg of cadmium. The reactivity worth of the aluminum drum was measured and its worth has been subtracted from the cadmium worth.

Extrapolation of the single drum worth to multiple drum worth is even more uncertain than with the sleeve worth extrapolations. However, control drums would be physically separated from each other by a significant amount of D_2O, and this effect probably would make the multiple drum extrapolation "more linear" than with the sleeve extrapolation. However, it is quite certain, from the above results, that multiple (4 or more) control drums could provide a very large amount of control, much greater than 5%Δk.

The reactivity data presented in this section were based almost entirely on measured differences in k-excess. In most cases the changes were large and could not be determined from simple period differences. In general, a set group of rods were used as a bank to evaluate k-excess. However, this was not always the case and it was found that when changing rod patterns from seven actuators to two actuators, where k-excess was low enough to do this, there was often a difference in the resulting k-excess values. These differences were taken into account when it was necessary to make changes in the rod pattern. Taking this and other factors into account, the data results giving the poison worths should be accurate to within a standard error of ±5%.

14.2 Power Distribution Measurements

Bare catcher foils were exposed in the cavity region over the top portion of the core both with and without the cadmium plate on the drum in the radial reflector. The cadmium, when in the reflector for these power mapping measurements, was placed in its most poisonous position, i.e., against the cavity wall. The primary purpose of the measurements was to show the effect of the cadmium on the fission power distribution in the core. The specific power measurements were actually extended beyond the core to the cavity wall as a matter of interest.

Table 14.4 contains the catcher foil data with no cadmium in the reflector. The relative axial profiles from the center of the cavity to the cavity wall are shown in Figure 14.6. Each of the axial profiles was averaged and these averages were plotted to give the composite radial profile shown in Figure 14.7.

The cadmium plate was then placed in the reflector against the cavity wall and the foil measurements repeated. Table 14.5 contains the foil data and Figure 14.8 shows the relative axial profiles across the core from the center to the cavity wall next to the cadmium plate. The change, of course, was very dramatic near the cavity wall. In the core, however, the comparison of the axial averages shows only an overall general 10% decrease in the axial averages with respect to the core center, approaching 12% at the radial edge of the core. However, at the cavity wall between the polyethylene and stainless steel liner, there was an

average decrease of 42% in specific power. Figure 14.9 shows the radial distribution of the axial averages with cadmium in the reflector.

The largest change in fission power occurred at the axial centerline of the core. To show this, the individual foil data were plotted through this region for both reactor conditions as noted in Figure 14.10.

The D_2O temperature for the foil exposure with no cadmium in the reflector was 21°C and Actuators 4, 5, 6, and 7 were withdrawn 1.1 cm. All other control rods were in the withdrawn position. When the cadmium was placed in the reflector and the cavity was power mapped, the D_2O temperature was still 21°C and Actuators 4, 5, 6, and 7 were 44.3 cm withdrawn. All other control rods were withdrawn. However, this difference in rod position probably had little effect on the shape of the radial profiles, even on those that were axially averaged.

14.3 Flux Changes in Reflector Due to Shortening of the Core

A special foil exposure was made in the end and radial reflectors using bare gold foils (0.0005 cm thick) to determine if any measurable change occurred in the reflector flux distribution from the removal of stage 1. The comparison was to be made with Configuration 9 prior to the rounding the core and removal of all of stage 1. The results, all with respect to the normalizer foils at the table separation plane, are shown in Figures 14.11 and 14.12. No change could be detected in the radial reflector but there was a change in the end reflector. Care was taken prior to the foil exposure to adjust k-excess so that the same rod positions were used as for the Configuration 9 base measurement so that only the effect of shortening of the core would be detected. Beyond the peak point, to which the data were normalized, for convenience of comparisons, there was a gradual decrease in the relative foil activity ranging from 2% to 21%. There was a corresponding decrease in rod worth when shortening the core as was pointed out in Section 13.1. The two effects are consistent, since an overall lower neutron flux would, of course, give lower rod worths.

TABLE 14.1

Control Measurements

Poison on an Aluminum Wand

Location (1) Radial (cm)	Axial (cm)	Cadmium Plate Worth (%Δk) (877 gm Cd)	Aluminum Worth (%Δk)	Net Cadmium Worth (%Δk)	Cadmium Worth (%Δk)
≈10.1	0	-1.685	-0.033	-1.652	-1.884
19.0	0	-1.232	-0.024	-1.208	-1.378
19.0	34.3	-1.109	-0.021	-1.088	-1.240
19.0	100.3	-0.221	-0.004	-0.217	-0.247
19.0	120.6	-0.095	-0.002	-0.093	-0.106
5.7	0	-1.710	-0.035	-1.675	-1.910
5.7	31.7	-1.661	-0.033	-1.628	-1.857
5.7	31.7 (3)	-1.676	-0.033	-1.643	-1.873
10.1	31.7 (3)	-1.488	-0.029	-1.459	-1.664
10.1	51.9 (3)	-1.152	-0.022	-1.130	-1.288
10.1	72.2 (3)	-0.717	-0.015	-0.702	-0.800
10.1	92.4 (3)	-0.364	-0.007	-0.357	-0.407
10.1	112.7 (3)	-0.148	-0.003	-0.145	-0.165
10.1	120.6 (3)	-0.116	-0.002	-0.114	-0.130
5.7	0	-0.933 (427 gm Cd)	-0.035	-0.898	-2.103
Between CH_2 & SS		-1.652	--	-1.652	-1.884
Between CH_2 & SS		-0.734 (427 gm)	--	-0.734	-1.719
Between CH_2 & SS		-0.919 (450 gm)	--	-0.919	-2.042

(1) Axial reference point is the wet surface of the cavity wall of the fixed table end reflector. The radial reference point is the axial center of the cavity.

(2) These are extrapolated values from one measurement at 5.7 cm from the cavity wall and at the axial center of the cavity.

(3) These measurements were taken with the plate shifted to the side 21.6 cm to clear a support beam in the reflector tank.

TABLE 14.2

Effects of Material Thickness

7.5 cm from Cavity Wall

Material	Thickness (cm)	Weight (gm)	ΣX	Worth (%Δk)
W	0..0254	435.7	0.030	-0.196
NiCr	0.0457	344.6	0.018	
Stainless Steel With 1.05% B	0.0254	166.8	0.088	-0.276
SS with 1.05 % B	0.0254	166.8	0.088	-0.349
W	0.0254	427.0	0.030	
Cadmium	0.0508	390.0	5.79	-0.892

TABLE 14.3

Control Measurements

Poison on an Aluminum Drum

Angle of Cd from Reference	Cadmium Plate Mass (gm)	Cadmium Plate Worth (%Δk)	Cadmium Worth (%Δk/kg)
0	877	-0.016	-0.018
45	877	-0.057	-0.065
90	877	-0.363	-0.414
135	877	-1.204	-1.373
180	877	-1.798	-2.050

TABLE 14.4

Catcher Foil Data - Run 1154

No Cadmium in Radial Reflector

Foil No.	Type	Location Radial (cm)	Location Axial (cm)	Normalized Counts	Local to Foil (X)
1	Bare	0	93.3	53103	2.964
2	Bare	0	120.6	14158	0.790
3	Bare	0	151.1	17916	1.000 (X)
4	Bare	0	181.5	30338	1,693
5	Bare	0	208.8	65905	3.679
6	Bare	15.2	93.3	54292	3.030
7	Bare	15.2	120.6	14498	0.809
8	Bare	15.2	151.1	19665	1.098
9	Bare	15.2	181.5	37305	2.082
10	Bare	15.2	208.8	59088	3.298
11	Bare	30.5	93.3	63032	3.518
12	Bare	30.5	120.6	17885	0.998
13	Bare	30.5	151.1	27350	1.527
14	Bare	30.5	181.5	45482	2.539
15	Bare	30.5	208.8	68520	3.825
16	Bare	45.7	93.3	79196	4.428
17	Bare	45.7	105.3	58652	3.274
18	Bare	45.7	120.6	23200	1.295
19	Bare	45.7	135.8	30724	1.715
20	Bare	45.7	151.1	45804	2.557
21	Bare	45.7	166.3	45162	2.521
22	Bare	45.7	181.5	71186	3.973
23	Bare	45.7	196.8	79568	4.441
24	Bare	45.7	208.8	86412	4.823
25	Bare	53.3	93.3	83452	4.658
26	Bare	53.3	105.3	77998	4.354
27	Bare	53.3	120.6	44339	2.475
28	Bare	53.3	135.8	51449	2.872
29	Bare	53.3	151.1	63734	3.557
30	Bare	53.3	166.3	72241	4.032
31	Bare	53.3	181.5	80717	4.505
32	Bare	53.3	196.8	89050	4.970
33	Bare	53.3	208.8	97620	5.449
34	Bare	61.0	93.3	86991	4.855
35	Bare	61.0	105.3	88754	4.954
36	Bare	61.0	120.6	72045	4.021
37	Bare	61.0	135.8	71738	4.004
38	Bare	61.0	151.1	78046	4.356
39	Bare	61.0	166.3	86761	4.843
40	Bare	61.0	181.5	92718	5.175

TABLE 14.4

(Continued)

Foil No.	Type	Location Radial (cm)	Location Axial (cm)	Normalized Counts	Local to Foil (X)
41	Bare	61.0	196.8	93233	5.204
42	Bare	61.0	208.8	97218	5.426
43	Bare	76.2	93.3	103163	5.758
44	Bare	76.2	105.3	100959	5.635
45	Bare	76.2	120.6	95706	5.342
46	Bare	76.2	135.8	98816	5.516
47	Bare	76.2	151.1	88318	4.930
48	Bare	76.2	166.3	93338	5.210
49	Bare	76.2	181.5	86545	4.831
50	Bare	76.2	196.8	84213	4.700
51	Bare	76.2	208.8	90092	5.029
52	Bare	91.4	93.3	130369	7.277
53	Bare	91.4	105.3	139889	7.808
54	Bare	91.4	120.6	143338	8.001
55	Bare	91.4	135.8	135008	7.536
56	Bare	91.4	151.1	135686	7.573
57	Bare	91.4	166.3	129443	7.225
58	Bare	91.4	181.5	129426	7.224
59	Bare	91.4	196.8	121105	6.760
60	Bare	91.4	208.8	100012	5.582

TABLE 14.5

Catcher Foil Data - Run 1155

Cadmium in Radial Reflector

Foil No.	Type	Location Radial (cm)	Location Axial (cm)	Normalized Counts	Local to Foil (X)
1	Bare	0	93.3	60299	3.130
2	Bare	0	120.6	14791	0.768
3	Bare	0	151.1	19265	1.000 (X)
4	Bare	0	181.5	34002	1.765
5	Bare	0	208.8	55339	2.873
6	Bare	15.2	93.3	52874	2.745
7	Bare	15.2	120.6	13443	0.698
8	Bare	15.2	151.1	18845	0.978
9	Bare	15.2	181.5	34496	1.791
10	Bare	15.2	208.8	58553	3.039
11	Bare	30.5	93.3	65316	3.391
12	Bare	30.5	120.6	18096	0.939
13	Bare	30.5	151.1	24975	1.296
14	Bare	30.5	181.5	44592	2.315
15	Bare	30.5	208.8	64192	3.332
16	Bare	45.7	93.3	77448	4.020
17	Bare	45.7	105.3	55237	2.867
18	Bare	45.7	120.6	25334	1.315
19	Bare	45.7	135.8	24891	1.292
20	Bare	45.7	151.1	33905	1.760
21	Bare	45.7	166.3	51143	2.655
22	Bare	45.7	181.5	70131	3.641
23	Bare	45.7	196.8	73161	3.798
24	Bare	45.7	208.8	85989	4.464
25	Bare	53.3	93.3	90830	4.715
26	Bare	53.3	105.3	75175	3.902
27	Bare	53.3	120.6	35035	1.819
28	Bare	53.3	135.8	41438	2.151
29	Bare	53.3	151.1	58861	3.055
30	Bare	53.3	166.3	65279	3.389
31	Bare	53.3	181.5	75127	3.900
32	Bare	53.3	196.8	91957	4.773
33	Bare	53.3	208.8	95744	4.970
34	Bare	61.0	93.3	89799	4.661
35	Bare	61.0	105.3	91521	4.751
36	Bare	61.0	120.6	69734	3.620
37	Bare	61.0	135.8	66355	3.444
38	Bare	61.0	151.1	70504	3.660
39	Bare	61.0	166.3	81639	4.238
40	Bare	61.0	181.5	84505	4.387

TABLE 14.5

(Continued)

Foil No.	Type	Location Radial (cm)	Location Axial (cm)	Normalized Counts	Local to Foil (X)
41	Bare	61.0	196.8	92358	4.794
42	Bare	61.0	208.8	97665	5.070
43	Bare	76.2	93.3	103141	5.354
44	Bare	76.2	105.3	96531	5.011
45	Bare	76.2	120.6	89692	4.656
46	Bare	76.2	135.8	80178	4.162
47	Bare	76.2	151.1	81571	4.234
48	Bare	76.2	166.3	82540	4.285
49	Bare	76.2	181.5	89528	4.647
50	Bare	76.2	196.8	90709	4.709
51	Bare	76.2	208.8	93909	4.875
52	Bare	91.4	93.3	157560	8.179
53	Bare	91.4	105.3	141791	7.360
54	Bare	91.4	120.6	77719	4.034
55	Bare	91.4	135.8	40748	2.115
56	Bare	91.4	151.1	38134	1.980
57	Bare	91.4	166.3	43408	2.253
58	Bare	91.4	181.5	77397	4.018
59	Bare	91.4	196.8	124196	6.447
60	Bare	91.4	208.8	116633	6.054

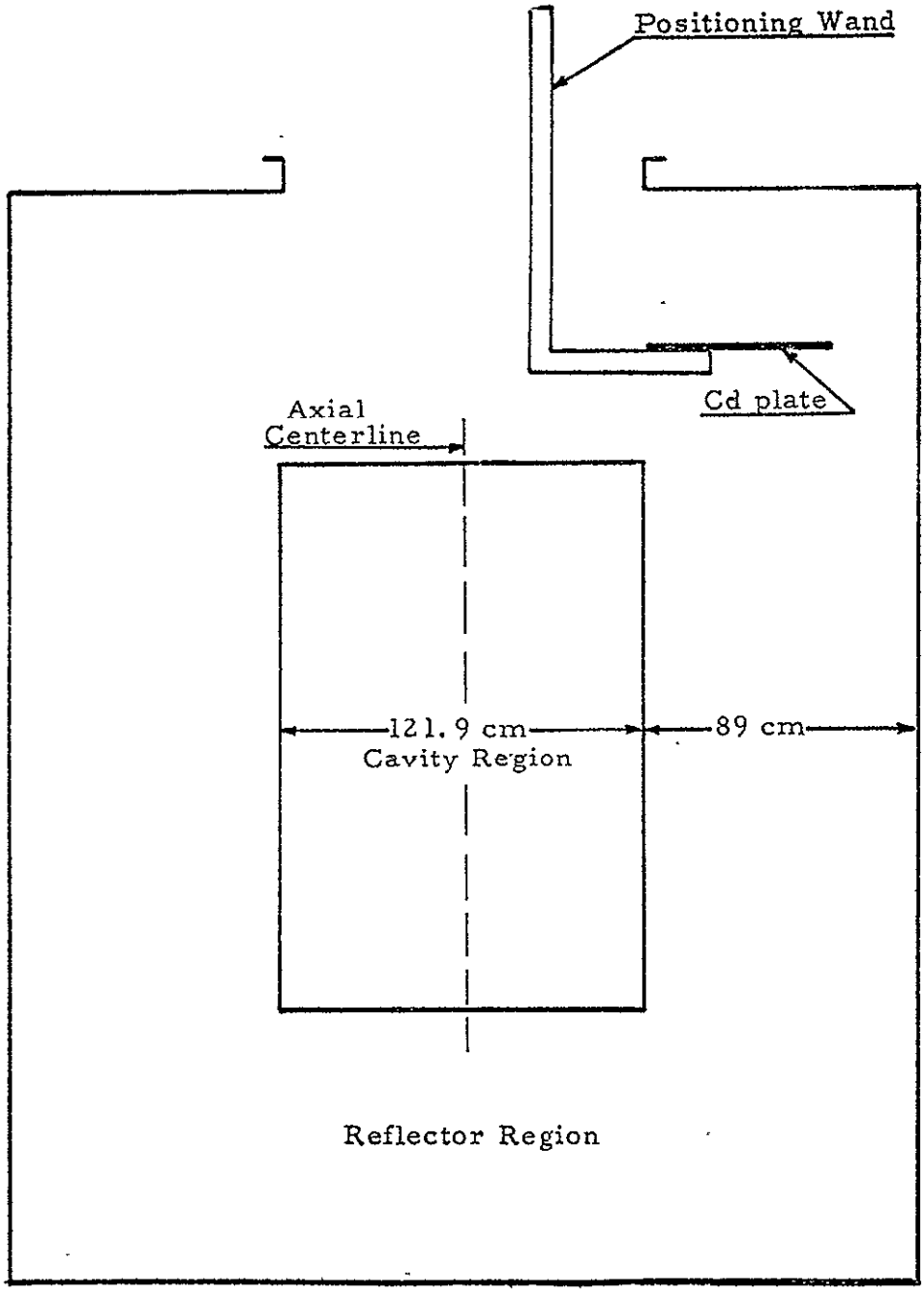

Fig. 14.1 Layout of control sleeve measurements

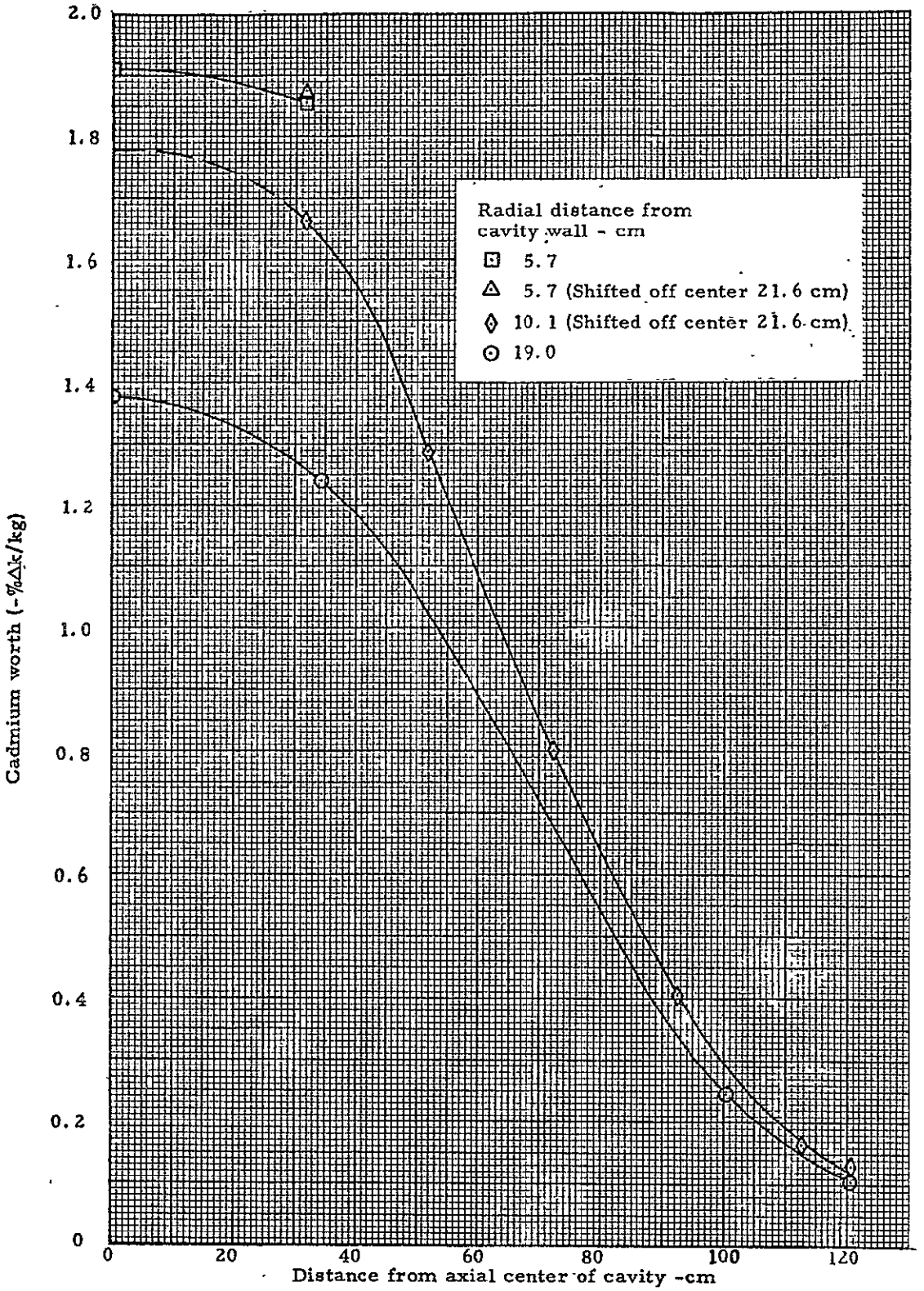

Fig. 14.2 Control sleeve simulation in the reflector using a plate of cadmium 30.5 cm wide by 61.0 cm long and 0.051 cm thick and weighing 877 gm

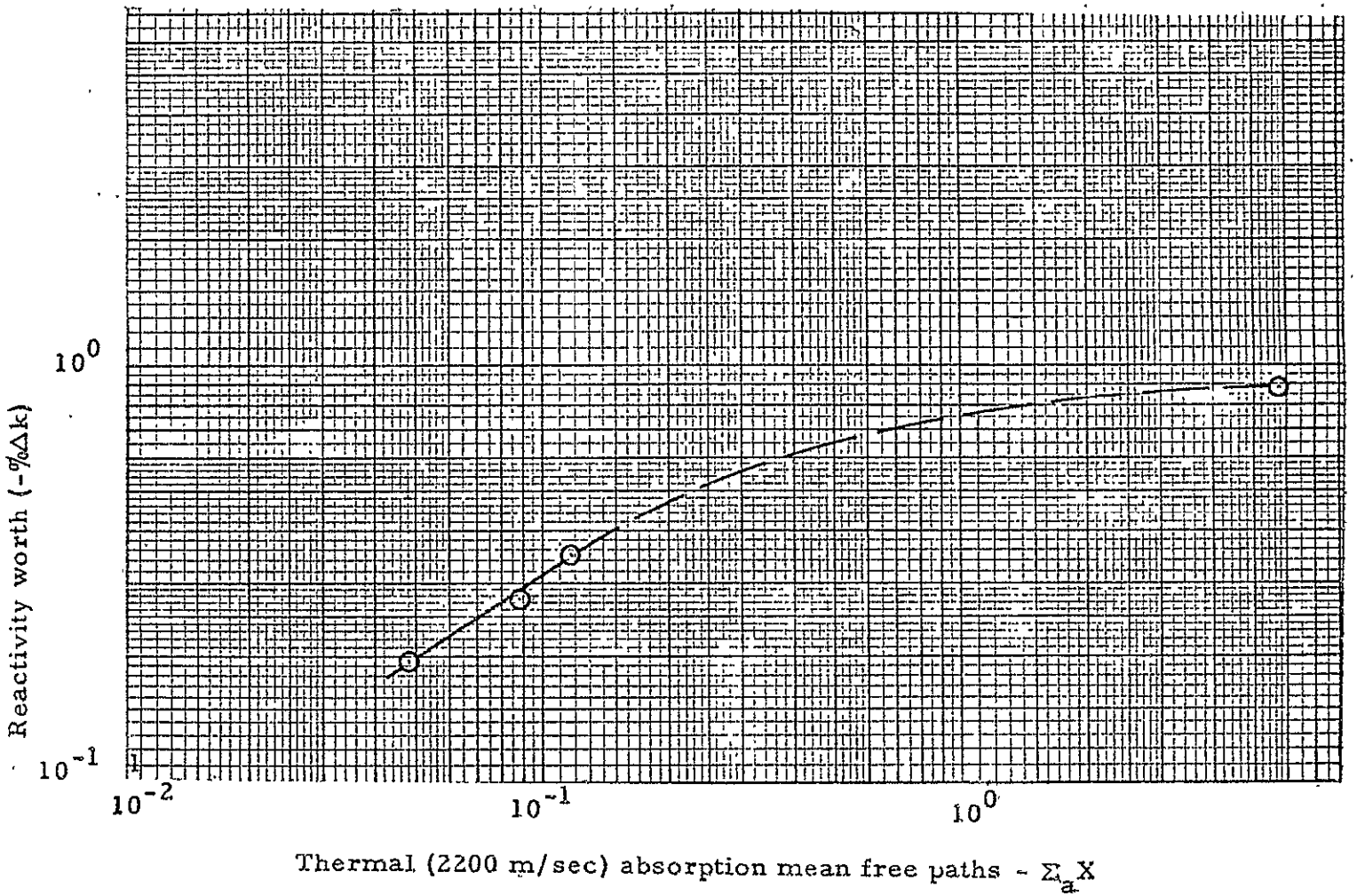

Fig. 14.3 Reactivity worth vs mean free paths from plates of material which were 22.1 cm wide by 40.0 cm long and placed 6.4 cm from the cavity wall in the radial reflector

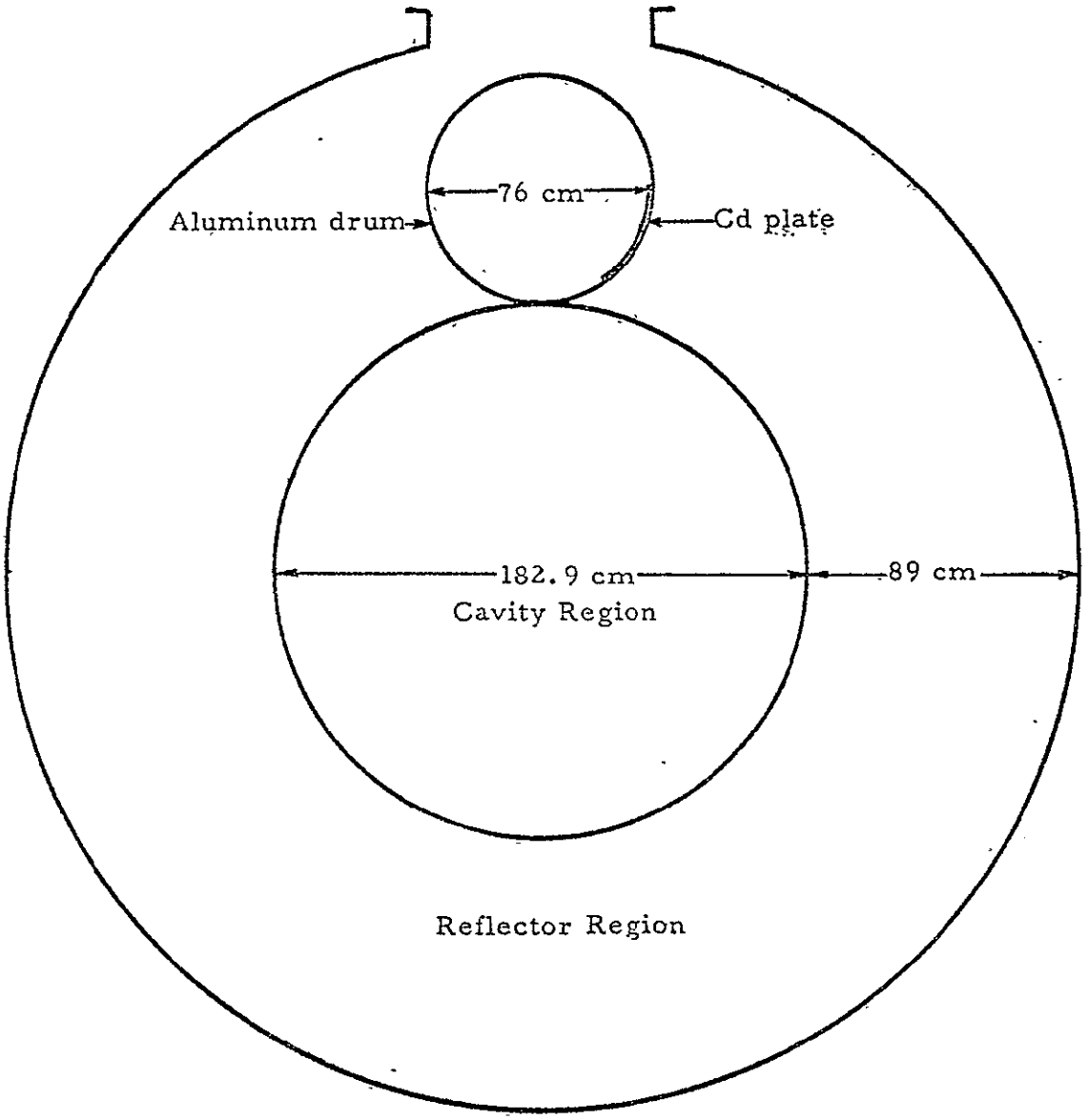

Fig. 14.4 Layout of control drum measurements

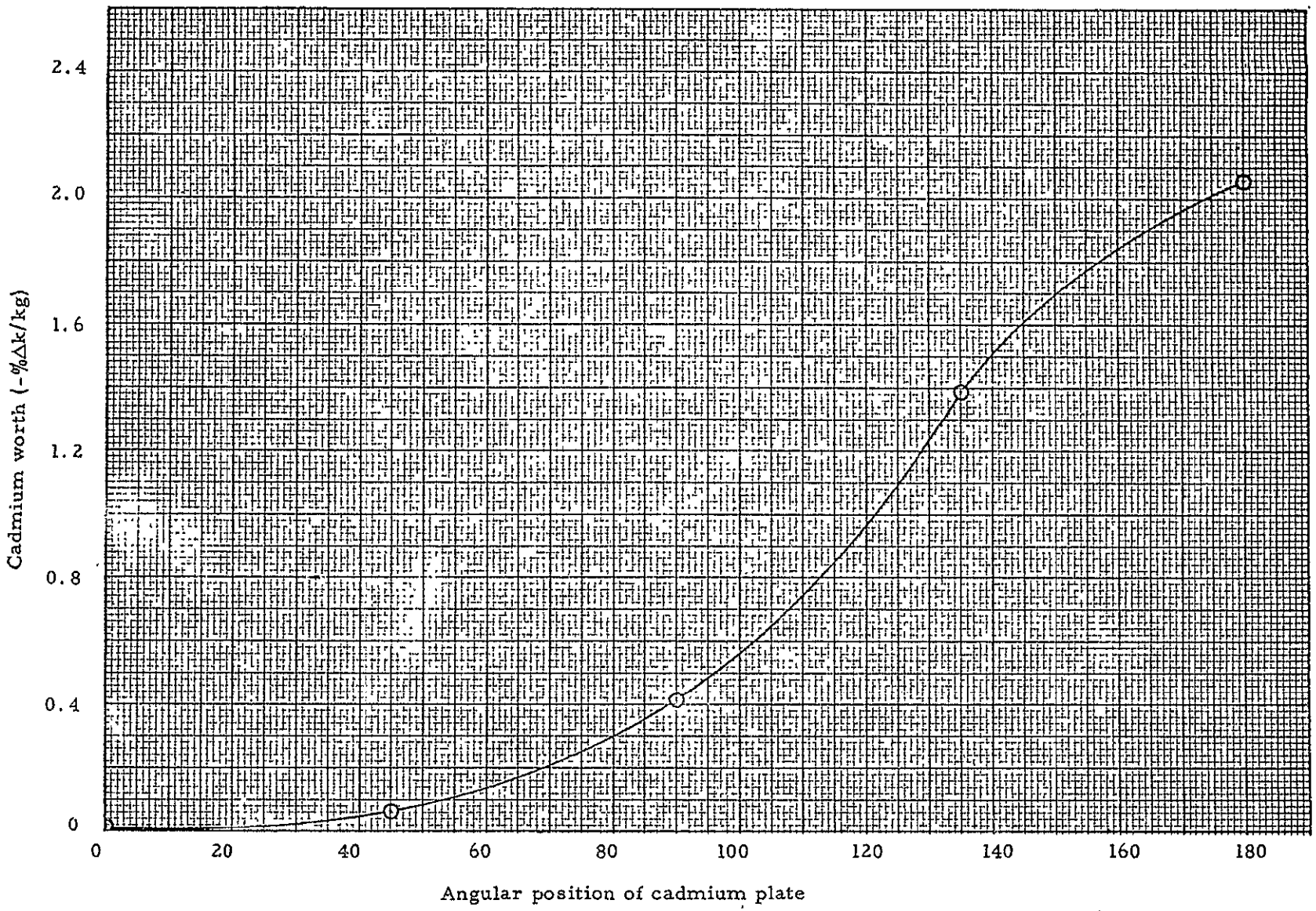

Fig. 14.5 Reactivity worth of rotating drum containing a sheet of cadmium 30.5 cm wide by 61.0 cm long and 0.051 cm thick and weighing 877 gm. Drum was located in the radial reflector centered over the cavity.

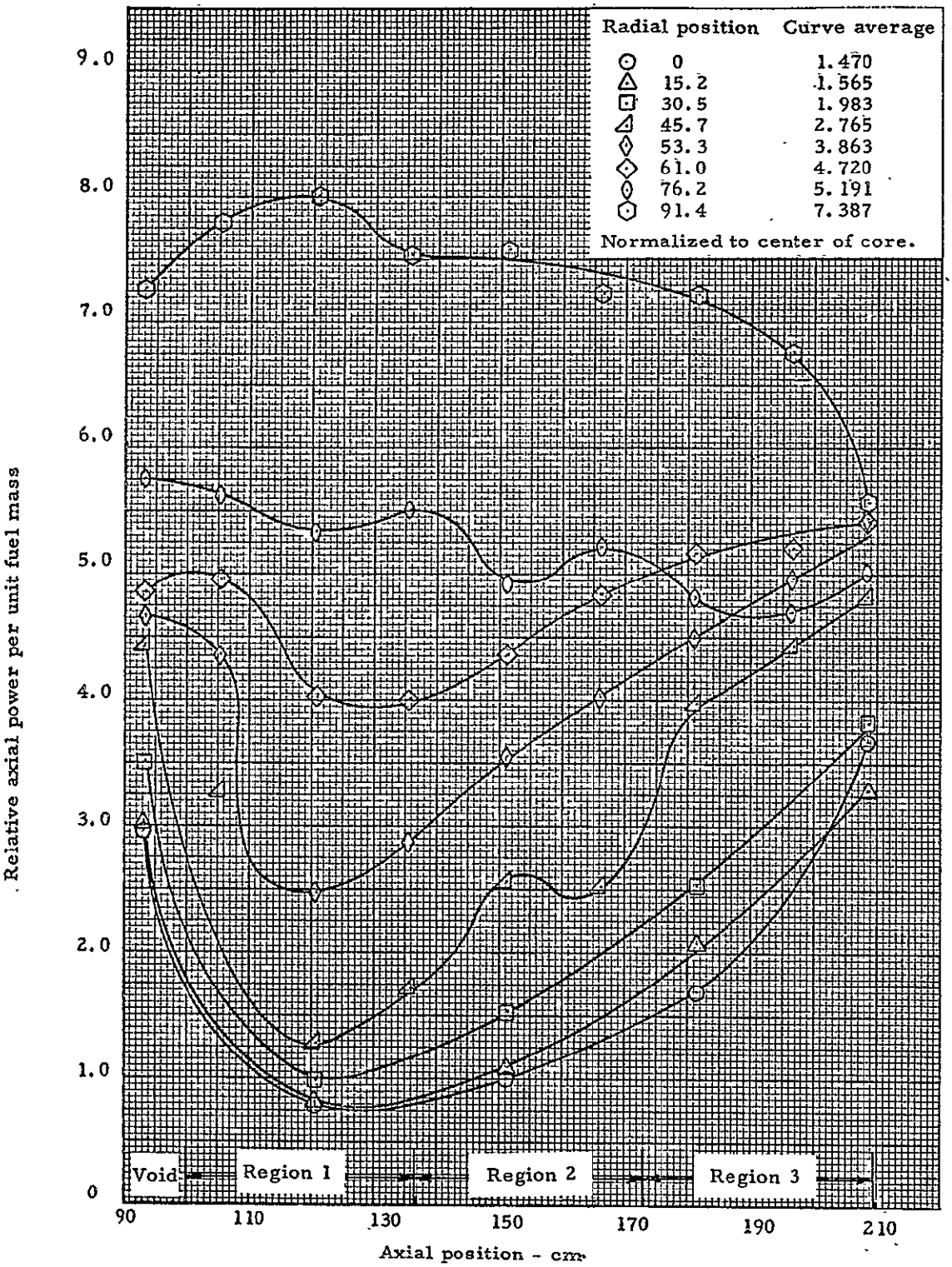

Fig. 14.6 Relative axial power distributions from bare catcher foils in the cavity region with no cadmium in the radial reflector.

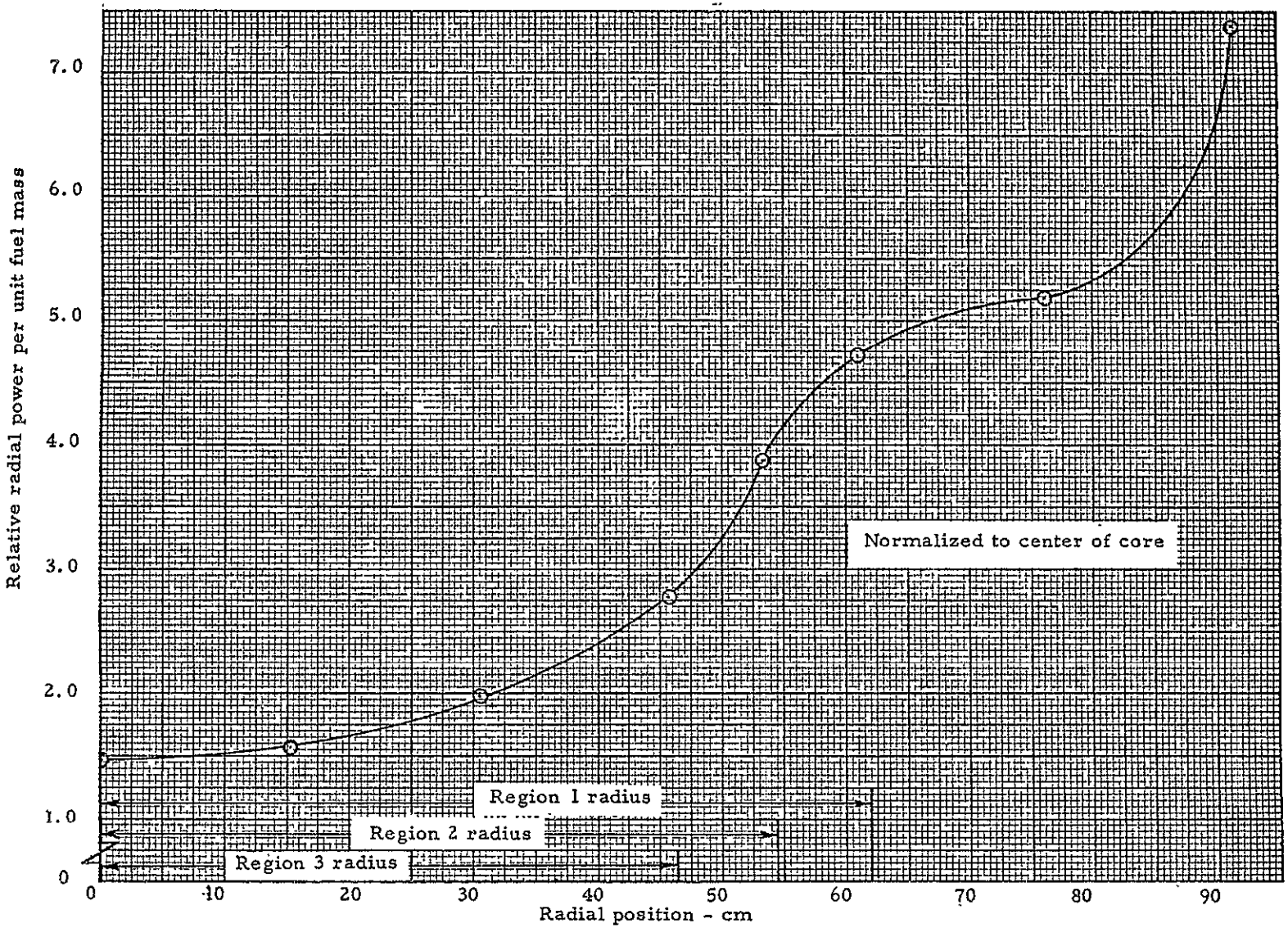

Fig. 14.7 Longitudinally averaged power distribution vs radius - without cadmium control elements in the reflector

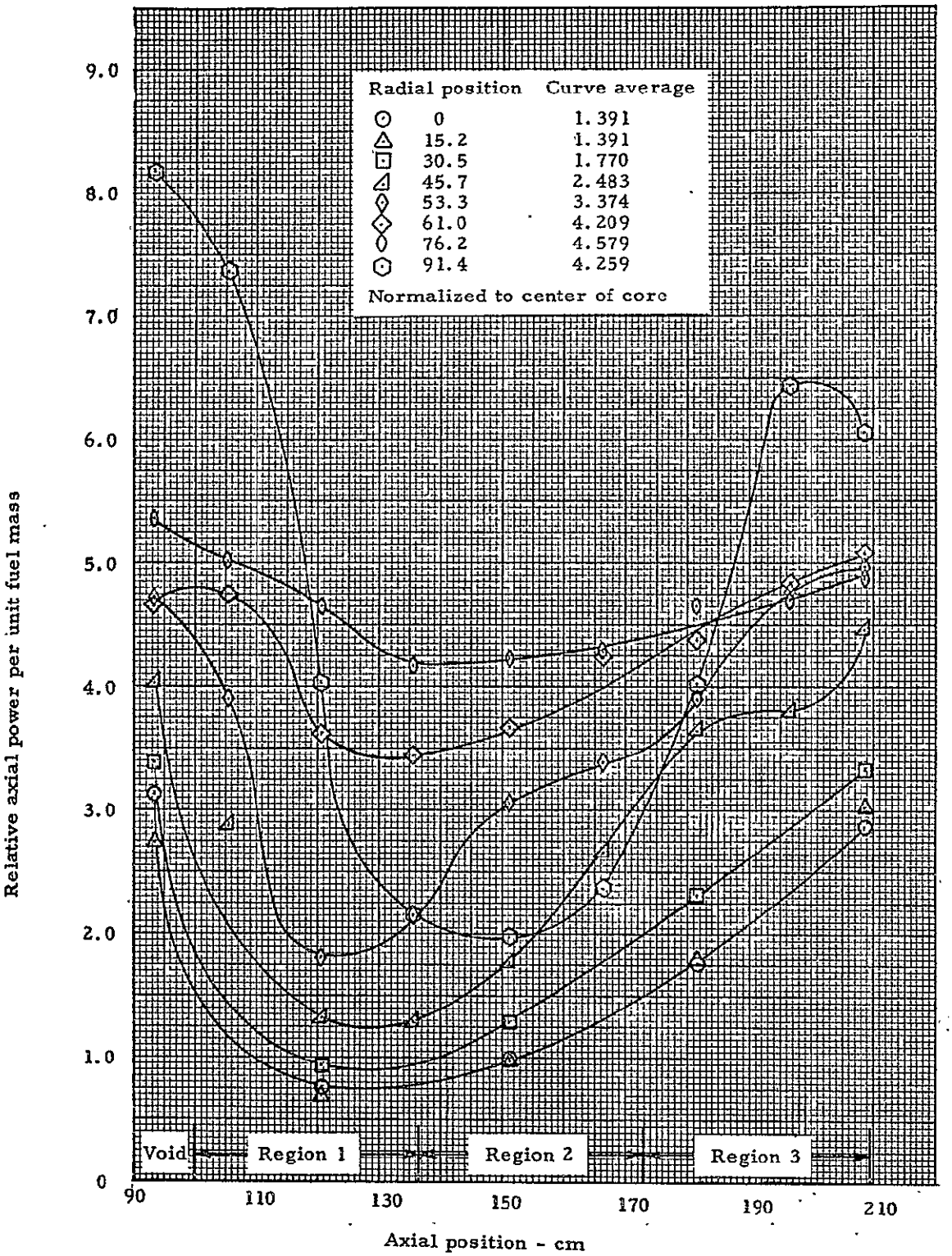

Fig. 14.8 Relative axial power distributions from bare catcher foils in the cavity region with 877 gm of cadmium near the cavity wall in the radial reflector

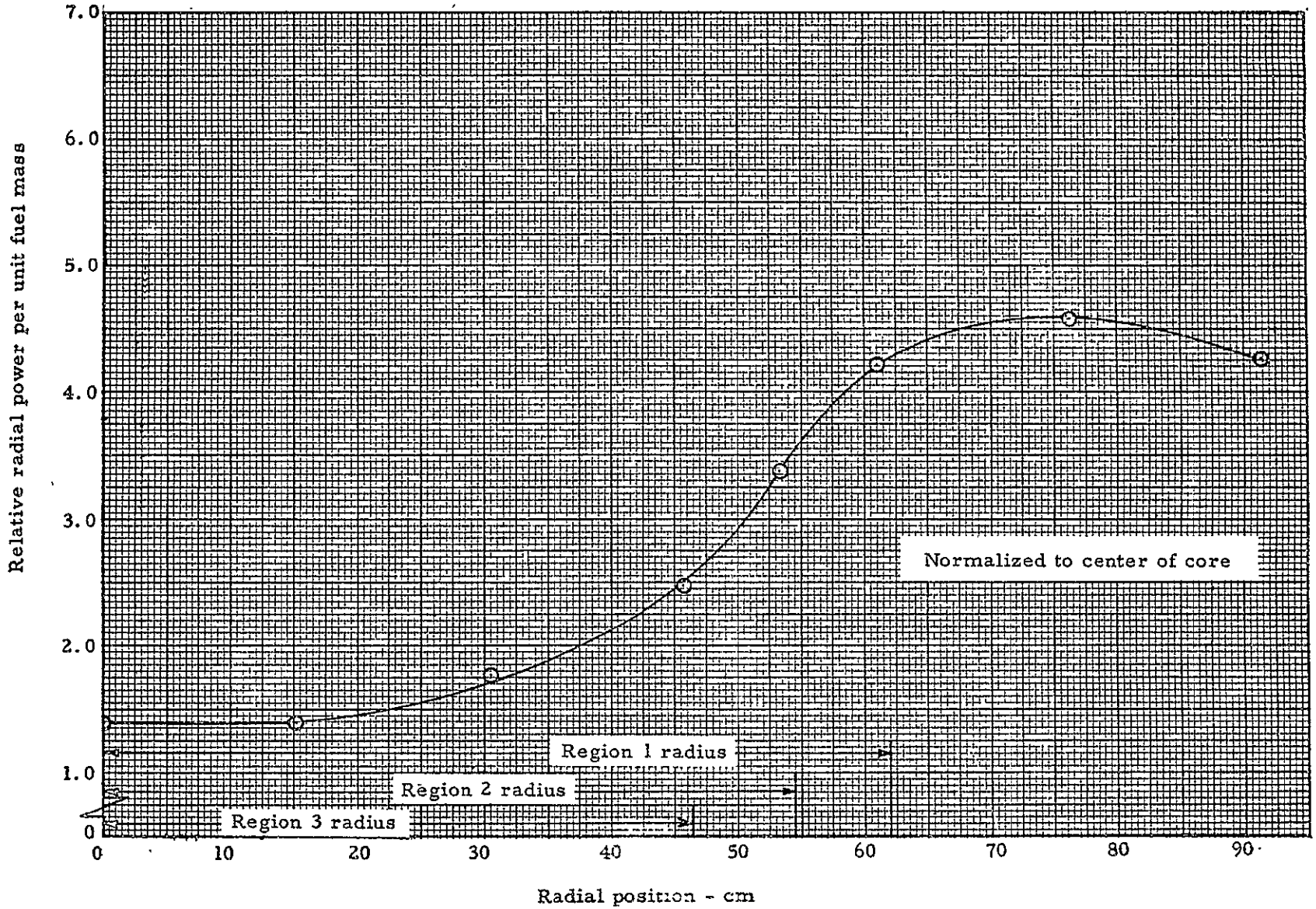

Fig. 14.9 Longitudinally averaged power distribution vs radius - with cadmium control element in the radial reflector

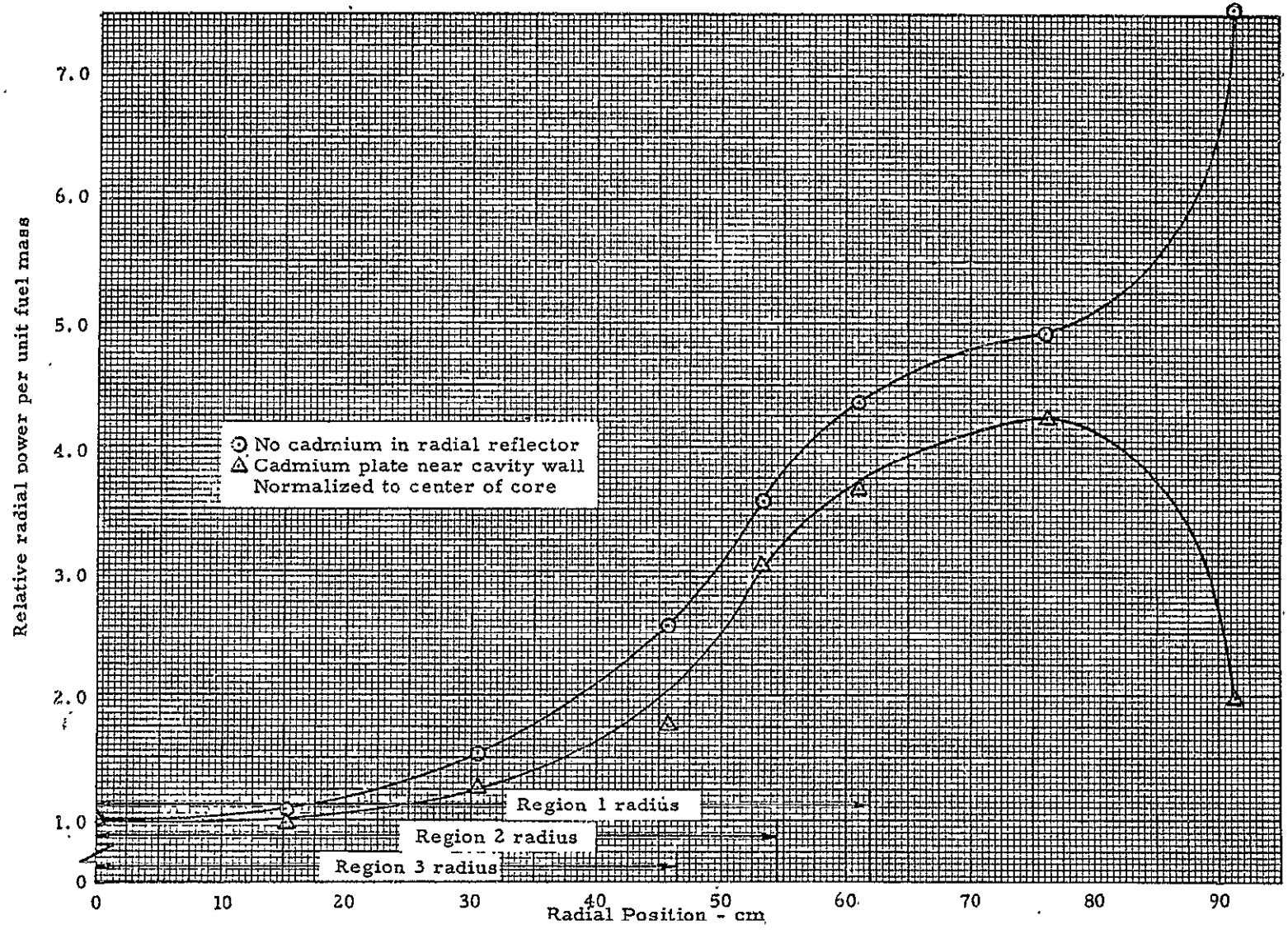

Fig. 14.10 Relative radial power distribution through the axial center of the core with and without cadmium in the radial reflector

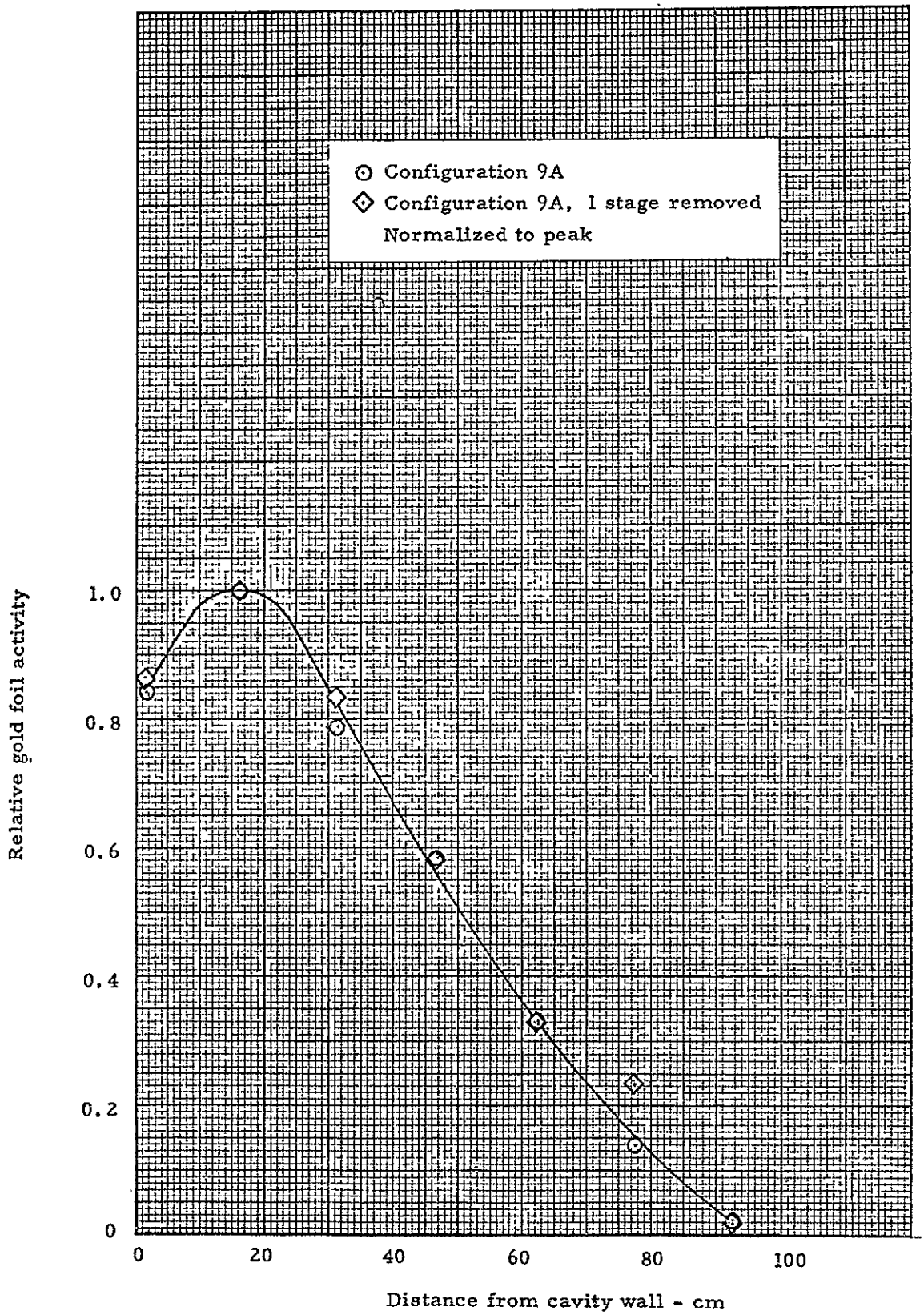

Fig. 14.11 Gold foil activity in radial reflector - configuration 9A

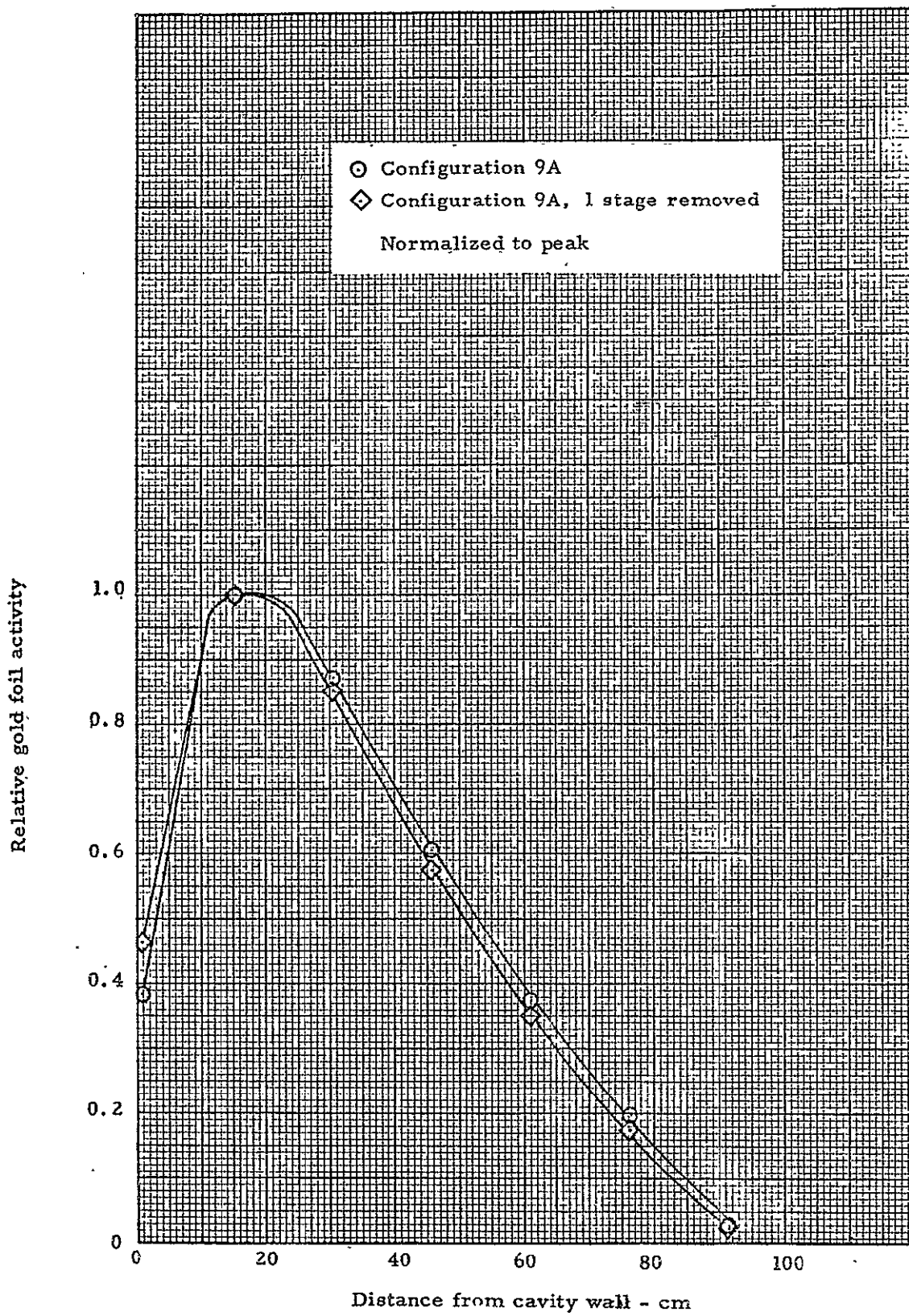

Fig. 14.12 Relative bare gold foil distribution in the end reflector showing the effects of shortening the core length one stage

15.0 CONCLUSIONS AND RECOMMENDATIONS

15.1 Pre-Wave Reactor Experiments

Prior to starting the wave experiments, two different core configurations were established. The first consisted of a uniformly loaded core with the ratio of the effective active core radius to the cavity radius of 0.68. The active core was radially surrounded by 20.6 kg of polyethylene. There was a stainless steel liner covering the ends and radial wall of the cavity which was 0.0965 cm thick and weighed 83.1 kg. There was also an annulus of MTR type fuel plates containing 823.2 grams of U^{235} in the radial reflector 19 cm from the cavity wall. The reactor was critical with 30.5 kg of uranium in the reactor and excess reactivity was 0.177%Δk. The basic core support structure described in Section 3.1 of this report was used for this reactor.

The primary purpose for this experiment was for a direct comparison with an earlier experiment which contained beryllium in the radial reflector (Reference 1, Section 5.0). With beryllium in the radial reflector, there were 18.1 kg of CH_2 surrounding the core and the critical mass was 54.1 kg of uranium. If the polyethylene were increased to 20.6 kg and corrections were made for differences in k-excess, the adjusted critical mass would be approximately 57.6 kg of uranium in the core.

The fuel annulus in the D_2O generated 13.5% of the total reactor fission power. This, of course, can be adjusted by varying the amount of uranium in the reflector which in turn would affect the core loading. The amount of fuel in this annulus would be governed by the power which could be tolerated but the point is clearly shown that very substantial saving in core loading can be achieved by having a uranium region in the reflector and by eliminating the beryllium heat shield in the reflector region. Note that by proper design, the uranium fuel element structure could serve as a heat shield as well. Addition of a 10 cm thick slab of Be to the radial reflector (using the uranium structure for support) would require the addition of approximately 5 kg to the original 30.5 kg uranium loading. (1), (3)

The base core for the wave measurements was then established. The core support structure was expanded so that it would accept and support the waves which extended beyond the normal active core boundary. This increased the total core aluminum mass 37.75 kg. For experimental convenience, the polyethylene was moved to the outer 8 cm of the cavity so that it would not interfere with the waves. With the other core components unchanged, the reactor was critical with 30.5 kg of uranium in the core, 34.9 kg of CH_2 near the cavity wall, and k-excess was 0.179 %Δk. Moving the CH_2 to the outer 8 cm of the cavity had a substantial positive effect on reactivity such that it more than compensated for the increase in aluminum mass in the core support structure. As a result, it was possible to increase the CH_2 mass 14.3 kg and still have sufficient operating k-excess.

15.2 Fuel Wave Measurements

15.2.1 Reactivity Measurements

In an operational cavity reactor, the outer surface of the active core is expected to contain irregularities in the form of waves. There will also be mixing of coolant (H) and uranium at the active core boundary. The intent of the wave experiments was to study the wave effects on reactivity and power distribution for both uniform and variable fuel density cores. Five general types of waves were measured during the course of the experiment. Examples of these are shown in Figures 15.1 to 15.6. In all cases only the worth of the addition or the re-location of the uranium was measured.

A summary of the core configurations is given in Table 15.1. As noted in the table, there were three major core configurations; (1) a uniform fuel density-uniform radius core (Configurations 1 to 6), (2) a uniform fuel density-variable radius core (Configuration 8), and (3) a variable fuel density-variable radius core (Configuration 9). The distribution of the fuel in Configurations 8 and 9 is given in Table 15.2 and the general layout of the three axial regions of the active core can be seen in Figure 15.7.

Configuration 1 core geometry was used for several types of waves which were numbered from 2 to 6. Each of these configurations had two or more wave measurements associated with it, numbered as described in Table 15.3. The reactivity worth of each of these waves is shown in Table 15.4. Configuration No. 2 waves represented the addition of a single stage of fuel on the outer surface of the core at several axial positions as shown in Figure 15.1. Configuration 2A gave the highest worth because of its location at the end of the reactor where a larger number of neutrons from both the end and radial reflectors could reach the wave without having to pass through some of the normal active core regions. The same reasoning also applies to Configuration 3A and 3B data where 2A was worth more than Configuration 3B.

The type of waves measured for Configurations 2 and 3 would not likely occur in an operating reactor unless transient type of eddy currents developed. Such have occurred near the exit end of scale model test, but here the central gas ("fuel") will probably be of lower than average density. Thus, the Configuration 2 and 3 type waves represent rather extreme cases which could be considered in the design of an adequate control system.

Configuration 4 waves consisted of the common "water type" waves (a crest and trough) that would normally occur at the core boundary. With this type of wave, there was no addition of fuel to the reactor. Configuration 4A was the type of wave shown near the separation plane in Figure 15.2 and was a single full wave. Configuration 4B was a double wave including 4A and a wave near the center of the core (which was measured to be worth 0.214%Δk by itself). The two waves together increased k-excess 0.433± 0.017%Δk where as the sum of the two individual waves was 0.457 ± 0.021%Δk.

Configuration 2C was also a double wave and included a wave near the axial center of the core and another over stages 1 and 2, In this case, however, the trough of the wave was on stage 1 and the crest on stage 2, whereas the wave for Configuration 4B at the separation plane had the crest on stage 15 and the trough on stage 15. The worth of Configuration 4C was only 0.222 ± 0.027%Δk which is only about half the worth of Configuration 4B. Configuration 4A was then reversed to determine the effect of interchanging the crest and trough of the wave at the end of the core. The reversed wave was worth 0.122 ± 0.017%Δk compared to 0.243 ± 0.017%Δk prior to making the interchange thus accounting for the lower worth for Configuration 4C compared to 4B. The reason for the lower worth with the trough of the wave at the end of the core is that the fuel at this location is worth more than in the stage next to the end of the core, whereas the crest of the wave is worth about the same over the first two stages.

Configuration 4D consisted of the three waves shown in Figure 15.2 and was worth 0.532 ± 0.024%Δk. In order to determine if the worth of the three waves together equalled the sum of the individual waves, the center wave worth was measured by itself to be worth 0.214 ± 0.013 %Δk. If it is assumed that the wave over stages 1 and 2 was worth the same as over stages 15 and 16 (Configuration 4A reversed) *, the sum of the individual waves was 0.579 ± 0.034%Δk. These results, along with the other data where mutliple waves were created, show some non-linearity in worth of the individual waves when several waves are summed to obtain a combination worth. The "sum of the parts" was always worth slightly more than the whole within the experimental uncertainty range.

The large waves associated with Configurations 3 and 5 had to be established in several increments. Because of the operational restrictions and the fact that the data from each increment indicated a nearly linear extrapolation could be made for the total wave worth, only half or a 180 degree sector of the large waves was measured. Thus, the values given in Table 3.4 for Configurations 3 and 5 are for the total wave extrapolated from the worth of half the wave. It will be noted that there was a significant decrease in wave worth between Configurations 5B and 5C. These were both double wave configurations with Configuration 5B being exactly as shown in Figure 15.5. The waves were then shifted two stages away from the separation plane to form Configuration 5C. This shift caused the trough of the wave to fall over stages 1, 2, and 3 for one of the waves. The reason for the decrease in worth is, therefore, the same as noted under the discussion of Configuration 4 where voids are created at the end of the core.

Configuration 6 waves were of the form shown in Figure 15.3 where the fuel was moved radially one stage thus forming a void directly under the wave. This represents a spalling off of the fuel from the core. Configuration 6D represents the sum of Configurations 6A, 6B, and 6C

---

* This assumption is not exactly valid as the data show a wave at the separation plane was worth more than at the other end of the core

and it will be noted that the measured worth of the three waves together was apparently higher by nearly 9% than the sum of the individual measurements. But the experimental uncertainty for 68% confidence was approximately 8%.

A comparison between Configurations 4 and 6 show that 6A falls between 4A and its reverse as might be expected. However, a comparison of the worth of the waves near the center of the core shows 6B to be worth 22% less than the center wave of 4D. Configuration 6D was also somewhat like Configuration 4D, each containing 3 waves, but the worth of 6D was 9% above 4D, but again the differences are within the experimental error. Although the comparison of the two types of waves is somewhat inconclusive, it can be deduced that their general magnitude is about the same and that in an operating reactor, the effects of the two types of waves would be essentially the same.

Configuration 8 contained a uniform fuel density throughout the active core but a variable radius. Waves were created at the end of each of the three axial regions as shown in Figure 15.6. As noted in Table 15.4, the amount of fuel involved in each of the single waves decreased as the core radius of the particular region decreased. If Configurations 8A, 8B, 8C, and 8D are compared on the basis of uranium worth-per-gram involved in the wave, the following values are obtained:

Configuration	Uranium Worth (%Δk/kg)
8A	0.588
8B	0.466
8C	0.420
8D	0.472

The above shows a decrease in specific worth of uranium as the core radius decreases. The three waves together gave a fuel worth of 0.472%Δk/kg. If the individual fuel worths for each wave is weighted by the amount of uranium used in each case, the weighted average is 0.497%Δk/kg which is 5% higher than the above number for all three waves together, again indicating a small amount of non-linearity and interation of the waves. These data are about like those for Configuration 4 if compared to the specific worth of uranium at approximately the same wave locations.

Configuration 9 was like Configuration 8 but with a variable fuel density. Only one wave measurement was obtained and it is referred to as Configuration 9E because the waves were at the same locations as for Configuration 8E. The results were essentially the same as the specific worth of the uranium in the waves for Configuration 9E was 0.476%Δk/kg compared to 0.472%Δk/kg for Configuration 8E.

The relative worth of various waves on all the configurations showed no unusual variations in worth. Table 15.5 is a summary of the wave worth per unit mass of uranium involved, classified as to whether there was a net addition of fuel or merely an interchange. The specific worths in

each category vary somewhat, but these variations are only ±30% maximum. Near the ends of the core, the shape of the wave has a noticeable effect on the worth, but otherwise there is very little change in worth as the wave moves down the core. The "interchange" uranium worth does become greater as the wave size grows. Finally, the specific worth of "uranium addition" waves is approximately three times the specific worth of "uranium interchange" waves.

The effect of wave size on reactivity and required critical fuel loading (using fuel worth data from Reference 1) is shown in Figures 15.8 and 15.9. A 30 kg base loading in a 122 x 122 cm cavity has been adopted as the reference configuration. Also shown in Figure 15.8 is the effect of a wave on the required fuel cavity pressure for criticality. For the latter, the ideal gas law has been assumed merely for the sake of simplicity in arriving at these conclusions. (Conditions in the power cavity with both ion and electron pressure are quite complex, and the ideal gas law is a gross simplification.) Since the crest-trough waves analyzed in Figure 15.9 involve essentially no change in fuel volume, the critical pressure curve will look the same as the critical mass curve.

Rounding of the fuel boundary and displacement of the inlet fuel region away from the cavity wall gave a total penalty of 5.5%Δk. Using the same reference 30 kg core as the base, this would translate to a penalty of 14 kg, giving a 44 kg loading.* This fuel loading penalty involved a simultaneous 25% reduction in active core volume as a result of these shaping measurements. The net effect would be approximately a factor of 2.0 increase in cavity pressure,--i.e., $P = 2.0\ P_o$, again assuming the ideal gas law. Thus, the sensitivity of critical fuel loading and cavity pressure to active core shape and size makes flow shaping studies of considerable importance. An increase of core to cavity radius ratio is a beneficial effect that can be used to compensate for fuel boundary rounding penalties. Data on the radius ratio effect may be found in Reference 3.

15.3 Control Methods

The three types of control methods measured were:

1. Control rods in end reflector. Thirty 1.7 cm diameter boron carbide rods worth 6%Δk.

2. Cadmium sleeve to be inserted around cavity. Assuming a steady geometric progression of the non-linearity factor, the total worth of such a blade is 22%Δk, and is believed to be a conservative estimate (underestimated).

3. Control drums (73 cm in diameter) with a 61 cm long by 30 cm wide cadmium poison strip on each drum. Assuming that six drums are worth 80% of 6 times one drum, a total control system worth of 10%Δk can be achieved.

---

* The fact that this result is the same as the 44.2 kg loading of Configuration 9A is fortuitous.

Figure 15.10 shows the effectiveness of these latter two control methods in providing adequate shutdown against high core loadings and the effectiveness for compensating for waves (the crest-trough type). Again a 30 kg, 122 x 122 cm reference core was used. It is obvious that the control sleeve provides virtually positive shutdown against any conceivable overloading. However, complete expansion of the fuel into the entire cavity will somewhat reduce the critical loadings shown in Figure 15.10.

15.4 Power Distribution

Power mapping measurements were obtained on Configurations 1, 4D, 9A, and 9E and on the control method configurations. Unusual effects of significance to the design and operation of a power cavity reactor were not discovered. The reader is referred to the section on the particular configuration for details on the power distribution.

TABLE 15.1

Major Core Configuration

Fuel Wave Measurements

Major Configuration Number	Number of Axial Regions	Ratio of Fuel to Cavity Radius	Critical Mass (kg) Uranium	CH_2
1	1	0.68	30.5	34.0
8	3	0.68, 0.59, 0.51	35.9	28.5
9	3	0.68, 0.59, 0.51	44.2	37.6

TABLE 15.2

Configuration 8 and 9 Fuel Distribution

	Fuel Fraction		Fuel Mass (kg of U)	
Region	Configuration 8	Configuration 9	Configuration 8	Configuration 9
1	0.476	0.658	17.1	29.1
2	0.304	0.244	10.9	10.7
3	0.220	0.098	7.9	4.4
	1.000	1.000	35.9	44.2

TABLE 15.3

Core and Wave Identification

Major Configuration Number	Wave Configuration (Base for waves)	Wave Size (1)	Stage Location (2)	No. of Waves
1	2A	7.3 cm-1/2	16	1
1	2B	7.3 cm-1/2	11	1
1	2C	7.3 cm-1/2	6	1
1	3A	21.9 cm-1/2	14 to 16	1
1	3B	21.9 cm-1/2	7 to 9	1
1	4A	7.3 cm-1	15 to 16	1
1	4B	7.3 cm-1	7 & 8, 15, 16	2
1	4C	7.3 cm-1	1 & 2, 9 & 10	2
1	4D	7.3 cm-1	1 & 2, 8 & 9, 15 & 16	3
1	5A	21.9 cm-1	11 to 13 & 14 to 16	1
1	5B	21.9 cm-1	3 to 5 & 6 to 8 11 to 13 & 14 to 18	2
1	5C	21.9 cm-1	1 to 3 & 4 to 6 9 to 11 & 12 to 14	2
1	6A	7.3 cm-1	16	1
1	6B	7.3 cm-1	9	1
1	6C	7.3 cm-1	2	1
1	6D	7.3 cm-1	2, 9, 16	3
8	8B	7.3	6	1
8	8C	7.3	11	1
8	8D	7.3	16	1
8	8E	7.3	6, 11, 16	3
9	9E	7.3	6, 11, 16	3

(1) Waves are either 7.3 cm square or 21.9 cm square. They are also either 1/2 or whole waves with a 1/2 wave representing addition of the wave to the outer surface of the cores. Whole waves always conserve fuel and consist of both trough and crests.

(2) Stage 1 is at the end of the cavity opposite the separation plane and Stage 16 is at the separation plane.

TABLE 15.4

Fuel Wave Measurement Results

Uniform Fuel Density Constant Fuel Radius Core

Wave Configuration	Uranium Addition (kg)	Wave Size (cm square)	Reactivity Worth (%Δk)
2A	0.44	7.3	0.725±0.029
2B	0.44	7.3	0.525±0.040
2C	0.44	7.3	0.524±0.049
3A	4.84	21.9	6.136±0.159
3B	4.84	21.9	5.743±0.126
	Uranium Interchanged (kg)		
4A	0.40	7.3	0.243±0.027
4B	0.81	7.3	0.433±0.017
4C	0.81	7.3	0.222±0.027
4D	1.21	7.3	0.532±0.024
4A (reversed)	0.40	7.3	0.122±0.017
4D (center wave only)	0.40	7.3	0.214±0.013
5A	3.30	21.9	2.812±0.144
5B	6.60	21.9	4.838±0.230
5C	6.60	21.9	4.196±0.279
6A	0.40	7.3	0.160±0.028
6B	0.40	7.3	0.167±0.019
6C	0.40	7.3	0.206±0.013
6D	1.21	7.3	0.579±0.026
8B	0.58	7.3	0.341±0.007
8C	0.56	7.3	0.261±0.007
8D	0.45	7.3	0.189±0.006
8E	1.59	7.3	0.751±0.022
9E	1.81	7.3	0.862±0.016

TABLE 15.5

Fuel Worth Comparison From

The Fuel Wave Experiments

Configuration	Uranium Addition (kg)	Uranium Worth (%Δk/kg)
2A	0.44	1.65
2B	0.44	1.19
2C	0.44	1.19
3A	4.84	1.27
3B	4.84	1.19
	Uranium Interchanged (kg)	
4A	0.40	0.607
4B	0.81	0.535
4C	0.81	0.274
4D	1.21	0.440
4A (reversed)	0.40	0.305
4D (center wave only)	0.40	0.535
5A	3.30	0.852
5B	6.60	0.733
5C	6.60	0.636
6A	0.40	0.400
6B	0.40	0.418
6C	0.40	0.515
6D	1.21	0.479
8B	0.58	0.588
8C	0.56	0.466
8D	0.45	0.420
8E	1.59	0.472
9E	1.81	0.476

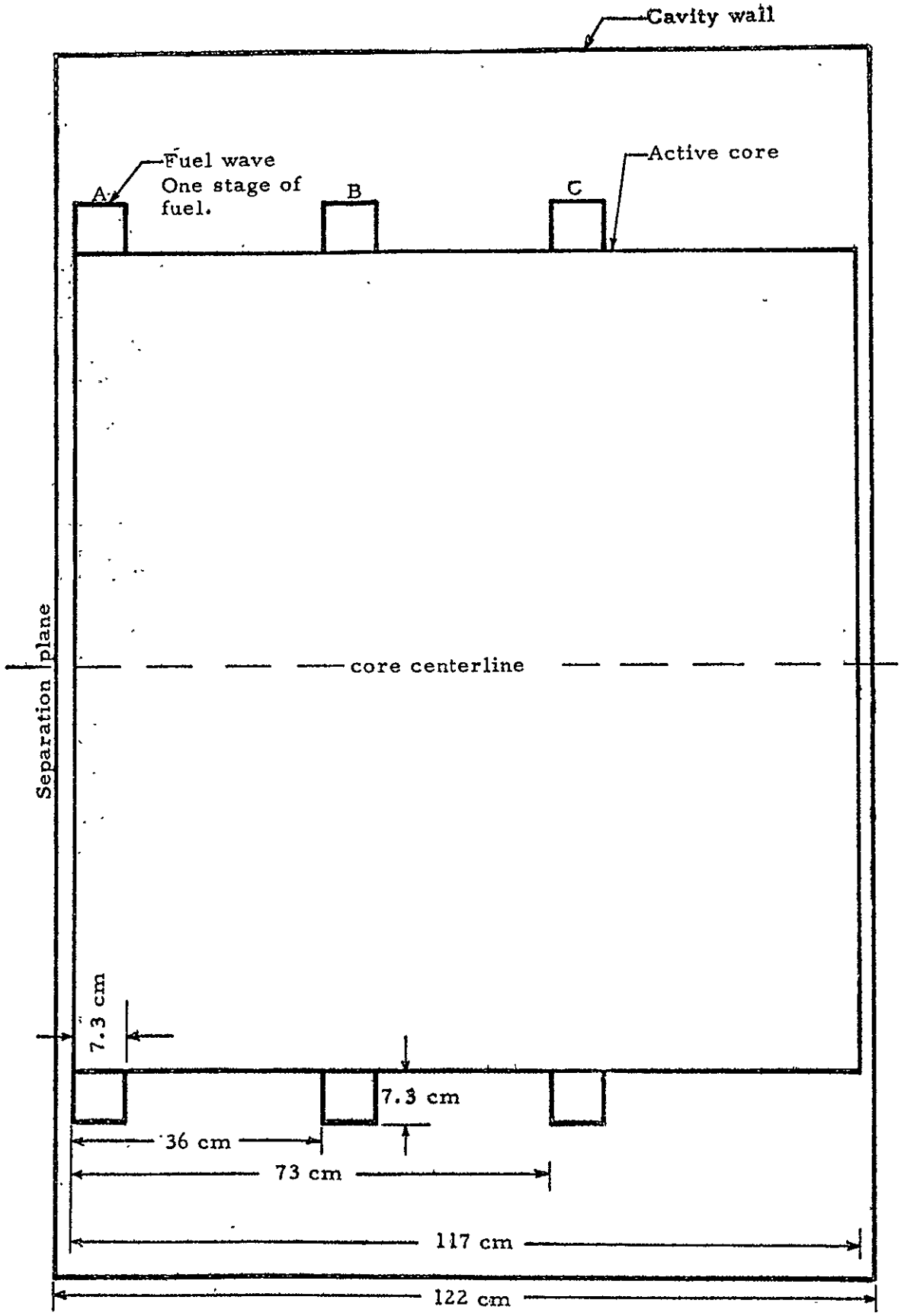

Fig. 15.1 Configuration 2 type waves

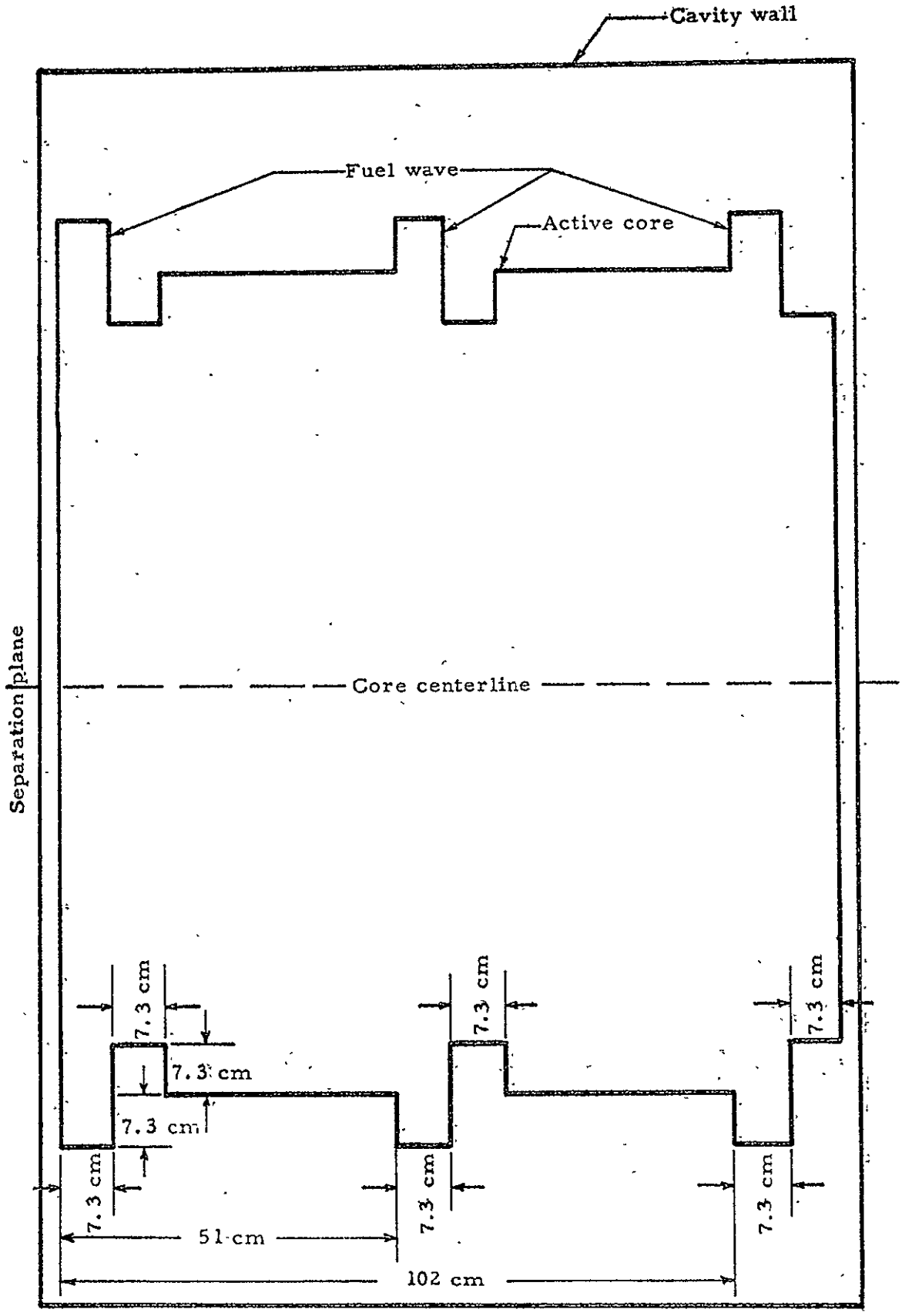

Fig. 15.2 Configuration 4 type waves

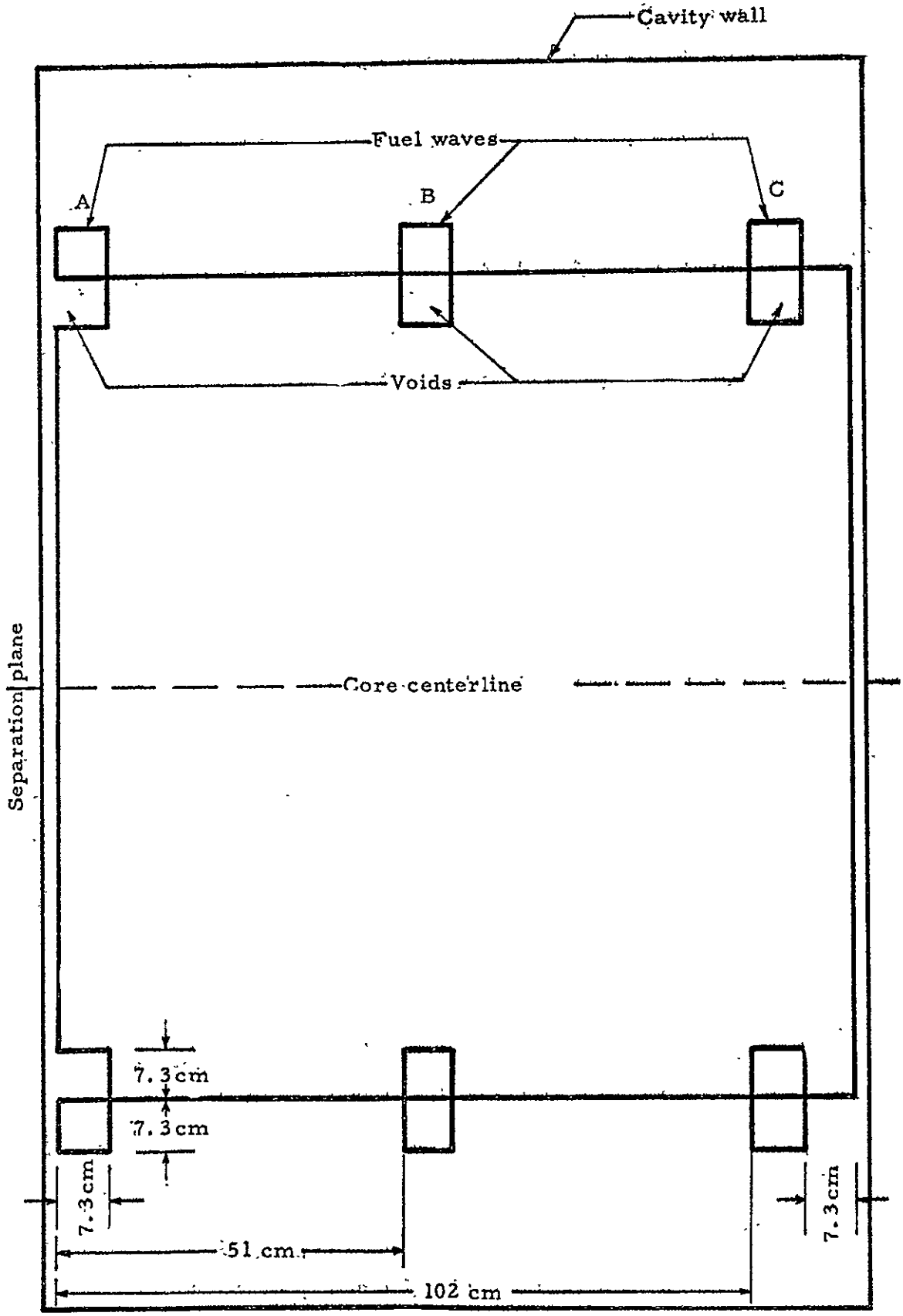

Fig. 15.3 Configuration 6 type waves

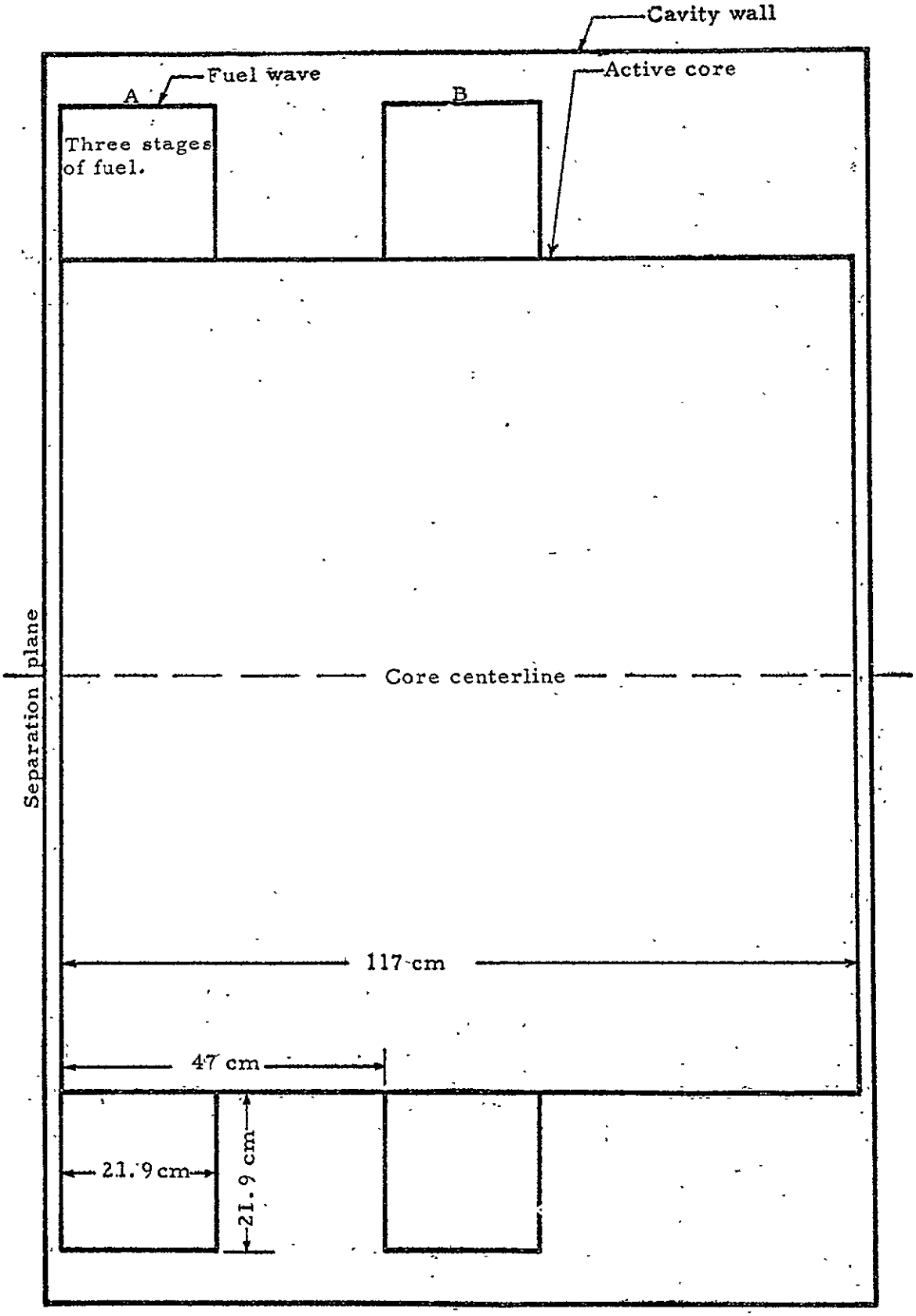

Fig. 15.4 Configuration 3 type waves

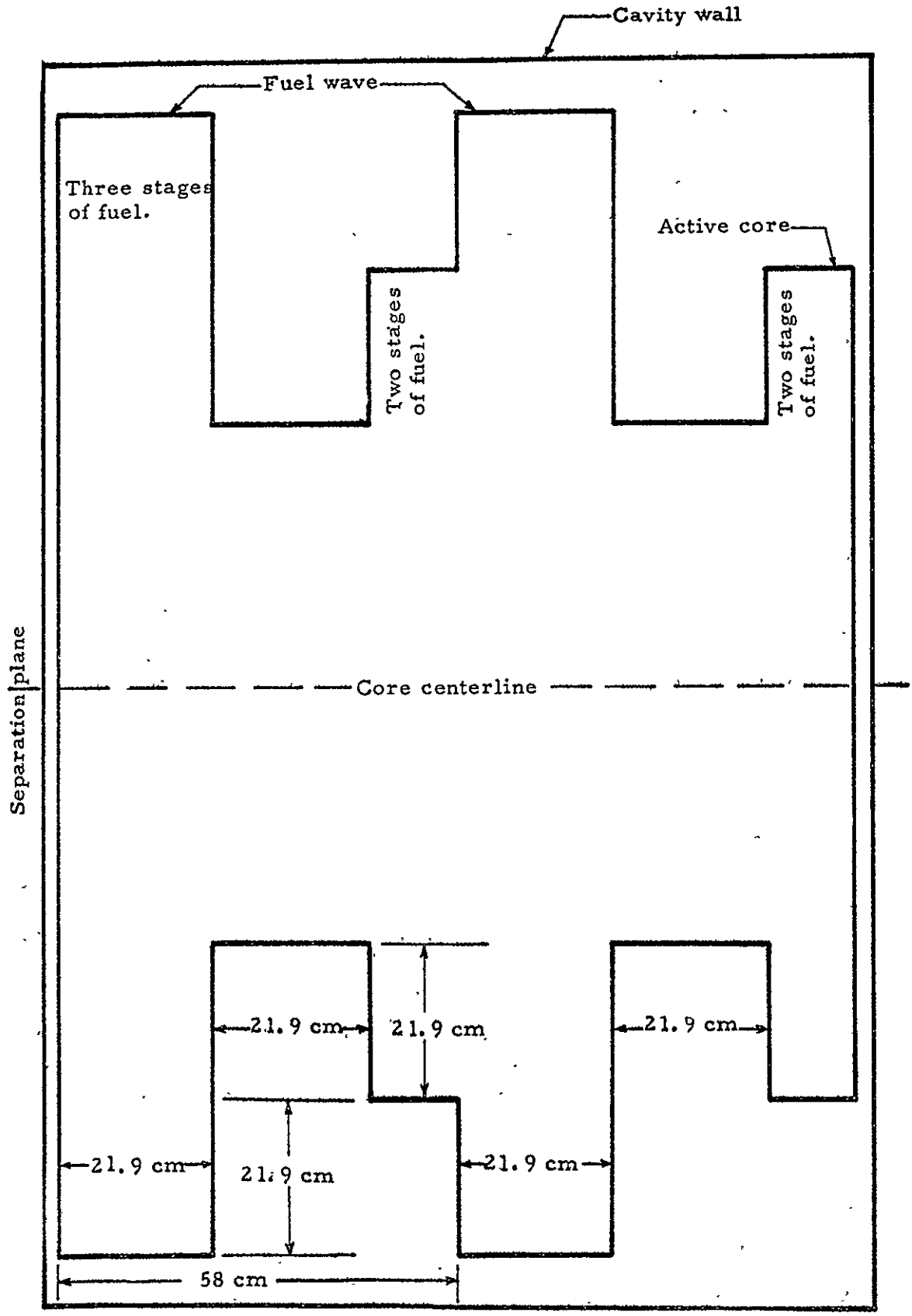

Fig. 15.5 Configuration 5 type waves

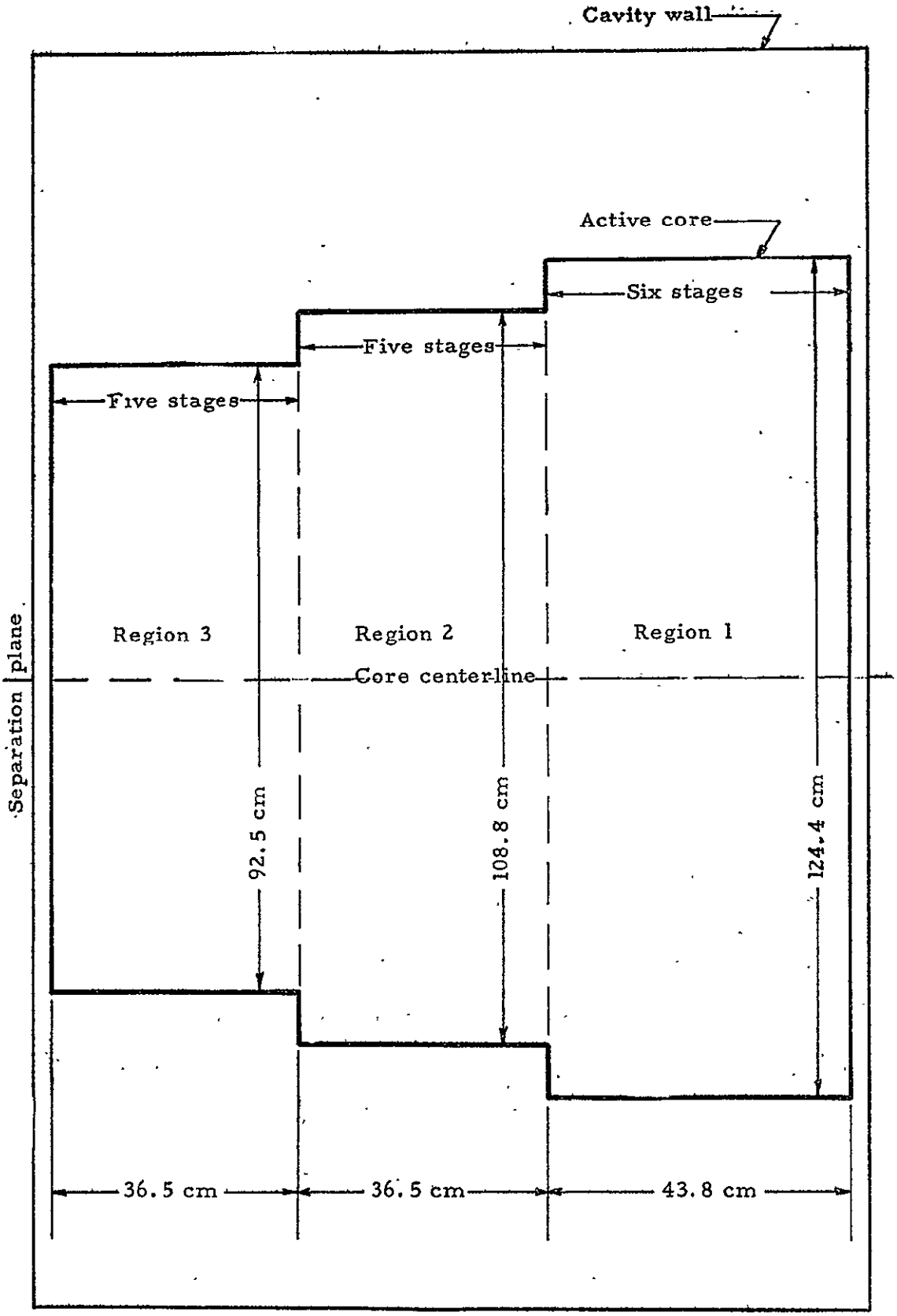

Fig. 15.6 Configuration 8 and 9 core outline

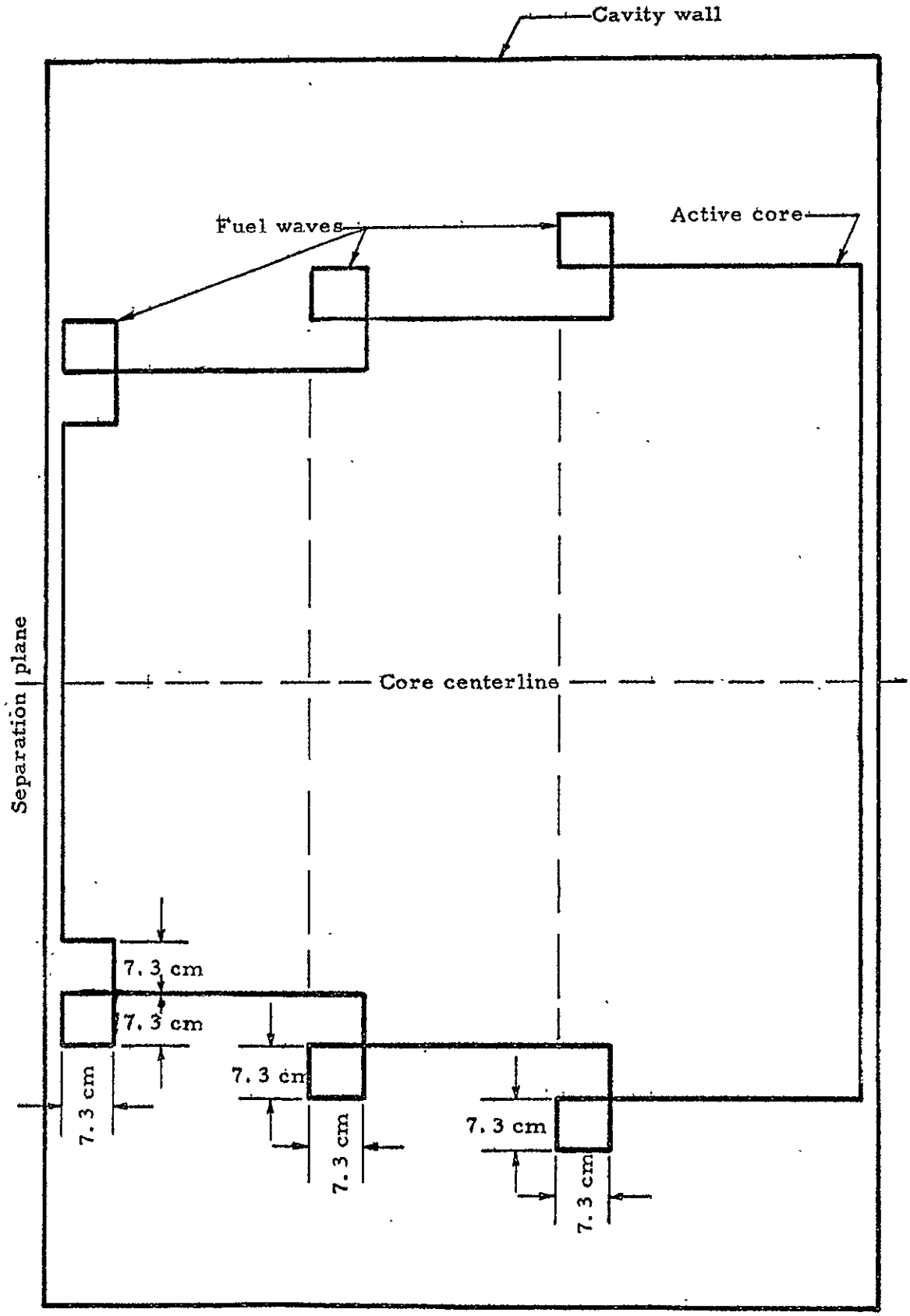

Fig. 15.7 Waves for configuration 8 and 9

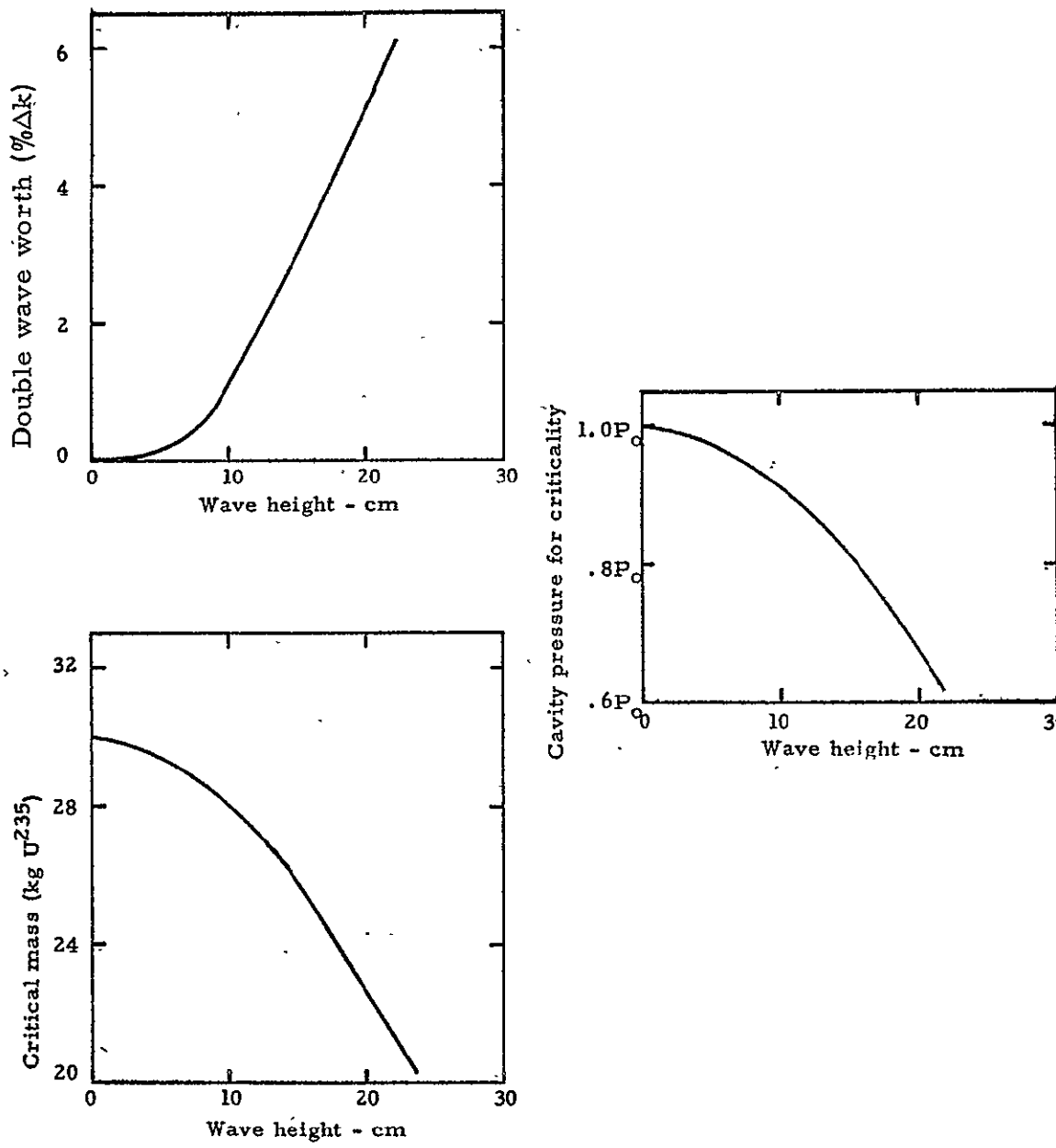

Fig. 15.8 Effects of double wave on criticality

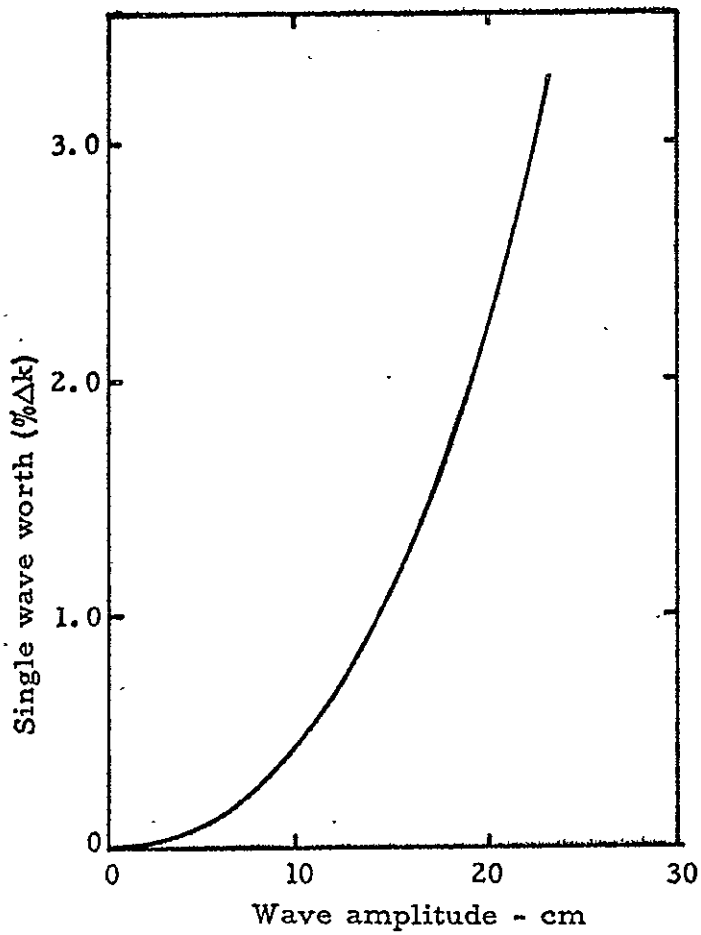

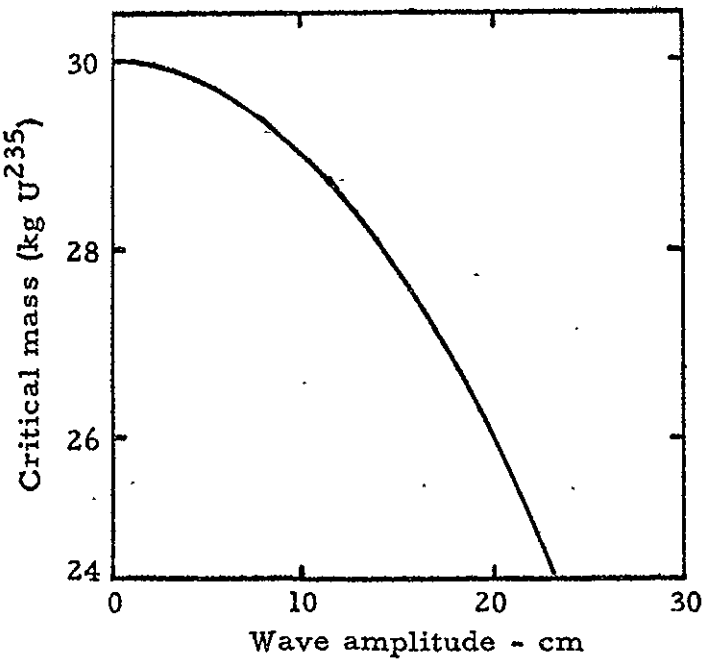

Fig. 15.9 Effects of single wave on criticality

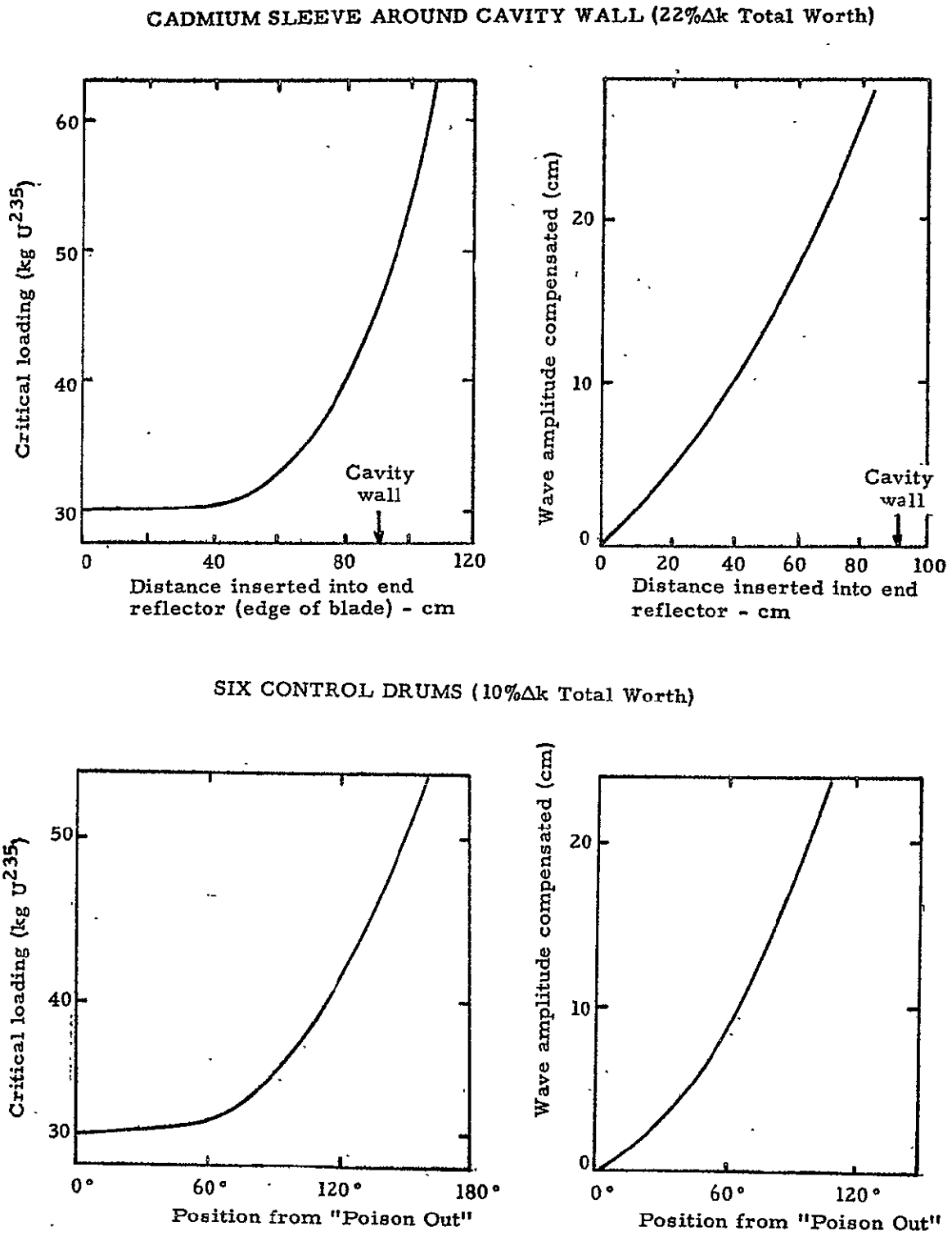

Fig. 15.10 Control method effectiveness of radial reflector

REFERENCES

1. Pincock, G. D., Kunze, J. F., "Cavity Reactor Critical Experiment, Volume III," General Electric Company, NSP-ITS, September 1968, (NASA-CR-72384).

2. Pincock, G. D., Kunze, J. F., "Cavity Reactor Critical Experiment, Volume II," General Electric Company, NSP-ITS, May 31, 1968, (NASA-CR-72415).

3. Pincock, G. D., Kunze, J. F. "Cavity Reactor Critical Experiment, Volume I," General Electric Company, NMPO-ITS, September 6, 1967, (NASA-CR-72234).

4. Cohn, C. E., Kaganove, J. J., (ANL), ANS Transactions, Vol. 5, No. 2, November 1962, p. 388.

5. Johnson, B. V, "Experimental Study of Multi-Component Coaxial-Flow Jet in Short Chambers," United Aircraft Corp. (G-910091-16), April 1968.

6. Ragsdale, R. G. and Hyland, R. E., NASA Lewis Research Center, Private Communication.

INDEX